UNIVERSITY OF SOUTHAMPTON

FACULTY OF ENGINEERING AND APPLIED SCIENCE

SCHOOL OF ENGINEERING SCIENCES

MATERIALS RESEARCH GROUP

Thesis submitted for the degree of Doctor of Philosophy

ANALYSIS OF A NEW APPROACH TO SIZING STAND-ALONE PV SYSTEMS

By Aikaterini Fragaki

March 2005

UNIVERSITY OF SOUTHAMPTON

ABSTRACT

FACULTY OF ENGINEERING AND APPLIED SCIENCES

SCHOOL OF ENGINEERING SCIENCE

Doctor of Philosophy

ANALYSIS OF A NEW APPROACH TO SIZING STAND-ALONE PV SYSTEMS

By Aikaterini Fragaki

The photovoltaic (PV) system design must allow for the variable nature of solar radiation and provide electricity to the load with optimum reliability and minimum cost. There are requirements both to understand the system operation and improve the available techniques. The aim of the current project is to improve the existing PV design concepts; by applying a predicting formalism of solar radiation based on day-to-day variations, and examine the possibilities of developing a new sizing methodology. An alternative methodology is suggested for system sizing, which determines the reliability of supply in terms of how long the system is expected to operate without shedding load. It is based, similarly to several traditional methods, on long-term system modelling. Unlike the traditional approach based on loss-of-load probability the method provides a clear relationship between the required system configuration and the length of the time series used in system sizing. The modelling work points out the importance of suitably designed array-size battery combination in terms of a sizing curve. Much of the modelling work is based on measured time series in the South of UK and Potsdam, Germany. The use of artificially generated solar radiation data from climate experiments for the prediction of the battery state of charge, however, is also examined, opening a new area of research. The model based on the daily energy balance that has been used for this purpose has been validated using a stand-alone system which has been constructed for this project and monitored. Furthermore, battery experiments have been conducted in the laboratory to examine detailed battery operation under conditions close to those encountered in a PV system. This part of the work focuses on loss of battery charge, which is shown to occur close to the full SOC. The electrical characteristics of PV generator are examined through a model developed in Matlab and validated experimentally. Following extensive literature research and modelling work, radiation data have been converted to the inclined plane for use as input in long-term system modelling, by applying the methodology of the European Solar Radiation Atlas.

CONTENTS

ACKNOWLEDGEMENTS

I would like to acknowledge the support, encouragement and guidance of my supervisor Dr. Tomas Markvart without which this work would not have been possible. I would also wish to acknowledge financial support from the School of Engineering Sciences, University of Southampton.

I am grateful to Prof. John Page for many useful conversations on the subject of solar radiation and on the use of ESRA software, to Dr. Neil Ross and Dr. David Spiers for valuable discussions on battery operation and efficiency and to Chris Goodbody for the calibration of the solar modules that I have used in the experimental PV system.

I would like to thank Dave Beckett, Peter Wilkes, Peter Malson, Rob Stansbridge and Ed Rayner for providing technical support during the experimental stages of this project. From the administration staff special thanks go to Gwyneth Skiller.

For proof reading, I wish to thank Charlene, Ed and Gerard.

I am indebted to my friends, my office mates and my sister. Their understanding and support made it possible for me to complete this work.

Finally, my deepest gratitude goes to my mother for her endless patience and encouragement.

NOMENCLATURE

β	Tilt angle of the PV panel
δ	Solar declination
θ_i	Angle of incidence of the solar rays on a surface
θ_z	Zenith angle of the sun
ρ_g	Ground reflectance
φ	Latitude
ω	Hour angle
ω_s	Sunset hour angle
G_{on}	Extraterrestrial solar irradiance normal to the sun rays
G_{sc}	Solar constant
G_o	Extraterrestrial solar irradiance on a horizontal surface
H_o	Daily extraterrestrial radiation on a horizontal surface
A_p	Area of the PV plane
I_T	Total hourly radiation on the inclined plane
E_{TILT}	Total energy of the radiation on the plane
I_b	Hourly beam radiation on the horizontal plane
R_b	The ratio of the beam radiation on the inclined plane to that on the horizontal surface
$E_{T,b}$	The energy of the beam radiation on the tilted surface
F_{1-2}	The fraction of object 2 visible from the surface of object 1
A_x	Area of the surface x
$I_{d,x}$	Part x of the hourly diffuse radiation on the horizontal plane
H	The daily total radiation on the horizontal surface
H_d	The daily diffuse radiation on the horizontal surface
K_T	Clearness index
$\overline{K}_T$	Monthly average clearness index
$\overline{H}_d$	Monthly average daily diffuse radiation on the horizontal surface
$\overline{H}$	Monthly average total radiation on the horizontal surface
$\overline{H}_T$	Monthly average total radiation on the tilted surface
$\overline{H}_b$	Monthly average beam radiation on the horizontal surface

E_c	Conduction bands
E_g	Band gap
E_v	Valence bands
E_F	Fermi level
J_h	Current density for the holes
k	Boltzman constant
D_h	Diffusion coefficient of the holes on the n-side
L_h	Diffusion length of the holes
T	Junction temperature
q	Charge of an electron
U	Net recombination rate
p_{no}	Equilibrium concentration of holes on the n-side
I_{ph}	Photocurrent
I_o	Dark saturation current
R_s	Series resistance of the cell
R_p	Parallel resistance of the cell
V_{oc}	Open circuit voltage
I_{sc}	Short circuit current of the cell
V_t	Thermal voltage
m	Ideality factor
FF	Fill factor
FF_o	Ideality fill factor
V_{bi}	Build in potential of the pn junction
I_{SCG}	Short circuit current of the generator
V_{OCG}	Open circuit voltage of the generator
R_{SG}	Series resistance of the generator
N_S	Number of modules in series in the generator
N_P	Number of modules in parallel in the generator
I_G	Generator current
V_G	Generator voltage
J_e	Current density for the electrons
D_e	Diffusion coefficient of the electrons on the n-side

L_e	Diffusion length of the electrons
T_a	Ambient temperature
T_c	Cell temperature
I_L	Load current
I_{PV}	PV current
I_B	Battery current
V_{DC}	Operating voltage of the system
$I_{PV(STC)}$	PV current under standard test conditions
n_{bat}	Battery efficiency
n_{con}	Controller efficiency
C_U	Useful capacity of the battery
C_B	Nominal battery capacity
L	Daily energy consumption of the load
F_{S1}	Generator sizing factor
F_{S2}	Storage sizing factor
C_S	Normalised storage capacity
C_A	Normalized generator capacity
E_{PV}	Daily energy produced by the PV
Q_{PV}	Charge produced by the PV daily
$\overline{L}$	Monthly average daily energy consumption of the load

1. INTRODUCTION

1.1 Aims and objectives

The aim of this project is to improve the sizing of stand-alone photovoltaic (PV) systems, by an experimental study and modelling of the photovoltaic system operation and battery state of charge, and an analysis of solar radiation statistics, reflecting the main issue of concern: the reliability of electricity supply by the system.

In more detail, the objectives of the current project are the following:

- To analyse a new sizing approach which determines the reliability of supply in terms of how long the system is expected to operate without shedding load. Therefore, to examine by modelling PV system operation on a daily basis using solar radiation data from the past. Of particular interest is the variation of storage requirement throughout the years when using long radiation series of historical daily solar radiation data. The focus is the link between the day to day variations of solar radiation and system sizing, as opposed to the monthly average values of solar radiation that are typically used as input in the sizing methods. An important parameter turns out to be the length of the time series that is considered for the system design.

- To project these results against a possible future evolution as determined by climate change studies. The investigation opens a new area of stand-alone PV system design. Thus, the research includes a preliminary comparison of the results with those using artificially generated data from Hadley centre.

- To validate a PV system model based on daily energy balance. The model is used in the new system sizing approach in order to find the storage requirement. Models of this type have been widely used in system sizing methods for the calculation of loss-of-load probability (LLP) but few attempts have been made to compare the modelling results with experimental data. To this end:

- A stand-alone system has been constructed and its performance monitored.
- The performance of the battery in a PV system has been studied with emphasis on the charging efficiency of the battery, both in the laboratory and as part of an experimental stand-alone system.

- To adapt an accurate and simple method of conversion of the daily radiation data on the horizontal surface to the values on the inclined surface, which is the input required by the daily energy balance model. In addition, to examine the effect of inaccuracies in the radiation conversion on the inclined surface on the battery state of charge in a stand-alone system. To this end a model of a selected method has been developed in Matlab, and compared with measured radiation values at Southampton.

1.2 Motivation of the work and structure of the Thesis

A satisfactory photovoltaic power supply is a well-designed system to provide electricity to a load with optimum reliability and minimum cost. To this end the system design must allow for the variable nature of solar radiation and incorporate the available knowledge of solar radiation in the design, particularly in the sizing of the PV generator and the energy storage.

The nature of solar radiation as a time series, and its use in system design studies constitutes the central topic of this research. Accurate conversion of solar radiation on the inclined surface forms the first step in system design. Using solar radiation as input to an energy-balance model, the optimum size of the PV array and energy storage (battery) can then be found. The main achievement of this work has been the development of an alternative approach, which uses the length of the daily radiation time series (and hence also the length of continuous operation) as an indicator of supply reliability, instead of the loss-of-load probability that is used typically in the design methodology. An important corollary of this result has been an improved understanding why the monthly average value of the radiation of the worst month that is being widely used in system design studies may be misleading as far as the required system size is concerned.

For the completion of the above research, a system model has been developed using previous versions of the programme available within the group. This model – based on daily energy balance – is similar to models used by others for PV system sizing. Although relatively simple in principle, one conclusion of this work has been that this model is adequate for system sizing purposes but there are limitations (for example, effect on battery degradation and lifetime) which may not be well represented in this model.

To validate the energy balance model, an experimental PV system has been constructed using state-of-the-art components. The operation of the system has been monitored over one winter of operation, to provide detailed data against which the system model could be compared. The experimental PV system work has been complemented by battery experiments in the laboratory. Particular emphasis has been given to a better understanding of battery operation in the PV system especially with

respect to battery charging efficiency, in order to fill the gap of adequate research in this area so far.

The results of this work have been applied to determine the sizing curves of three locations which specify detailed system configurations. In addition, they have been applied to recommend optimum system sizing for two locations where long time series of data are available: Efford, near Southampton, and Potsdam in Germany. The principal novel component has been to determine the required storage size as a function of the length of the time series of data used in the analysis. These results are related with climate change studies, and constitute the first attempt so far in the PV system research to account for possible effects of climate change (in particular, any change of persistence in solar radiation) on sizing results.

The work also includes a thorough literature review. This review covers solar radiation on the inclined surface, the operation of the PV generator, the batteries for PV systems and PV system sizing and modelling. Modelling work was carried out with the aim to convert radiation values on the inclined surface, using transposition methods from the literature. Matlab software has been used for this part of the work. ESRA software has been used for conversion of solar radiation from the horizontal to the inclined surface.

The structure of the report is as follows:

It starts with the introduction, presented in this chapter, Chapter 1, that includes the aims and the objectives of the project in section 1.1, the current work and the report structure in section 1.2 and the background of the study area in section 1.3.

Chapter 2 is a study of the radiation conversion on the inclined plane. It includes the following main sections: Section 2.2 discusses the astronomical considerations 2.3 the calculation of the extraterrestrial radiation. Section 2.4 analyses the effect of the atmosphere on the solar radiation. Sections 2.5 to 2.7 focus on the problem of radiation conversion on the inclined surface of the PV panel. An application on local radiation data is presented in section 2.8. Section 2.9 is a brief overview of the algorithms adopted by ESRA software. This software will be used in the current work

for the radiation conversion on the inclined. Section 2.10 discusses the optimum orientation of the PV panels.

Chapter 3 describes the experimental set-up of the experiments conducted in this work. Section 3.2 describes the set-up for the experiments on the PV generator conducted for the validation of the PV generator model developed in the next chapter. Chapter 3.3 describes the construction and monitoring of an experimental stand-alone system, the measured data of which will be used in the following chapters for the validation of the model based on daily energy balance and for the analysis of the batteries and the PV system operation. Section 3.4 describes the set up for battery experiments in the laboratory.

Chapter 4 is the operation of the PV generator. Section 4.2 is the literature review on the PV generator. Section 4.3 analyses the development of a PV generator model in Matlab. Section 4.4 presents the results. Section 4.5 discusses the model validation by comparison with experimental data and section 4.6 is the conclusions.

Chapter 5 is about the batteries used in PV systems. Section 5.2 is the literature review, section 5.3 examines the limits of accurate battery modelling and compares experimental results with Copetti and Chenlo model[65]. The conclusions are presented in section 5.4.

Chapter 6 describes the operation of the PV system, firstly using monitored data from the experimental PV system in section 6.2, then section 6.3 analyses the concept of a typical model based on daily energy model and section 6.4 describes the operation of the PV system using this model concentrating on the main factor that affects the results-the accuracy of the solar radiation conversion on the inclined. The conclusions are presented in section 6.5.

Chapter 7 describes the battery operation in the PV system through literature review in section7.2, from measured data of the experimental stand alone system in section 7.3 and through experiments in the laboratory in 7.4. Section 7.5 is the conclusions.

Chapter 8 is the validation of the model based on daily energy balance. Section 8.1 is the introduction. Section 8.2 introduces two models for the estimation of the battery SOC from the monitored data of the experimental PV system. Section 8.3 analyses the first model and presents the results. Section 8.4 analyses the second model and presents the results 8.5 is the discussion and comparison of the results and section 8.6 the conclusions.

Chapter 9 is about the sizing of PV systems. Section 9.1 is the introduction. Section 9.2 is an overview of the system sizing methodology and a brief reference to some sizing methods. Section 9.3 analyses the methodology of the new sizing approach developed here and discusses the variations in the storage requirement through the years based on historical solar radiation data. Section 9.4 is the discussion of the results and section 0 the conclusions

Chapter 10 relates studies about the prediction of future climate with the design of the PV systems. Section 10.1 is an introduction. Section 10.2 is an overview of the climate change and 10.3 is an application of artificially generated data from climate change experiments in Hadley Centre in the PV system sizing approach analysed in the previous chapter.

Chapter 11 is the conclusions of the work and

Chapter 12 is the further work

1.3 Background

1.3.1 PV systems

Photovoltaic (PV) systems generate electricity, using the energy from the sun. They constitute an environmentally friendly alternative way for energy production. They operate quietly without emissions and they can be installed quickly. They are modular which has the advantage that we can add more units if the load increases. Their long lifetimes and little maintenance requirements make them an ideal solution for remote applications when used as autonomous systems. When they are used as

embedded generation PV systems can be located close to the sites where the electricity is to be consumed. Generator systems near the end-user can reduce transmission and distribution costs. They can provide with peak load high quality power and increase reliability of electrical services delivered. At the moment, major barrier to the widespread adoption of photovoltaic technology is its high cost.

There are two types of PV systems: stand-alone and grid connected. The two types aim at different applications and are best studied separately because there are different issues that should be considered for each type.

Most stand-alone systems are often installed in remote locations, using energy determined exclusively by the presence the sun. Therefore, the most important design considerations are adequate reliabilility of energy supply and low maintenance requirements. This is not the case for grid-connected systems, which are usually found in industrialized countries to supplement the conventional power generation.

The most important consideration regarding grid-connected systems is their interface with the utility network. This "grid connection" must ensure sufficient power quality and safe operation; the requirements for this are determined by technical issues and by national regulations. These issues are discussed in more detail later in this chapter.

Optimal sizing is a very important issue in stand-alone systems, to ensure adequate reliability of the energy supply for a given solar radiation pattern and load demand. The sizing of the grid-connected systems is determined by cost consideration of the components and the system installation. We do not need to know the load to size the grid-connected system. However if we know the expected load pattern we can access the proportion supplied by the PV and determine the system economics.

Because of the variation of solar resource the storage of the excess energy in stand-alone systems is a critical consideration. For grid-connected systems all the energy generated by the PV system is consumed because it can be exported to the utility. However, in some cases on-site storage can increase the value of the grid connected PV system.

1.3.2 Grid-connected systems

There are two principal types of grid-connected systems[6,5]: Large-scale PV power generation in PV power stations and a distributed form of power generation,

usually integrated in buildings. Most grid-connected PV systems are embedded generators, that is to say, they are connected to the distribution network. A schematic diagram of a grid-connected system is shown in Figure 1[1]. The inverter usually contains a DC interface which implements maximum-power-point tracking, and an AC interface which ensures sufficient power quality and safety of operation such as islanding protection.

Figure 1 Grid-connected system[1]

The PV power plant feeds the generated power instantaneously into grid by means of one or more inverters and transformers. At present, the cost of generated electricity from PV plants is competitive with the conventional power sources (e.g. thermal plant) only in special cases. To connect a PV plant at the end of a distribution line may be cheaper than to upgrade the line. It may also be cheaper to connect a PV plant to the local distribution in order to meet the peak demand, instead of constructing another power station.

In the building integrated PV (BIPV) systems the photovoltaics are incorporated into the building structure. PV arrays are mounted on the roofs or the facades. In the most usual type the excess of electricity that the PV may produce is fed into the grid to earn revenue, while the system draws energy from the grid in case the energy supplied from the photovoltaics is not enough to meet the demand.

In the case of building integrated systems, energy storage can be beneficial because it can be used as a demand side management tool, firstly, by providing peak load power to the building; secondly, by storing excess energy when it is unfavourable to sell electricity to the grid while providing high value peak load power to the grid. The load on the grid during peak times is reduced and this ensures the quality of supply.

Within Europe[2,3] there are several countries with extensive experience with grid-connected systems. These include Austria with its 200kW Photovoltaic Rooftop Programme, Germany with its 1000 Roofs Programme (now 100,000 Roofs

Programme), which led to the installation of more than 2250 systems by 1999, Italy with ENEL's 3.3MW PV plant, the Netherlands with an expanding research and demonstration programme (several MW of PV have been installed, mainly on roofs) and Switzerland with its Energy 2000 programme. In the USA there are many grid-connected building mounted PV systems, mainly on domestic houses. There are also, many experimental systems PV power stations and demonstration projects. Japan with its 70,000 roofs programme plans to increase its installed capacity from 10000 systems in 1997 to 4600MWp by 2010. In the UK the potential is seen for building integrated PV systems. The increasing international activity is resulting in cost reduction of PV systems, especially in the area of building integration.

There are some important considerations related with the incorporation of the PV systems into the network.

Public electricity supply in most countries comprises generation, transmission and distribution[3]. Generation usually takes place in large centralized power stations. A high voltage transmission system transmits the energy to primary substations. A local (low voltage) supply network distributes energy to the end user.

Power flows from higher voltage levels to lower voltage levels via transformers and the direction of current flow is from the primary distribution transformers to customer loads. This assumption is used to predict the voltage profiles along the cables and overhead lines which supply the customers. The size and ratings for the network plant such as the distribution transformer associated switchgear; cables, overhead lines and protection are determined using the predicted consumer load profiles and known local topology. The addition of dispersed generation makes these original design calculations no longer valid since the embedded generation will affect the actual voltage profiles on the network, as well as the associated fault levels and protection settings.

The development of international standards facilitates the development of PV market. However, it has been found difficult to establish a complete unanimity amongst the international community on grid-connected PV standards because of the differences in electrical network topologies in different countries, and sometimes even among different local electricity companies.

1.3.3 Stand-alone systems

The simplest stand-alone system consists of a generator that (usually via a controller) supplies a load (e.g. water pumping systems). However, most stand-alone systems include a battery for energy storage. There are also hybrid systems where a diesel or petrol generator is used as a back up. Stand-alone systems often include power electronics that consists of charge regulators and DC-DC converters. PV systems can power both AC and DC appliances but to power AC loads, an inverter needs to be added to convert the DC from the array to AC. All the other components (such as the wiring, fuses, switches connectors) are called balance of system components (BOS). A schematic diagram of a hybrid stand-alone system which supplies AC current is illustrated in Figure 2[4].

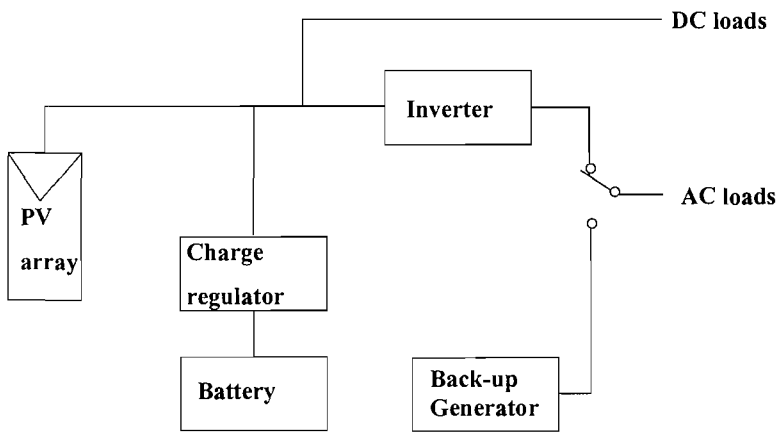

Figure 2 Stand-alone ac system with battery and back up

Applications of the stand alone systems may include telecommunications, cathodic protection, railway crossings, navigational aids and warning devices, consumer products like calculators and watches, battery charging, refrigeration, water pumping, lighting, residential power. This wide range of applications encompasses wide differences in demand for supply reliability, maintenance, and economics. In certain class of systems (e.g. telecommunications), the reliability must be high but can be achieved by using straightforward economic arguments. In domestic systems, lower reliability can usually be tolerated to reduce the cost of the system.

The cost-effective region for using a stand-alone system in comparison with connection to the grid varies with the load distance from the grid and the type of stand-alone system chosen. Small loads in conjunction with long grid extensions required favour stand-alone systems. If the load is small, a stand-alone system can be

cost effective even very close to the grid. In the US, for example, systems smaller than 2KW can be cost effective at grid extensions as short as 1/3 of a mile[5].

2. IN-PLANE SOLAR RADIATION

2.1 Introduction

Irradiation or sometimes simply radiation is the radiant energy per unit area on a surface and is measured in J/m^2 or Wh/m^2. Irradiance is the power per unit area on a surface and is measured in W/m^2. Our prediction of solar radiation at a certain location is based on radiation data from the past. The solar radiation data are usually recorded on the horizontal surface.

The solar radiation on a surface of an arbitrary orientation at any time depends on the angle of the solar rays with the surface in question, that is to say, on the relevant position of the surface with respect to the sun. This is determined by the surface orientation and the astronomical parameters. PV system modelling requires the knowledge of radiation on the inclined surface of the PV panel which usually has to be calculated using the radiation on the horizontal surface. The steps in the radiation conversion are as follows: Firstly, the radiation has to be decomposed into the two components; beam and diffuse. The next step is the transposition of each onto the inclined plane. The total (global) radiation contains a sum of the two components as well as the ground reflected radiation. The key procedure is the calculation of diffuse radiation. The key quantity in this calculation is the clearness index which expresses the effect of the atmosphere on the extraterrestrial solar radiation.

A review of several methods that have been developed for the conversion of solar radiation to the inclined surface is presented here, with the aim to adopt an accurate method for the conversion of daily solar radiation data. A model for radiation conversion has been developed in Matlab that incorporates Liu and Jordan algorithm with the aim to assess the differences between model and observed data and discuss a possible improvement.

It was found that although using correlations of the diffuse radiation based on recorded data can improve the results, the discrepancies between measured and modelling results seem to be still significant especially in winter months.

The surface orientation and the astronomical parameters are analysed in section 2.2. The clearness index is discussed in sections 2.3 and 2.4. The problem of the calculation of diffuse radiation consists of two parts: to find the diffuse radiation on

horizontal surface from the clearness index (section 2.5) and then to determine the diffuse radiation on the inclined surface 2.6. Section 2.7 compares the main two methods for the conversion of the monthly average daily radiation on the inclined surface, the Liu and Jordan method and the Klein and Theilacker method. Section 2.8 is an application of Liu and Jordan algorithm to solar radiation data recorded at Southampton University, followed by a discussion and an attempt of improving the results. Section 2.9 is a brief reference to the algorithms used in ESRA software for the radiation conversion on the inclined plane. ESRA software will be used in this work for radiation conversion on the inclined plane. Section 2.10 discusses the optimum orientation of PV panels.

2.2 Astronomical considerations

The earth goes round the sun in an elliptical orbit, with the sun at one focus of the ellipse[6,7]. The plane of this orbit is called the ecliptic plane. The time that the earth takes to complete this orbit defines one year. Simultaneously, the earth spins around its own central axis, (the polar axis), once a day. Viewed from the earth the motion of the earth, around the sun is pictured by the apparent motion of the sun within the celestial sphere (Figure 3).

The position of the sun at any instant can be described by the position angles in two coordinate systems. The base of the first coordinate system is the celestial equator (Figure 3). The celestial equator is the intersection of the equatorial plane of the earth and the celestial sphere. The polar axis which intersects the celestial sphere in the celestial north pole and the celestial south pole defines this system. The daily rotation of the earth is depicted by the rotation of the celestial sphere about the polar axis. The sun makes two apparent motions. Firstly, it travels with the celestial sphere and marks out a circle about the earth parallel to the equator of the celestial sphere. The instantaneous position of the sun is described by the hour angle ω, which is the angle passing between the meridian of the sun and the meridian of the site. Secondly, it travels through a great circle of the celestial sphere, the ecliptic that forms an angle 23.45^{o} with the celestial equator. The sun's rotation around the ecliptic is in the opposite direction to that of the celestial sphere around the earth. We define a second coordinate system, for an observer on the earth's surface (Figure 4). The base here is the observer's horizon. This system is defined by a vertical line at the observer's

position, which intersects the celestial sphere in two points (zenith-nadir). The angle between this vertical line and the celestial equator is the latitude (φ) at the observer's position. The angle between the sun at solar noon and the celestial equator is the solar declination (δ), where $-23.45^{\circ} \leq \delta \leq 23.45^{\circ}$.

The zenith angle of the sun (to be denoted by θ_z) is the angle between the vertical and the line to the sun (or the angle of incidence of solar rays on a horizontal surface). It varies between 0° and 90°, when the sun is above the horizon. It depends on the latitude (φ), through the declination (δ) on the day of the year, and on the hour angle (ω) that reflects the time of the day. It is given by the equation:

$$\cos\theta_z = \cos\varphi \cdot \cos\delta \cdot \cos\omega + \sin\varphi \cdot \sin\delta \qquad (2.2.1)$$

We also determine as solar altitude angle α_s the angle between the horizontal and the line to the sun, i.e., the complement of solar zenith angle.

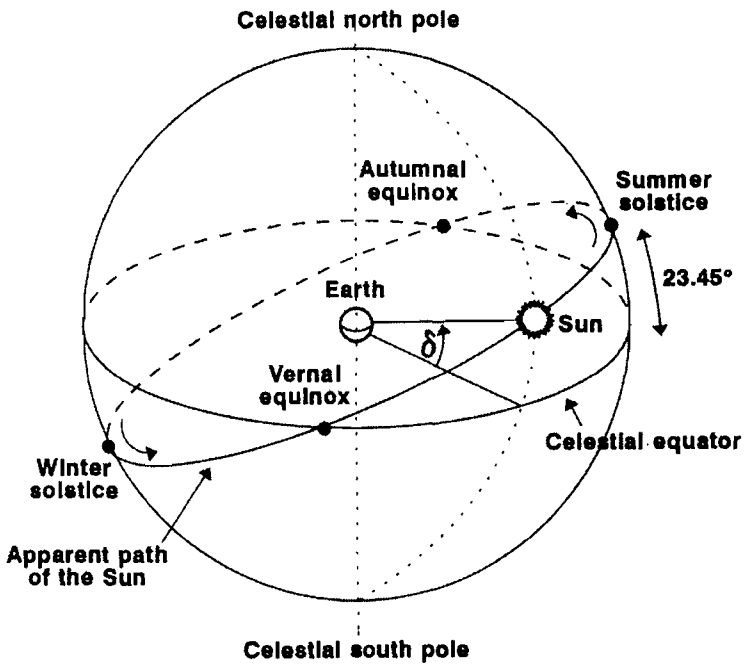

Figure 3 The celestial sphere's coordinate system showing the yearly motion of the sun[6].

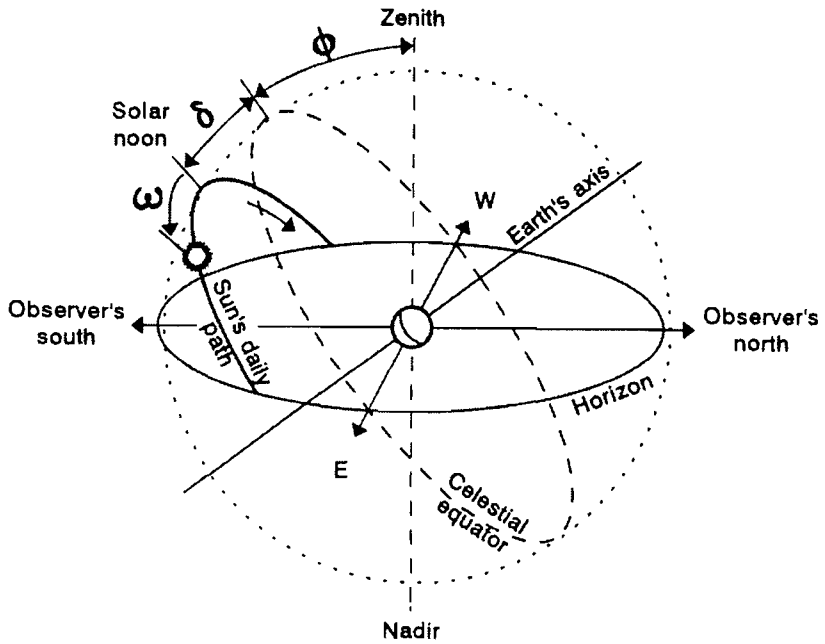

Figure 4 The observer's coordinate system showing the apparent daily motion of the sun[6].

2.3 Extraterrestrial radiation

Figure 5 shows the extraterrestrial solar irradiance as a function of the time of the year, measured on plane normal to the sun rays (G_{on}), and given by the equation[8]:

$$G_{on} = G_{sc}\left(1 + 0.033\cos\frac{360n}{365}\right) \quad (2.3.1)$$

Where n is the day of the year and G_{sc} is the solar constant. Solar constant is the irradiance on a surface perpendicular to the direction of the sun rays, at mean earth sun distance outside the atmosphere. The most generally accepted value for the solar constant is G_{sc}=1367W/m^2.

For future reference we note that the extraterrestrial irradiance on a horizontal surface is:

$G_o = G_{on} \cdot \cos\theta_z$ (2.3.2)

Clearly, the extraterrestrial irradiance depends on the latitude and the day of the year and the hour of the day.

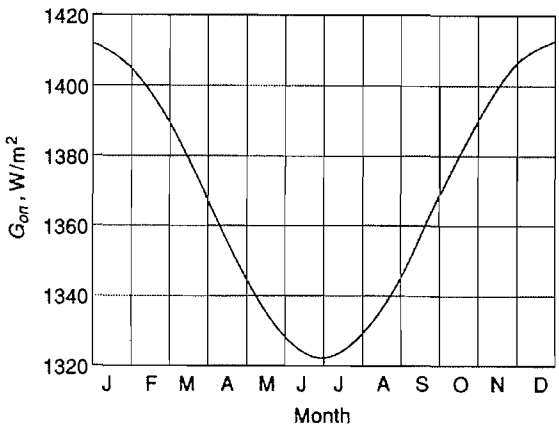

Figure 5 Variation of the extraterrestrial solar irradiance with the time of the year[8]

By integration of the extraterrestrial irradiance on the horizontal surface (2.3.2) from sunrise to sunset we can find the daily extraterrestrial radiation (in joules/m^2) on a horizontal surface:

$$H_O = \frac{24 \cdot 3600}{\pi} G_{sc}\left(1 + 0.033\cos\frac{360n}{365}\right)\left(\cos\phi\cos\delta\sin\omega_s + \frac{\pi\omega_s}{180}\sin\phi\sin\delta\right) \quad (2.3.3)$$

where ω_s is the sunset hour angle in degrees.

The monthly mean daily extraterrestrial radiation ($\overline{H}_O$) can be calculated[8] for latitudes in the range +60 to –60 with equation (2.3.3) substituting for n, δ and ω_s their values at the mean day of the month- the day for which the hourly and the daily extraterrestrial radiation on the horizontal surface are equal to their corresponding monthly mean values[7].

2.4 Effect of atmosphere on solar radiation

The amount of radiation on a surface on the earth consists of three components:

- Direct (or beam) radiation is the radiation received directly from the sun without having been scattered by the atmosphere.
- Diffuse radiation is the radiation received from the sun after its direction has been changed by scattering by the atmosphere.
- Albedo (or ground reflected radiation) is the radiation reflected from the ground.

As it passes through the atmosphere, solar radiation is affected by absorption and scattering. Scattering represents a wavelength dependent change in the direction of the radiation, and can be caused by interaction of the radiation with air molecules, aerosols and by clouds. Atmospheric absorption in the solar energy spectrum is due to uniformly mixed gases, (e.g. oxygen); ozon and water vapour; aerosols; and absorption by clouds[9]. The degree to which scattering and absorption occurs is a function of the number of particles through which the radiation must pass and the size of particles relative to the wavelength of the radiation[8].

The changes in spectral distribution of the solar radiation that reaches the earth's surface, as modified by scattering and absorption, is characterized by the concept of air mass. Air mass is the ratio of the mass of atmosphere through which beam radiation passes to the mass it would pass through if the sun were directly overhead[8]. It is equal to the relative length of the direct beam path through the atmosphere. The air mass characterizes the effect of any atmosphere on sunlight[6]. The standard PV spectrum assumes solar spectrum corresponding to air mass 1.5. However, a more detailed analysis which includes changes in the solar spectrum can be carried out but their effect is generally small[10]. The value of the radiation falling on the inclined surface of a PV panel can be modified to account for reflection losses from the surface of the glass of the PV panel. These depend on the angle of incidence θ_i and the fraction of the reflected radiation can be calculated using Fresnel formulas[7]. Correction factors should be applied to all three components: beam diffuse and albedo radiation in order to account for reflection losses. Reflection losses mainly occur when the sun is at a high angle of incidence. They are due to the increased reflectance

of the cover glass of the PV modules for angle of incidence greater than approximately 60°[11,12]. The northern hemisphere has small solar altitude in winter, resulting in small incidence angles at modules set at large tilted angles, and therefore small reflection losses. For example, the reflection losses for the month of December for Netherlands is 2% at tilt angle 52°[13]. Given that the critical period for PV system operation is when the solar radiation is low, that is, winter for the locations considered in this work (see sections 6.4 and 9.3), and the modules are set at large tilt angles (e.g. 66°), the reflection losses should be small and have not been taken into account.

Two types of solar radiation data are widely available[8]. The first is the monthly average total radiation on a horizontal surface, that is to say mean values over many years of data of the average daily values of each month. The second is hourly total radiation on a horizontal surface for each hour for extended periods such as one year or more.

2.5 The diffuse radiation

Diffuse radiation reaches the observer after scattering by the atmosphere. It depends on the cloudiness and the atmospheric clarity which are highly variable and it is therefore difficult to describe its distribution over the sky dome. Based on clear sky data we tend to describe diffuse radiation as being composed of three parts[8] presented schematically in Figure 6. The first is the isotropic part, received uniformly from the entire sky dome. The second is the circumsolar diffuse, resulting from forward scattering of solar radiation and concentrated in the part of the sky around the sun. The third is referred to as horizon brightening.

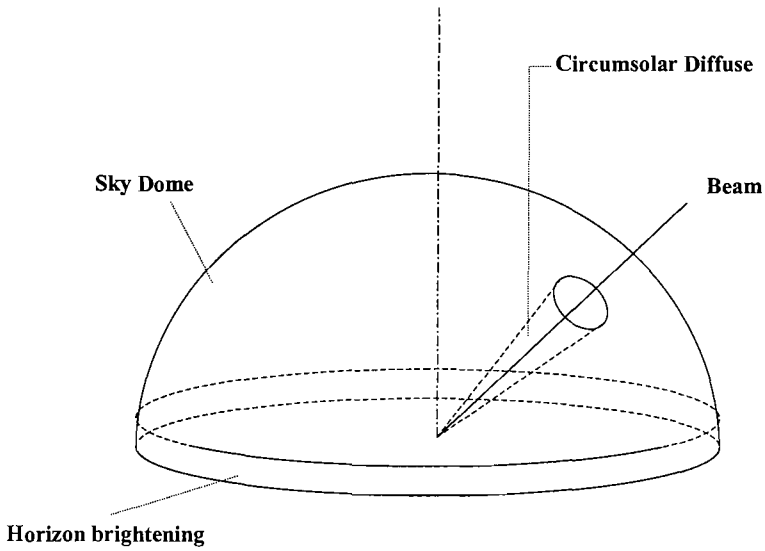

Figure 6 Schematic of the distribution of diffuse radiation over the sky dome

If the area of the PV plane is A_p and I_T is the total hourly radiation on the inclined plane, the total energy of the radiation on the plane is given by:

$$E_{TILT} = A_p I_T \quad (2.5.1)$$

Denoting by I_b the beam radiation on the horizontal plane then, the energy of the beam radiation on the tilted surface is equal to:

$$E_{T,b} = I_b R_b A_p \quad (2.5.2)$$

Where R_b is the ratio of the beam radiation on the inclined surface to that on the horizontal surface. In general, R_b is a function of the transmittance of the atmosphere. It is seen from Figure 7 [8], that R_b is a geometrical variable, which is equal to the ratio of the cosine of the solar incidence angle onto the inclined surface to the solar zenith angle:

$$R_b = \cos\theta_i / \cos\theta_z \quad (2.5.3)$$

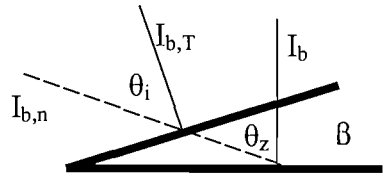

Figure 7 Beam radiation on the horizontal and tilted surfaces. $I_{b,n}$ is the hourly beam radiation on a normal surface $I_{b,T}$ is the hourly beam radiation on a tilted surface and I_b is the hourly beam radiation on a horizontal surface and β is the tilt angle of the inclined surface.

In order to calculate the diffuse and the ground reflected radiation on the tilted surface we have to determine the view factor. For two objects 1 and 2, with surface areas A_1 and A_2 we define the view factor F_{12} as the fraction of object 2 visible from the surface of object 1[14]. The view factor ranges from zero to one. For two surfaces that emit diffuse radiation, i.e., that the intensity of the radiation is the same in all directions the following relation applies, known as a reciprocity relation[14]:

$$A_1F_{1-2}=A_2F_{2-1} \quad (2.5.4)$$

The energy of the diffuse radiation on the tilted surface is:

$$E_{T,d} =I_{d,iso}A_sF_{s-p}+ I_{d,cs}R_bA_p+ I_{d,hz}A_{hz}F_{hz-p} \quad (2.5.5)$$

The subscripts iso, cs and hz stand for isotropic, circumsolar and horizon, and the three terms represent the corresponding parts of the diffuse radiation. A_s and A_{hz} are areas of the sky and the horizon band of the sky respectively, while F_{s-p} and F_{hz-p} are the view factors from the sky dome to the array plane and from the horizon band to the array plane. The unknown areas A_s and A_{hz} can be eliminated by taking into account the reciprocity relations (2.5.4) for the view factor.

Similarly, the energy of the reflected radiation on the tilted surface is:

$$E_{T,r}= I\rho_gF_{p-g}A_p \quad (2.5.6)$$

Where ρ_g is the ground reflectance and F_{p-g} is the view factor from array plane to the ground. We should note here that the importance of accurate estimation of the ground reflected irradiance increases, naturally, with the tilt angle β, as the proportion of the sky dome viewed by the inclined surface diminishes, and the proportion of the ground viewed by the inclined surface increases[41].

Adding the three components we find from equations (2.5.1), (2.5.2), (2.5.5),A_p (2.5.6), that the hourly total radiation on the inclined surface is:

$$I_T = I_b R_b + (I_{d,iso} F_{p-s} + I_{d,cs} R_b + I_{d,hz} F_{p-hz}) + I \rho_g F_{p-g} \qquad (2.5.7)$$

where I is the total hourly radiation on the horizontal plane.

2.5.1 Isotropic and anisotropic assumptions

For the calculation of the diffuse radiation on the inclined plane, the results depend on the assumptions that we make regarding where the solar radiation comes from. These are the isotropic and anisotropic assumptions.

If we assume that the diffuse radiation is isotropic (Liu and Jordan model)[15,16], the third and the fourth terms of equation (2.5.7) become zero and we obtain the following simplified equation for the solar radiation:

$$I_T = I_b R_b + I_d \frac{(1+\cos\beta)}{2} + I\rho_g \frac{(1-\cos\beta)}{2} \qquad (2.5.8)$$

where $(1+\cos\beta)/2$ and $(1-\cos\beta)/2$ are the view factors of the surface to the sky (F_{p-s}) and to the ground (F_{p-g}) respectively. The values of radiation view factors can be derived analytically from simple geometries and are tabulated in several references on heat transfer[14,17].

Given that the diffuse radiation is isotropic, $(1+\cos\beta)/2$ is also the ratio of diffuse radiation on the tilted surface to that on the horizontal surface, which is denoted by R_d. Klucher[18] concludes, using hourly data and tilt angles of 37° and 60°, that Liu and Jordan isotropic distribution model provides a good fit to empirical data under overcast skies but underestimates the amount of solar radiation incident on tilted surfaces under clear and partly clouded skies.

The most important anisotropic models are the HDKR (Hay, Davies, Klucher, Reidl) model and the Perez model. Hay and Davies[19] first developed a model assuming that the diffuse is composed of the isotropic and circumsolar parts. This model was modified by Klucher and Reidl[8] to account for the horizon brightening on clear days and also for cloudiness, by applying a correction factor to the isotropic diffuse.

The most detailed model regarding the analysis of the three diffuse components of solar radiation is the Perez model.[8,20,21] The Perez diffuse irradiance model describes the sky as a hemisphere, where a circumsolar disk and a horizon band are superimposed on an isotropic background.

This original model has been improved and simplified by Perez[20] using redefined brightness coefficients: the normalized contributions of the circumsolar and horizon regions to the total diffuse energy received on the horizontal. As a result, the final model yields noticeable performance improvements for climates where cloudy conditions prevail.

From the three models for the calculation of the instantaneous radiation on the tilted surface the isotropic model gives the lowest values of radiation on the inclined plane and Perez model gives the highest values, which also agree best with the measurements. Duffie and Beckman recommend the Perez model for surfaces with azimuth far from zero (or 180 for southern hemisphere). However, the Perez model is far more complex to use than the two others. Instead of the anisotropic models, correction factors to the isotropic models have been also developed that account for the anisotropic diffuse radiation[32,22].

2.6 Calculation of the diffuse fraction on the horizontal plane

Using the available data, Liu and Jordan in 1960[23] investigated the relationship between the diffuse and total radiation on a horizontal surface. The ultimate aim was to estimate the diffuse radiation for locations where only the total radiation is known. The fraction of the diffuse to total radiation on the horizontal was found to be a function of the clearness index: the ratio of the total radiation on the horizontal surface to the extraterrestrial radiation. This empirical functional dependence is known as correlation. Subsequently, such studies have been repeated on a number of

occasions and several such functions have been proposed. There are correlations of daily diffuse radiation data, correlations of monthly average daily diffuse radiation data and correlations of hourly diffuse radiation data with the corresponding clearness indices.

2.6.1 Correlations of daily diffuse data with the clearness index

Liu and Jordan assumed that the declination during a month (and therefore the daily extraterrestrial solar radiation (H_o) on the horizontal plane at a locality remain constant. Consequently, the day-to-day variations of the daily total (H) on the horizontal surface are due to the variation of the atmospheric conditions, mainly the variation of the atmospheric cloudiness. However, the variability of the atmospheric cloudiness is largely responsible for the day to day variations in the daily diffuse (H_d) on the horizontal as it can be assumed given the origin of the diffuse radiation. Using 10 years of data from Blue Hill, Massachusetts Liu and Jordan finally found a correlation between the daily total to the daily extraterrestrial radiation on the horizontal surface (denoted as clearness index, $K_T=H/H_o$), which expresses the cloudiness of the sky, with the ratio of the daily diffuse radiation to the daily total radiation ($\frac{H_d}{H}$).

In 1963 Choudhury[24] derived a statistical relationship between the daily diffuse and the daily total for New Delhi using Liu and Jordan's method and in 1963 Stanhill[25] derived a similar relationship for Israel. The differences between these curves and Liu and Jordan curve were attributed to insufficient data in deriving the experimental curves and to a greater dust content of the atmosphere in New Delhi and Israel. In 1976, Ruth and Chant[26] derived a correlation for the daily diffuse fraction using data from four Canadian stations. Taking advantage of the newly developed computer technology they calculated the value of the extraterrestrial radiation daily in an attempt to improve the accuracy of the correlation. They concluded that the correlations show latitude dependence.

In 1979, Collares-Pereira and Rabl[27], found that the shade ring of the pyranometers, typically used by that time for diffuse solar radiation measurements blocks not only the solar disk but also a sizable portion of the diffuse radiation and

therefore a correction, which depends on irradiance and incidence angle should be applied to the data. Furthermore, Collares Pereira and Rabl found a seasonal trend (the season is indicated by the sunset hour angle), especially at large values of clearness index, where summer has a higher ratio of diffuse to total than winter. Erbs[28] in his investigation on the daily diffuse fraction in 1982, also found a seasonal dependence.

To conclude, there are many correlations of the daily radiation with the daily clearness index[8 and 23-29,] from different authors and there are some disagreements (Figure 8). There is a seasonal dependence of the daily diffuse fraction, with the winter data showing somewhat lower diffuse fractions for high values of K_T. According to Lorenzo[7], the reliability of applying the correlations of daily radiation to daily values is good only if we use daily values averaged over many years of data.

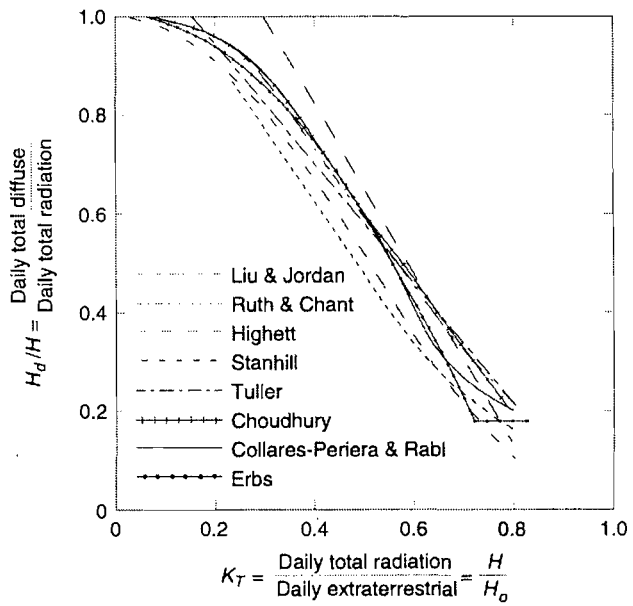

Figure 8 Correlations of the daily diffuse fraction with the daily clearness index[8]

2.6.2 Probability distribution of the clearness index

In order to calculate the monthly average diffuse radiation Liu and Jordan[23] constructed statistical distribution curves of daily total radiation. These curves show the fraction of time f that the daily clearness index K_T is below a certain value, for a month characterized by a given $\overline{K}_T$. Liu and Jordan plotted graphs for $\overline{K}_T$ 0.3,0.4, up to 0.7 (Figure 9). They found that curves from a wide range of localities are almost identical. This means that the number of days in a month with certain sky clearness

depends only on the monthly average clearness index and is independent of the location. This result was later confirmed by Bent[30] with study of 90 US locations.

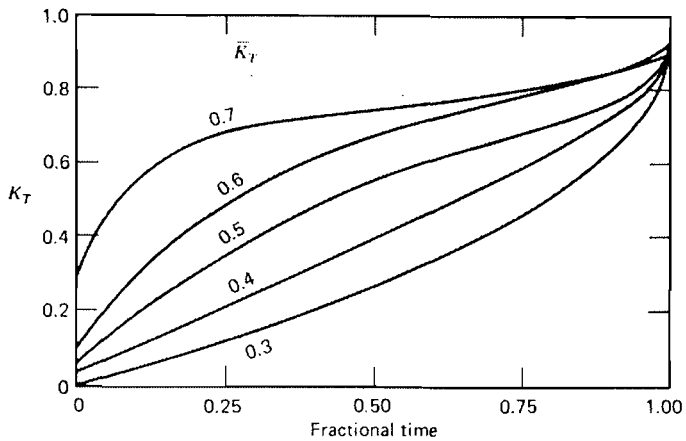

Figure 9 Generalized distribution of days with various values of K_T as a function of $\overline{K}_T$ [8]

2.6.3 Correlations of monthly average diffuse data with the clearness index

There are several correlations[8] of the monthly average daily diffuse fractions $\frac{\overline{H}_d}{\overline{H}}$ with the monthly average daily clearness index $\overline{K}_T$ (Figure 10) like those of Liu and Jordan[23], Choudhury[24], Stanhill[25], Collares-Pereira[27], Erbs[28], Page[31,32] and Bannister[33]. Among the above correlations there is significant disagreement. Monthly average correlations are obtained in two ways[34]. The first method uses monthly average data of diffuse and total [27,31]. The second method is based on the Liu and Jordan observation that cumulative distributions of K_T having the same value of $\overline{K}_T$ are remarkably similar for wide range of locations, as discussed in section 2.6.2.

The monthly average diffuse fraction is more strongly dependent upon the season than the daily diffuse fraction. The accuracy of applying to a particular year's monthly average daily values the correlations of monthly average daily data is small, although better than in the case of particular daily values and correlations of daily data[7]. The use of correlations of monthly average daily data is very accurate when we use monthly average daily values (over many years of data).

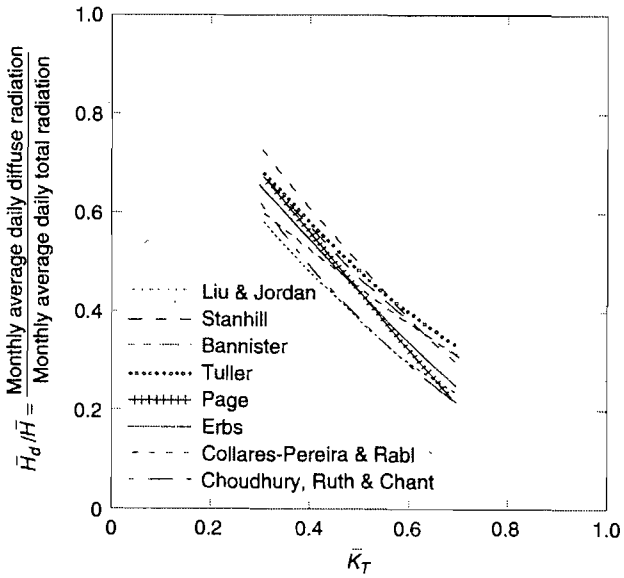

Figure 10 Correlations of the monthly average daily diffuse fractions with the monthly average daily clearness index[8]

2.6.4 Correlations of hourly diffuse data with the clearness index

Orgill and Hollands[35] were the first to derive a correlation equation for diffuse radiation based upon hourly measured values rather than daily totals. Although derived from three separate databases, correlations of hourly data of different[28,34,35,36] authors are essentially identical (Figure 11). The correlations give accurate results only if we use hourly values averaged over many years of data.

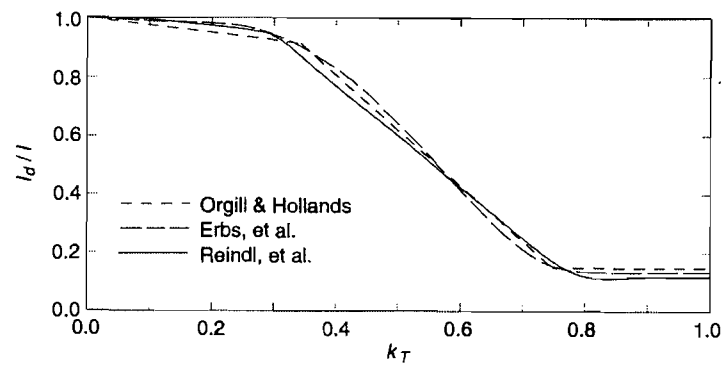

Figure 11 The ratio of I_d/I as a function of hourly clearness index[8]

The validity of correlations of daily monthly and hourly radiation data is not completely general as they are not applicable to all locations. When there is a correlation available based on the analysis of data obtained from a nearby weather station, Lorenzo[7] suggests that it should be used in preference to the general correlations that exist in literature. As an example he refers to the work of Macagan[37,38]. Macagnan obtained hourly daily and monthly correlations for Madrid, which give much better fit to the recorded data than all the existing correlations.

2.7 Calculation of monthly average daily radiation on an inclined plane

PV system design is usually based on the monthly average daily radiation on a tilted surface. There are two basic methods to calculate the monthly average daily radiation on the inclined surface of the PV panel from the monthly average daily radiation on the horizontal panel[8]. These are the Liu and Jordan method[15] (Figure 12) as extended by Klein[39] and the Klein and Theilacker or K-T method [40].

Both methods rely on assumptions concerning the long-term average distributions of the radiation (10 years). Both assume that the diffuse and ground reflected radiation are isotropic. The isotropic assumption for the diffuse component generally results in underestimation of the monthly average daily radiation on surfaces oriented towards the equator and overestimation of radiation on surfaces directed east or west of south. In addition, both methods assume that the radiation is symmetrically distributed about the solar noon, giving the same values of R_b for surfaces facing east as they do for surfaces facing west.

The two methods differ in the calculation of the average beam radiation on the tilted surface. The difference is due to the way that they calculate the monthly mean ratio of the beam fraction $\overline{R}_b$. In winter months Liu and Jordan method gives a higher estimate of solar radiation. The situation is reversed in summer months.

Here we analyse Liu and Jordan's method, which is the simplest and the more widely used.

The validity of correlations of daily monthly and hourly radiation data is not completely general as they are not applicable to all locations. When there is a correlation available based on the analysis of data obtained from a nearby weather station, Lorenzo[7] suggests that it should be used in preference to the general correlations that exist in literature. As an example he refers to the work of Macagan[37,38]. Macagnan obtained hourly daily and monthly correlations for Madrid, which give much better fit to the recorded data than all the existing correlations.

2.7 Calculation of monthly average daily radiation on an inclined plane

PV system design is usually based on the monthly average daily radiation on a tilted surface. There are two basic methods to calculate the monthly average daily radiation on the inclined surface of the PV panel from the monthly average daily radiation on the horizontal panel[8]. These are the Liu and Jordan method[15] (Figure 12) as extended by Klein[39] and the Klein and Theilacker or K-T method [40].

Both methods rely on assumptions concerning the long-term average distributions of the radiation (10 years). Both assume that the diffuse and ground reflected radiation are isotropic. The isotropic assumption for the diffuse component generally results in underestimation of the monthly average daily radiation on surfaces oriented towards the equator and overestimation of radiation on surfaces directed east or west of south. In addition, both methods assume that the radiation is symmetrically distributed about the solar noon, giving the same values of R_b for surfaces facing east as they do for surfaces facing west.

The two methods differ in the calculation of the average beam radiation on the tilted surface. The difference is due to the way that they calculate the monthly mean ratio of the beam fraction $\overline{R}_b$. In winter months Liu and Jordan method gives a higher estimate of solar radiation. The situation is reversed in summer months.

Here we analyse Liu and Jordan's method, which is the simplest and the more widely used.

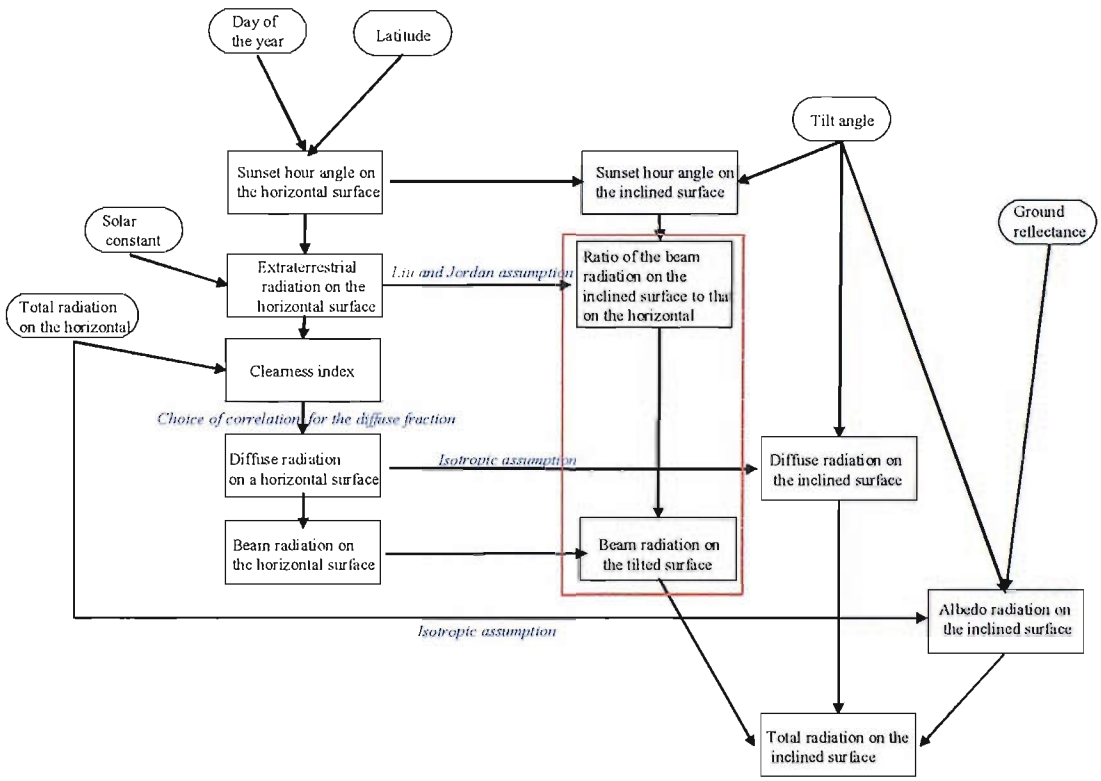

Figure 12 The diagram shows the procedure to find the monthly average daily radiation on a tilted surface, for surfaces facing the equator, using Liu and Jordan method. Rounded boxes represent input data, and rectangular boxes represent steps in the calculations. The process is the same in K-T method apart from the calculation of beam radiation (shown by doted rectangular box).

Liu and Jordan calculate the monthly average daily solar radiation on the inclined surface by replacing in formula (2.5.7) the hourly values by the monthly average daily values:

$$\overline{H}_T = \overline{H}_b \overline{R}_b + \overline{H}_d \frac{(1+\cos\beta)}{2} + \overline{H}\rho_g \frac{(1-\cos\beta)}{2} \qquad (2.7.1)$$

Liu and Jordan assume that $\overline{R}_b$ can be estimated as the monthly average extraterrestrial radiation on the inclined surface to that on a horizontal surface.

2.8 Application

The purpose of this application is to convert the daily radiation on horizontal surface to radiation of the inclined surface for the case of Southampton. The assumptions that are incorporated in the conversion algorithms will also be critically examined. The data on the inclined surface are needed to be used as input at the long term PV system modelling. The importance of accurate conversion is analysed in section 6.4. It was found that a simple technique based on Liu and Jordan model and existing correlation in literature for the diffuse fraction does not provide accurate results. An attempt to improve fit to experimental data by deriving new correlations for the diffuse fraction based on recorded data is presented here.

The solar radiation data have been measured on the roof of Lanchester Building at Southampton University. The latitude of Southampton is 50.92°. Irradiance (W/m^2) on the horizontal surface every 2.5 seconds is recorded by a pyranometer adapted from a solar cell. The data are averaged and logged in a file over every five minutes. A second pyranometer (also based on a solar cell) is attached to the PV panels and records the irradiance on the inclined surface of the panels. The panels are set at a tilt angle equal to the latitude (50°) and are oriented towards the south. The available data are daily values from December 99-00, January 01, February 00-01, March 00-01, April 00, June 99, July 99, August 99, September 99, November 99,00. A programme was developed in Matlab, for the conversion of daily radiation on the inclined plane, based on the Liu and Jordan isotropic model. To this end, equation (2.7.1) was used applying daily values instead of monthly average data.

The ground reflectance, in practice, does change throughout the year and increases significantly at low angle of incidence[32]. Here these changes were neglected and a constant value of 0.2 has been chosen, which is a recommended typical value[7]. Several daily correlations found in the literature were tried in the programme. Those of Erbs and Collares Pereira[28,27], do not give a good fit to the measured data. The correlation that gives the best fit is the Page correlation usually applied to monthly average values:

$$\frac{\overline{H}_d}{\overline{H}} = 1 - 1.13\overline{K}_T \quad (2.8.1)$$

Even using this correlation the modelling results are not in good agreement with the measured daily tilt radiation especially for values far from the average value (Figure 13). The discrepancies may be due to a number of factors, including the failure of the isotropic assumption, an incorrect way that the daily R_b is calculated, bad choice of the correlation for the diffuse radiation or due to changes in the ground reflectance (see sections 2.5 to 2.7). It is easily verified that the effect of albedo is of minor significance. Therefore, it remains to study the effect of the other three factors.

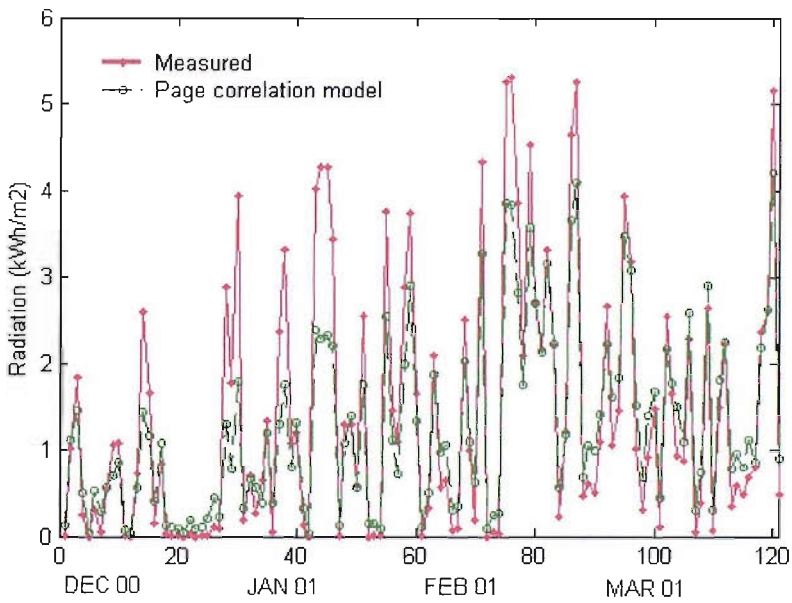

Figure 13 The radiation on an inclined surface at Southampton for the months December 2000 to March 2001. The inclination is 50°.

As mentioned in section 2.6, the correlations for the diffuse fraction may depend on the location. Therefore, it may be worthwhile to derive a correlation based on data measured at a local weather station. In addition, only when we apply daily values averaged over many years of data we can achieve high reliability of the daily correlations. Unfortunately, we do not have records of long-term radiation data on tilted surface for this purpose.

To determine the correlation for Southampton, a relationship between the ratio of the diffuse to total radiation and the clearness index was first derived based on the

existing data. From (2.7.1) we can relate the ratio of the diffuse to the total radiation on the horizontal with the recorded data:

$$\frac{H_d}{H} = \frac{1}{C_2 - C_1} \cdot \left[\frac{Data\ of\ the\ total\ on\ the\ tilted}{Data\ of\ the\ total\ on\ the\ horizontal} - (C_1 + C_3) \right] \quad (2.8.2)$$

where $C_1=R_b$ (daily), $C_2=(1+\cos\beta)/2$ and $C_3=((1-\cos\beta)/2)\cdot\rho_g$

We can now relate the K_T to the daily recorded data in the horizontal plane:

$$K_T = \frac{\text{Data of the total on the horizontal}}{\text{Calculated exraterrestrial}} \quad (2.8.3)$$

and H_d/H versus K_T can then be plotted as a function of K_T, as shown in Figure 14. A piece-wise linear approximation was chosen for simplicity. The process was repeated for all months and a plot was also constructed for all months of the year combined.

In plotting these graphs we excluded the measured data at low irradiances where the accuracy of the measurement is low. For the months June and July it was not possible to find a correlation based on the existing data because the values of the diffuse fraction (2.8.2) were found to be far beyond the allowable limits. This is an indication that the isotropic model may not be adequate.

We also repeated the process for winter months ($\omega_s \leq 81.4$-October to February) and summer months ($\omega_s > 81.4$-March to September). An example of a diffuse fraction correlation is shown in Figure 14. Figure 15 shows a comparison of the results between the correlations for the diffuse based on measured data and Page correlations for the diffuse.

The difference between the summer and the winter graphs is that for winter we get lower diffuse radiation at low k_T ($k_T<0.48$ app.) and a higher diffuse fraction at high k_T ($k_T>0.48$ app.). In other words, the summer curve is steeper than the winter curve. Regarding line of the linear data fit to the recorded values and line that represents Page correlation the former is steeper than the latter. The data indicate

higher diffuse fractions than those predicted by Page for $k_T < 0.38$ approximately and lower diffuse fractions for $k_T > 0.38$. However, although the two linear approximations, Page and the new one are different they lead to very similar inclined radiation values. This implies that there are other factors apart from the correlation of the diffuse fraction that affect the results.

The resulting equations for each month give some improvement for values where the difference from the average over the month is large. The results are shown in Figure 16. Larger amount of data would be needed to derive correlations with higher reliability. We should also note that both Page correlation model and measured data based correlation model are less accurate for the winter (Figure 16 a), when the solar radiation is low. However this is exactly the period that has the greatest impact on the PV system design.

The remaining discrepancies are therefore due mainly to the method of calculation of R_b, and to the isotropic assumption. The next section presents ESRA software for the calculation of the radiation on the inclined plane which deals in more detail with the above two issues.

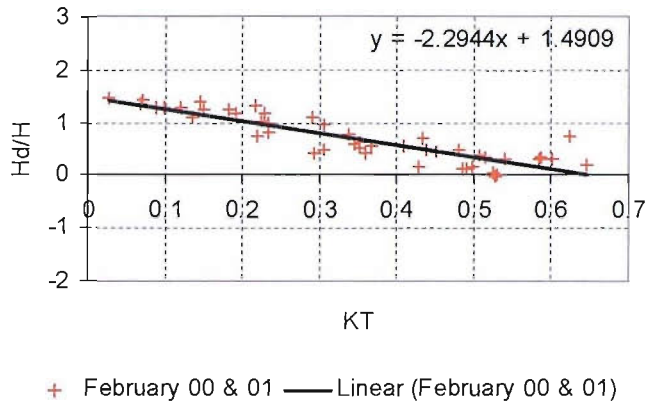

Figure 14 Example of diffuse fraction correlation. Linear data fit was applied to the data.

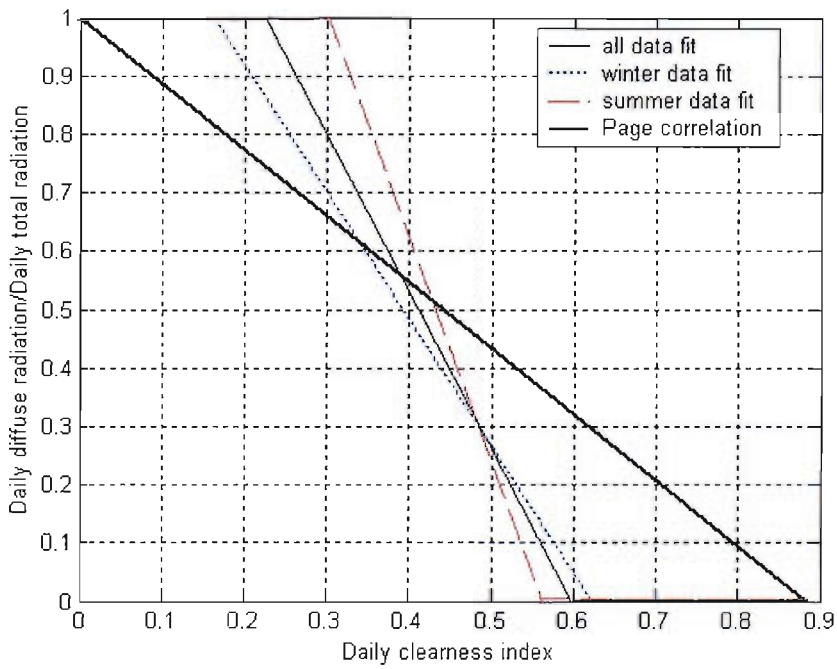

Figure 15 Correlations of the daily diffuse fraction (Southampton). A linear data fit to the measured values and a comparison with Page correlation.

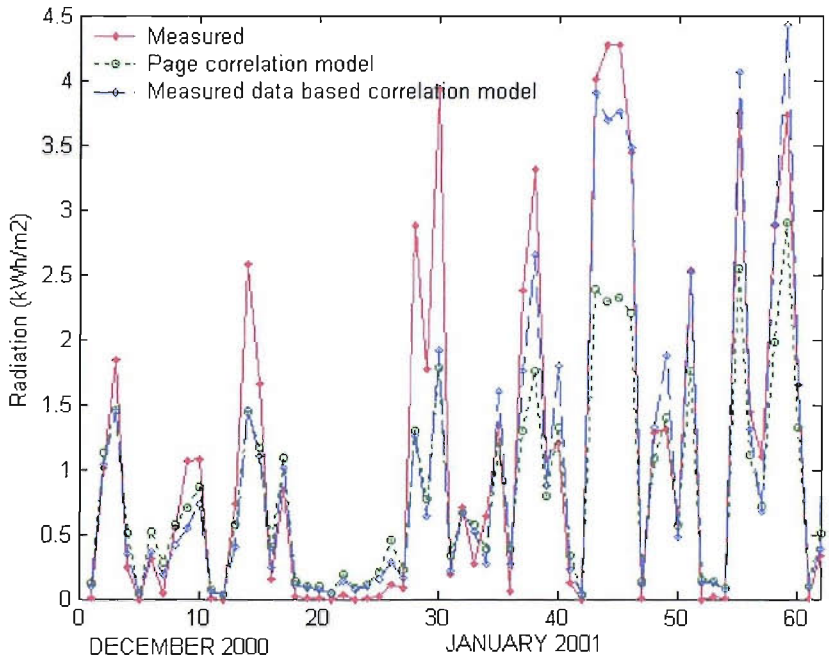

a.

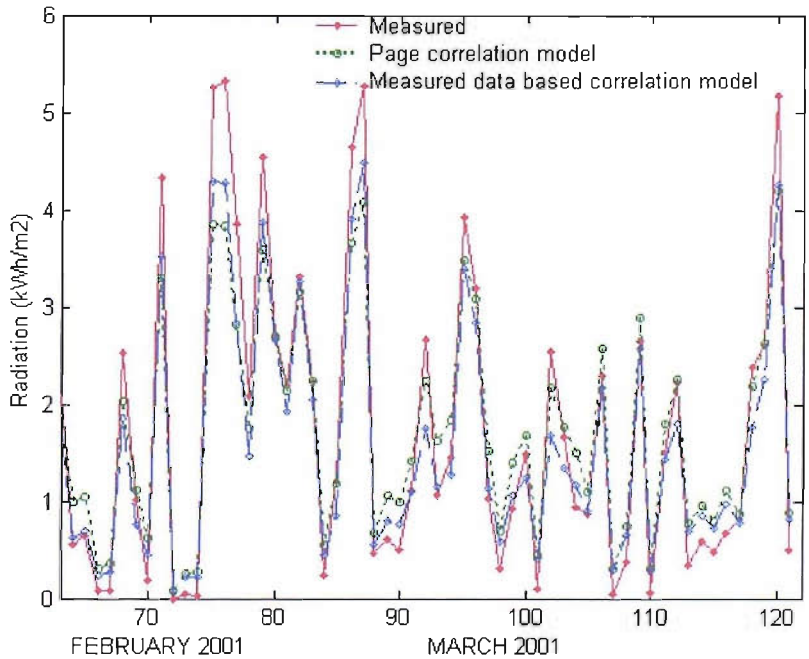

b.

Figure 16 Graphs (a) and (b) show the radiation on the inclined surface at Southampton for the months December 2002 to March 2001. The inclination is 50°.

2.9 ESRA software

The European Solar Radiation Atlas (ESRA)[41] uses a more sophisticated way to calculate R_b and uses a second generation of anisotropic model for the conversion of the diffuse radiation on the inclined plane. It is therefore expected that will lead to more accurate results and has been used in this work to obtain the daily radiation values on the inclined surface from the measured data on the horizontal surface.

The principal development in ESRA software takes into account that the sun may only be on the surface for a part of any selected hour. The precise times the sun shines on the surface can be calculated. A method of using a 10 minutes time step has been adopted for the calculation of the beam radiation algorithm on the inclined surfaces and similarly for the diffuse radiation.

Muneer's[42] diffuse model was adopted in ESRA software for the calculation of the diffuse radiation on the inclined plane. The choice was made after testing nine selected models from the existing ones[43]. These were the Liu and Jordan (1961) basic isotropic model; the Bulger[44], Klucher[18], Hay[19] and Reindl et al.[34] representing the first generation of anisotropic models already describing the sky dome as incorporating circumsolar and/or horizon band enhancing of diffuse irradiance; and the Gueymard[45], Skartveit and Olseth[46], Perez et al.[47], and Muneer[42] models representing a second generation of yet more sophisticated models.

The Muneer method distinguishes between sunlit surfaces (under non-overcast sky), potentially sunlit (that is sunlit surfaces under overcast sky) and shaded surfaces. Non-overcast is the sky when the (hourly) global radiation is larger than the (hourly) diffuse radiation and overcast when it is equal.

Further improvements in the Muneer's model in ESRA software was the removal of a discontinuity in the sky irradiance in the model when the sun moved from being just off the surface to just being on the surface. An improvement was also introduced at low solar altitudes, because the adjustments for the beam component became unrealistically large.

2.10 Orientation of PV panels

Ideally the solar generator should always face the sun at a right angle to the sun's rays, or for a cloudy sky should lie horizontally to accept diffuse irradiation. In an actual application, the tilt angle (β) of the solar generator depends on the purpose of the PV installation[48]. For a grid connected system one often aims at the maximum yield over the year. A stand-alone system may be designed to give the maximum possible energy yield over the winter months. A tilt angle less than 15^0 should be avoided to ensure self-cleaning by rain, while inclination angles greater than 60^0 can let the snow glide off easily.

There are several rules of thumb referred to in literature regarding the optimum orientation of PV panels. They could be summarised in the following:

The total annual energy received is maximized when the tilt angle of the panels is equal to latitude ($\beta=\phi$). For the northern hemisphere the optimum tilt angle for the summer, is equal to the latitude (ϕ) minus 10^0 to 15^0, and the optimum tilt angle for the winter (December, January, February and March) is equal to the latitude (ϕ) plus 10^0 to 15^0. Deviations about 15^0 from the optimum tilt angle result in 5% reduction in the annual energy (small).

The optimum azimuth angle (γ) is 0^0 for the northern and 180^0 for the southern hemisphere (the surface faces the equator). A 20^0 change from the optimum will make small difference in the total annual energy.

Figure 17 and Figure 18 show the effect of the tilt angle on the energy received on a surface in Efford (UK), latitude 51^o, while Figure 19 shows the effect of azimuth. The results are from E.S.R.A software and are in accordance with the rules of thumb mentioned above.

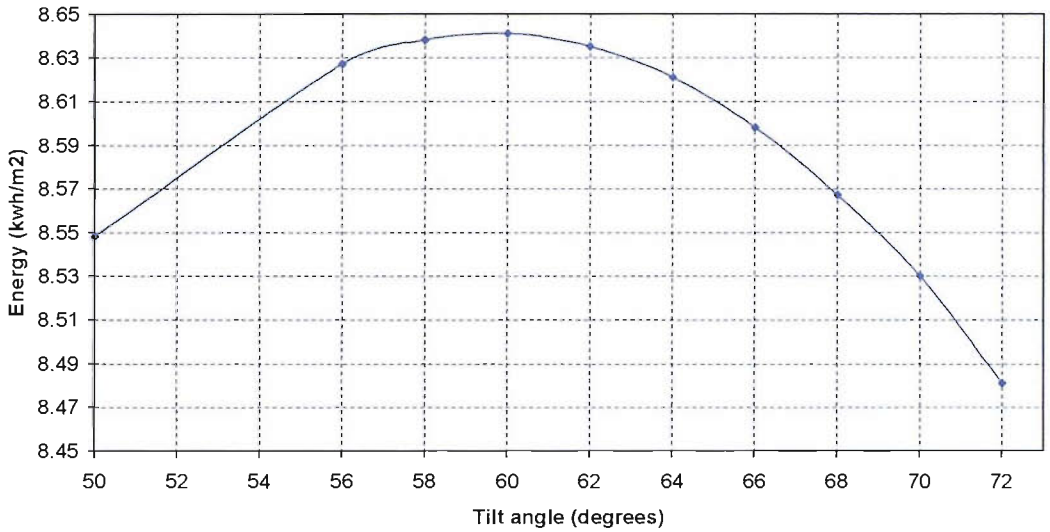

Figure 17 The energy received in winter months at various tilt angles and at zero azimuth in Efford (latitude 51°). The values were obtained using E.S.R.A. software

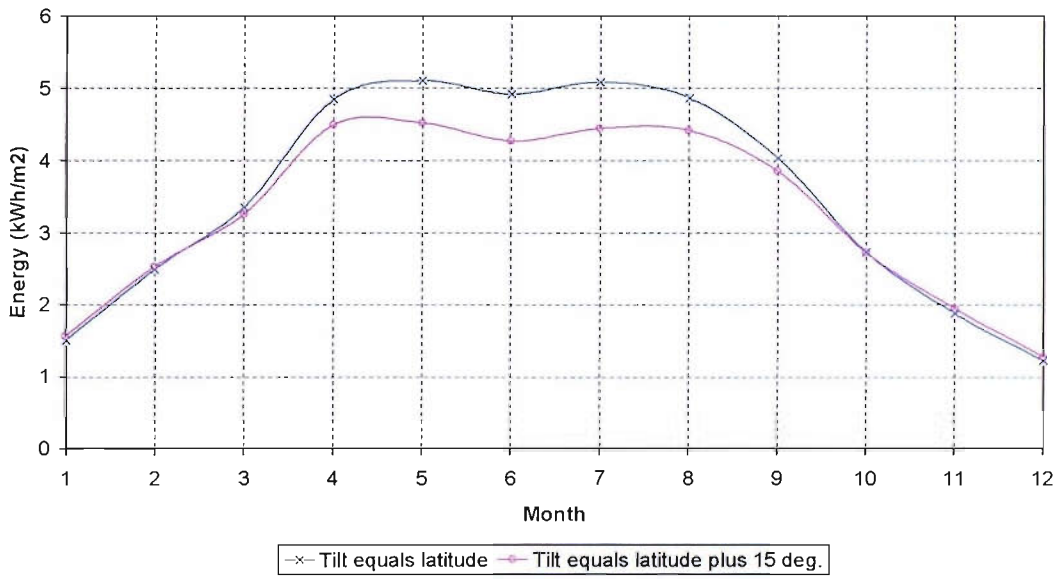

Figure 18 The energy received at tilt equal to latitude and at the optimum tilt angle

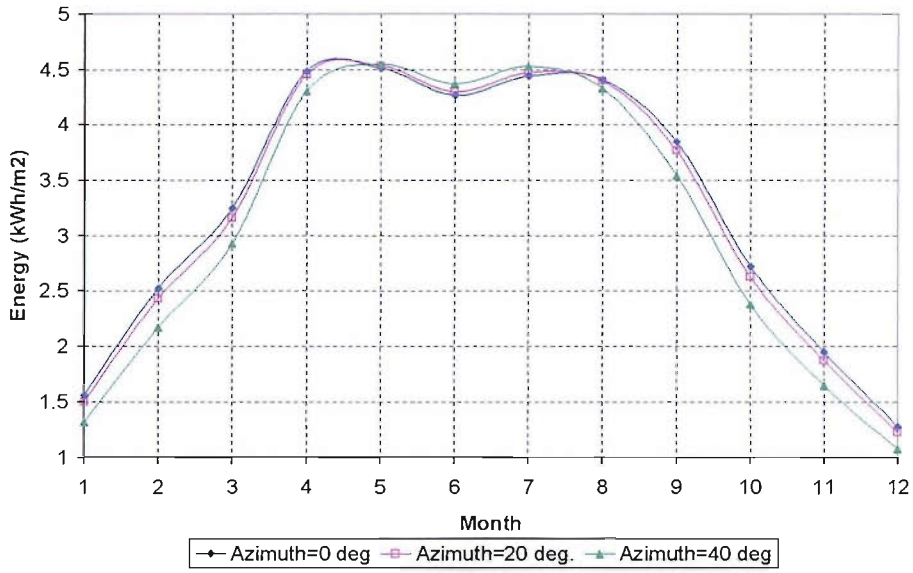

Figure 19 The effect of azimuth on the energy received

2.11 Conclusions

We have discussed the conversion of measured solar radiation data on the horizontal plane, to solar radiation value in the plane of the PV array. The procedure focuses on daily radiation as these data are needed as input to the modelling procedure which will be discussed in Chapter 6. Following the decomposition of global radiation into the beam and diffuse components, key to this procedure is the calculation of the diffuse fraction by using the clearness index: the ratio of the global to the extraterrestrial radiation.

Several concepts have been discussed related with the nature of the diffuse radiation and the calculation of the beam fraction. Liu and Jordan's method which has been widely used due to its simplicity has been analysed. The results have been compared with the values measured at STaR Facility at Southampton University. We have found that the procedure results in significant discrepancies, especially during the winter months – precisely when accurate data are needed for the modelling of the PV system. A new correlation based on the recorded data has been developed, resulting in some improvement with observation. The improvement refers to the values where the difference from the average value for the whole month is large. The

remaining discrepancies are mainly due to the way that the daily R_b is calculated, and to the isotropic assumption. The most advanced methodology that currently exists for this purpose – presented in the latest edition of the European Solar Radiation Atlas (ESRA) - was then discussed, and will be used in the remainder of this work. The resulting uncertainty, however, is the source of possibly one of the greatest errors in the model, and we shall return to this question in Chapter 6.

3. EXPERIMENTAL SET-UP

3.1 Introduction

This chapter describes the experimental set-up of the three types of experiments conducted during this work. These experiments are:

- Experiment to monitor the performance of a PV generator
- Construction and monitoring of a stand-alone system
- Battery experiments in the laboratory

A simple configuration of two modules in series connected to a resistive load will be used in this work in order to study the performance of a PV generator and validate a model in section 4.3.

From the several types of stand-alone systems, with respect to the variability of the load or the type of the load (e.g., AC, DC) the type of lead-acid battery used, the as well as the type of the charge regulator, here the research will focus on the basic type of stand-alone system, with constant resistive load that operates continuously 24 hours daily, lead acid batteries and simple on-off charge regulator. An experimental stand-alone system was constructed on the roof of Lanchester Building, at Southampton University and its operation has been monitored for six months – November to April- with the aim to analyse and understand its performance. The monitoring period includes the winter months because it is in winter when the battery reaches the lowest state of charge and this period is therefore critical for system sizing. During the summer months the battery becomes full during the day. The monitoring data will be used latter on in this work (chapter 8) for comparison with simulation results from an energy model. The main objectives are:

- To obtain a detailed record of the overall performance of the system, by recording the voltages and the currents at the PV the battery the load.
- To validate the predictions regarding the system sizing and performance

- To analyse the measured values of the monitoring parameters (current, voltage, irradiance)
- To monitor the battery operation in the PV system
- To obtain the necessary experimental data to validate (in chapter 8) the model based on daily energy balance of PV systems of section 6.3.

In addition this chapter describes the experimental set-up for battery charging and discharging experiments that where conducted in the laboratory with the aim the better understanding of battery operation as a PV system component and the use of the results in the validation of the model based on daily energy balance. The battery experiments and the results are presented in section 5.3 and chapter 7.

This chapter is organized as follows:

Section 3.2 describes the set-up for the PV generator experiment. Section 3.3 describes the construction and monitoring of the stand-alone system. Section 3.3.1 gives details of the physical arrangement of the system and the electrical interconnection (including the orientation of the modules). Section 3.3.2 discusses component specification. Section 3.3.3 discusses cables and grounding issues. The sensors of data acquisition system are described in section 3.3.4. Section 3.3.5 is a presentation and analysis of the experimental data. Section 3.4 describes the experimental set-up for battery experiments in the laboratory.

3.2 PV generator set-up

The experimental set-up described in this section has been used for the validation of the PV generator model described in section 4.3. The validation of the model is presented in sections 4.4 and 4.5.

The system consisted of two façade-integrated Eurostare polycrystalline silicon modules of vertical inclination. These modules were connected in series, to power a resistive load (Figure 20). The module parameters are given in Table 1.

In the absence of vertically mounted sensors, the short-circuit current of another two modules was recorded in the place of the in-plane solar irradiance. For the same reason, the open circuit voltage of yet another two modules, was used. The existing data acquisition system has been used (see appendix B). The in-plane

irradiance and the cell temperature were then obtained using the mathematical formalism discussed in sections 4.2.1. and 4.2.2.

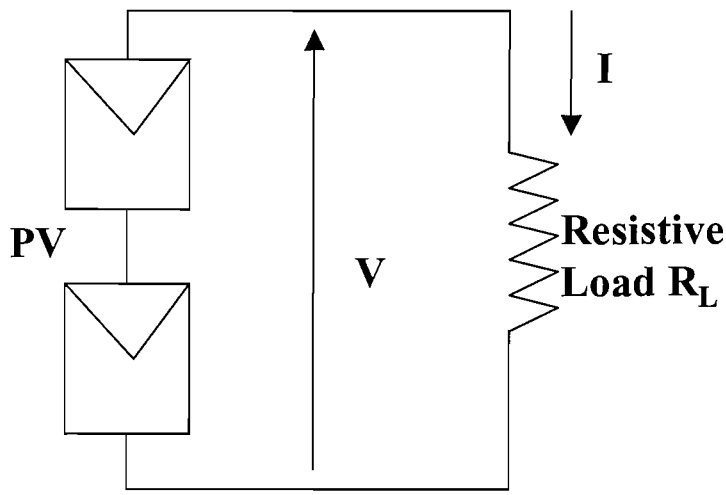

Figure 20 Experimental set-up for performance study of the PV generator.

Manufacturer's data
P_{MPP}=38.81W
I_{SC} =2.59A
I_{MPP}= 2.31A
V_{OC}= 21.88V
V_{MPP} =16.81V

Table 1. The manufacturer's data of the modules at STC

3.3 Stand-alone system construction and monitoring

3.3.1 System layout

The experimental set-up described in this section has been used in order to obtain the experimental data needed for the validation of the model based on the daily energy balance of section 6.3. The validation procedure is analysed in chapter 8. The experimental data have also been used to analyse the operation of the PV system in section 6.2 as well as the battery operation in section 7.3.

The tilt angle of the panels is set at 66° according to the rules of thumb described in section 2.10 and to calculations made using Esra software, in order to find the tilt angle which maximises the winter output in Southampton. The system is facing south. Figure 21 and Figure 22 show the physical arrangement of the components of the system at the roof of Lanchester building and the physical arrangement of the components in the battery box, respectively. The electrical drawings of the system are shown pages 55, 56.

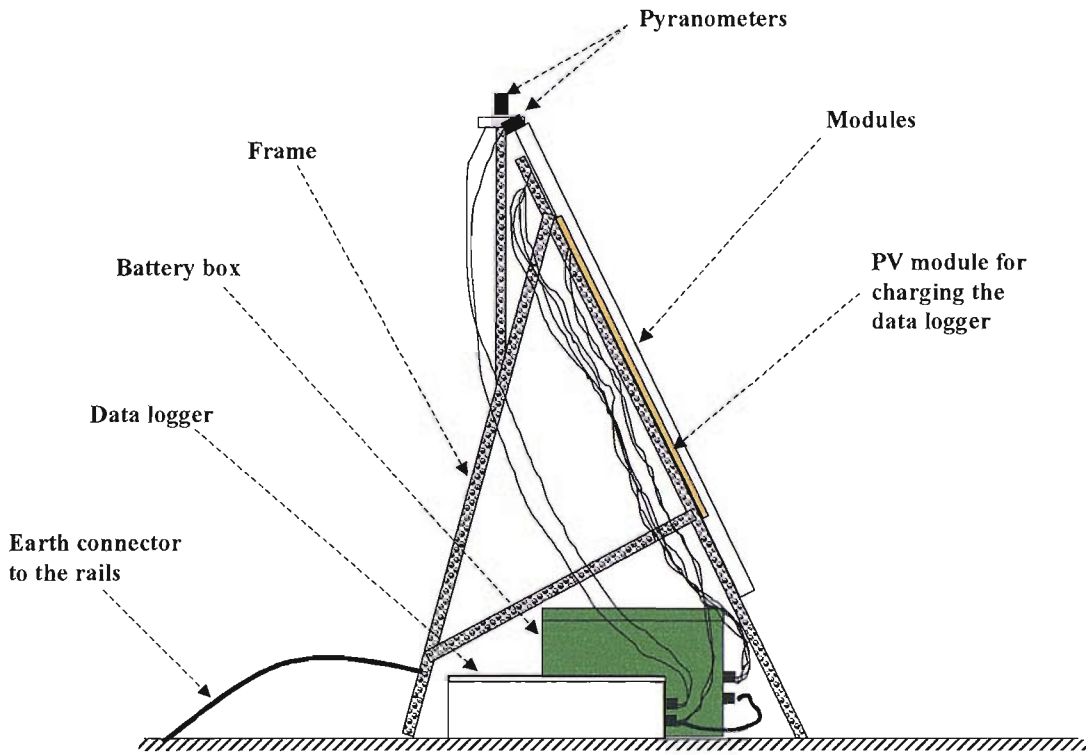

Figure 21 Physical arrangement of the stand-alone PV system at Lancaster building

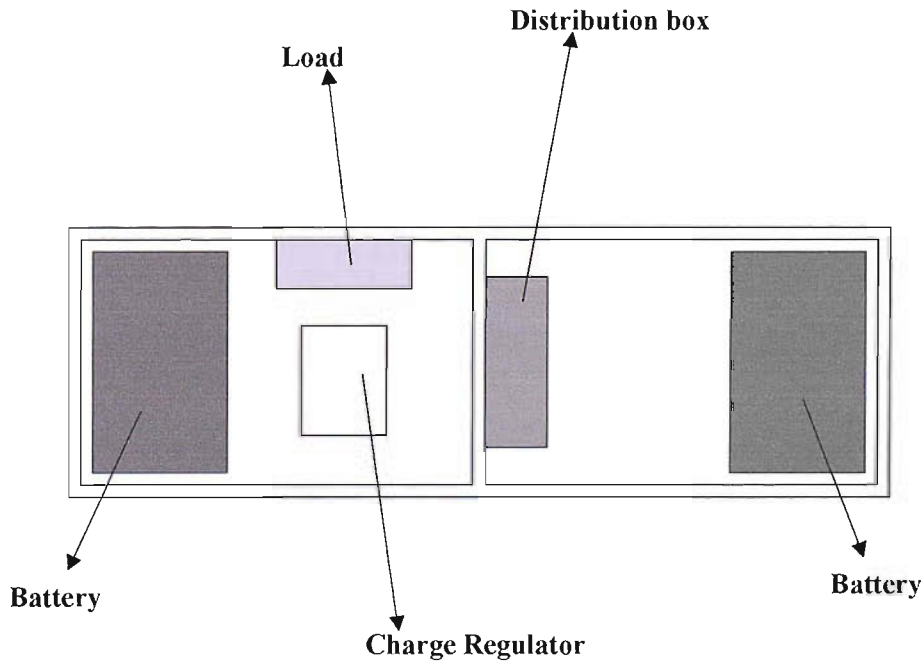

Figure 22 Physical arrangement of the components in the battery box

STAND-ALONE PV

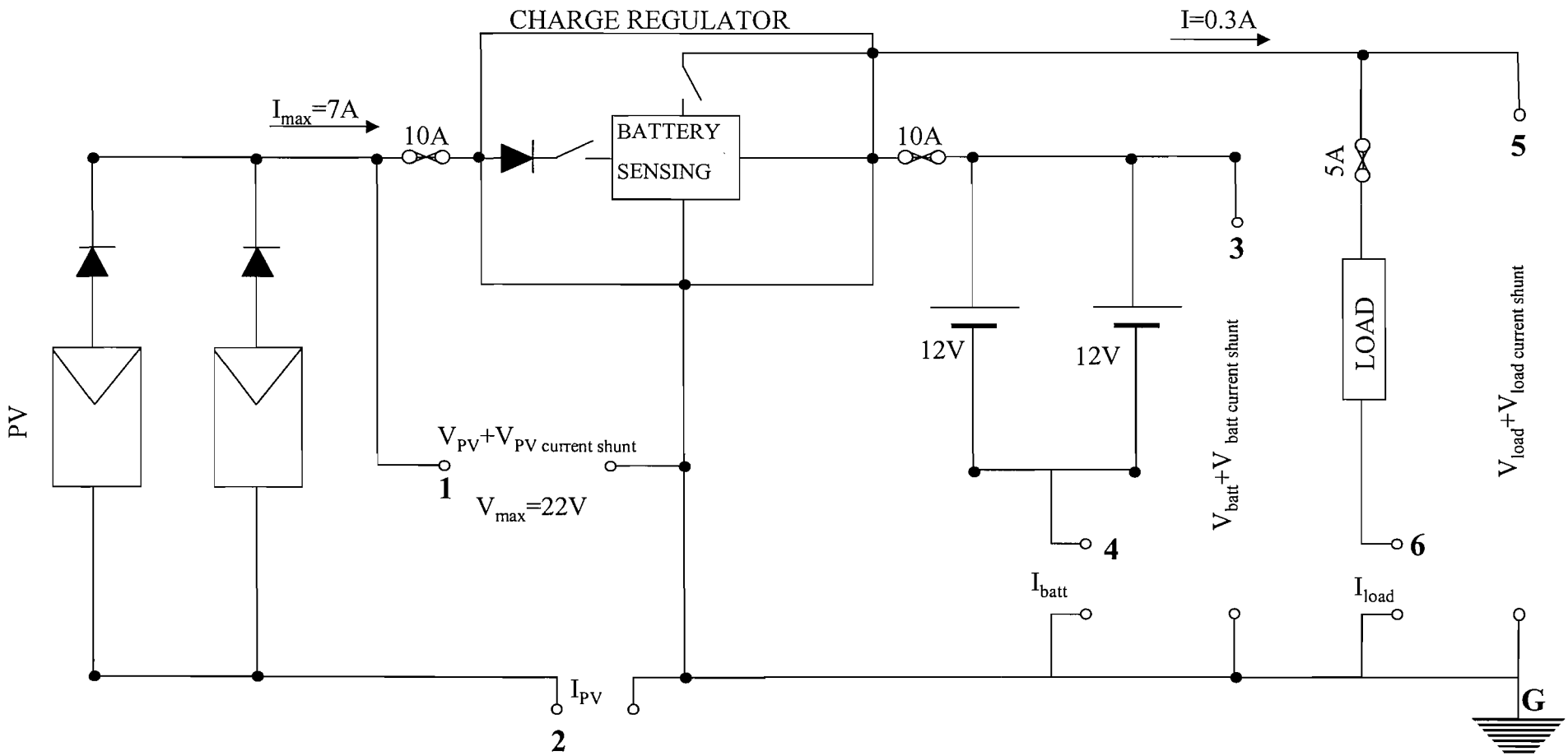

STAND-ALONE PV

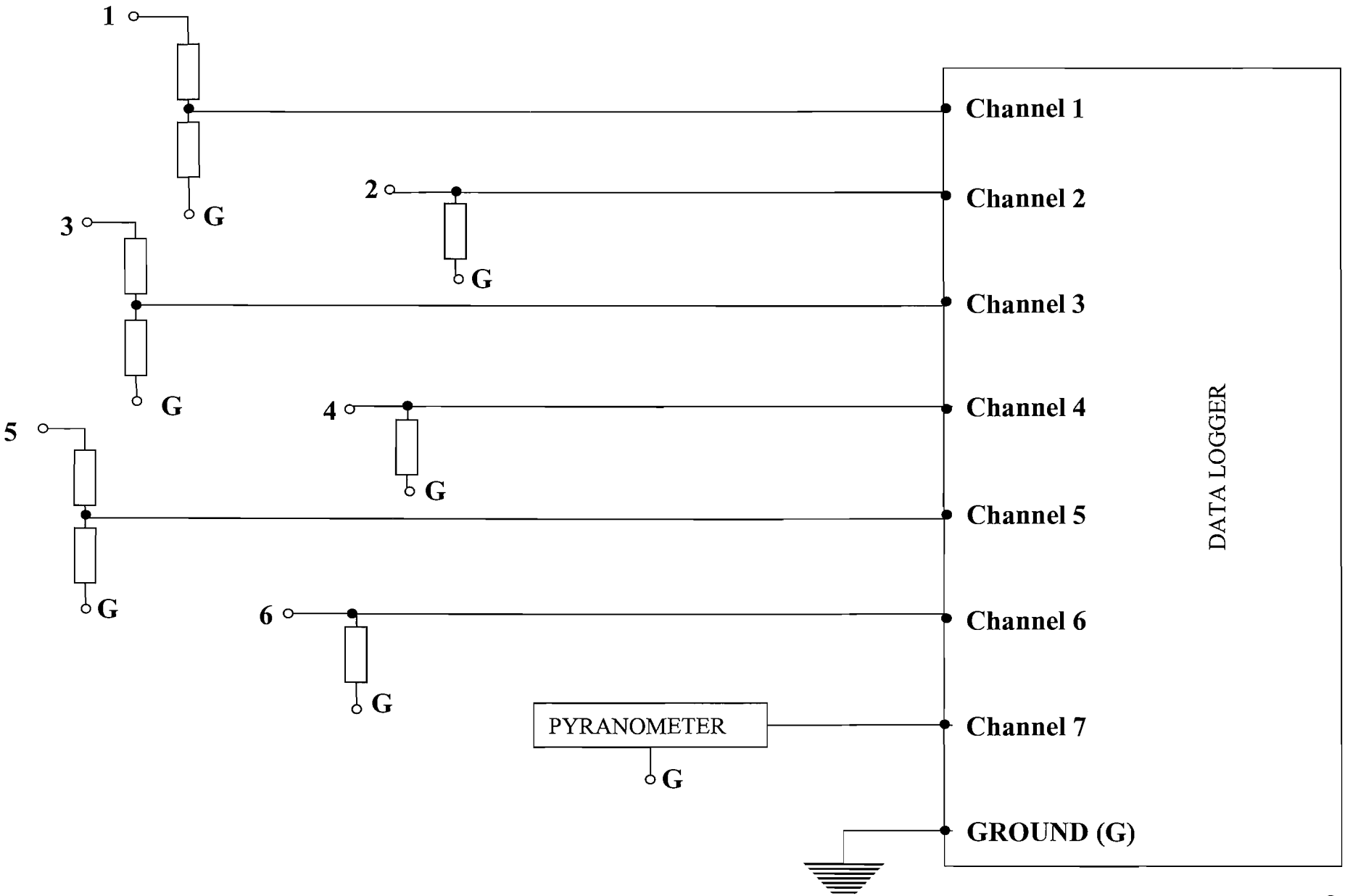

LAYOUT DRAWING 2

3.3.2 Components specifications

The modules used are Sharp NT9075 modules consisting of 36 cells in series. After calibration it was found that they have the following characteristics:

Module a: Isc=3.6 A, Voc=21.9 V, Pmax=51W,
Module b: Isc=3.5 A, Voc=21.8 V, Pmax=51.5 W

The load is a variable resistor set at 40 Ohms.

The system sizing was made according to the method described in section 9.2.3. Two low maintenance sealed valve regulated lead-acid batteries, SunLyte 12-5000X, of 100 Ah capacity each and nominal voltage of 12 V, were installed connected in parallel.

A simple on/off shunt charge regulator SOLLATEK SPCC10E was used, with Low Voltage Disconnect (LVD) and temperature compensation of –3mV/°C/cell. A diode, which protects the regulator against reversed polarity[49], is incorporated in the regulator's circuit. The operation of the regulator in the PV system is explained in section 6.2 and Chapter 7. The voltage thresholds are as follows:

- Charge disconnect, 12.9 V
- Charge reconnect, 14.4 V
- Load disconnect, 11.3 V
- Load reconnect, 12.3 V

A fuse of 10 A is connected in series between the solar panel and the charge regulator in the positive line[49], and a second one between the charge regulator and the battery, while a fuse of 5 Amps is connected in series with the load. The reason of using fuses is to protect the cables from overcurrent. It should be noted that the most potentially dangerous situation for both charge regulator and the load is operation without a battery which can happen for example when maintaining the battery or when the battery protection fuse blows. Then the PV generator imposes the voltage and this can raise enough to destroy the electronic devices.

A bridge rectifier KBPC 25005 of 50 Volt and 25 Amps was connected in series with the PV panels. The purpose is to make use of the two blocking diodes, therefore

to connect in series with each module a blocking diode for the reason described in section 4.2.3.

3.3.3 Cables and grounding

The heavy current leads, for the connections among the batteries the PV and the charge regulator, use a 7 stranded 4mm diameter and 30 Amps nominal current cable. It should be noted that all the specifications of the cables are again in accordance with those suggested by Lorenzo for a solar home system. The minimum acceptable cross section of the wire is 2.5mm^2 for the wire from the PV module to the charge regulator and 4mm^2 wire from the charge regulator to the battery, while all charge regulator terminals should easily accommodate at least 4mm^2 section cables[49]. Furthermore is recommended that the sections of cables must cause less than 3% of the voltage losses between PV modules and charge regulator, less than 1% between battery and charge regulator, and less than 1% between charge regulator and load. All of these apply at the maximum current condition. For copper cables (specific resistance =0.01724 Ohm*mm2/m at 20°C) and for 12 V nominal voltage the following formula can be used:

$S(mm^2)=0.3*l(m)*I_M(A)/\Delta V(\%)$, where S is the minimum cross-section of the cables, l is the cable length, I_M the maximum current and ΔV the allowable voltage losses. The cross-section of the cables used in the current application satisfies the above.

The load wiring is of 0.75 mm^2 diameter and 6 Amps nominal current; the same goes for the ground wiring. For connection with the data logger a multicore cable was used of 2 Amps nominal current. All wiring is coloured coded and labelled[49].

The system is connected with the existing lightning conductors[50] of the building, using a bolded connection at each end (the PV frame and the lightning conductors).

Regarding earthing the system is left to float.

3.3.4 Data recording

For data recording a CR10X Campbell scientific data logger was used and the software used for data recording is the PC208W software. The power supply of the data logger is a PS12E-LA power supply and includes a 12V, 7Ah lead-acid battery and a temperature-compensated charging circuit, which is attached to the side of the PS12E carrier. The datalogger and its power supply are fixed in an ENC10/12 Campbell Scientific weatherproof enclosure. A small PV module of approximately 19 V open circuit voltage is used to charge the battery of the data logger and is installed at the same inclination with the rest two modules.

SKS 1110 Skye pyranometers are used for solar radiation recordings on the horizontal and inclined surfaces.

The system quantities that we want to measure are the voltages across the PV, the battery and the load and the corresponding currents. Using the data logger we will also record solar radiation on the horizontal and inclined plane. Eight single ended channels of the datalogger were used for data recording.

The voltage range at the dataloger channels for voltage measurements had to be set so to cope with about 22 V voltage input which is the maximum voltage that can be provided by the PV panel. To this end for the voltage measurements there were used voltage dividers with 1/10 ratio. The final values for the resistors used are in appendix C.

Current was measured by shunts (see appendix C for the values used). The datalogger 0.25 V range was chosen for the measurements. The voltage error of the measurements was estimated as follows:

Voltage error (%)=Voltage range/operating voltage=0.25V/12V=0.02=2% (1. 1)

The resolution at 0.25 V voltage range is 66.6 μ V for the single ended measurement.

The channels for the irradiance measurement were set at 0.025 V sensitivity. The corresponding resolution for single ended measurements is 6.6 μ V.

3.3.5 Experimental data processing

This section analyses the difficulties of accurate monitoring of the measuring variables and explains some corrections that have been applied to the monitored data.

Measurement of irradiance

Pyranometers often return negative readings at night and this was also found to be the case with the pyranometer used in this study. Small positive values are also sometimes observed, probably due to stray light. It is safe to assume that no power is produced at this low level of illumination due to the nonlinearity of PV response. These readings are discarded by setting the nighttime irradiance to zero during the data processing stage. The nighttime period was estimated from the monthly average sunset and sunrise time using ESRA software.

Load voltage

The monitored values of PV and battery voltage do not need to be corrected because the current sensing resistors for the PV and the battery current measurements are very small and the very small voltage error that they introduce has already been taken into account in the calibration of the corresponding channels so that the voltage error in the measured data is less than 1%. However, a correction was applied to the monitored values of the load voltage to account for the voltage drop on the load current sensing resistor (see Layout drawing 1). The accuracy of the corrected readings of the load voltage is better than 1%.

Current measurements

The measurement of the battery and PV currents poses the difficulty that these currents vary widely (between zero to over 7 A). It is particularly the small values that need to be measured accurately since the battery is charged by a low current in winter, often over periods of several days. Since the datalogger needs to be set to measure also high currents over the summer months, the low current measurements incur high error, as can be seen from the following argument. The data logger is measuring voltages and the voltage readings can be converted to current readings by setting the multiplier equal to $1/R_s$, where R_s is the value of the current sensing resistor in mOhms. The offset error of the data logger is a function of the full-scale reading-

±0.1% of the full-scale reading. This means that if 2500 mV voltage range is used, the error in the voltages for the single ended measurements is ±5mV. The value of the current sensing resistor used for the measurements of the battery and the PV currents is 33mOhms. The offset error of the current is ±0.15 Amps. The relative offset error is therefore inversely proportional to the measured current (Figure 23). This implies that there is a linear relationship between the measured values of current and the accurate values of current, which gives the possibility to correct the offset error of the datalogger. The data logger was calibrated using a FLUKE 79 series II multimeter. In the battery and PV current values we had additionally to adjust the settings as mentioned above in order to correct the offset error of the datalogger. Furthermore, because of the rapid fluctuations of the radiation and therefore of the currents, it was difficult to take recordings of the battery and PV currents and most of the readings were taken with the PV replaced by a D30 4 FARNELL dc power supply.

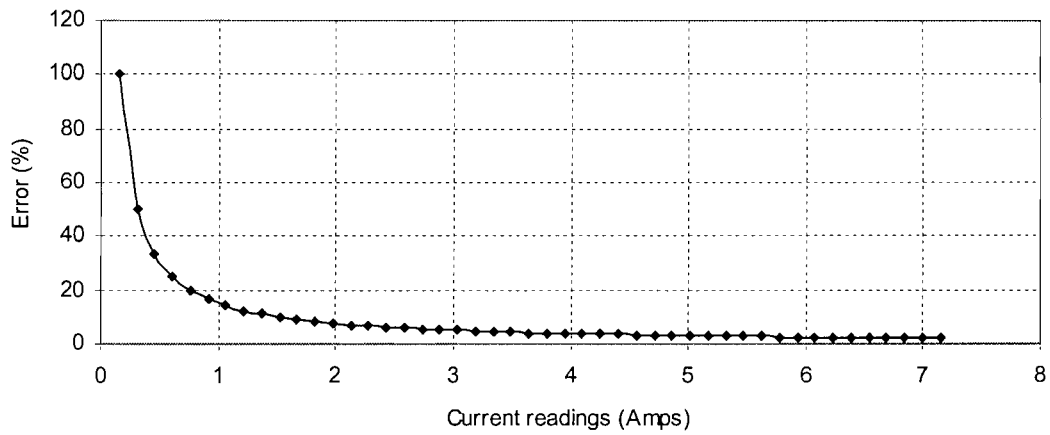

Figure 23 Theoretical curve of the percentage error of the data logger

A further improvement in the accuracy is possible by the use of Kirchhoff's laws. The greatest errors occur in the measurements of the PV and the battery currents on account of their wide range of variation. In contrast, the almost constant load current can be measured with high accuracy, and can be used to produce more accurate values of the PV and battery currents, as follows:

The following sum S according to the Kirchhoff's law should be zero (Figure 24):

$S=I_{PV}+I_B+I_L+I_R$ (3.3.1)

Where, I_{PV}, I_B and I_L are PV, battery and load currents, and I_R is the current consumed by the regulator. The current consumption of the regulator is constant and equal to 8 mA, according to the manual provided by the manufacturer. Even a small deviation from this value when the regulator operates (unlikely to be larger than 1 or 2 mA) introduces an error that is negligible compared to the values of the measured currents.

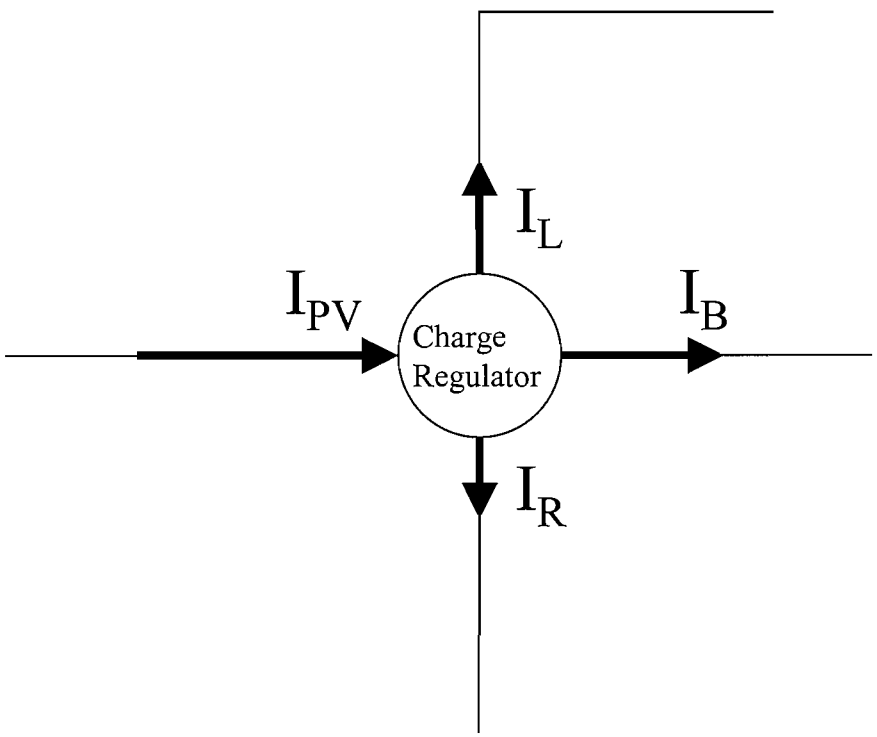

Figure 24 Kirchhoff's law applied on the stand-alone system of the layout 1

Case one

When the PV is disconnected (e.g. at night) the current to the system is provided only by the battery. In this case, the battery current is set equal to the load current plus the current consumption of the regulator.

Case two

When both the battery and the PV are connected to the system, the deviation from Kirchhoff's laws S (3.3.1) in the measured values is attributed equally to the PV and the battery currents:

$I_{Bcorrected} = I_B - S/2$

$I_{PVcorrected} = I_{PV} - S/2$

3.4 Set-up for battery experiments in the laboratory

The battery voltage and currents were monitored using a pico ADC-11/12 data logger connected to a laptop. According to manufacturers data the accuracy of the data logger is ±0.5 % of the full- scale reading. The readings are recorded every second and averaged and logged in a file every 5 minutes. Two different channels were used for current monitoring since the sign of the current changes between charge and discharge while the data logger can only record positive signals. An inverting amplifier circuit was used to invert the negative signal. The circuit used in battery experiments is shown in

Figure 25 and the amplifier circuits that are used for the data logger channels are shown in Figure 26.

The channels of the data logger were calibrated using a Keithley 197 A six digit multimeter with the following accuracy: ±(0.015%+2) for the voltage readings and ±(0.2%+15) for the current readings of the 200mA scale and ±(0.2%+15) for the 2000mA scale. The temperature is kept constant during each experiment using a heater with a thermostat. The values of the open circuit voltage were measured after leaving the battery 48 hours at rest, as recommended by the manufacturer.

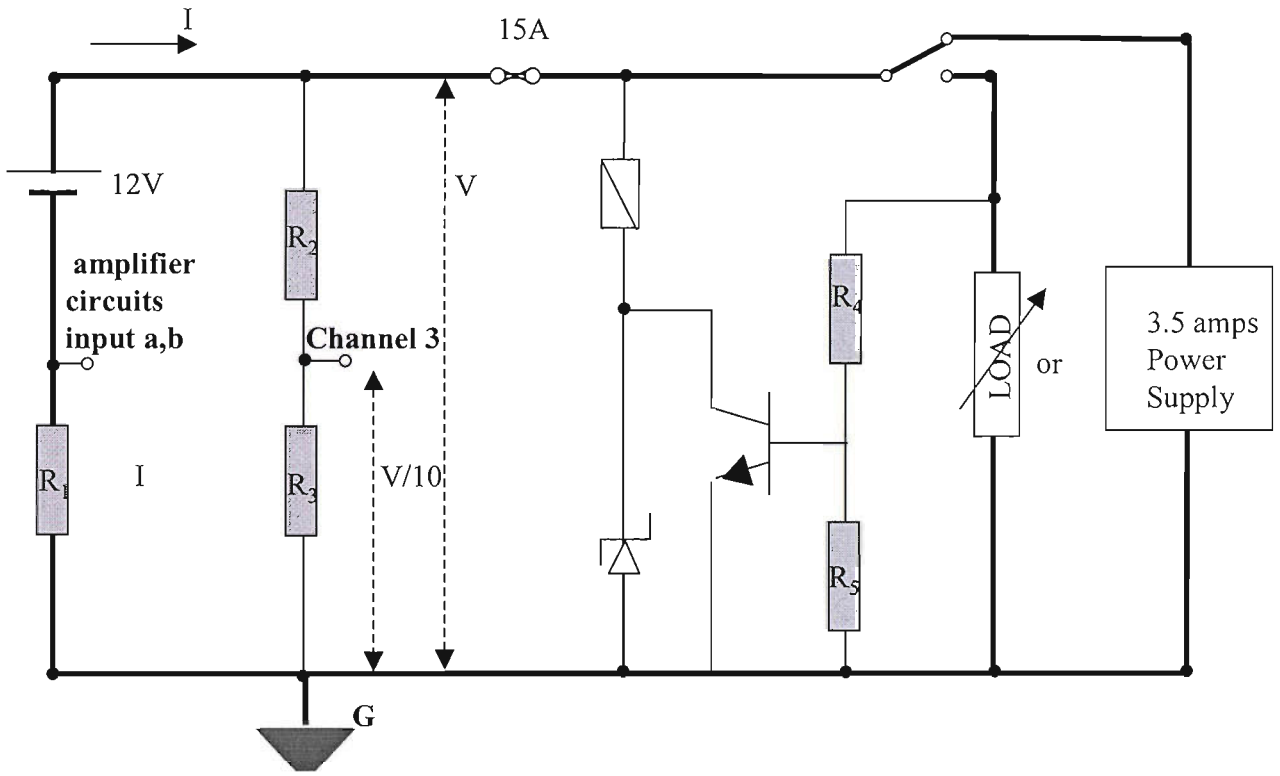

R_1=33 mOhm, R_2=246.6 kOhm, R_3=27.4 kOhm, R_4=10 kOhm, R_5=10 kOhm

Figure 25 Circuit used in battery experiments

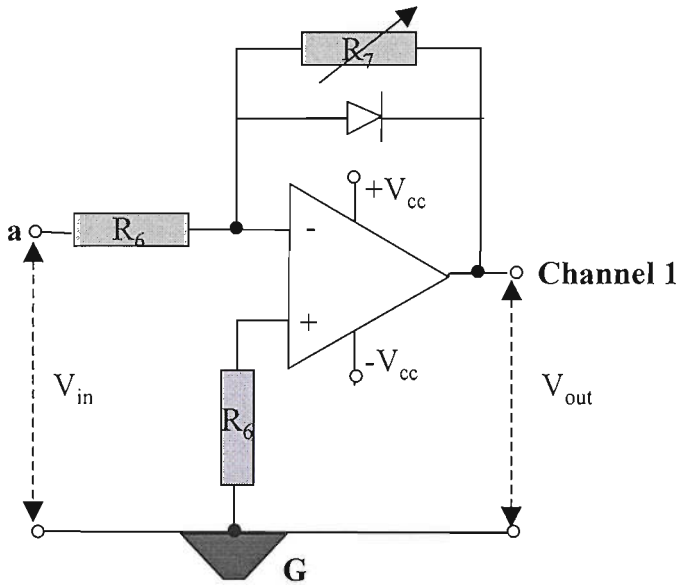

a.

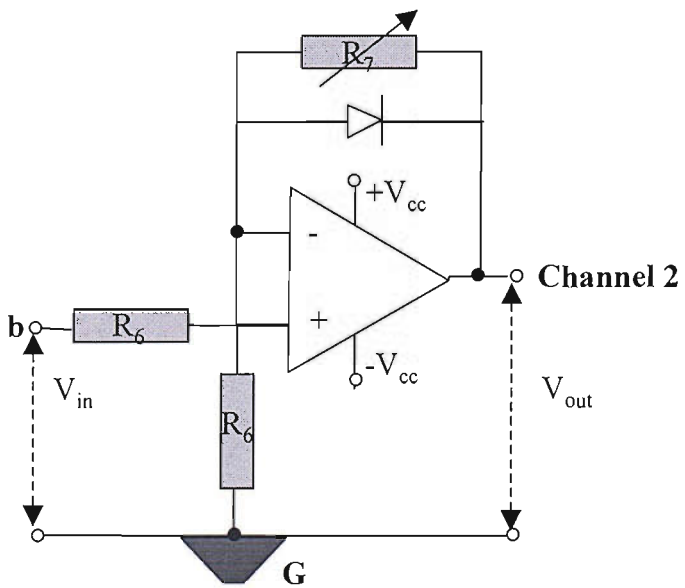

b.

R_6=10 kOhm, R_7=100 kOhm-1000 kOhm

Figure 26 Inverting (a) and non-inverting (b) amplifier circuits

4. OPERATION OF THE PV GENERATOR

4.1 Introduction

The PV generator is the energy producing component of the PV system, and this chapter reviews its operation. We consider the electrical characteristics, both under standard and operating conditions. We also examine the effect of interconnecting solar cells into modules, and modules into an array, or PV generator. We illustrate these concepts with the use of a model. This time-dependent model was developed with the use of Matlab[51,52] software. The instantaneous current, voltage and power output of the generator at the operating conditions are calculated and analysed in section 4.2. Although the detailed simulation of system components is necessary for certain purposes (like component design, assessment of system stability and determination of power quality) the usefulness of such simulation in system sizing has been put into question by several authors[90,53]. This issue appears to be that the uncertainties in the input radiation series seem to be larger than the uncertainties introduced by modelling the system components. The results of the Matlab model are compared with experimental data obtained in section 3.2. It was found that although the PV generator can be modelled with high accuracy some parameter adjustment is needed for the generator model to be adapted to the specific array used in the experiment.

Section 4.2 explains the operating principles of a solar cell and the influence of environmental parameters on solar cell operation. It also considers the solar module and how to determine the module current during practical operation, mismatch losses and the module interconnection in a PV generator. Section 4.3 describes the model developed in this work. The experimental and modelling results are presented in section 4.4. Section 4.5 discusses the results while the conclusions are presented in section 4.6.

4.2 Literature review

4.2.1 Solar cell

Solar cells form the energy conversion part of the PV system. The classical model of a solar cell is a semiconductor p-n junction.

The properties of the semiconductors are determined to a significant degree, by the crystal structure. The band structure of a crystal solid is defined by the energy momentum relationship of the electrons[54]. For any crystalline solid there are forbidden energy regions in which allowed states cannot exist. In a semiconductor (or insulator for that matter), one band is exactly filled with electrons, at least at the absolute zero of temperature. Energy states or energy bands are allowed above and below this energy gap. The upper bands are called the conduction bands (E_c); the lower bands, the valence bands (E_v). The separation between the energy of the lowest conduction band and that of the highest valence band is called the band gap (E_g). In a n-type semiconductor extra electrons from the valence band are promoted to the conduction band. In a p-type semiconductor there is an electron deficiency in the valence band. A quantity for describing the concentration of electrons and holes at any point in a semiconductor is the fermi level E_F.

A semiconductor junction (for example a p-n junction) creates a space charge region. The associated electric field and the built-in potential V_{bi} play an important role in solar cell operation. When the diffusion effect is exactly cancelled by the built-in electric field, the junction is at equilibrium. At equilibrium, the Fermi level is constant across the junction and, indeed, throughout the device. In equilibrium the fermi level can be determined from the charge neutrality condition. In operation, however, separate Fermi levels (usually called quasi Fermi levels) need to be defined for electrons and holes.

Figure 27 illustrates the p-n junction.

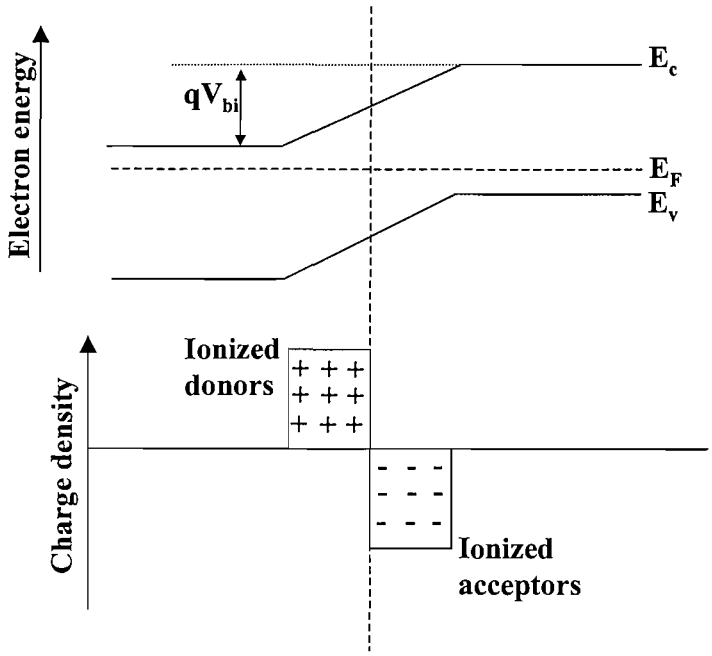

Figure 27 A schematic band diagram of a p-n junction at equilibrium

The thermal equilibrium condition is the one with no applied voltage and no current flow and no other external perturbation such as illumination. At thermal equilibrium, the pn product is equal to n_i^2. At forward and reverse bias condition the electrostatic potential across the junction is equal to the external bias V.

When voltage is applied, the potential difference between the two sides of the diode will change, the minority carrier densities on both sides of a junction are changed and the pn product is no longer given by n_i^2.

We can now find the minority carrier distribution in the quasi-neutral regions, for example the concentration of holes into n-side of the junction[55].

The continuity equation for the holes reads:

$$\frac{1}{q}\frac{dJ_h}{dx} = -(G - U) \quad (4.2.1)$$

Where J_h is the current density for the holes, G is the net generation rate by external processes such as illumination and U is the net recombination rate.

The transport equation on the n-type side of the diode is:

$$J_h = -qD_h \frac{dp}{dx} \qquad (4.2.2)$$

An approximate solution[56] of the equations (4.2.1) and (4.2.2) in the dark (i.e., for a diode) is:

$$J=J_h+J_n= J_o(e^{qV/kT} -1) \qquad (4.2.3)$$

Where,

$$J_o = \frac{qD_e n_{po}}{L_e} + \frac{qD_h p_{no}}{L_h} \qquad (4.2.4)$$

where q is the charge of an electron, k is Boltzman constant, T is the junction temperature, V is the electrostatic potential difference across the junction, D_h is diffusion coefficient of the holes on the n-side, (similarly D_e for the electrons), L_h , L_e have the dimension of length and are known as the diffusion lengths, p_{no} is the equilibrium concentration of holes (minority carriers) on the n-side (similarly n_{po} for electrons).

The equation (4.2.4) is the Shockley equation, or the ideal diode law. In the dark, the junction acts as a rectifying diode to the current: at forward bias there is a carrier transport across the junction which produces current that varies approximately as $e^{qV/kT}$. At reverse bias, only a small number of carriers will cross the junction, and this reverse current saturates at some value of current density J_o. For a planar diode, it is a simple matter to convert current densities in currents by multiplying with the area of the device A, say. The I-V characteristic of an ideal diode is shown in Figure 28.

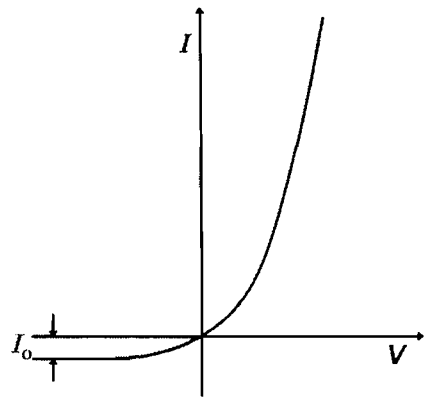

Figure 28 The diode I-V characteristic

Under illumination by light, photons with sufficient energy are absorbed and generate in the semiconductor electron-hole pairs (one photon generates one electron-hole pair). Those, which are collected at the junction are pulled apart by the electric field and give rise to photo-generated current I_{ph}. This transforms the diode characteristic (4.2.3) to:

$$I=I_{ph}+ I_o(e^{qV/kT} -1) \quad (4.2.5)$$

Equation (4.2.5) is known as the ideal solar cell I-V characteristic. We should note that the illuminated characteristic is approximately the dark characteristic of Figure 28 shifted down by a current I_{ph}. This gives a region in the fourth quadrant of the final plot where power can be extracted from the diode. For practical considerations one must consider deviations of solar cell behaviour from the ideal operation described by equation (4.2.5). The equivalent circuit of the solar cell is shown in Figure 29.

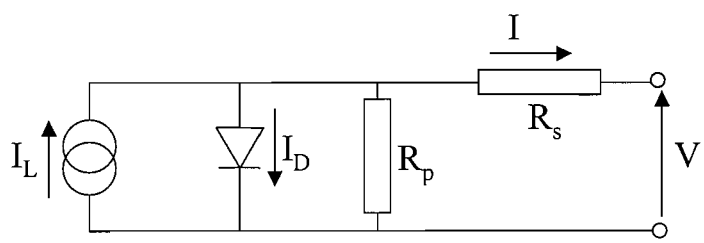

Figure 29 Equivalent circuit of a photovoltaic cell

The series resistance R_s of a cell in Figure 29 consists of several contributions[57], including contact resistance and bulk resistance. In a system there is also the resistance of the external circuit. R_p the parallel resistance, due mainly to leakage currents through the junction, is usually large and can be omitted.

The I-V characteristic of a solar cell is usually measured under standard test conditions (STC), which are universally recognized measuring conditions. The standard test conditions are 1000W/m^2 radiation, with a spectrum corresponding to air mass 1.5 (see section 2.4), normal angle of incidence and cell temperature of 25^{0}C. A typical I-V characteristic is shown in Figure 30.

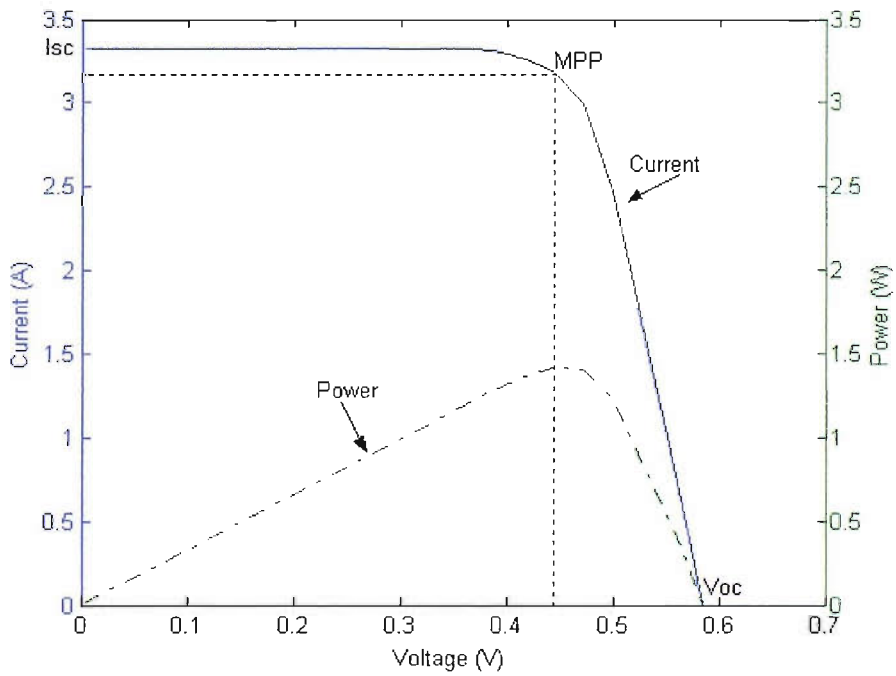

Figure 30 The typical I-V curve and the power output of a BP250 crystalline silicon photovoltaic cell of area 100 cm^2 under standard conditions

The quantities of importance that are associated with a given I-V curve are:

- The open circuit voltage V_{oc}
- The short circuit current I_{sc}

- The maximum power point (MPP), which is the optimal operating point on the curve
- The fill factor which is the ratio of the maximum power that can be delivered to the load divided by the product $I_{sc}V_{oc}$

The fill factor gives a quantitative measure of the form of the characteristic curve. The fill factor of an ideal solar cell is approximately[7]:

$$FF_O = \frac{v_{oc} - \ln(v_{oc} + 0.72)}{v_{oc} + 1} \qquad (4.2.6)$$

where $v_{oc}=V_{oc}/V_t$ and V_t is the factor kT/q, called the thermal voltage

The open circuit voltage does not depend on the surface area of the cell, and is a function principally of the material. It is of the order of 590mV for $1kWm^{-2}$ of irradiance for a single crystal silicon solar cell at 25°C and between 0.6-0.9V for amorphous silicon cells[48]. The open circuit voltage does not depend strongly on the irradiance. The short circuit current is of the order of $30mAcm^{-2}$ for an irradiance of $1kWm^{-2}$ for a single crystal silicon solar cell at 25°C. Only a weak dependence of the current on temperature is usually observed (Figure 36).

An ideal solar cell is electrically equivalent to an ideal current source connected in parallel with an ideal diode. In other words if we omit the series and the parallel resistance, the electric circuit of Figure 29 represents an ideal solar cell. Figure 31 compares the characteristic of a solar cell when only the series resistance is taken into account (as we usually do in practical applications) with the ideal one.

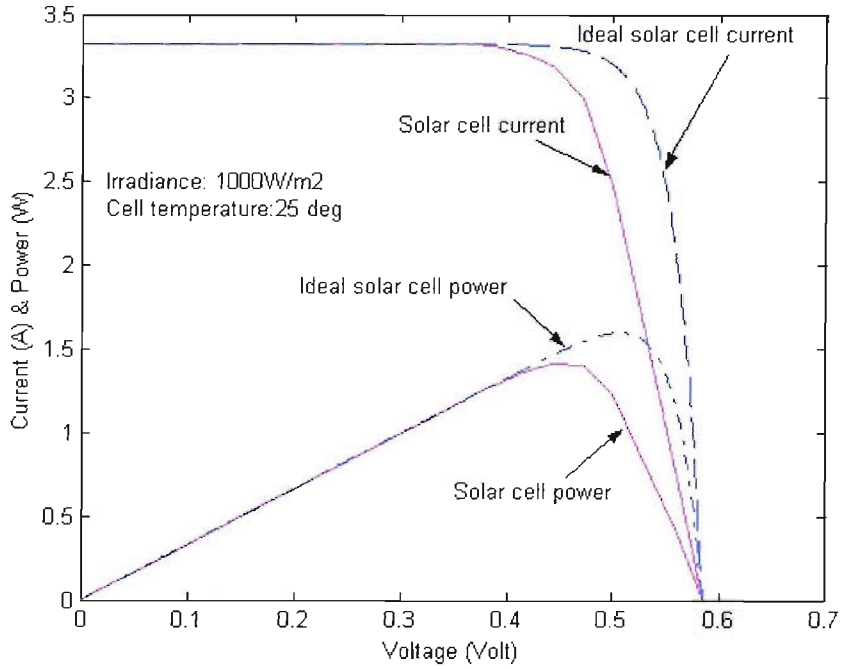

Figure 31 Comparison on the current and the power curves of a solar cell in practice (Figure 30) with the ideal solar cell, under standard conditions.

In addition to series and parallel resistance further effects may arise from recombination in the space-charge region and non-linear recombination in the emitter and the base. These effects can be described phenomenologically by introducing the so called ideality factor (m). Figure 32 shows the effect of the diode ideality factor on the I-V curve of an ideal solar cell. The effect of the series resistance on the I-V curve of a solar cell is shown in Figure 33. Both factors seem to affect mainly the fill factor but not the short circuit current or the open circuit voltage. The series resistance causes a reduction in the slope of the I-V curve in the region between the MPP and the point that corresponds to the open circuit voltage. The shunt resistance causes an increase in the slope of the I-V characteristic in the region between the point that corresponds to the short circuit current and the MPP. The effect of shunt resistance is less pronounced. A good solar cell has small R_s, large R_p and m close to 1.

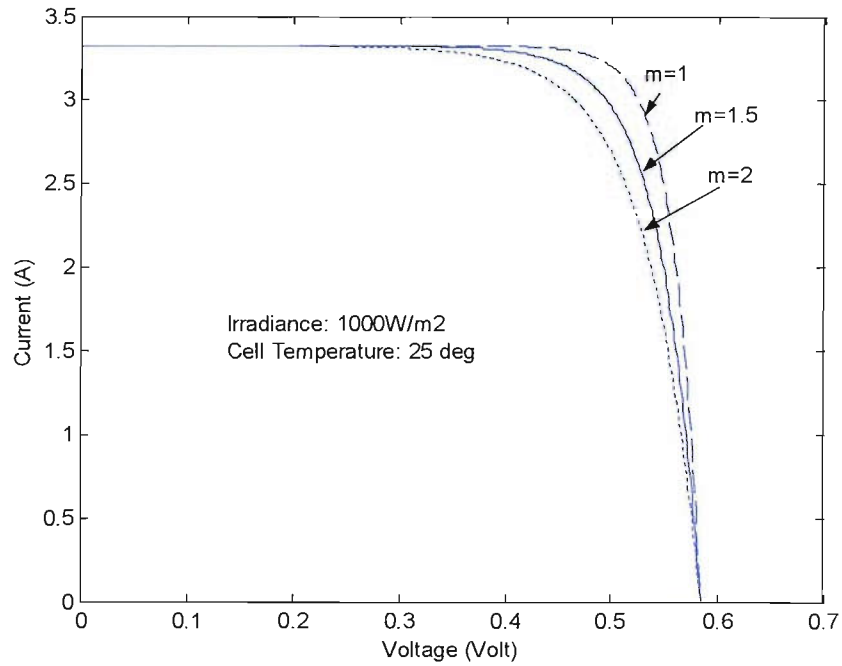

Figure 32 The effect of the ideality factor on the I-V curve of the solar cell of Figure 30 under standard conditions.

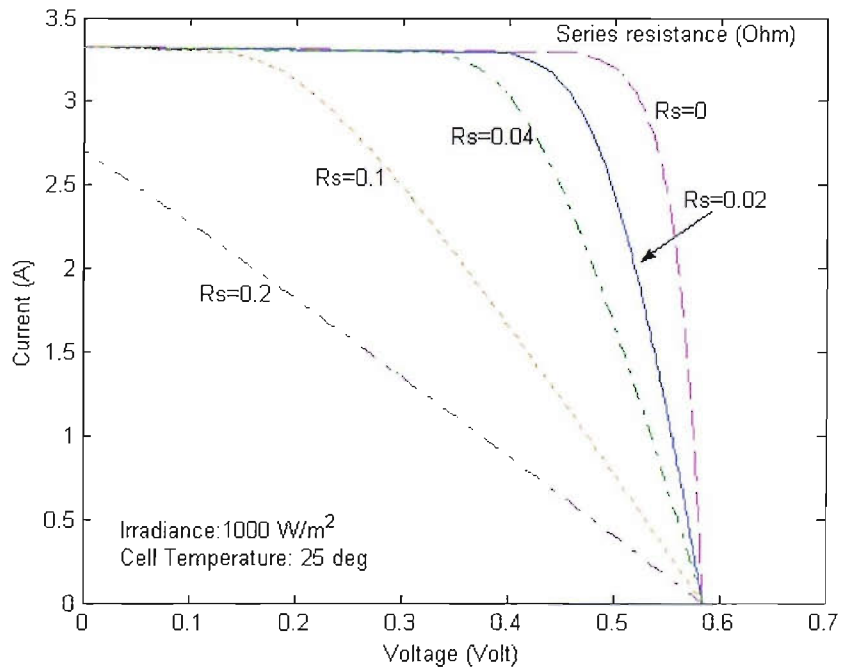

Figure 33 The effect of series resistance on the I-V curve of the solar cell of Figure 30 under standard test conditions.

The equation that describes the I-V curve of a solar cell represented by the equivalent circuit of Figure 29 is:

$$I = I_{ph} - I_o\left(e^{q(V+IR_S)/mkT} - 1\right) - \frac{(V + IR_s)}{R_p} \qquad (4.2.7)$$

In many instances, the effect of shunt resistance can be neglected and the ideality factor is chosen equal to 1. Then equation (4.2.7) becomes:

$$I = I_{ph} - I_o\left(e^{q(V+IR_S)/kT} - 1\right) \quad (4.2.8)$$

Figure 34 shows the calculated I-V curve of a solar cell when only the series resistance is taken into account and the experimental I-V curve. We will see now how from equation (4.2.8) we can derive the equation from which the I-V curve of a solar cell can be calculated:

First, we find the expressions for the open circuit voltage and the short circuit current as follows:

In the open circuit condition I=0 from (4.2.8) we can derive the equation that gives the open circuit voltage:

$$V_{oc} = \frac{kT}{q} \ln \frac{I_{ph} + I_o}{I_o} \qquad (4.2.9)$$

In the short circuit condition V=0 and from equation (4.2.7) we can find the short circuit current:

$$I_{sc} = I_{ph} - I_o\left(e^{qI_{sc}R_S/kT} - 1\right) \quad (4.2.10)$$

Under 1 sun irradiance the series resistance is negligible in the short circuit condition and the short circuit current can be considered equal to the photocurrent:

$I_{sc}=I_{ph}$ (4.2.11)

Now, the equation from which we calculate the I-V curve of a solar cell can be derived as follows:

Under operating conditions we usually have $\exp((V+IR_s)/kT)\gg 1$[7] and from equation (4.2.9) we can find the dark saturation current I_o.

$$I_o = I_{sc} e^{-\frac{qV_{oc}}{kT}} \quad (4.2.12)$$

Then from (4.2.8), (4.2.11) and (4.2.12) we find:

$$I = I_{sc}\left[1 - e^{\frac{V - V_{oc} + IR_s}{V_t}}\right] \quad (4.2.13)$$

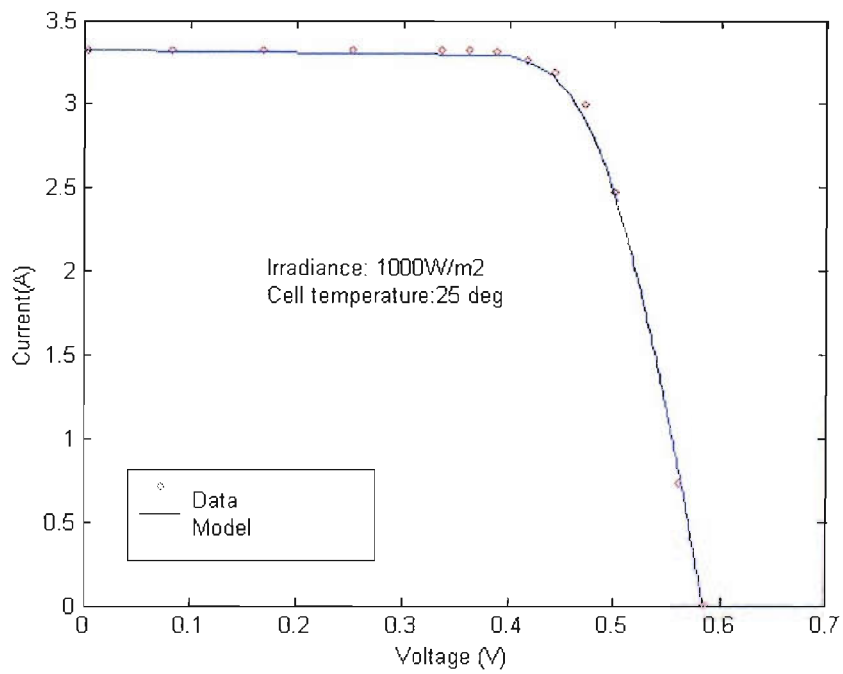

Figure 34 The I-V curve of a solar cell (see also Figure 30) obtained by fitting the I-V characteristic to the experimental data using the series resistance as the fitting parameter.

We shall now consider the effects of changing irradiance and temperature on the I-V curve of the solar cell. The open circuit voltage increases logarithmically with increasing irradiance level (4.2.9) and this dependence is therefore weak. In PV system design this effect is usually neglected. It can be shown[54] that the dark saturation current I_o increases exponentially with cell temperature as: $I_o \propto T^{(3+\gamma/2)} e^{-\frac{E_g}{kT}}$, where γ is constant. Therefore, it is seen from equation (4.2.9) that the open circuit voltage decreases linearly with temperature. For crystalline silicon cells at ambient temperature it is approximately:

$$\frac{dV_{oc}}{dT} = -2.3 mV/^{O}C \quad (4.2.14)$$

An increase in temperature also leads to a slight increase in photocurrent. The principal reason for this is the temperature variation of the semiconductor bandgap. In PV system design this effect is usually neglected.

It can be seen from (4.2.11) that the short circuit current is proportional to the irradiance (W/m^2), approximately proportional to the number of incident photons:

$$I_{sc} = C_1 G \quad (4.2.15)$$

$$C_1 = \frac{I_{sc}(1000 W/m^2)}{1000 W/m^2} \quad (4.2.16)$$

Based on the above discussion, the effects of irradiance and temperature on the I-V curve of a solar cell are shown in Figure 35 and Figure 36. It can be seen (Figure 35) that the dependence of the open circuit voltage on irradiance as well as the dependence of the short circuit current on temperature (Figure 36) is weak and can be neglected.

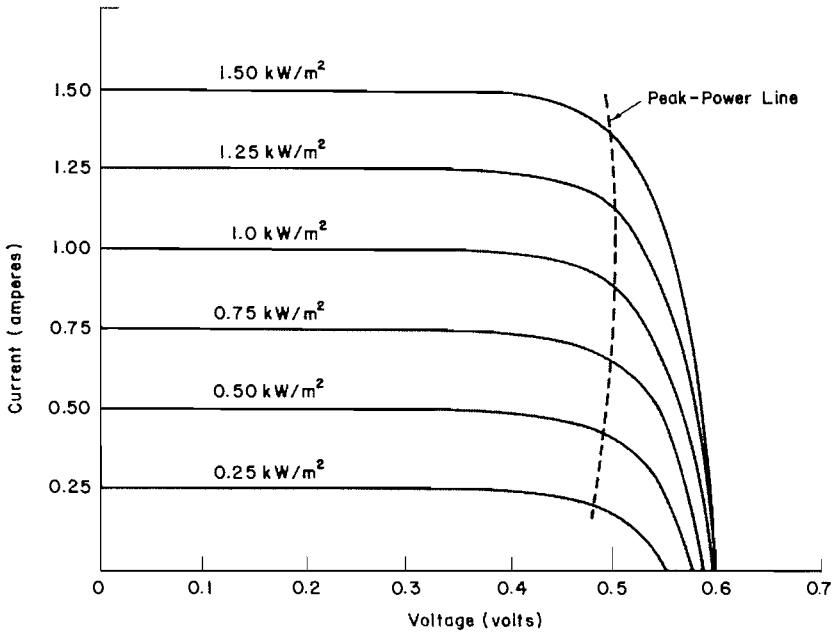

Figure 35 Influence of irradiance on the current and voltage output characteristics at constant cell temperature[58]

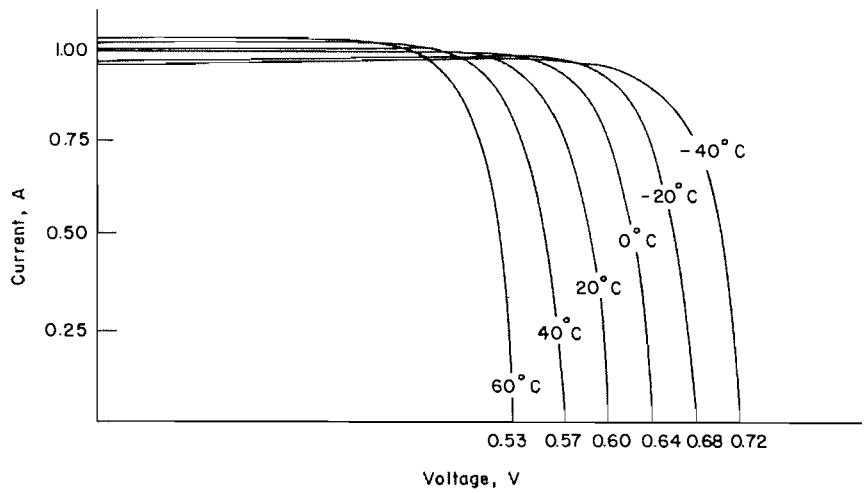

Figure 36 Influence of the temperature on the current and voltage output characteristics at constant irradiance[58]

If the cells terminals are connected to a variable resistor R and we consider that the temperature and irradiance are constant, then the working point will be determined by the intersection of the I-V characteristics of the solar cell and the load[58] (Figure 37. For a resistive load the load characteristics is a straight line with slope 1/R. Then the

power delivered to the load depends only on the value of the resistance. Only for a given value of the resistance the system operates at its maximum power point. If the resistance is small, the system will operate at the region MN of the I-V curve. In this region the cell behaves as a constant current source, with current almost equal to the short circuit current. If the load is large, the system will operate at the region PS of the I-V curve, the cell behaves as a constant voltage source, with voltage almost equal to the open circuit voltage if the series resistance is small.

In the region NP neither the voltage nor the current are constant.

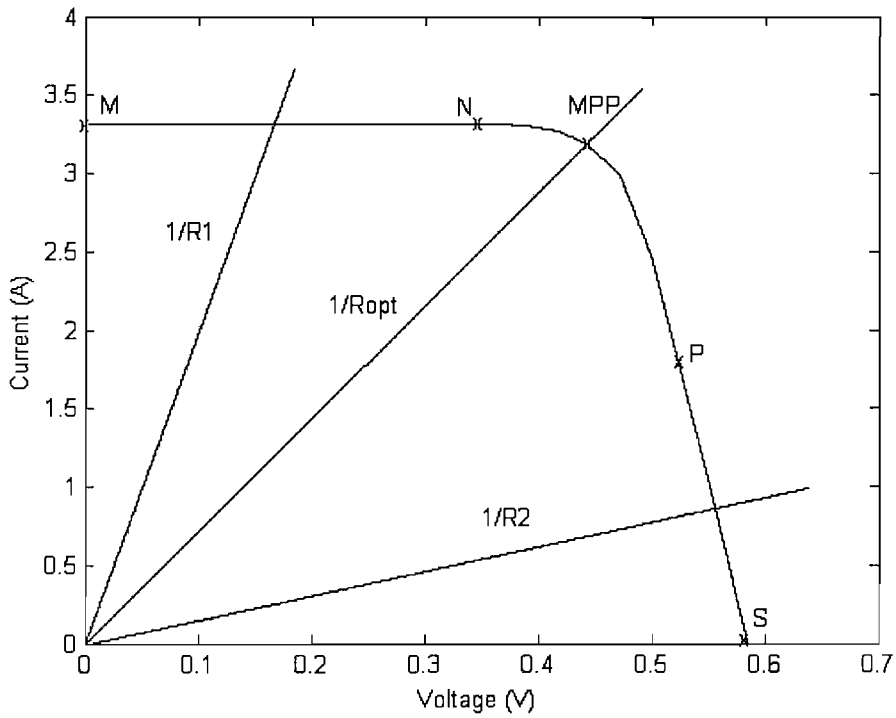

Figure 37 The operation of the solar cell of Figure 30 connected to various resistive loads, at constant irradiance and temperature. The working point is each time the intersection point of the I-V characteristic of the cell and the load curve

The operation at the area NS is strongly affected by temperature as can be seen from Figure 36. Therefore, if the output of the cell is desired to be independent of temperature it is desirable for the cell to operate at the MN part of the curve, but not too far from N.

4.2.2 PV module

The number of cells in a module is governed by the desired voltage of the module[59]. In a stand-alone system the nominal operating voltage of the system usually has to be matched to the nominal voltage of the storage subsystem, usually a lead-acid battery. Modules therefore are manufactured to work with 12V batteries. Modules that feed power to inverter at a higher voltage are now also available. As mentioned in section 1.1 we want that the system operate as a constant current source at the linear part of the I-V curve (and the power curve), so that the current and the power output are not affected by temperature changes (see Figure 36 and Figure 38). Therefore, a system of one module operating at constant voltage of 12V at STC, should operate below the MPP. This is the reason that we use 36 cells connected in series for a solar module. This number of cells gives the maximum power at standard test conditions (STC) at a voltage sufficiently above the 12 Volts. A smaller number of cells would cause problems at high operating temperatures; in a module with larger number of cells, too large a part of the voltage would be wasted. The nominal power output of a module at STC is usually called peak power of a module, and expressed in peak watts, W_p.

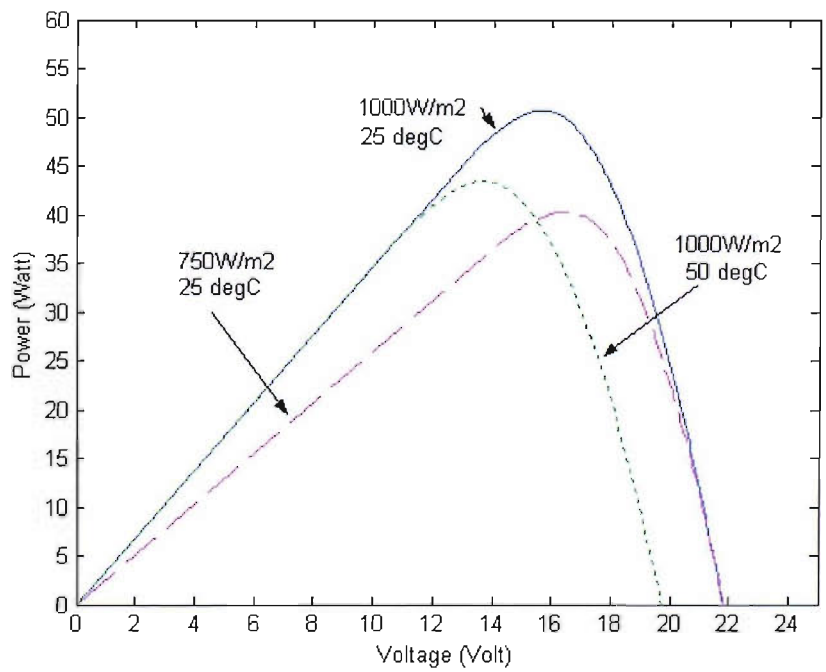

Figure 38 Power changes of module output at possible operating conditions.

The information that is usually available from the manufacturer's data for a module is the maximum power delivered by the module P_{MAX}, the short circuit current $I_{SC,}$ the open circuit voltage V_{OC} and, sometimes, the nominal cell operating temperature NOCT[7]. The first three quantities refer to the standard test conditions (STC). The nominal cell operating temperature NOCT is the temperature that is reached by the cell under conditions that resemble the way the module operates in practice (irradiance 800 W/m^2, spectrum corresponding to air mass 1.5, normal angle of incidence, ambient temperature 20^0 and wind speed 1m/sec). Given the above information it is possible to find the I-V curve of the module under any conditions of irradiance and ambient temperature. The process is shown in Figure 38:

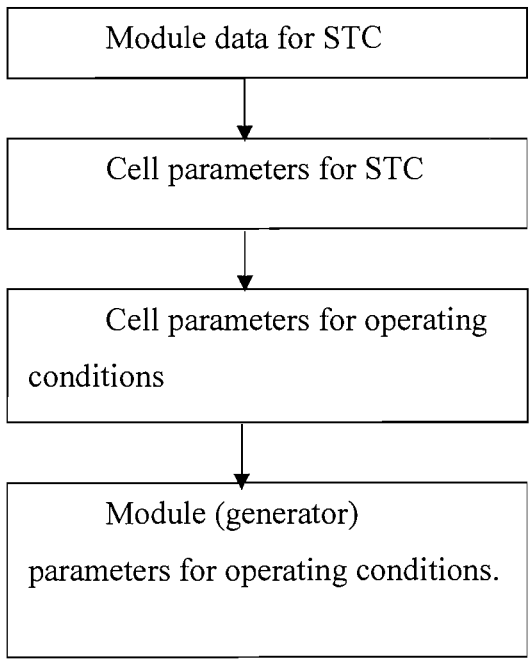

Figure 39 The diagram shows the steps in the calculations of the I-V curve of the module (generator)

The calculated parameters are the short circuit current, the open circuit voltage, the series resistance and the thermal voltage. (see sections 4.2.1, 4.2.2 and Appendix A for the detailed calculations).

In order to calculate the I-V curve of the module, under different operating conditions than the STC, usually we make the following assumptions:

- The short circuit current is proportional to the irradiance (4.2.15)
- The open circuit voltage reduces linearly with cell temperature (4.2.14)
- The difference between cell temperature and ambient temperature is proportional to the irradiance:

$$T_c - T_a = C_2 G \qquad (4.2.17)$$

where $C_2=(NOCT(^{\circ}C)-20)/80mW/cm^2$, or with a reasonable approximation[7] $C_2=0.03^{\circ}C/mW/cm^2$ if NOCT is not known.

The series resistance is unaffected by operating conditions and, in terms of the parameters of the I-V characteristic it is given by[7]:

$$R_s = \left(1 - \frac{FF}{FF_o}\right)\frac{V_{oc}}{I_{sc}} \qquad (4.2.18)$$

The above procedure neglects features such as:
The effects of temperature and spectrum on short circuit current (this implies an error less than 0.5%), the effects of irradiance on open circuit voltage and the effect of wind velocity on solar cell temperature. Also in some occations we ignore additional reflection losses when the angle of incidence of the radiation is not normal (see section 2.4).

In any case, cell temperature matters little if the module operates below the MPP, as referred to in the previous section. Figure 40 shows the I-V curves of a module under possible operating conditions.

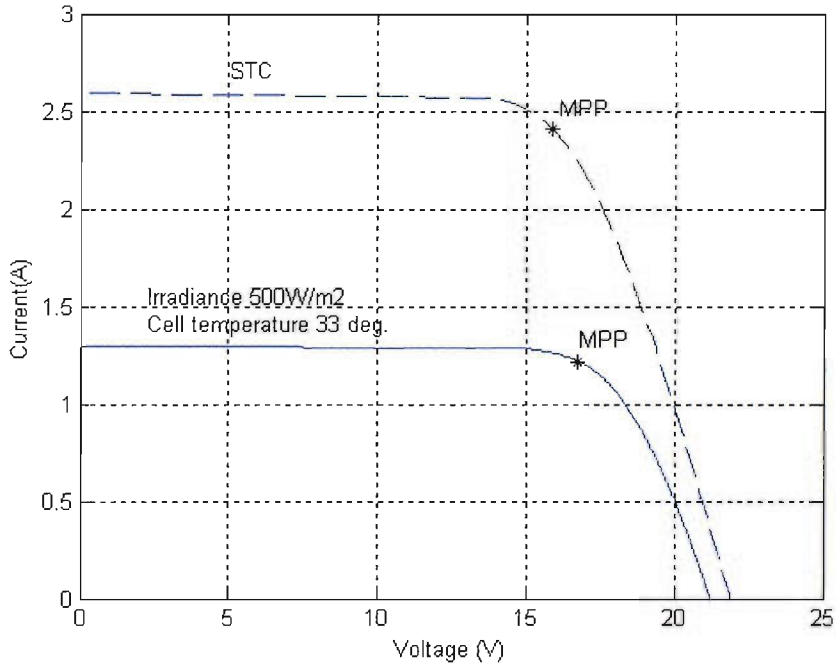

Figure 40 I-V curves of a module under possible operating conditions

4.2.3 Mismatch losses

Solar cells and modules are not identical and do not operate under the same conditions in practice. For example, sometimes a cell may have a lower short circuit current than other cells connected in series either due to the manufacture or because the cell is partly shadowed. In these cases it may act as a load and will consume the power generated by the other cells. The same will happen if a cell has lower open circuit voltage than other cells connected in parallel. The same arguments go for modules and arrays. The maximum power that the generator can deliver is therefore less than the sum of the outputs of the constituent modules. The difference is called mismatch losses[7].

Mismatch losses can be lowered or avoided all together by employing by-pass diodes-for example, across a part of a series string, or, across each module. The polarity of the diodes is reversed with respect to the polarity of the cells. As a result, the current will flow through the diode instead of flowing through the module that contains the faulty or shaded cell.

In addition, we usually connect blocking diodes in series with the module string to prevent current from flowing from the battery into the modules.

Figure 41 shows the use of blocking and by-pass diodes in a PV generator.

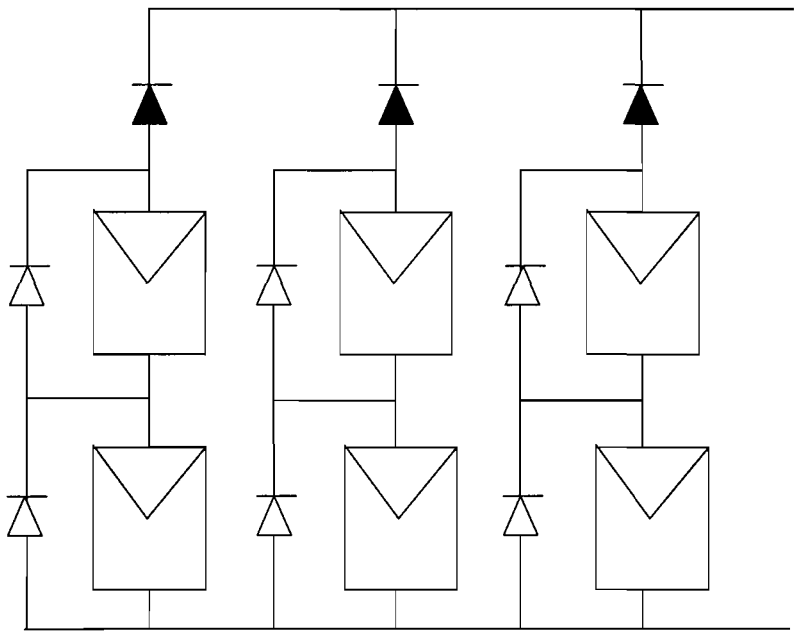

Figure 41 Photovoltaic generator with by-pass diodes (white) and blocking diodes (black)

If we neglect mismatch losses and losses in the diodes, the simplified equation of the I-V curve of the solar cell (4.2.13) gives the I-V curve of the generator as follows:

$I_{SCG}=I_{sc}N_P$ (4.2.19)

$V_{OCG}=V_{oc}N_S$ (4.2.20)

$R_{SG}=R_sN_S/N_P$ (4.2.21)

$$I_G = I_{SCG}[1-\exp\left(\frac{V_G - V_{OCG} + I_G R_{SG}}{N_S V_t}\right)] \quad (4.2.22)$$

where I_{SCG} V_{OCG} R_{SG} are the short circuit current the open circuit voltage and the series resistance of the generator respectively, N_P is the number of cells in parallel in the generator, N_S is the number of cells in series in the generator.

4.3 Modelling

This section describes the programme developed in Matlab that simulates the PV generator.

The input to the programme is the in plane irradiance the ambient temperature, the manufacturer's data for the generator, and the value of the resistive load.

The process of the calculations is as described below:

- Calculation of the series resistance of the generator from the manufacturer's data We assume that the series resistance is constant for all operating conditions (see section 4.2.2).The steps of the calculations are:
    - Calculation of the fill factor (FF_o) of the ideal solar cell (series resistance equals to zero) under standard test conditions,(see section 4.2.1)
    - Calculation of the fill factor (FF) of a solar cell under standard test conditions, (see section 4.2.1).
    - Calculation of the series resistance, of the cell the module and the generator (see section 4.2.2) using the fill factors calculated in the two previous steps.
- Calculation of the cell temperature under operating conditions using the in-plane irradiance and the ambient temperature (see section 4.2.2)
- Calculation of the open circuit voltage under operating conditions, using the cell temperature, from the previous calculation and the manufacturer's data, (see section 4.2.1).
- Calculation of the short circuit current of the generator under operating conditions from the in plane irradiance and the manufacturer's data
- Calculation of the I-V curve of the generator under operating conditions solving iteratively the equation (4.2.22).
- Calculation of the maximum power output of the generator, assuming that it is always operating at its maximum power point.

- Calculation of the power output of the generator, when it is connected to a resistive load, using interpolation to find the intersection point between the load curve (I=V/R) and the generator I-V curve at any instant.

The analytical calculations as used in Matlab programme are in Appendix A. The flow chart of the programme is shown in Figure 42.

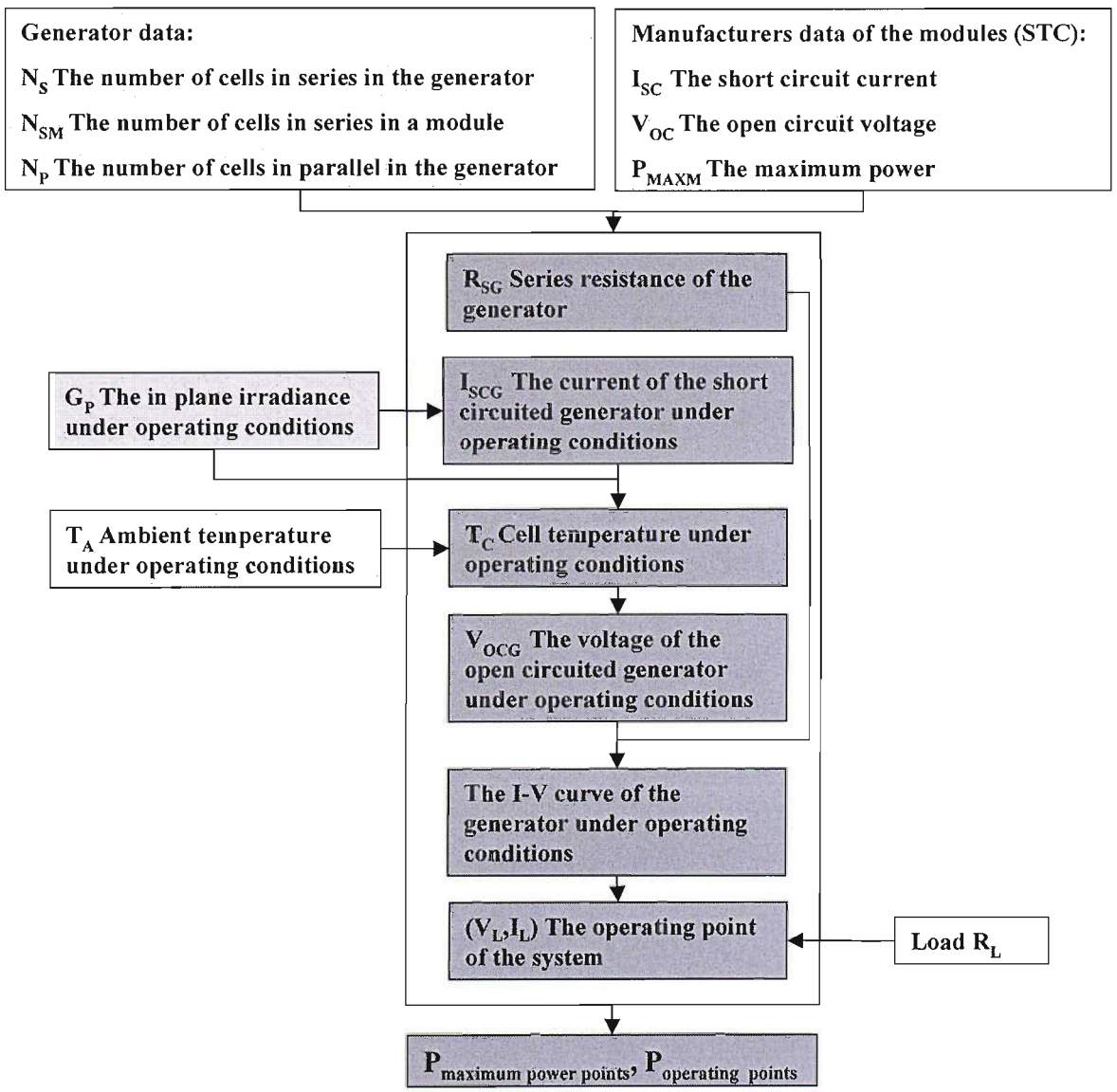

Figure 42 Flow chart of Matlab Modelling

4.4 Results

The graphs in Figure 43 to Figure 48 illustrate the power produced by the system at the corresponding in-plane irradiance variations, also illustrated in each figure. The measured and the calculated power are illustrated on the graphs, as well as the power that the system would produce if it were operating continuously at the maximum power points. The PV generator model developed here was used for the simulation of the power output. The experimental results were obtained using the set-up described in section 3.2.

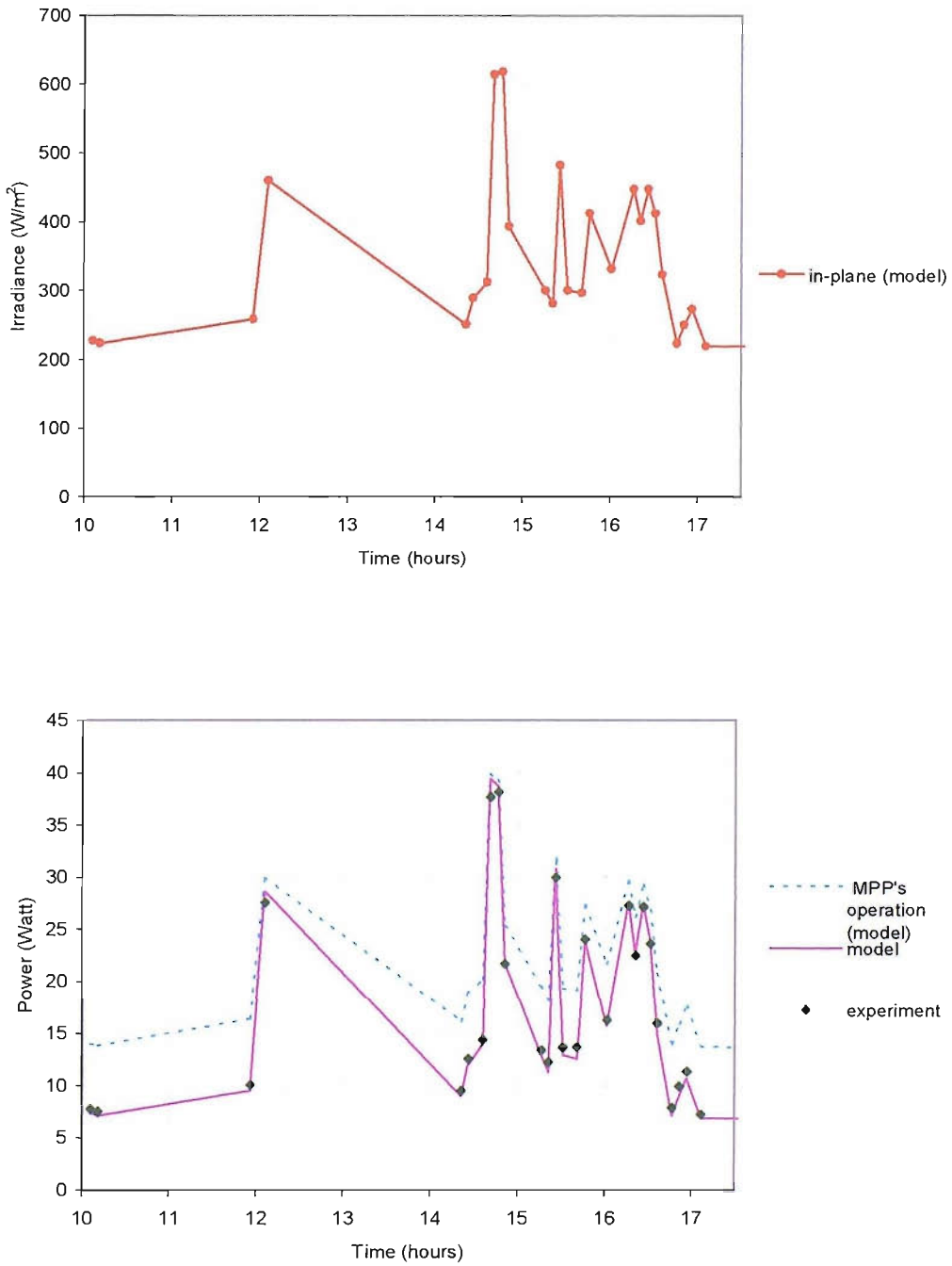

Figure 43 In-plane irradiance and power produced on the 18/6/01 that the generator is connected to a 24 Ohm resistor

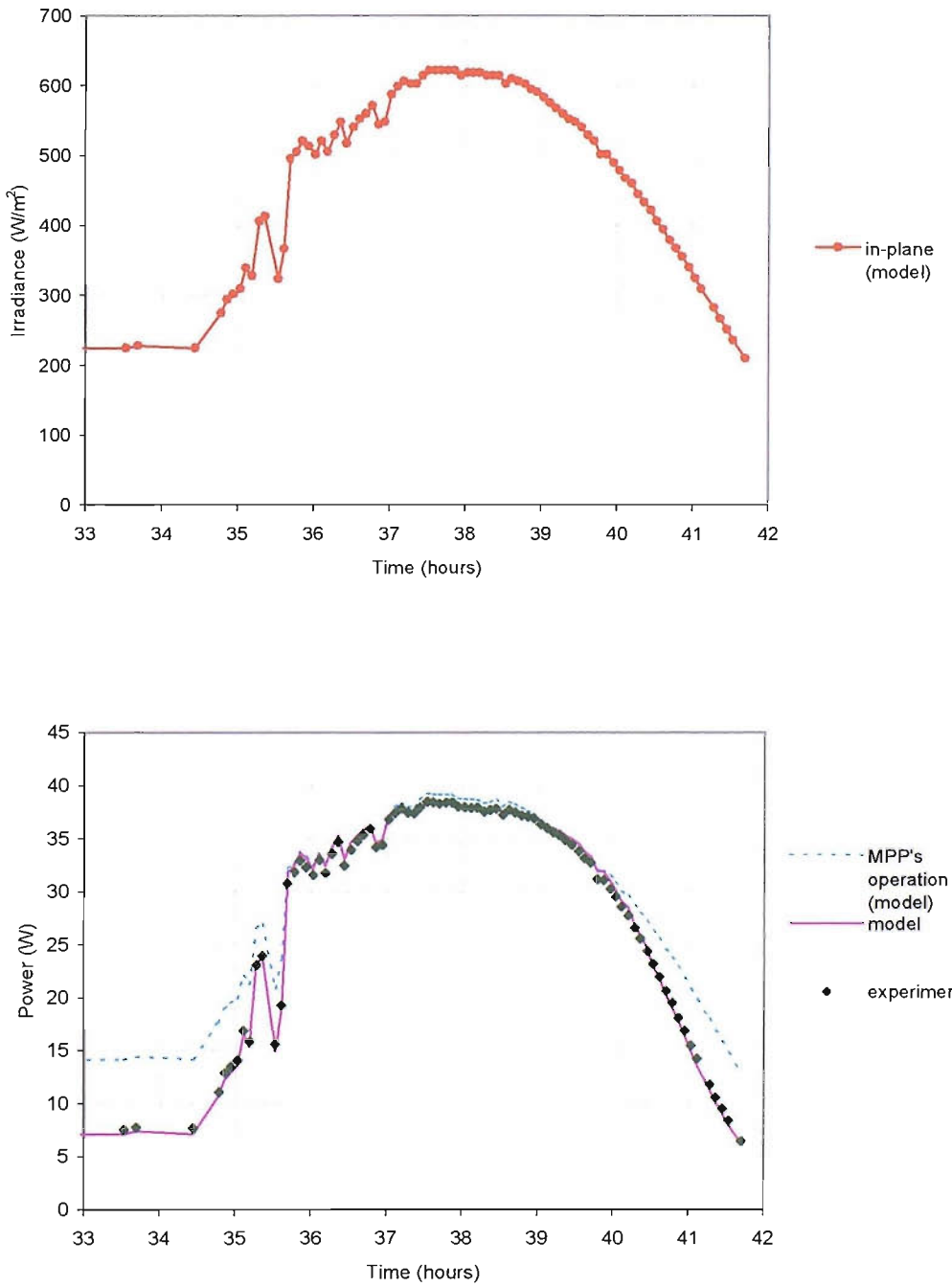

Figure 44 In-plane irradiance and power produced on the 19/6/01 that the generator is connected to a 24 Ohm resistor

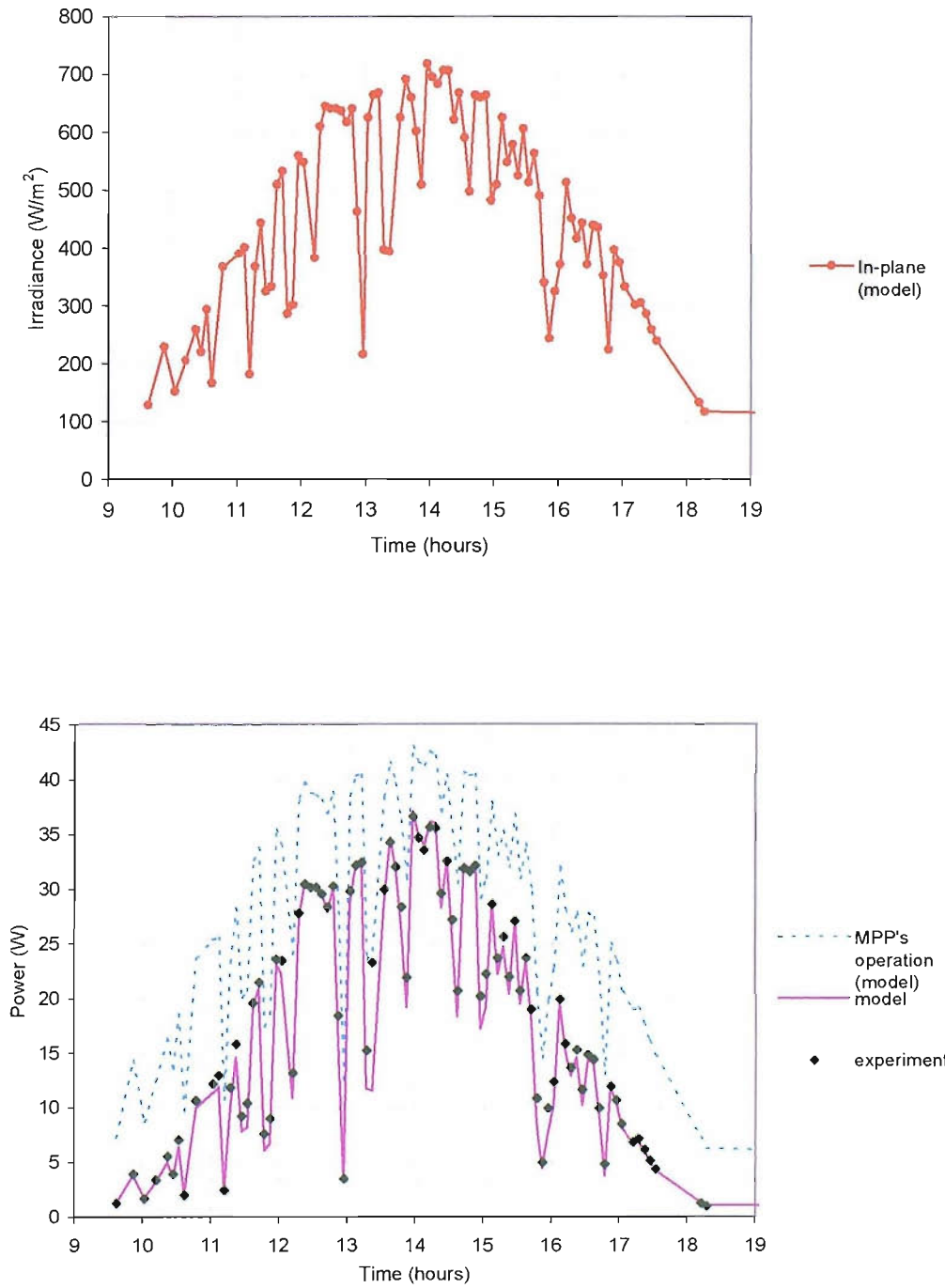

Figure 45 In-plane irradiance and power produced on the 21/6/01 that the generator is connected to a 12 Ohm resistor

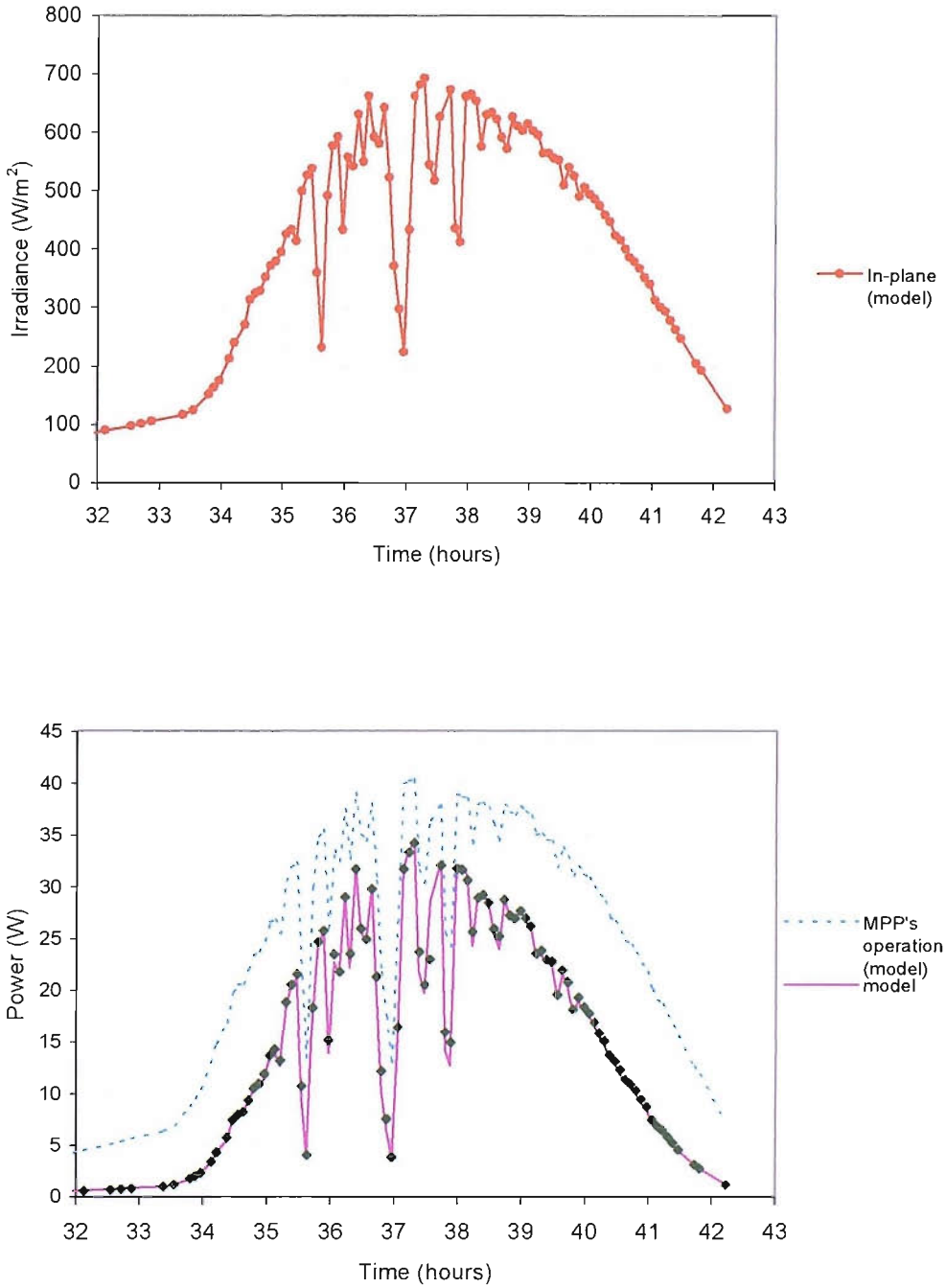

Figure 46 In-plane irradiance and power produced on the 22/6/01 that the generator is connected to a 12 Ohm resistor

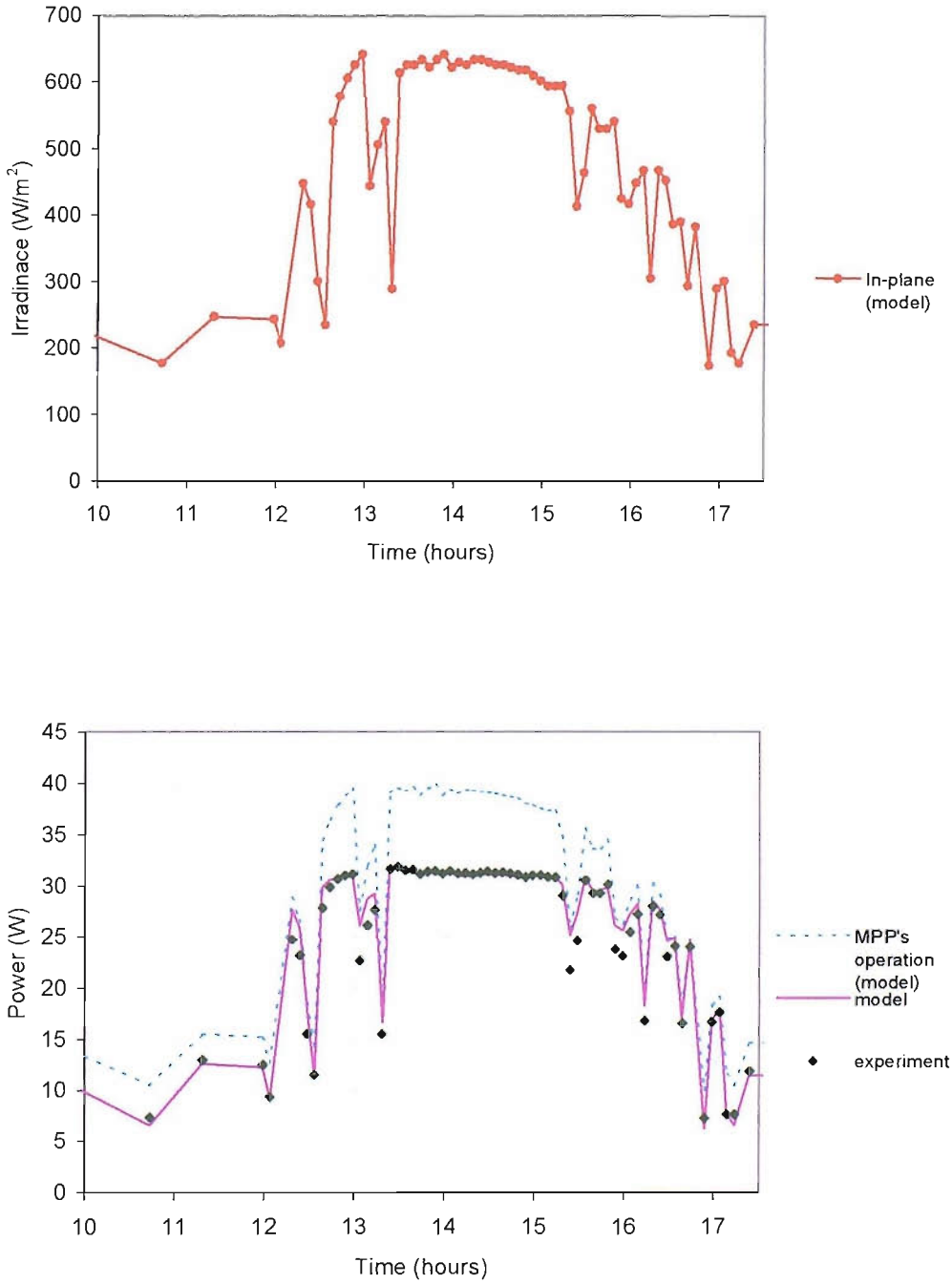

Figure 47 In-plane irradiance and power produced on the 27/6/01 that the generator is connected to a 36 Ohm resistor

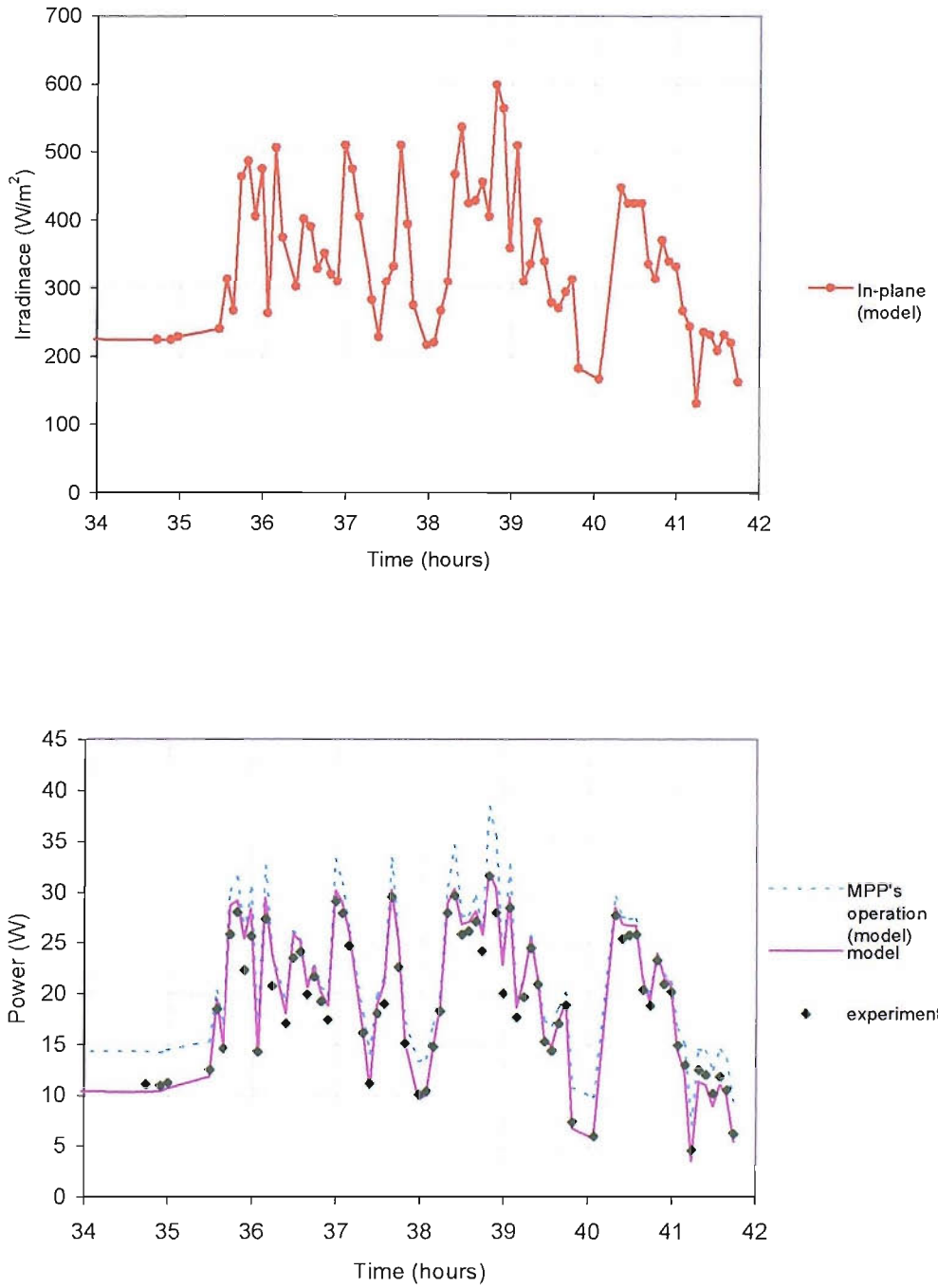

Figure 48 In-plane irradiance and power produced on the 28/6/01 that the generator is connected to a 36 Ohm resistor

There are three parameters that had to be adjusted to fit the calculated power curves to the experimental data presented from Figure 43 to Figure 48. Those are the series resistance, the parallel resistance and the ideality factor (see section 4.2.1). Taking into account the effect of those parameters on the I-V curve together with our conclusions from Figure 49 regarding the system operating points we can easily understand the following:

Firstly, the sensitivity of the power output to the value of series resistance is higher when the 36 Ohm, or the 24 Ohm load is connected (Figure 33, Figure 48). Secondly, the power output is affected mainly by the value of the parallel resistance when the 12 Ohm load is connected. Finally, the effect of the ideality factor is more pronounced when the 24 Ohm load is connected and under some conditions with the 36 Ohm load.

It has been found here that the calculated value of series resistance according to the formalism presented in section 4.2.1, that was used in Matlab modelling (see appendix A) does not result in good agreement with the measured values of power. An improvement can be made if we use the value of 3.1 Ohm instead of 2.95 Ohm, the calculated value. The higher value used, accounts for the additional losses in the leads and was found by trial and error. The values of the measured current are found to be less than the values of the short circuit current when the 12 ohm resistor was connected. This means that the parallel resistance (see equation (4.2.7)) should be taken into account. Parallel resistance of 600 Ohms gives a good fit to the recorded data. The ideality factor was set at 1.3.

We should note, that in the data analysis, in order to obtain the power curves (Figure 43 to Figure 48), we consider the values that correspond to recorded voltage and current, with ratio 1% plus or minus the value of the load resistance used.

In addition, it was verified that the short circuit current of the generator is the same (within an error of less than1%) with that of the modules used for current sensing. However in some cases, for short periods of time (less than 5 min) this error can reach values 5-9%. This is due to variations in shading and received irradiance, arising from the different position of the modules on the façade.

The errors between the measured values of power and the calculated ones for the three cases of different load connection are presented in Table 3.

Resistive load	12 Ohm	24 Ohm	36 Ohm
Average error (%) in the calculated power output	4.5	2.4	4.6

Table 2 Average error (%) in the calculated power output of the system

The disagreement between the calculated power and the recorded values in some cases of rapid change (e.g. Figure 48) in the power output should be attributed to the experimental error. In particular, to the averaging procedure, used by the interface program of the data acquisition system for the calculation of the power: The power is calculated every 2.5 sec from the measured values of voltage and current and averaged and logged every five minutes. This results in underestimation of power when the actual power curve is concave and an overestimation when is convex.

4.6 Conclusions

The operation of the photovoltaic generator has been reviewed, including the operation of the solar cell under standard conditions, the operation under variable illumination and temperature in practice, and the effect of mismatch losses. A model has been developed using the Matlab software. This model is based on the mathematical formalism suggested by Lorenzo, based on the irradiance dependence of the short circuit current and the dependence of the open circuit on the temperature of the solar cell.

The model has been compared with experimental data obtained by operating an experimental array under solar illumination for several days with a resistive load. We have found that, after an allowance is made for system components such as the series and parallel resistances, the model gives a good agreement with experiment, and can be used as a tool for further work.

5. BATTERIES FOR PV SYSTEMS

5.1 Introduction

The energy storage for a stand-alone system is usually a lead acid electrochemical battery. Although various advanced batteries might be used in specialized applications (for example, NiCd batteries at low temperatures or where rugged performance is needed, redox batteries for utility applications, etc.), lead acid batteries remain the usual choice for stand-alone systems. The main lead-acid battery types include SLI (starting, lighting and ignition) for automotive applications, traction batteries with good resistance to cycling, and back-up (or floating) batteries which operate near full charge. Some manufacturers make batteries with plates as in traction battery but having larger case to increase the reserve of electrolyte. These batteries combine the advantages of low cost and low maintenance requirement, so they are often a good choice for PV applications[7]. In other applications with shallow daily discharge cycle, floating batteries may be more appropriate. Due to the different types of batteries, there is not a battery model of general validity and for different types of battery the existing models have to be adjusted.

This section gives an overview of lead-acid battery operation and modelling. The possibility of modelling the battery operation is examined by comparing Copetti and Chenlo model-one of the basic existing battery models- with results from experiments conducted in this work.

It was found that the parameters of the Copetti and Chenlo model should be readjusted in order to describe the battery operation.

Section 5.2 explains the operation the construction, and a brief overview of the philosophy of the existing battery models, with the main emphasis given in the Copetti and Chenlo model. Section 5.3 is a comparison of experimental data with Copetti and Chenlo model. This includes determination of model parameters, model sensitivity to parameter change and sensitivity to temperature. Section 5.4 presents the conclusions.

5.2 Literature review

5.2.1 The operation of lead-acid batteries

The principal components of a lead-acid battery include: an anode of lead oxide (PdO_2), the positive electrode, a cathode of lead (Pb), the negative electrode and an electrolyte of sulphuric acid (H_2SO_4) diluted in water. Battery operation (Figure 50) is based on chemical reactions in the battery during charge and discharge process. During charge[6] current flows from the generator to the battery. At the anode, electrons are produced and lead oxide is formed on the electrode. At the cathode, electrons are absorbed and lead is formed on the electrode. During discharge, current flows from the battery to the load. At the anode (positive electrode) electrons are absorbed and lead sulphate is formed on the electrode. At the cathode (negative electrode) electrons are produced and lead sulphate is formed on the electrode.

The chemical reactions are:

Anode:

$$PbO_2 + SO_4^{-2} + 4H^+ + 2e^- \underset{charge}{\overset{discharge}{\rightleftarrows}} PbSO_4 + 2H_2O$$

Cathode:

$$Pb + SO_4^{2-} \underset{charge}{\overset{discharge}{\rightleftarrows}} PbSO_4 + 2e^-$$

The whole reaction is:

$$Pb + PbO_2 + 2H_2SO_4 \underset{charge}{\overset{discharge}{\rightleftarrows}} 2PbSO_4 + 2H_2O$$

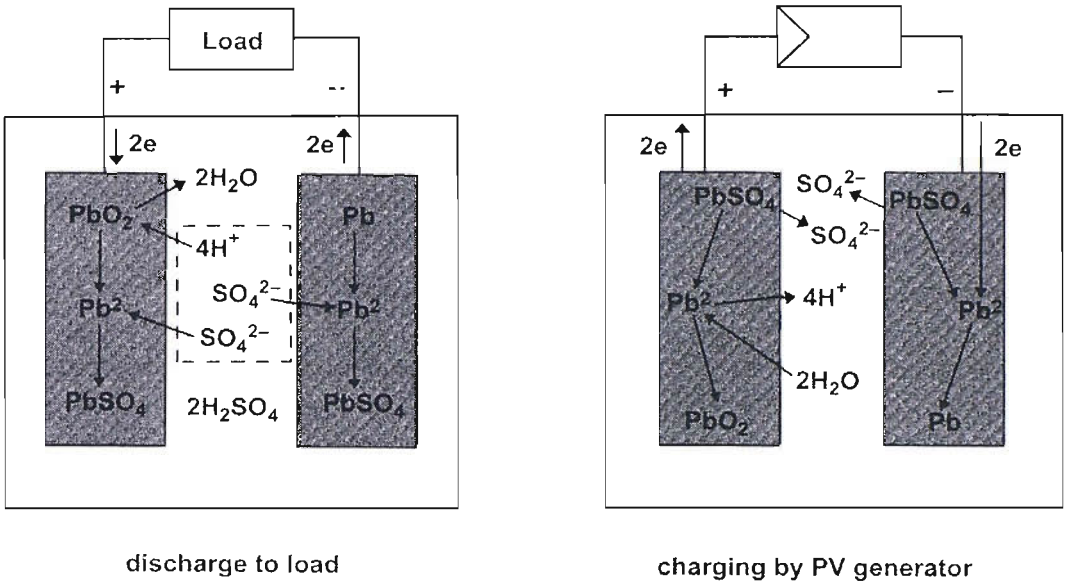

Figure 50 Battery operation

5.2.2 Battery construction[7]

The anode (positive electrode) consists of a grid of solid lead and a porous sponge of lead oxide (PbO_2) that is filling the grid. In batteries that are frequently discharged, porous covers (made of plastic or fiberglass) in form of a line of tubes side by side, may be used to cover the positive plate. The reason of these covers is to prevent active material being lost during discharge, due to mechanical stresses caused by variations in volume of active material of the plates: the volume of lead sulphate that is formed in the electrodes during discharge is 3 times the volume of lead and 1.5 times the volume of lead oxide. The cathode consists of a grid of solid lead and a porous sponge of lead (Pb) that is filling the grid. In addition to the electrodes the battery contains separators of porous plastic material

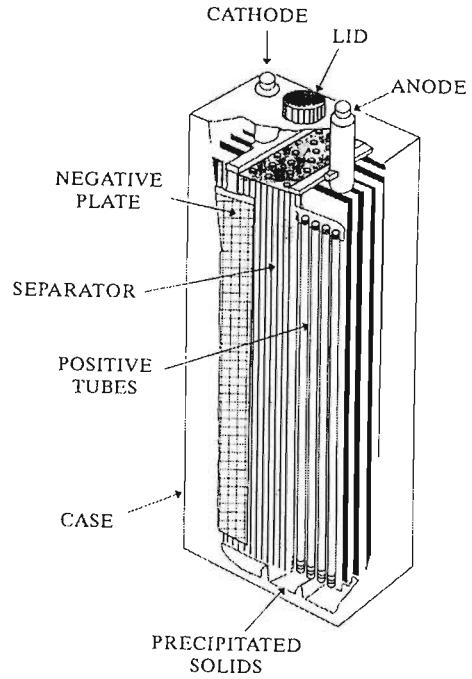

Figure 51 Battery construction[7]

5.2.3 Battery performance concepts

This section explains the basic concepts that are needed to describe the battery operation.

Polarization losses[60]

Not all the energy of the electrochemical reactions in the battery can be converted to useful electric energy and this is due to polarization losses. The amount by which the voltage of the cell deviates from its equilibrium (zero current) value is called the polarization voltage. It occurs when a current passes through the electrodes and can be associated with two causes:

- The ohmic drop in the electrolyte, separators, electrodes and connectors
- Electrode losses, which are related with physical phenomena within the battery that follow the chemical reactions.

Specific gravity

The decrease in the electrolyte concentration –traditionally termed specific gravity is a convenient means of determining the degree of discharge which has taken place or, conversely, for checking the state of charge of the battery (see latter in this

chapter). In a fully charged battery the specific gravity is normally between 1.24 and 1.28 and in a fully discharged battery is 1.08-1.14[61] depending on the discharge rate and the amount of free acid. During the charge process the specific gravity cannot be correlated with the state of charge of the battery until near the end of the charge when gassing provides a good mixing of the electrolyte.

Voltage of a cell or a battery[62]

Different references are made to the voltage of a cell or battery:

- *The open circuit voltage* is the voltage under a no-load condition. The open circuit voltage is determined solely by concentrations of acids at the plates and takes a stabilized value after sometime of rest, when the acid becomes uniform everywhere in the cell. After charging the open circuit voltage decreases until it reaches the stabilized value, while after discharging increases. The open circuit voltage is also influenced by temperature-for specific gravity >1.04 it increases with increasing temperature.
- *The nominal voltage* is one that is generally accepted as typical of the operating voltage of the battery and is the value of voltage given by the manufacturer.
- *The working voltage* is representative of the actual operating voltage of the battery. The working voltage is lower than the open circuit voltage during discharge and higher during charge. The actual values depend on the state of charge, the current and especially at the end of charge the type of battery.
- *The end or cut-off* voltage is designed as the end of the discharge. Usually it is the voltage above which most of the capacity of the cell or the battery has been delivered. It is standard practice to assume that the voltage has reached 100% depth of discharge at the 'knee' of the voltage curve (Figure 52). The value of the cut off voltage for the cell is dependent upon both the discharge rate and the temperature.

For the lead-acid batteries, the open circuit voltage is 2.1 V, the nominal voltage is 2.0V, the working voltage is between 1.8 and 2.0V, and the end voltage is typically 1.75V. The working voltage on charge may range from 2.3 to 2.8V.

The initial voltage of the cell under a discharge load is lower than the open circuit voltage due to the internal cell resistance and the resultant IR drop as well as polarization effects at both electrodes. The voltage also drops during discharge as the cell resistance increases (Figure 52). Curve 2 represents a cell with higher internal resistance or a higher discharge rate, compared to the cell represented by curve 1. As the cell resistance or the discharge current increase the discharge voltage decreases and the discharge is faster.

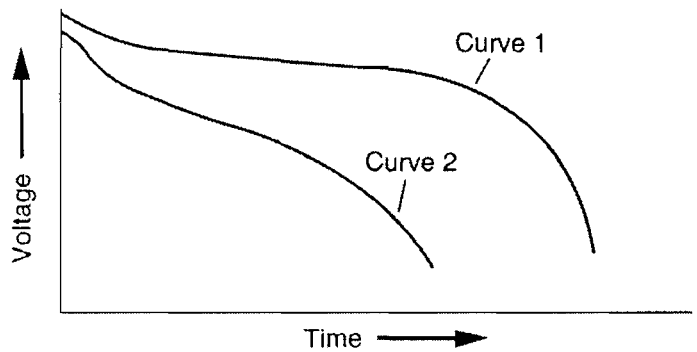

Figure 52 Characteristic discharge curves

When the battery stands idle after discharge, certain chemical and physical changes take place, which can result in a recovery of battery voltage. Thus the voltage of a battery, which has dropped during heavy discharge will rise after a rest period, giving a shawtooth shaped discharge (Figure 53).

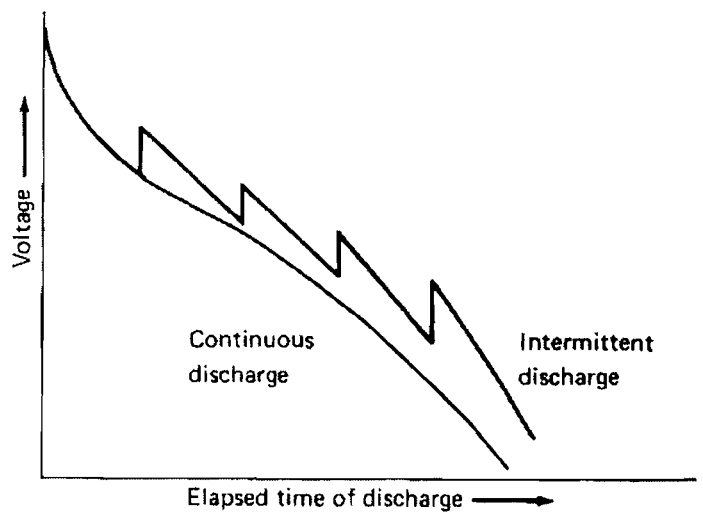

Figure 53 Intermittent discharge

Battery capacity

The nominal (or rated) capacity of the battery C_B refers to the charge (Ah) that can be extracted from the battery[7] during discharge at constant current to the cut off voltage. The capacity obtained from a lead-acid cell is strongly dependent on the rate of discharge (in other words the discharge current). During a rapid discharge, the electrochemical reactions take place mainly on the surface of the plates because of the limited time available for adequate diffusion of acid into the pores of the active material. Moreover, the reaction product (PbSO4) tends to close off the pores, a process which further restricts the ingress of acid. Thus capacity is severely reduced at heavy rates of discharge. Figure 54 shows the dependence of battery capacity on the discharge rate. The battery capacity also depends on the battery temperature.

In order to compare battery capacities[61] the rated capacity is written with the symbol C_x where x refers to the number of hours until the discharge is complete. The rated capacity should be accompanied by the appropriate end voltage (final discharge voltage) and the battery temperature. The rated capacity is often given as the 10 hour capacity, and written as C_{10}: for example C_{10}=100Ah to 10.8V at 20°C. The nominal capacity of the battery and the current at which it is charged or discharged can be described in terms of a charge or discharge regime, or a discharge rate. For example, if a 100Ah battery is discharged at 5 A, the discharge regime (or discharge rate) is said to be 20 hours and the value of the discharge current is written as I_{20} or $C_{20}/20$.

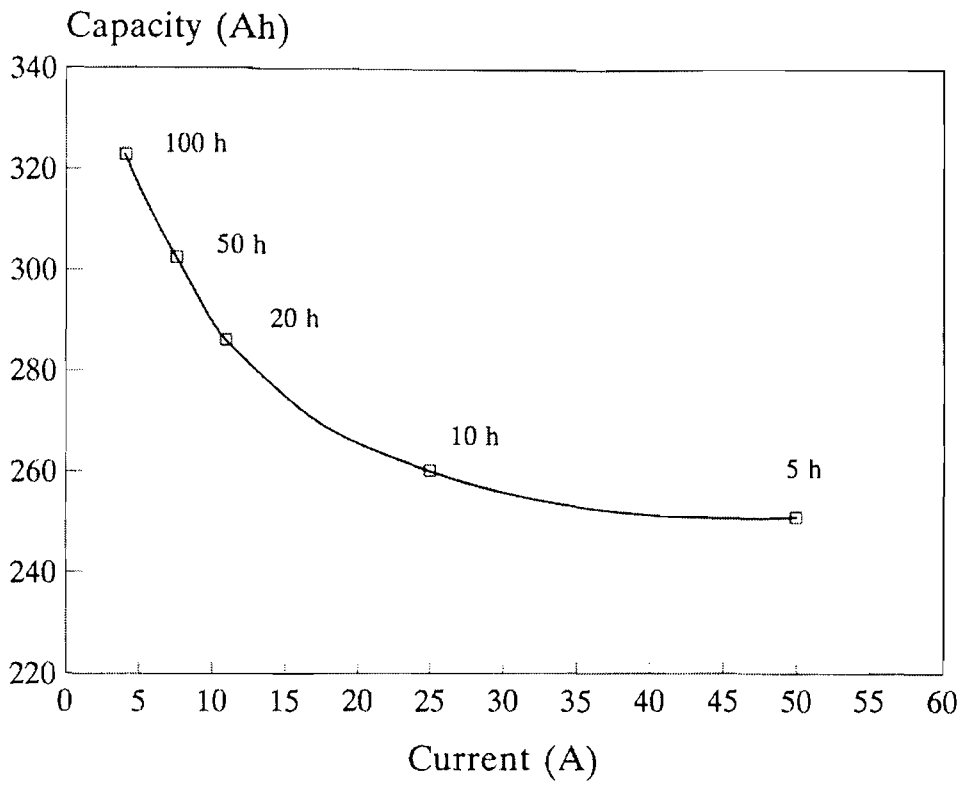

Figure 54 Variation of the capacity with the discharge regime at constant temperature. The numbers show the discharge time

Battery state of charge (SOC)

State of charge of the battery SOC is the fraction of the nominal capacity still available in the battery. The depth of discharge (DOD) is defined as 1-SOC, the complement of the state of charge.

Battery efficiency

The battery efficiency[5] is very important due to the relative high cost of the PV array. However, there is no much information in the literature about ways of measuring the battery efficiency-especially given the fact that the concepts of the 'full' battery and the battery SOC are not in practice clearly defined. There are three characterizations of battery efficiency in the literature, the coulombic or storage or charging efficiency, the voltage efficiency and the energy efficiency. However, it is most common to refer to the charging efficiency of the battery, as a way to characterise the battery efficiency. The three ways to characterize the battery efficiency are analysed as follows:

- Coulombic or storage or charging efficiency, is about 90% at 25°C[4] (or 95% according to other authors[61]) and refers to the amount of charge (Ahs) able to be retrieved from the battery, relative to the amount put in during charging. It is affected by self-discharge.

  Until a lead acid battery is 90-95% charged[61], almost no current is wasted in producing gases. The exact charge efficiency of the battery depends on the depth of discharge (DOD), and the current at which it is recharged. Battery manufacturers do not often (or routinely) measure the Ah efficiency of batteries, and when they do their definitions and measurement conditions can vary quite a lot[63]. Most commonly, we find Ah efficiencies quoted as the Ah removed by constant current discharging to some DOD divided by the Ah delivered in some 'complete' recharge which will include some overcharging. It is rare to find reports of measured Ah efficiencies where the recharging has been made with a constant current, or even a current that varies as a typical PV recharging current would.

- Voltage efficiency is the ratio between discharge and charge voltage. It is about 87%[4] and reflects the fact that the charge retrieved from the battery at a lower voltage level than was necessary to put the charge into the battery.

- Energy efficiency is the ratio between the energy discharged and the energy consumed during charge. It is about 78% and is the [coulombic efficiency]*[voltage efficiency].

5.2.4 Battery models

Simplified sizing models (as described, for example, in section 6.3) are based on the energy flux in and out of battery[7]. A more complete description of the battery operation (for example the voltage at battery terminals, the extent of overcharge (or discharge), or the likelihood of stratification) requires a more detailed model.

A battery model may give a macroscopic view of the parameters that describe the battery operation, describe in detail the chemical and physical phenomena that take place within the battery structure, or model the battery as an electrical circuit. In the first category belongs the Shepherd model[64], an improvement by Copetti and

Chenlo[65], and a further improvement by Guasch and Silvestre[66,67,68]. In the second category belong a model by Hiram Gu[69] and the improvement of the model by W.B. Gu[80]. The third category includes the recent models by Salameh[70] and by Ross[71].

This work follows principally the paper by Copetti and Chenlo which has been used with success in photovoltaic applications[7,67].

The Copetti and Chenlo model is based on the observation that the product of the capacity and the internal resistance of the battery is very similar from one battery to the other. By writing the equations as functions of C_{10} battery capacity rated the model is claimed to be valid for any size of lead/acid battery.

This model consists of the following equations which describe the discharge and charge:

$$V_D = [A_D - B_D \cdot (1 - SOC)] - \frac{I}{C_{10}}\left(\frac{C_D}{1 + I^{D_D}} + \frac{E_D}{SOC^{F_D}} + G_D\right) \cdot (1 - H_D \cdot \Delta T) \qquad (1)$$

$$V_C = [A_C + B_C \cdot SOC] + \frac{I}{C_{10}}\left[\frac{C_C}{1 + I^{D_C}} + \frac{E_C}{(1 - SOC)^{F_C}} + G_C\right) \cdot (1 - H_C \cdot \Delta T) \qquad (2)$$

The parameter A_D has the meaning of the open circuit voltage. The parameter B_D relates the open circuit voltage to the battery state of charge. The parameters C_D, D_D, E_D, F_D, are coefficients which describe losses related with the internal resistance of the battery. The parameter H_D gives the temperature dependence.

5.3 Comparison of experimental data with Copetti and Chenlo model

5.3.1 Determination of model parameters

Experiment

The voltage and the current are monitored during two discharge-charge processes. Each discharge process starts from rest and the initial values of open circuit voltage are recorded. The discharging occurs under constant load-different for each discharge. Because the discharge is slow, the value of discharge current is almost

constant during the process. Charging starts immediately after discharge and is at constant current. The charging current-different value for each charge- is selected to be similar to the charging currents of each battery of the stand-alone system of section 3.3 when the radiation is high.

The values of voltage are averaged over every hour to be compared with modelling results using Copetti and Chenlo model (see section 5.2.4). The results are the same if instead of using averaged values of voltage we have used the voltage value at the end of each hour. This is because the voltage changes very slowly.

The discharge is modelled here from fully charged battery down to the value of the cut off voltage. The charge is modelled from 12 V voltage values up to full state of charge. The initial value of charging voltage for the model validation is chosen to be about the minimum value reached by the voltage of the stand-alone system of section 3.3.

No attempt was made to fit the model during overcharge as the charging efficiency is very low in this regime, and the model has little relevance to the present work.

The parameters of the model were extracted by visual fitting of the curves to the experimental data. Table 4 shows the original parameters and the estimated parameters for the discharge and charge in correspondence.

DISCHARGE		
	Copetti-Chenlo model	Present work
A_D	2.085	*2.133*
B_D	0.12	*0.19*
C_D	4	*3*
D_D	1.3	*2*
E_D	0.027	0.027
F_D	1.2	*0.8*
G_D	0.02	0.02
H_D	0.007	0.007

Table 3 Parameter fitting of discharge curves

CHARGE		
	Copetti-Chenlo model	Present work
A_C	2	*1.948*
B_C	0.16	*0.31*
C_C	6	*3.5*
D_C	0.86	0.86
E_C	0.48	0.48
F_C	1.2	1.2
G_C	0.036	0.036
H_C	0.025	0.025

Table 4 Parameter fitting of charge curves

Results

The results are presented in Figure 55 which shows the discharge curve and in Figure 56 which shows the charge curve.

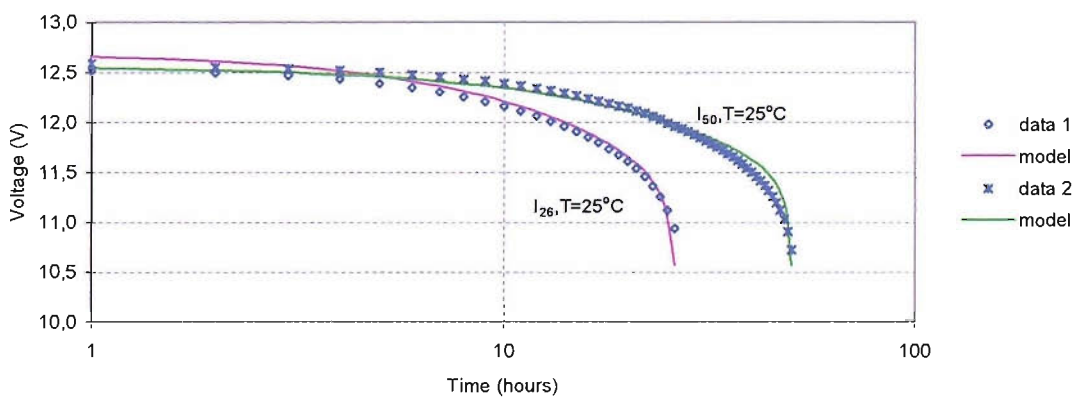

Figure 55 Experimental and modelling discharge curves

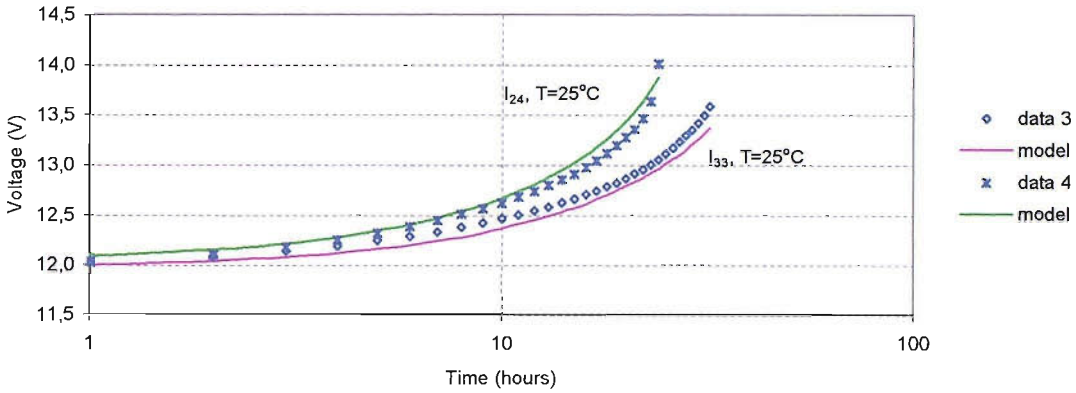

Figure 56 Experimental and modelling charge curves

Discussion

After the parameter adjustment, as it can be seen from the graphs in Figure 55 and Figure 56 the model agrees well with the experimental data.

Regarding the modelling of discharge process:

The second discharge (data 2) starts from a slightly higher value of initial open circuit voltage than the first does (see Figure 55). It can be seen from Figure 55 that the model with the adjusted parameters approximates better the beginning of the second discharge than the beginning of the first discharge. Therefore, certain values of adjusted parameters can model discharges that start from approximately the same open circuit voltage, (or the same SOC). Otherwise, different parameters should be used in the model of each discharge.

Regarding the modelling of charging process the same argument goes regarding the adjusted parameters.

The adjusted values of the parameters for both the discharge and charge process are very similar with the values used by Daniel Guasch Murillo in his model[72,73,74] (an improvement of the Copetti and Chenlo model) extracted using the Levenberg-Marquardt algorithm[75,76].

5.3.2 Model sensitivity to parameter change

In this section we are discussing the sensitivity of the model to the parameters, using some experimental results from the previous section.

Regarding the modelling of discharge process:

The parameter A_D shifts the whole curve to lower or higher values as it can be seen from Figure 57 and Figure 58. The parameter B_D changes the shape of the curve after the initial hours of the discharge (smaller B_D means slower discharge and sudden reduction of the voltage at the final stages of the discharge). The rest of the parameters have less effect on the discharge curve.

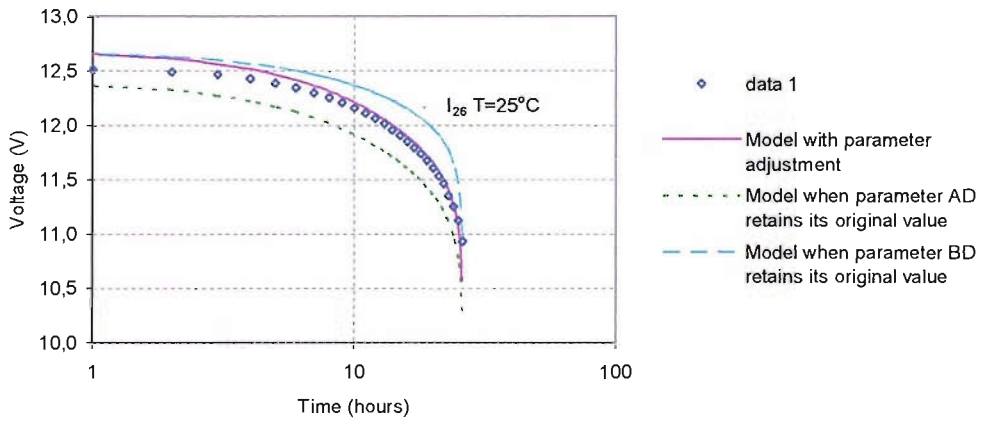

Figure 57 Sensitivity of the model to the parameters A_D and B_D. Discharge at I_{26}, T=25°C-Experimental data and modelling results

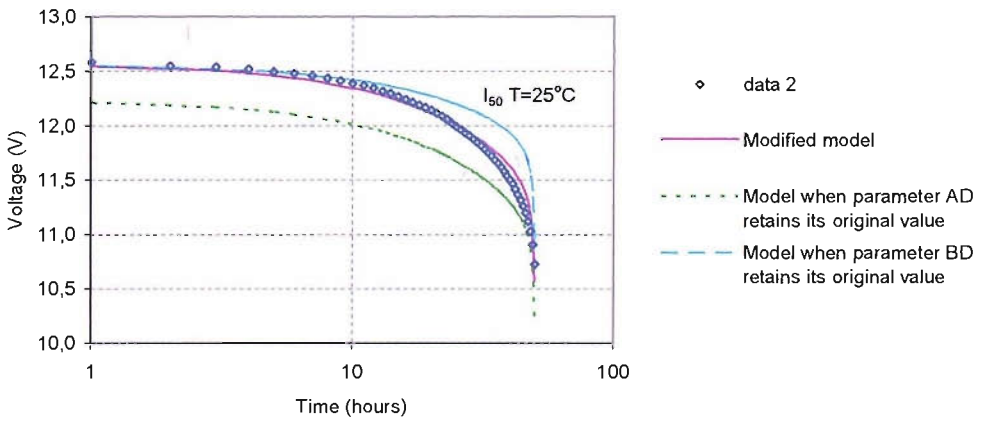

Figure 58 Sensitivity of the model to the parameters A_D and B_D. Discharge at I_{50}, T=25°C-Experimental data and modelling results

Regarding the modelling of charging process:

Similarly with discharge, the parameter A_C shifts the whole curve upwards or downwards, while the parameter B_C simulates slower charge when it takes a lower value.

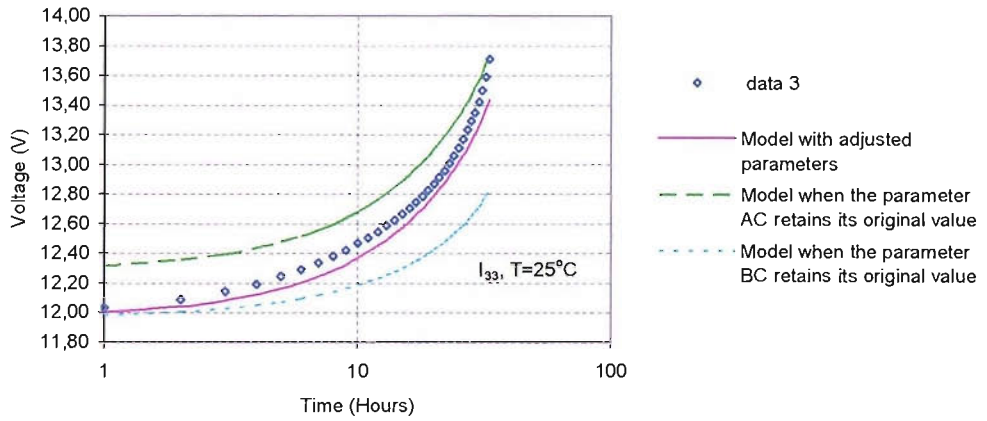

Figure 59 Sensitivity of the model to the parameters A_C and B_C. Discharge at I_{33}, T=25°C-Experimental data and modelling results

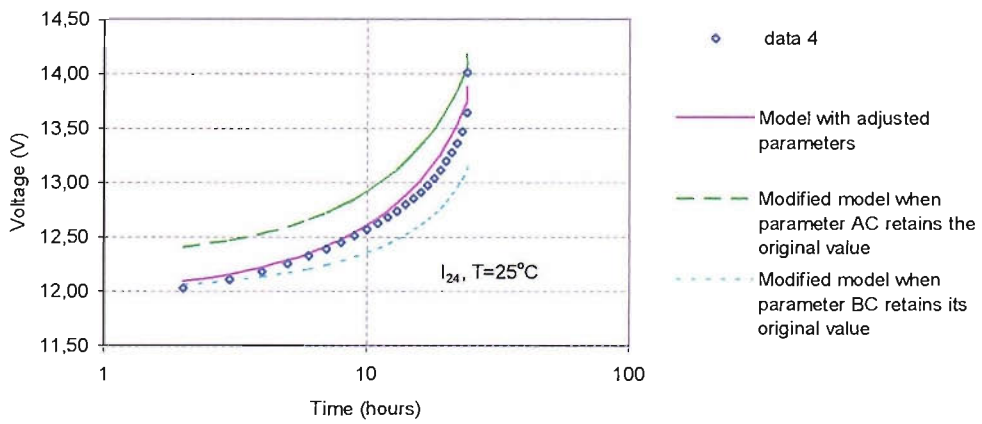

Figure 60 Sensitivity of the model to the parameters A_C and B_C. Discharge at I_{24}, T=25°C-Experimental data and modelling results

5.3.3 Dependence of characteristics on temperature

A charge at 3.5 amps current was repeated at 17° C with the aim to compare with the results from the model.

The graph in Figure 61 shows experimental and modelling charge curves at different temperatures.

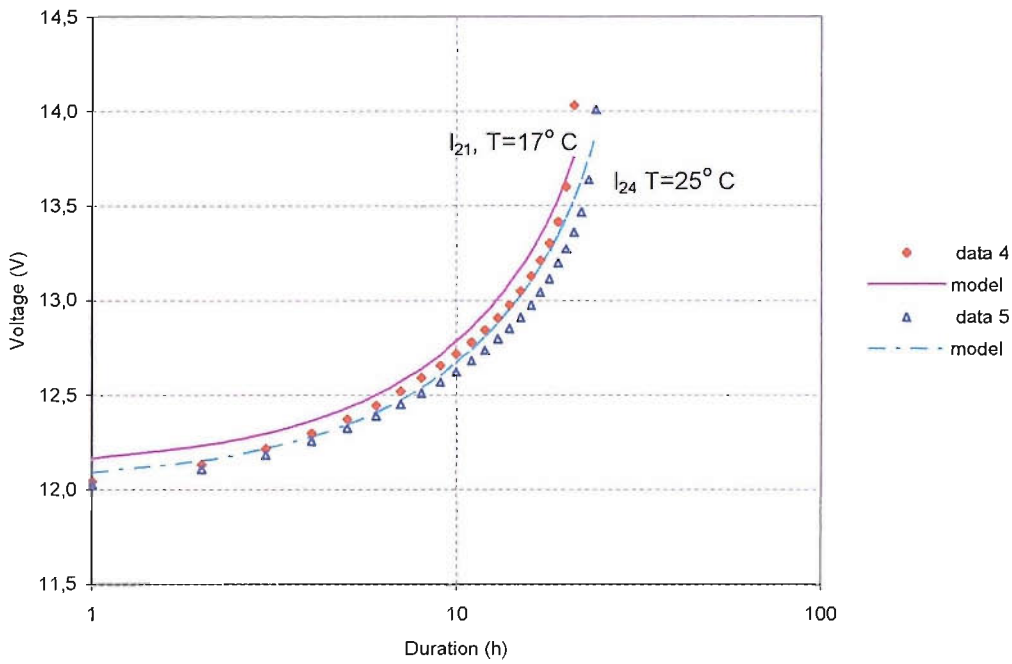

Figure 61 Charge at 3.5 Amp current at two different temperatures-experimental and modelling results

From Figure 61 it is seen that lower temperatures lead to more rapid charge. This result is expected[65]. The nominal parameter for the temperature corrections has been used here. It seems that some adjustment of the parameter is needed so that the resulting curves at different temperatures do not fall within the discrepancy between the modelling and the experimental results as it is seen from the graph in Figure 61. This wouldn't have been the case had we work with greater temperature differences (e.g. Greater than10°C). However, more specialized and complicated experimental set-up[65] is needed to achieve battery temperatures constant and low enough for the comparison. We should also note that the model should be able to simulate accurately the battery behaviour for temperature range between –5 and 25 deg C, which is the

highest temperature variation during the monitoring period of the stand-alone system of section 3.3.

5.4 Conclusions

An overview of the lead-acid batteries construction, performance and modelling has been presented. Models have been created to simulate the charge and discharge at constant current between two predefined states of charge (or, equivalently, two values of V_{oc}). The parameters in the models can be adjusted for a specific type of battery. The Copetti and Chenlo model has been applied to a specific battery experimental charge/discharge curves. It was found that although the normalized Copetti and Chenlo model is claimed to be valid for every battery, some readjustment of the parameters is needed. In addition, the discharge and charge of a battery in a PV system starts each time from a different state of charge (different values of the open-circuit voltage) and occurs at variable rates. The analysis of the parameters in this chapter has shown how the values of the parameters depend on the initial state of charge of the battery and of the charge or discharge rate. A different approach has been applied in this thesis to show that, even subject to these limitations, a reasonably accurate description of the battery can be developed using a model based the daily energy balance. (see Chapter 8).

6. OPERATION OF A PV SYSTEM

6.1 Introduction

A photovoltaic system operates in a complicated way mainly because of the fluctuating nature of the solar radiation that imposes the production of fluctuating current. This chapter includes an analysis of the PV system described in section 3.3 in terms of voltages and currents of the PV the battery and the load, charge produced, stored and consumed and battery regulation. This behaviour is simplified in models based on daily energy balance that they are typically used to assess the long-term performance of PV systems. Long data series can be used (10-30 years) as input and the system components are considered as 'black boxes', in other words only the input and the output is taken into account. The energy balance is found for the desired period of time taking into account the energy flows and estimating the rate of the energy production and the load consumption. According to the energy balance the daily energy produced by the PV generator is used to power the load; any surplus is stored in the battery and retrieved when solar radiation is below the value used in the design of the system. Figure 1 illustrates the energy flows in a stand-alone photovoltaic system with a DC load.

The first objective of this chapter is to give a detailed analysis of the actual PV system performance.

The second objective is to assess the results of modelling a PV system using a model based on daily energy balance when we use as input solar radiation data converted on the inclined surface using different methods (chapter 2).

A typical model based on daily energy balance developed in Fortran in previous work in Southampton University has been converted here in Matlab and is used in the rest of the work for system sizing purposes. (see chapters 9,10). The validation of the model is presented in chapter 8.

As it was found here, it is possible that, small differences in solar radiation series, used as input in the model based on daily energy balance, result in substantial differences in the battery SOC in winter months, when the solar radiation is generally low.

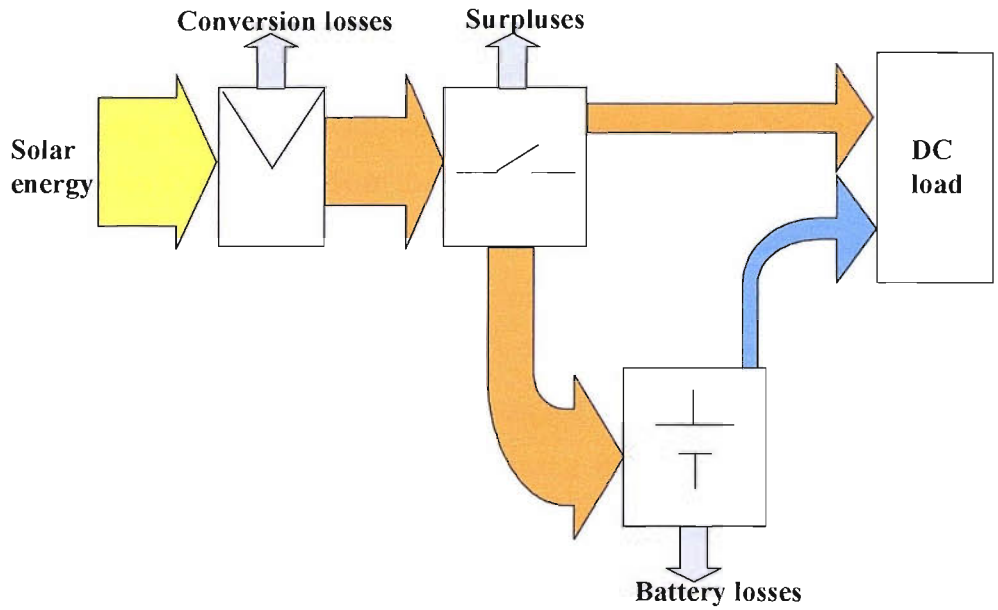

Figure 62 Energy flows in a stand-alone photovoltaic system with a DC load[48].

In section 6.2 the detailed operation of the stand-alone system of section 3.3 is analysed and explained. Section 6.3 discusses the development of the model based on daily energy balance. Section 6.4 presents the modelling results that show the effect of inaccuracies of the solar radiation conversion to the inclined plane on the battery SOC. Section 6.5 is the conclusions.

6.2 Operation of the experimental stand-alone PV system

The study described in this section is based in a detailed monitoring of the PV system of section 3.3 in 5 min intervals, as described in more detail in sections 3.3.4 3.3.5. As a result, a large volume of data has been collected and analysed. Examples of the (corrected) data are presented in this section with the aim to explain the operation of the PV system.

Figure 63 shows the in plane solar irradiance on 12/11/02 between 9:05 and 16:55. Figure 64 shows the corresponding variation of the PV the battery and the load voltage, while Figure 65 shows the corresponding variation of the PV, battery and load current. It can be seen from Figure 64 that between 9:30 and 12:40 as well as between 13:55 and 16:10, the PV array is connected to the system since the battery

and the load voltage follow the changes of the PV voltage. The difference between the PV voltage and the battery voltage is due to the voltage drop on the diode incorporated in the regulator circuit. Similarly, there is a difference between the battery voltage and the load voltage due to the voltage drop in the charge regulator circuit- possibly on a second diode in the charge regulator. The two large peaks during early afternoon, between 12:40-13:05 and 13:05-13:55, illustrate a situation where high solar irradiance generates high PV current which, in turn raises the voltage monitored by the charge regulator. When this voltage increases past the cut-off limit of the regulator 14.3V, the regulator disconnects the PV array. Since the battery is not yet fully charged (see Figure 67), this illustrates a limitation of this simple type of charge regulator. The value of PV voltage during these peaks appears lower than the open circuit voltage of the module (22V) because the measured data are averages over 5 min intervals of when the PV array is intermittently connected and disconnected from the rest of the system. Figure 64 shows the percentage of the 5 minutes interval time that the PV is disconnected, as calculated from the value of the open circuit voltage and an estimated average value of voltage (14.5V) when the PV is connected. After 16:15 the irradiance (Figure 63) drops to zero and as a result the PV voltage (Figure 64) also drops to zero, while the battery voltage is decreasing slowly as the battery starts discharging. From the current curves in Figure 65, it is also clear that after 16:15 only the battery provides current to the load. For the PV to provide current to the system the value of the irradiance should be such that the PV voltage exceeds the battery voltage, e.g., after 9:35 in the morning (see Figure 63 to Figure 65). Figure 64 and Figure 65 also illustrate another type of PV system operation when, during low irradiance, the PV current is sufficient to provide only a part of the load current, and an additional current is needed from the battery. This is the case between 10:20 and 10:55, and between 15:55 and 16:10. Between 11:00 and 11:40, the battery current is close to zero and the PV current is just about enough to feed the load.

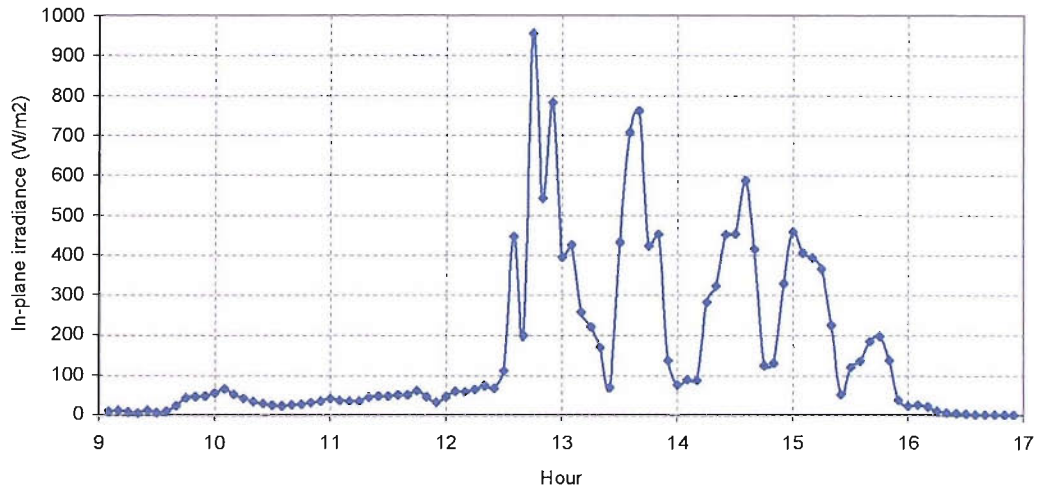

Figure 63 In-plane solar irradiance during the daytime on 12/11/02

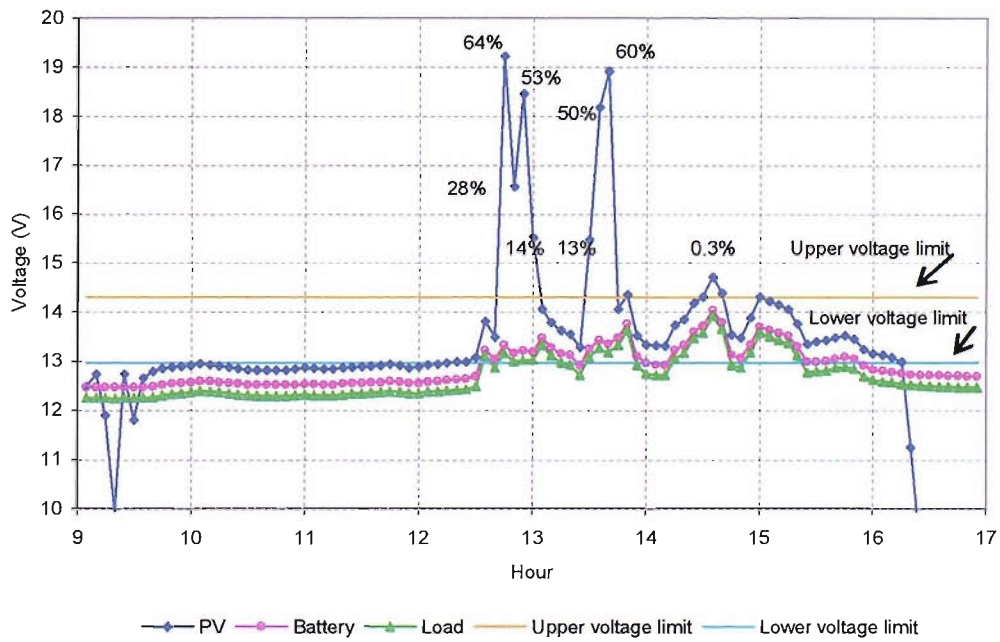

Figure 64 PV, battery and load voltage during the daytime on 12/11/02. The percentage of time that the PV is disconnected

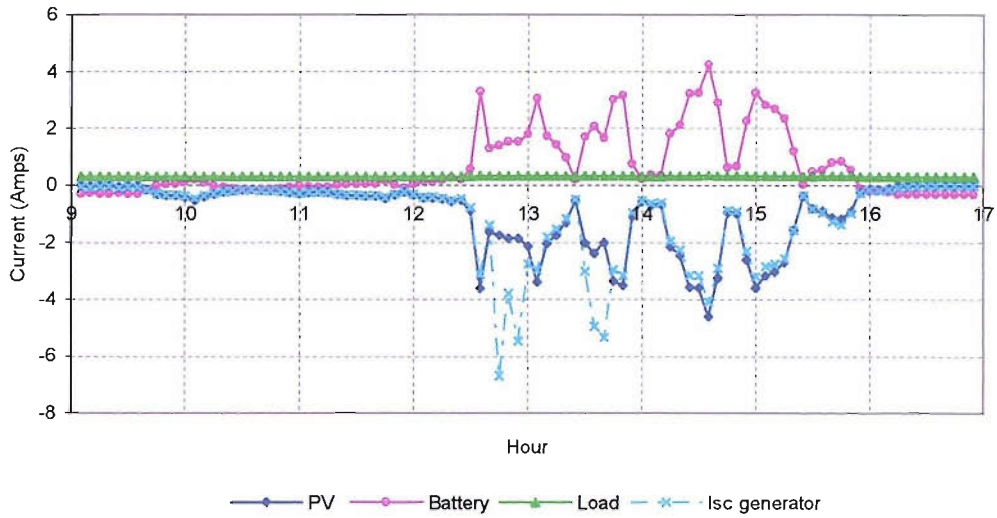

a.

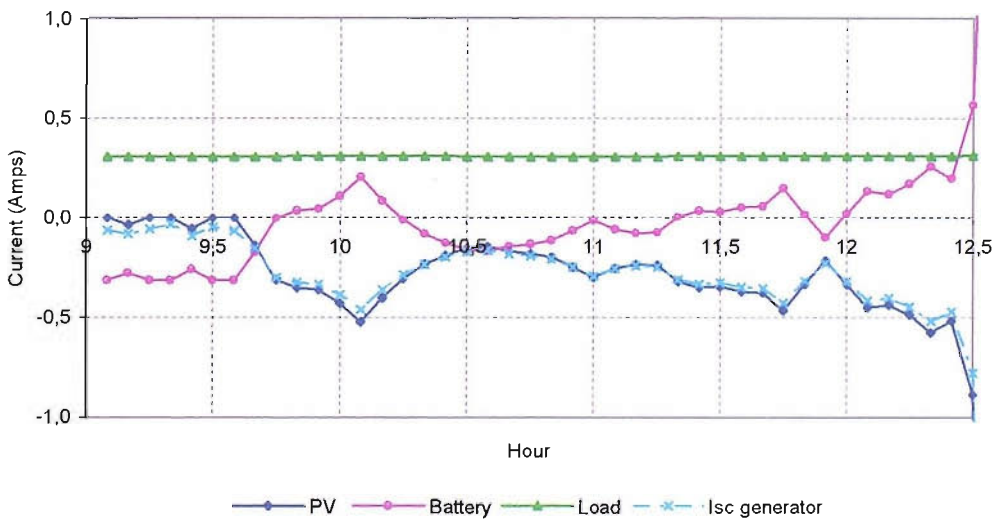

b.

Figure 65 PV, battery and load current during the daytime on 12/11/02 (a), detail of the graph in figure (a), from 9:00 to12:30 (b); Generator's short circuit current (Isc) for the irradiance in Figure 63. Note that, for clarity, the PV current is plotted as negative

Figure 66 to Figure 68 show the operation of the PV system between the 7th and the 15th November 2002, and illustrate an important concept in the design of stand-alone PV systems: the climatic cycle.

Figure 66 shows the solar radiation time profile from 7/11/02 to 15/11/02 and Figure 67 the relative cumulative charge received/given out by the battery relative to the sunset of the 7/11/02, just before the battery starts discharging. It can be seen that every day starts (12:00 at night) with charge leaving the battery. Then charge is received by the battery as the sun rises and at the sunset the net charge received by the battery reaches the highest value for the day just before the sunset, when the discharge starts again and continues until the end of the day (12:00 midnight). Obviously, when the radiation is very low (e.g. on 8/11 and 11/11) almost no charge enters the battery during the daytime (see Figure 66 and Figure 67).

The discharge segments in Figure 67 are almost parallel since the discharge current at night is almost identical. Any differences in the slope are due to differences in the voltage at the battery (and the load) as well as the state of charge of the battery.

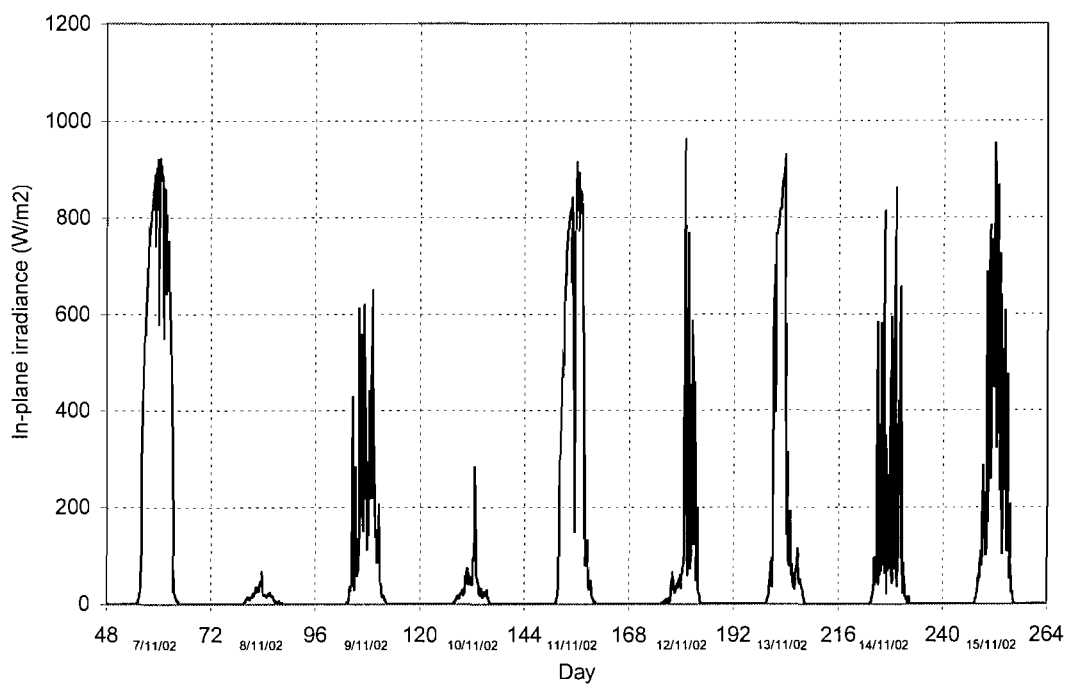

Figure 66 In-plane irradiance from 7/11/02 to 15/11/02

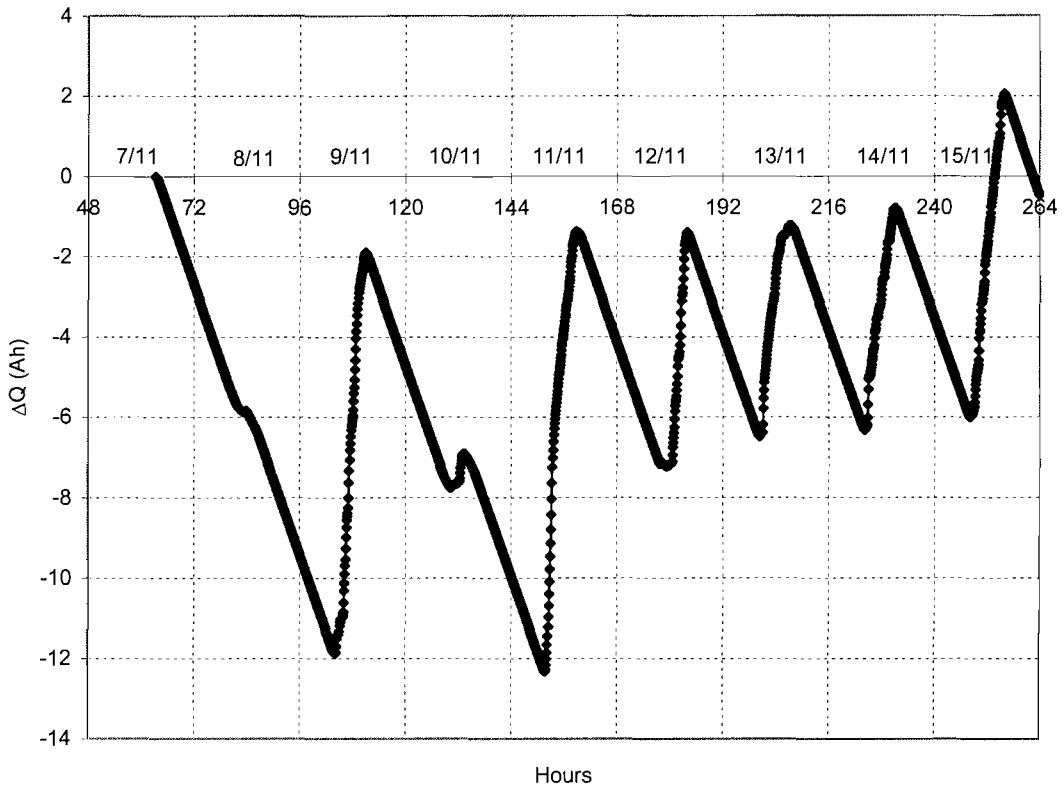

Figure 67 Relative cumulative charge ΔQ received/given out by the battery from sunset of 7/11/02 to midnight of 15/11/02

Figure 68 shows the total daily charge produced by the PV and the total daily charge in and out of the battery from 7/11/02 to 15/11/20. It also show the charge that could have been produced by the generator if it was always connected to the system and the operating point of the system was such that the value of the generators current were equal to the short circuit current. The total daily charge produced by the PV array is not proportional to the total daily charge that could have been produced if the PV were always connected to the system because of the operation of the regulator that disconnects the PV when the battery voltage reaches the upper limit. For example, as shown on 14/11/02 the PV array converts to charge a larger part of the available radiation than on 11/11/02.

A small part of the radiation is also lost when the radiation values are too low for the PV voltage to exceed the battery voltage and produce current to the system. However, we should note that even irradiance values higher than 10 W/m^2 are large enough for the generator to supply current.

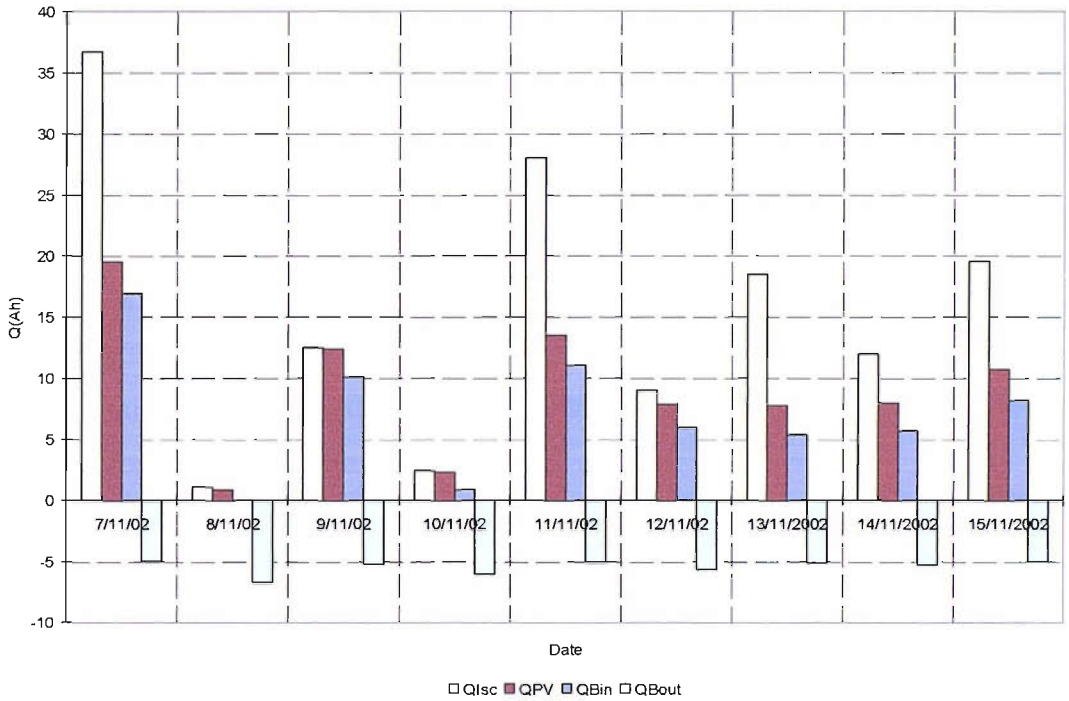

Figure 68 The total daily charge transfer from 7/11/02 to 15/11/02. Q_{Isc} is the maximum charge that could have been produced by the PV. Q_{PV} is the charge produced by the PV, Q_{Bin} is the charge that enters the battery and Q_{Bout} is the charge that is given out by the batttery

6.3 Model based on daily energy balance

The time profile of the battery SOC of the system can be obtained from daily solar radiation data on the plane of the generator using a model based on daily energy balance (see section 6.1). The program, based on daily energy balance, which is used in this work for long-term system modelling, was firstly developed in previous research in Southampton and was now converted to Matlab. The flow chart of the program is shown in Figure 69.

It is common practice in these programming applications to assume that there are no losses in the battery. The concept of daily energy balance is based on a simplified system where the load is always fed by the battery. This would happen, for example, if there were only nocturnal energy consumption. Therefore, the day is divided into two periods:

- Daytime, from the sunrise to the sunset, during which we have energy production from the PV generator, energy storage in the battery and energy loss if the available energy exceeds the storage capacity. (By 'available energy' we mean here the energy that is already in the battery at the sunrise of the day plus the energy produced by the generators during a day) and
- Nightime, from the sunset to the sunrise of the next day during which we have only energy consumption by the load.

The load can be either connected to the system (load on) or disconnected (load off). We should clarify that when we are referring to load on or off we are always referring to the nightime since as mentioned before during the day the load is always disconnected.

To have for the first day the load on, it should be ensured that there is enough energy in the battery at the sunset to feed the load for this day, no matter whether the generators will produce energy this particular day or not. Therefore, the initial storage capacity of the battery should be at least equal with one day of storage (equal to the energy that the load consumes in one day). Therefore, from the total battery capacity, one part, equal to one day's load demand aim to cope with the daily cycle (see section 7.2.1), while the rest of the battery capacity aim to cope with the seasonal and the climatic cycle and can vary depending on the location (see section 7.2.1).

So:

Battery storage=[seasonal/climatic storage]+[daily storage]

When on a given day the demand is not completely met, then the load disconnects and we have loss of load for this day. The next day will start with the load off and the battery empty. The load will turn on again when the energy in the battery at the sunset is at least enough to meet the daily load demand.

The state of charge of the battery is calculated for the sunset of each day as follows:

$$SOC = \frac{\text{The energy that the load consumes at night + The energy that is stored in the battery the sunrise of the next day}}{\text{Total battery capacity (Wh)}}$$

The long term LLP is calculated using the definitions in section 9.2.1:

$$LLP = \frac{\text{Energy load demand for N days - Energy used by the load over N days}}{\text{Energy load demand for N days}}$$

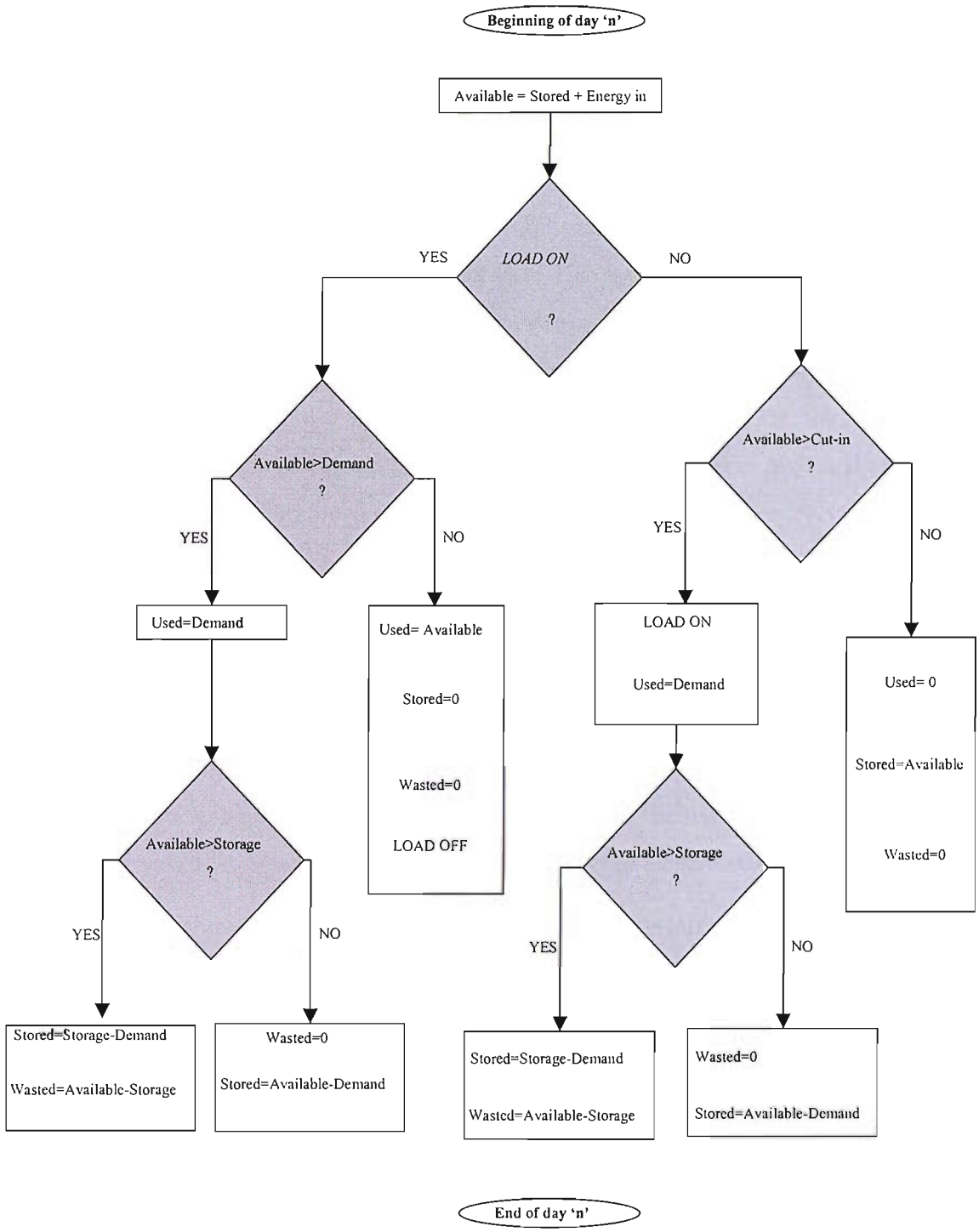

Figure 69 Flow chart of the simulation programme for system sizing

6.4 Modelling results: Radiation pattern-Battery SOC

The effect of inaccuracy in converting solar radiation onto inclined plane on the SOC of the battery is discussed in this chapter.

The results are based on modelling work. For the model based on daily energy balance the programme described in the previous section was used. The system is the one described in the example in section 9.2.3, in this case at 50 degrees panel inclination and 1.2 oversizing of the generator. The system was sized for 50^{o} panel inclination because the diffuse correlations were derived for this tilt angle. The storage capacity was chosen Cs=10.2 days of storage, a typical value for the UK. Liu and Jordan isotropic model[15] was used to convert the daily data on the horizontal surface to values on the inclined surface. The ground reflectance is assumed constant and equal to 0.2, a recommended typical value[7].

Figure 70 shows the calculated values of solar radiation on the inclined surface using solar radiation data on the horizontal surface (see section 2.7 and 2.8). The data on the horizontal surface are from Efford provided by the Met. Office. 25 years of daily data from 1970-1994 were used in the modelling. The worst period between the years 1970 and 1994 is November and December 1994, and this period is shown on the graphs. The first pattern was taken using Page correlation for the diffuse and the second using correlations based on measured data from StaR facility as described in section 2.8.

Figure 71 shows the battery state of charge of the system, as it is obtained from the Matlab model for the long-term performance prediction of the system, using as input the solar radiation patterns of Figure 70.

As it can be seen from Figure 70 and Figure 71, slight differences in the calculated radiation data on some days can lead to quite significant differences in the state of charge of the battery (note, in particular, the time interval between days 9082 and 9095). On other days, however, large differences may have no effect, as much of the energy produced is lost anyway. The effect on the battery SOC depends on the system design. The relative differences between the resulting SOCs profiles may become smaller or larger for different generator sizes. Figure 72, shows the resulting radiation patterns if we use twice the size of the generator. The relative differences are significantly increased in this case.

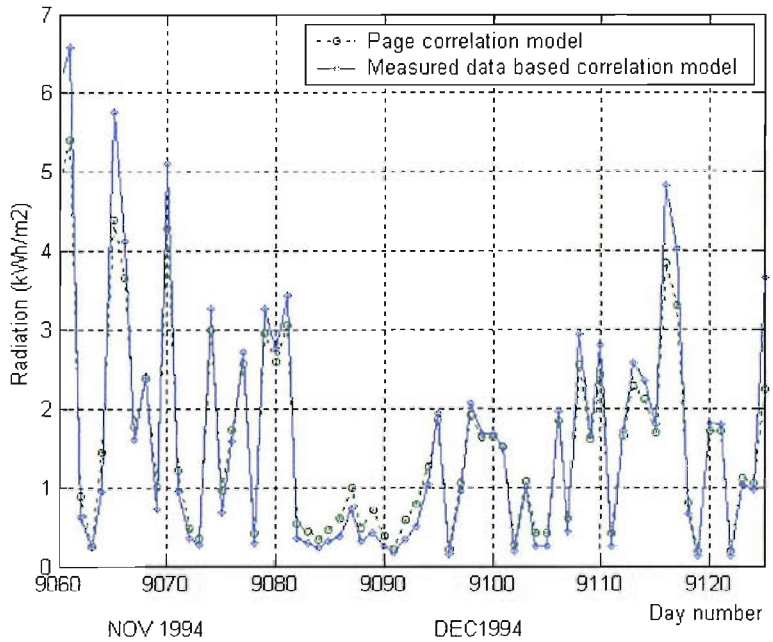

Figure 70 Two different values of solar radiation were found for the radiation on the inclined plane (50°) in Efford using two different models for conversion.

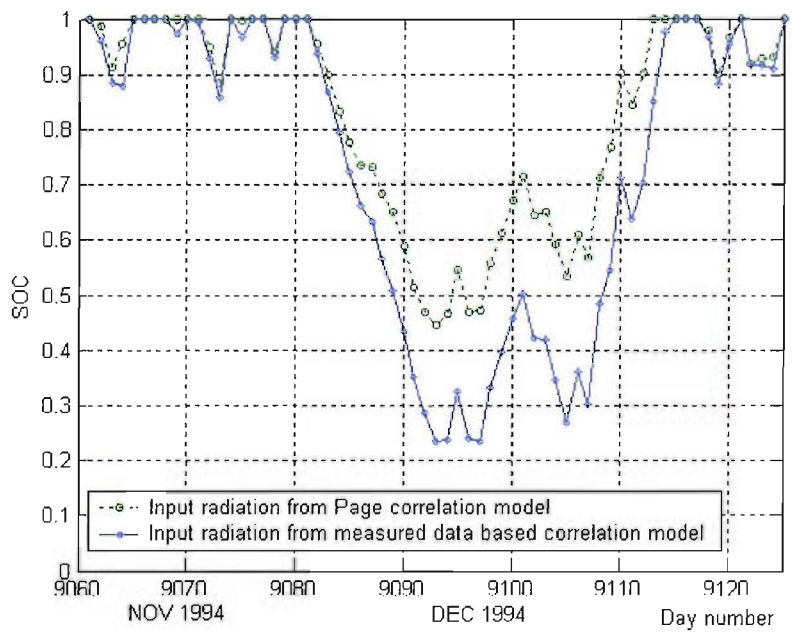

Figure 71 The corresponding battery state of charge of the system for the radiation data of Figure 70. Note the effect of the slight difference in the radiation patterns during the time interval between days 9082-9095, on the battery SOC

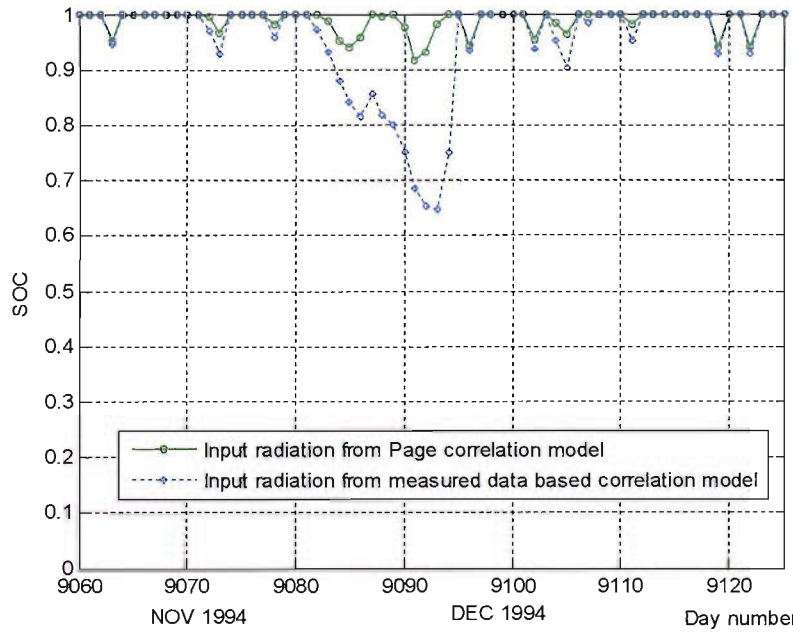

Figure 72 The corresponding battery SOC of the system for the radiation data of Figure 70 and twice the generator we used to obtain the results in Figure 71

6.5 Conclusions

The operation of the experimental stand alone system has been described in detail. This description includes the operation during one day, with a close examination of the effects of charge regulator switching and of the state of charge of the battery on the output from the generator. This complex behaviour is difficult to describe in detail but appears to have little effect on the overall energy balance in the system, as we shall see in Chapter 8.

We have also analysed the operation of the PV system during a sequence of several days and introduced the concept of climatic cycle. This concept was then used to develop a model based on daily energy balance. Based on a computer model developed during previous work at Southampton, a refined model has been created in Matlab which will be used in Chapters 9 and 10 to study system sizing. The results of this Chapter will be discussed further in Chapter 8 where we discuss validation of the model by a detailed look at the battery state of charge.

Using the results of Chapter 2, we have also examined the sensitivity of the predicted state of charge of the battery on the solar radiation profile. The results highlight the importance of a reliable method for the conversion of measured solar radiation data to radiation on the inclined plane of the PV panels. We have shown that even small differences may lead to substantial discrepancies in the pattern of the battery state of charge during system operation in practice but these discrepancies may be reduced or enhanced depending on the ratio of the generator size to the battery size.

7. BATTERY OPERATION IN A PV SYSTEM

7.1 Introduction

The model based on daily energy balance (section 6.3) treats the battery as a 'black box' that receives, stores, and gives out energy. The fundamental question therefore arises, to what extent does this model describe the battery operation in the PV system? One important issue is the charging efficiency of the battery in the PV system. So far, the concept of the charging efficiency of batteries in general and the way of measuring it is not clearly stated in the literature (see section 5.2.3). Even less information is available regarding the battery efficiency in stand-alone PV systems, where only one paper[77] has been found.

The principal aim here is to understand better the battery operation in the PV system and to acquire the necessary information for the validation of the model based on daily energy balance (chapter 8). To this end, the battery operation in the experimental stand-alone system of section 3.3 was analyzed. A series of experiments was conducted in the laboratory using the same type of battery used in the experimental PV system (section 3.3). The first part of the experiments has already been presented in section 5.3. This chapter presents experiments that were conducted with the aim to understand the battery cycles in the PV system and to estimate the battery charging efficiency. These experiments can be divided into three groups. The first and the second group include the experiments that reproduce the climatic, the daily and the daytime battery operation in the PV system to give a qualitative description of battery operation as a PV system component. The third group focuses on the charging efficiency, and includes experiments where a battery is partially charged and discharged at various levels of the state of charge. It was found that the loss of charge should be very small- at least when the battery is not overcharged as it happens when we have a simple on/of regulator- and only occurs when the battery is close to the full state of charge. For reasons that will become apparent below, only a qualitative study was possible within the scope of this project.

Section 7.2 includes the literature review of the battery operation as a PV system component and the charge regulation. Section 7.3 describes the battery

operation in the experimental stand-alone system of section 3.3. Section 7.4 describes the experiments and presents the results and the discussion. Section 7.5 presents the conclusions.

7.2 Literature review

7.2.1 Battery as a PV system component

Typical operation of a battery in a PV system will usually include the daily cycle where the battery is charged during the day and discharged by the night-time load. Superimposed on the daily cycle is the climatic cycle due to the variable climatic conditions. This cycle occurs any time when the daily load exceeds the average energy supply from the PV generator (Figure 73).

There are a number of considerations that are related to batteries used in PV systems due to the fluctuations of solar radiation that affect the discharging and charging process and the depth of discharge. The depth of discharge due to the daily cycling depends only on the ratio between the nocturnal consumption and the capacity of the battery. The daily cycle is normally shallow (typically 5-10% of the battery capacity). The depth of discharge and the duration due to the seasonal/climatic cycling depends on the daily consumption, the size of the generator and the local climate and has to be limited below a maximum value. This is typically done using charge regulators (see section 7.2.2. The seasonal cycling is demonstrated in Figure 73. Seasonal cycling can be much deeper than daily cycling. The DOD_{MAX}[7] varies between 0.5 and 0.75 the exact value is determined by the setting of the charge regulator. However, this means that from the total (nominal) battery capacity C_B, the useful battery capacity (C_U), that is, the capacity that can be actually extracted from the battery is:

$$C_U = C_B \cdot DOD_{MAX} \quad (7.2.1)$$

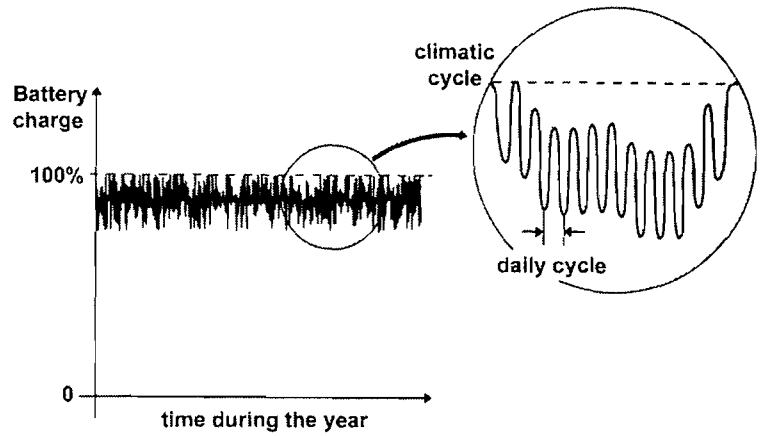

Figure 73 The cyclic operation of the battery in PV systems

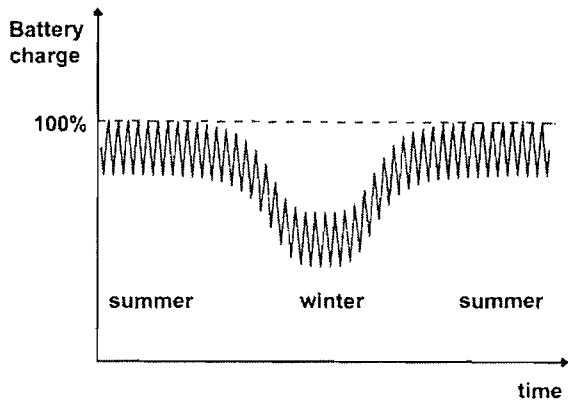

Figure 74 The seasonal cycle

It is sometimes pointed out that, the battery (with lifetime sometimes as low as 3-6 years) appears to be the 'weakest point' of a PV system since its lifetime expectancy is usually an order of magnitude lower than of other components.

In addition to regular daily and seasonal cycling, other chemical phenomena take place during the battery operation that affect maintenance requirements and battery life. These are gassing, during the charging, electrode corrosion and sulfation, and electrolyte stratification.

Gassing is the generation of hydrogen and oxygen at the electrodes by electrolysis of water due to lack of lead sulphate when at the end of the charging process. Gassing is desirable to some extent because the stirring action of the bubbles homogenizes the electrolyte and eliminates stratification[7].

Electrode corrosion is the slow oxidation of the lead of the positive plate grid to lead oxide due to the potential of the positive plate[78]. It is promoted by high positive plate potentials usually occurring at high state of charge of the battery. Corrosion decreases the cross section of the grid wires eventually leading to collapse of the plate[79].

Sulfation is the formation of large lead sulphate crystals at the plates which hinder the reversible chemical reactions. This occurs mainly when the battery remains in a low charge state for extended periods of time. Lead sulphate is not very soluble in the sulphuric acid electrolyte, but the solubility increases at higher temperatures[79]. When the temperature of the battery is increased even slightly, the smaller crystals of lead sulphate dissolve and when the temperature falls again this lead sulphate slowly crystallizes out. As a result, the large crystals grow at the expense of the smaller ones. The crystals on the positive plate are usually larger than those on the negative plate.

Stratification is a non-uniform electrolyte distribution. In the charging process[80], the electrolyte adjacent to the electrodes becomes heavier due to the acid production and moves downwards. Because of mass conservation there is an upward motion of the electrolyte in the middle of the cell. Furthermore, the maximum velocity of the electrolyte near the lead oxide electrode is significantly larger than near the lead electrode, simply because of a higher rate of acid production. This natural convective flow reverses during discharge. Both charge and discharge therefore produce a higher density of the electrolyte at the bottom than at the top of the battery.

7.2.2 Charge regulation

Overcharge and excessive discharge of the battery lead to phenomena within the battery that are harmful to its life (see section 7.2.1). In order to cut or reduce the current entering or leaving the battery and therefore avoid overcharge and excessive discharge in correspondence we use charge regulation.

Parallel or series regulators are used to avoid overcharge. For simple applications self-regulation may be sufficient on account of the IV characteristic of the array. To protect the battery against excessive discharge the load is disconnected when the voltage at battery terminals falls below a certain threshold. Usually a temperature sensor is fitted in the charge controller and the set point is temperature compensated, that is reduced at high battery temperatures and vice versa.

Parallel regulators (Figure 75)[61] are used to divert the array current through a low resistance path, parallel with the battery terminals, which effectively short circuits the array, when the battery voltage exceeds a certain threshold. A blocking diode has to be included in the shunt controller to prevent the battery discharging through the same pathway. When PV charging current is being passed it has to pass through a blocking diode, where there will be some voltage drop which causes heat production.

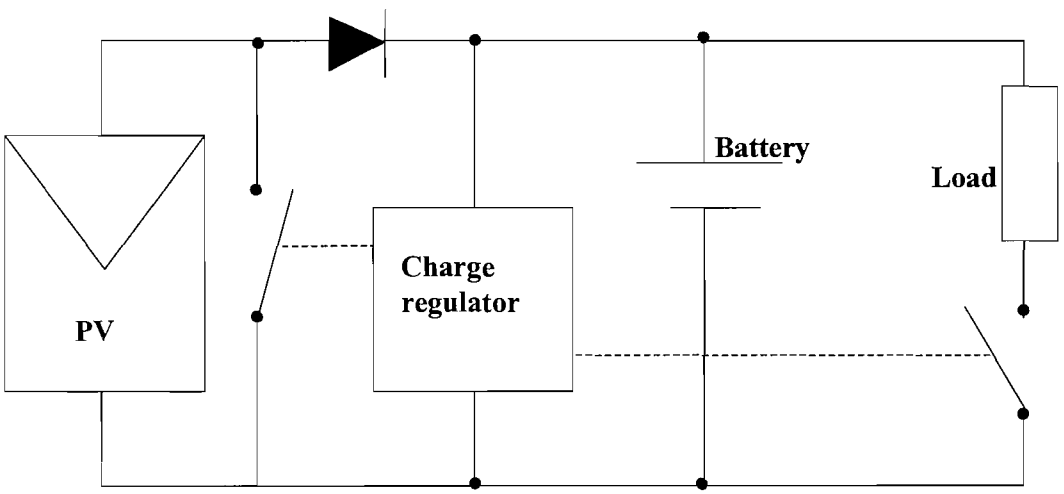

Figure 75 Operating principles of a parallel regulator[48]

Series regulators (Figure 76) disconnect the array when the battery voltage reaches a certain threshold. They do not need to have blocking diodes included.

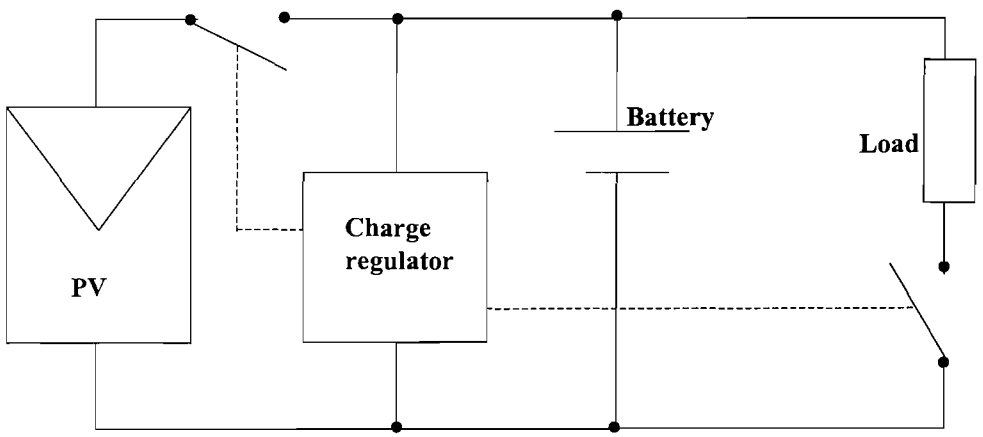

Figure 76 Operating principles of a series regulator[48]

Controllers may use either a relay or a solid-state switching device (such as a MOSFET or a power transistor) or a solid-state linear device, which can increase its resistance to reduce the current passed.

Apart from the simple one-step control that can be achieved with the simple on/off type controller, other types of regulation are possible:

In some series relay controllers, the PV current may still be passed to the battery after the set point has been reached, but now through a power transistor, or even a simple resistor that reduces the charging current and continues to reduce the current as the battery voltage continuous to rise more slowly. This is two-step control.

Multiple series relay controllers comprise more than one relay, each one connected to an independent PV sub-array. The threshold is different for each relay so that they can operate in sequence keeping the battery voltage almost constant.

Solid-state switching controllers (either shunt or series) and can operate at very fast rates (even thousands of times per second). When the threshold is reached, they can pulse current on and off in order to keep the battery voltage almost constant. The drawback is that they can cause interference with certain types of loads such as radio equipment.

Solid-state series linear controllers apply an increasing resistance to the current in order to keep the battery voltage as constant as possible. The main drawback is that they produce heat, often higher than the solid-state switching controllers.

In special circumstances a self-regulated system may be used. Self-regulated systems[5] are best suited to batteries which can tolerate substantial amounts of overcharging such as the Ni-Cd. The operating principle is as follows. The operation of the system takes place between the upper and the lower voltage limits that battery is allowed to operate. The operating point of the generator in a self regulated system should be chosen so as the upper end of the voltage range is above the MPP. This is usually achieved by using a smaller number of solar cells (typically 33) in a module. Since the slope of the I-V curve progressively increases when shifting from the MPP to the open circuit condition a slight increase in battery voltage sharply reduces the charging current from the PV generator and prevents overcharging. However, due to the large temperature sensitivity of the voltage of the solar cell it is difficult to design a reliable self-regulating system, particularly one suitable for a range of locations.

7.3 An experimental study of battery operation in a stand-alone PV system

In a stand alone PV system the pattern of battery charge and discharge depends on the availability of solar radiation, and on the variation of the load. The aim of this section is to study the battery operation and behaviour, on a daily basis, as a component of a PV system. It includes a description of the charging /discharging cycles, resulting from varying radiation availability, observed in the stand-alone system of section 3.3. For simplicity, the load has been chosen as constant and continuous.

The following principal features characterize the daily cycle of battery operation:

- At night only discharge occurs with almost constant current equal to the load current plus losses in the regulator
- During the daytime when there is enough radiation to feed the load there are two occasions:
    - The battery is charged with varying current. This occurs when the battery voltage does not reach the upper voltage limit set by the regulator (because the battery SOC is low and/or the radiation is low).
    - The battery is charged until the battery voltage reaches the upper voltage limit set by the regulator. Then the battery is discharged until the battery voltage reaches the lower voltage limit set by the regulator and then is charged again etc. This type of interruptive charge/discharge occurs when the battery is close to the full state of charge and/or when the radiation is high.
- When the radiation is too low to meet the load demand but sufficient for the PV voltage to exceed the battery voltage (this is often the case at sunset and sunrise), the PV array remains connected to the system and the battery is discharged with varying current less than the load current.

The contribution of the battery energy to the energy demand of the load on a daily basis will now be illustrated by data obtained in the experiment. If the in-plane solar radiation is greater than $50W/m^2$ the PV produces enough charge to feed the load. However, we have found that during all six months of monitoring, no matter

how sunny a day is, during the day (daytime and night) the system needs some energy from the battery more than half of the day. Let us take, as an example, a sunny day in March, 14/03/03. The battery was full before the sunset of the previous day, and by the morning of 14/3, it has therefore only been subject to a discharge during the night. After the sunrise it takes about one hour for the battery voltage to reach the value for the PV disconnection. From 7:45 until 17:40 (10 consecutive hours), solar radiation can provide at least the charge needed by the load. In April, the time period that the generator produces at least the charge to feed the load is about 11.5 hours while this period lasts about 7 hours on a sunny day in December. The number of hours that the battery should contribute to the load's demand, on a typical sunny day, therefore is: 16h in November, 17h in December, 16.5h in January, 15h in February, 14h in March and 12.5h in April.

It is interesting to consider briefly the macroscopic behaviour of the battery during charging. To this end the change of battery voltage during the charging process in relation to the state of charge of the battery can be visualized by analogy with filling a glass with beer. When the content reaches the level of the rim, the glass may still be partly empty, because of the foam. The more quickly we try to fill the glass the more foam is formed and the more misleading is the impression, regarding amount of beer in the glass (state of charge for the battery for our system), depending on the level of the foam (voltage at the battery terminals during charging). The 'real' level of the beer in the glass is the level of the content after some time of rest, when the foam disappears. In the case of battery, this level corresponds to the open circuit voltage which is typically measured after rest section 5.2.3.

The interruptive charging/discharging of the battery during the daytime can last from a very short time to many hours. For example, in April, the interruptive/charge discharge takes place from about 8:50 until 16:10 that is more than 7 consecutive hours. The duration of the charge and discharge during the interruptive charging discharging process depends on the value of solar radiation

Let us consider the case of a battery that operates near the full state of charge and the in-plane solar radiation is below 700W/m^2. This occurred, for example, on 12/4/03 (Figure 77a). It is seen (Figure 77b) that we do have recorded data of negative

battery current equal in absolute value to the load current. Given that the battery current is recorded as negative when the battery is discharged (section 3.3.5), this means that the battery discharge lasts more than 5 min (otherwise the averaging process would have result in positive value for the current or larger negative value).

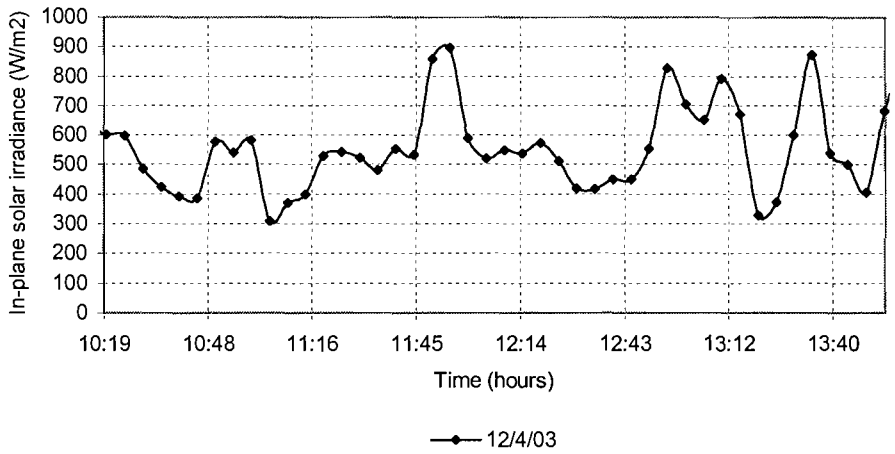

a

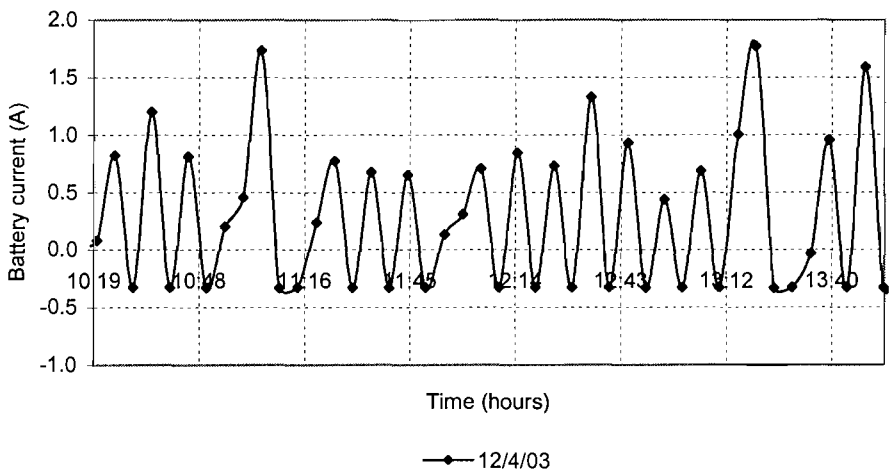

b

Figure 77 The in-plane solar irradiance (a) and the corresponding measured data of battery current (b) for a typical irradiance below 700 kw/m^2

When the in–plane irradiance is higher than 700 W/m^2 (Figure 78a), it can be seen (Figure 78b) that we only have measured data of positive battery current. The value of the battery current appears positive due to the averaging procedure over 5 min intervals. The battery discharge (negative values of battery current) during the

interruptive charge/discharge process is not apparent from the measured data because is faster than in the previous case (in-plane irradiance lower than 700 W/m^2). Therefore, the interruptive process which is characterized by a faster charge, is also characterized by a faster discharge (Figure 78b). This means that the fast charge does not really fill the battery and as a result the battery voltage falls below the lower voltage limit very quickly, usually in much less time than 5 min. For example, when the irradiance is as high as 950W/m^2, a closer observation of the regulator's operation can show that the charging time is less than 5sec and the discharging time about 35 sec.

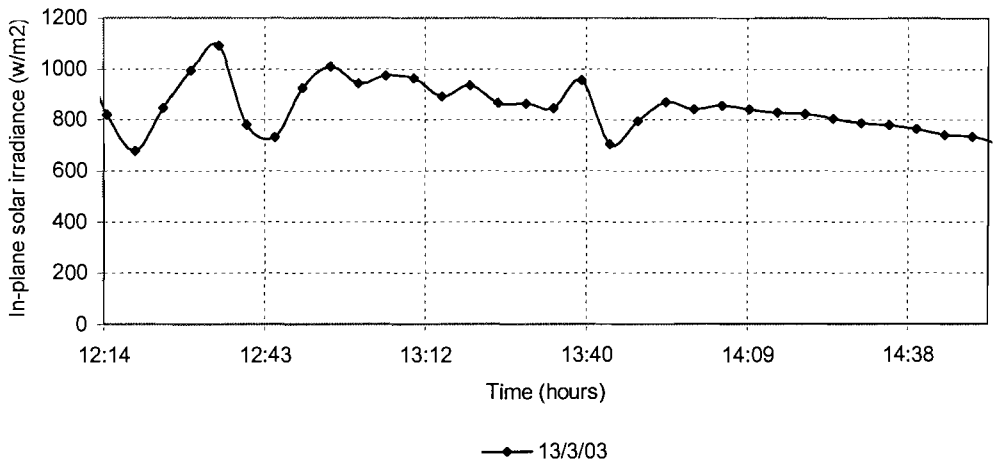

a

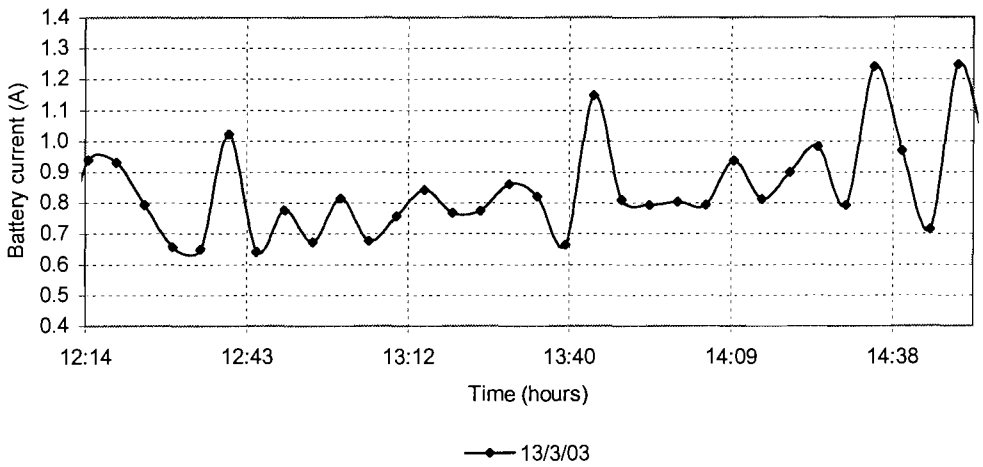

b

Figure 78 In-plane solar irradiance (a) and the corresponding measured data of battery current (b) for a typical irradiance in excess of 700 W/m^2

In a PV system the battery state of charge fluctuates on a daily basis. On a sunny day (for example on 14/3/03, Figure 81), the battery continuously operates close to the upper voltage limit. The SOC of the battery should therefore reach its highest value at the sunset of the day, just before the discharge starts. This is not the case, however, if the radiation fluctuates from high to very low values during the day. In this case, the battery may discharge and charge again reaching a lower SOC at the sunset.

At sunset, the charging current gradually decreases. As a result the voltage at the battery terminals decreases. This phenomenon may appear as a paradox since judging from the voltage at the battery terminals -the battery appears to empty while it is actually being charged. What happens is that the slow and decreasing current rate allows enough time for the battery voltage to settle down to a value closer to the open circuit voltage in rest, which is –in general (see section 5.2.3)- lower than the voltage during charging. An example is shown Figure 79.

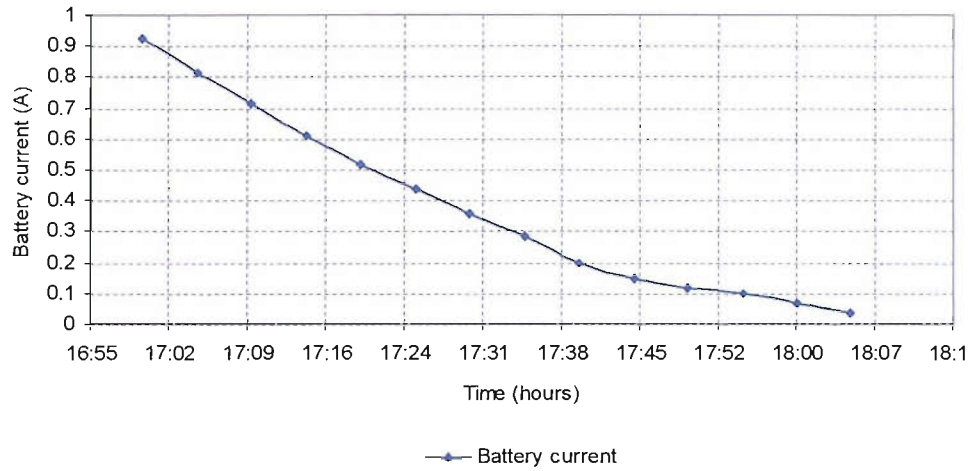

a

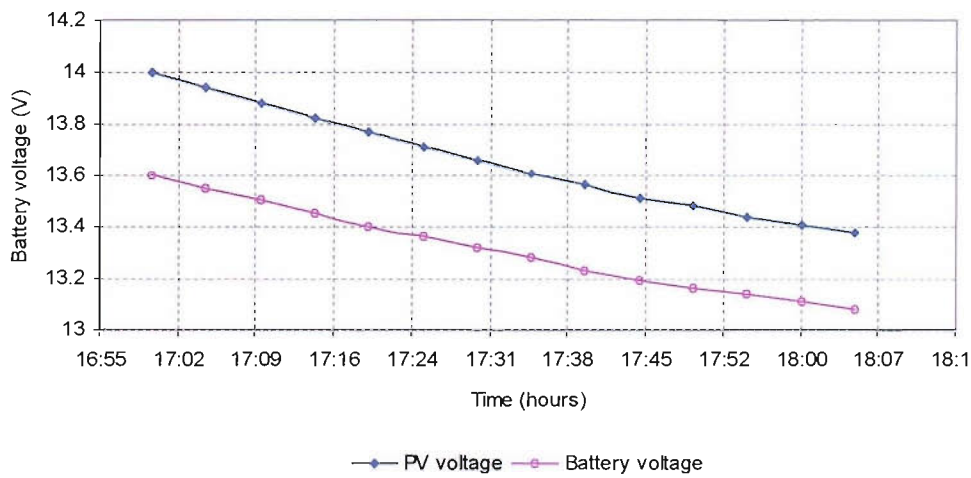

b

Figure 79At the sunset, the battery charging current decreases (a) and the battery voltage also decreases (b).

We will examine now how the amount of charge received by an almost full battery is related with the available solar radiation. Let's consider two days, 30/3/03 and 31/3/03. Both days the battery is almost fully charged as we can assume from the

high in plane solar radiation values (Figure 81). The total amount of charge received and given out by the battery is shown on Table 5.

Two interesting observations can be made:

The first observation is that the rapid increase in the net charge received by the battery occurs at the sunset (Figure 80 c), after16:30 at low radiation -lower than 400kW/m^2 (Figure 80 a). It is seen from the battery current data, (Figure 80 b), that after 16:30 there are no changes in the battery current sign. Given that the solar radiation values are relatively low this means that the PV remains connected to the system until its voltage drops below the battery voltage. Therefore more charge enters the battery at low radiation values, when there is no interruptive charge/discharge process, than at high radiation values when the interruptive charge/ discharge takes place.

The second observation is related to the radiation values in conjunction with the total charge received /given out by the battery during the two days mentioned above. During most of the daytime -from 8:10 until 15:30- the radiation is higher on the 31st (Figure 80 a). However, the corresponding net increase in the charge entering the battery is larger on the 30th (Figure 80 c). Two reasons may have caused this: The first is that the interruptive charge/discharge process probably allows more charge to enter the battery when the radiation is lower and the charge current is smaller. The second is that the, the battery might be at higher state of charge (SOC) on the 31st and can therefore accept less charge. As a result the daytime ends with higher net amount of charge entering the battery on the 30th than on the 31st.

	CHARGE GIVEN OUT	CHARGE RECEIVED	TOTAL
30/03/03	-4.518	5.091	0.575
31/03/03	-4.159	3.969	-0.189

Table 5 The charge received/given out by the battery two sunny days (30/03/03 and 31/03/03)

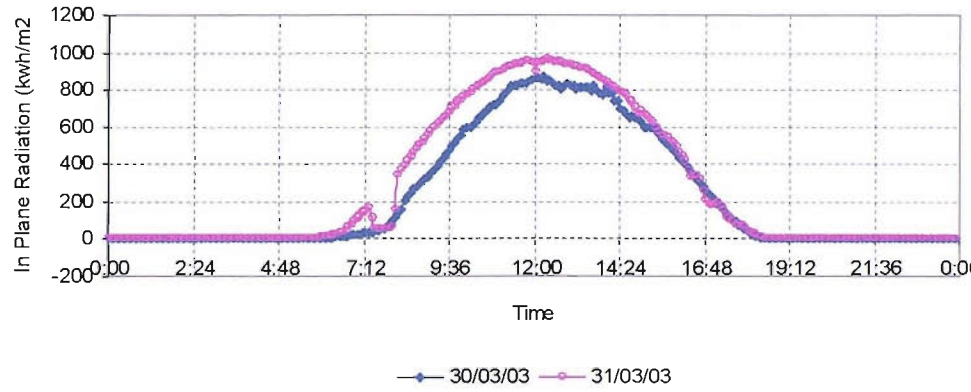

a

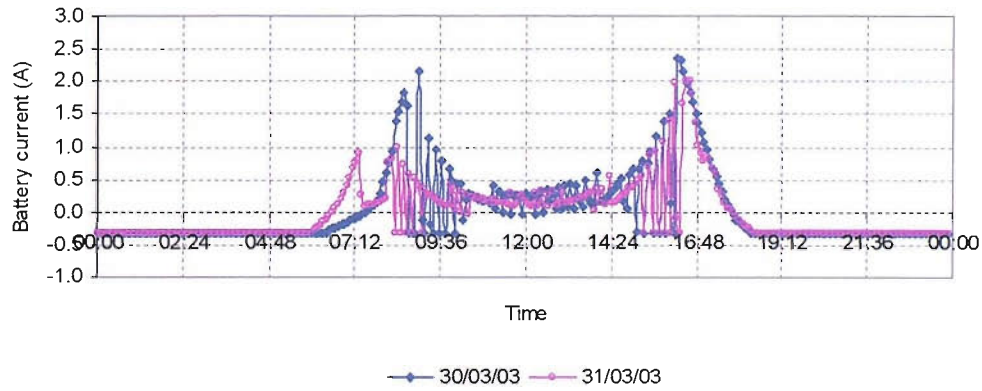

b

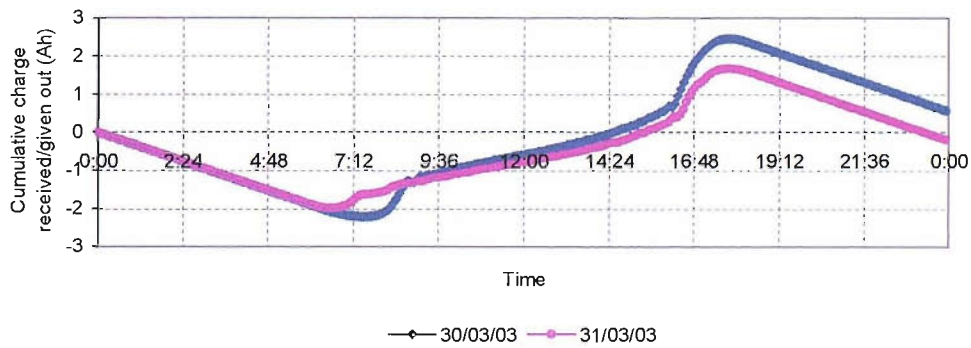

c

Figure 80 The in-plane solar radiation (a), the battery current (b) and the cumulative charge received and given out by the battery (c), of two days for which the battery operates at full state of charge

Based on the discussion in this section we may attempt to attribute daily values of charging efficiency to the battery current data. In order to estimate the battery

charging efficiency from the measured data we should focus on a period for which it is expected that the battery operates at the full state of charge because the main losses in the efficiency occur at this state due to gassing (see section 7.2.1). We expect that the battery is fully charged from 14/3/03 to 30/3/03 since the in-plane radiation values during this period are high (Figure 81). Table 2 shows the daily efficiencies as they are calculated (see section 5.2.3) from the measured data. It can be seen that the daily efficiencies take a wide range of values. This probably means that the efficiency depends on the particular way that the battery is charged/discharged during a day and therefore it is difficult to attribute one particular value of daily charging efficiency to the battery when it operates at full state of charge. We shall return to this question in section 8.3.

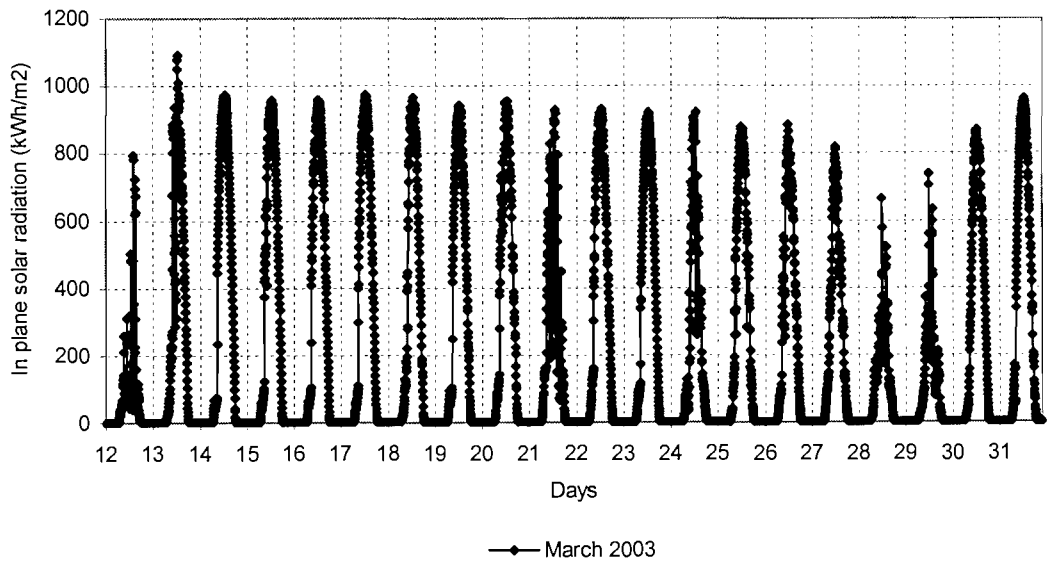

Figure 81 The in-plane solar radiation during a part in March 2003. From 14/03/03 till 31/03/03 the battery reaches the full state of charge every day

Date	Charge in	Charge out	Efficiency (%)
14	7.08	-4.11	0.58
15	6.21	-4.12	0.66
16	6.31	-4.08	0.65
17	6.44	-4.18	0.65
18	5.21	-4.36	0.84
19	5.89	-4.16	0.71
20	5.42	-4.29	0.79
21	5.47	-4.65	0.85
22	5.04	-4.24	0.84
23	5.73	-4.19	0.73
24	5.68	-4.43	0.78
25	6.04	-4.23	0.70
26	6.42	-4.38	0.68
27	6.13	-4.57	0.75
28	6.13	-4.85	0.79
29	6.73	-4.71	0.70
30	5.09	-4.52	0.89

Table 6 Charge received and given out by the battery and daily charging efficiency

7.4 Simulation of the battery operation in the laboratory

We have seen in section 7.3 that the battery charge and discharge in a PV system (especially when viewed over the short scale of seconds and minutes), is a complex process. It is difficult to depict this process satisfactorily by monitoring the system as the battery state of charge is unknown. For this reason, these processes have been studied under simulated conditions in the laboratory.

Three groups of experiments are included in this section, an experiment that simulates the daily and climatic cycles, an experiment that simulates the battery charging during a sunny day, and battery efficiency experiments. The results of these experiments are reported in sections 7.4.1, 7.4.2 and 7.4.3.

For the estimation of the initial and the final state of charge of the battery a relationship between the open circuit voltage and the SOC of the battery is needed. This is found by curve fit (Figure 82) to manufacturer's data.

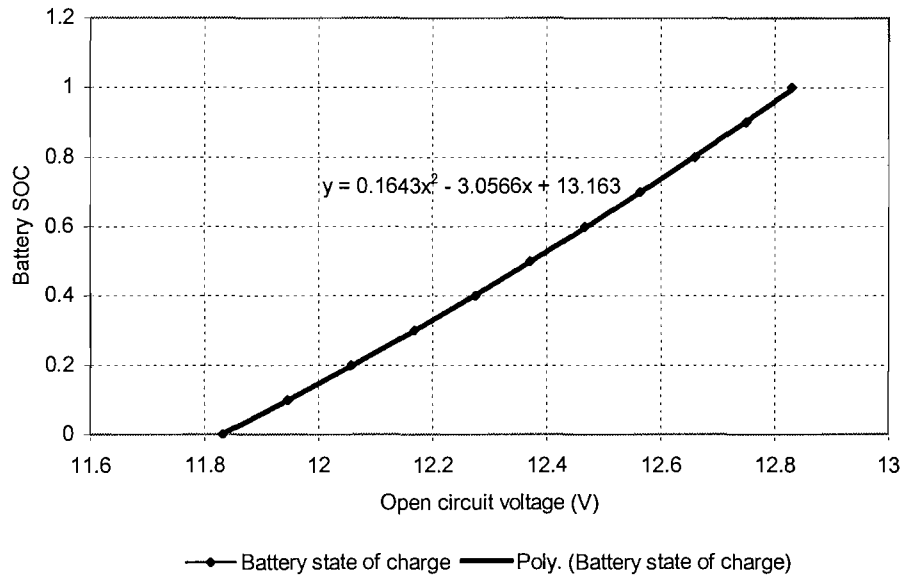

Figure 82 The relation between the open circuit voltage and the battery state of charge-curve fitting to manufacturer's data

7.4.1 Simulation of daily and climatic cycles

A. Experiment

In this experiment the purpose is to study the battery operation during the daily and climatic cycles of the stand-alone system of section 3.3. The cycles of night - discharge and day-charge are simulated. Also reproduced is a period of a continuous discharge-which is then followed by a continuous charge. The 'daily' consumption in the experiment is the same as in the model based on daily energy balance and in the stand-alone system, while the current rates are chosen so that they are close to those observed in the stand-alone system operation.

In details, here the load operates at 'night', which lasts 12 hours during which the discharge current is 0.350A. This would be the value of the discharge current of each battery in the stand-alone system if we had only nocturnal energy consumption.

The battery is then charged ('day') until the regulator interrupts charging, when the battery voltage reaches 14.3V. The value of the charge current used here-0.985A- is an approximate average value of the current that charges the battery of the stand-alone system since the sunrise of a day and until charging is interrupted by the regulator for first time. After rest in a full state of charge (Voc=12.88V) the battery is firstly charged up to 14.3V and the daily charge-discharge cycles start as soon as charging is interrupted for the first time. After two daily cycles a seasonal cycle starts. That is 72 hours (six days) discharge followed by charge up to the 14.3V. The final open circuit voltage after rest is Voc=12.84V. The diagram in Figure 83 shows the experimental process. The letters in italics stand for the results. Table 1 shows the charge in and out of the battery in each cycle.

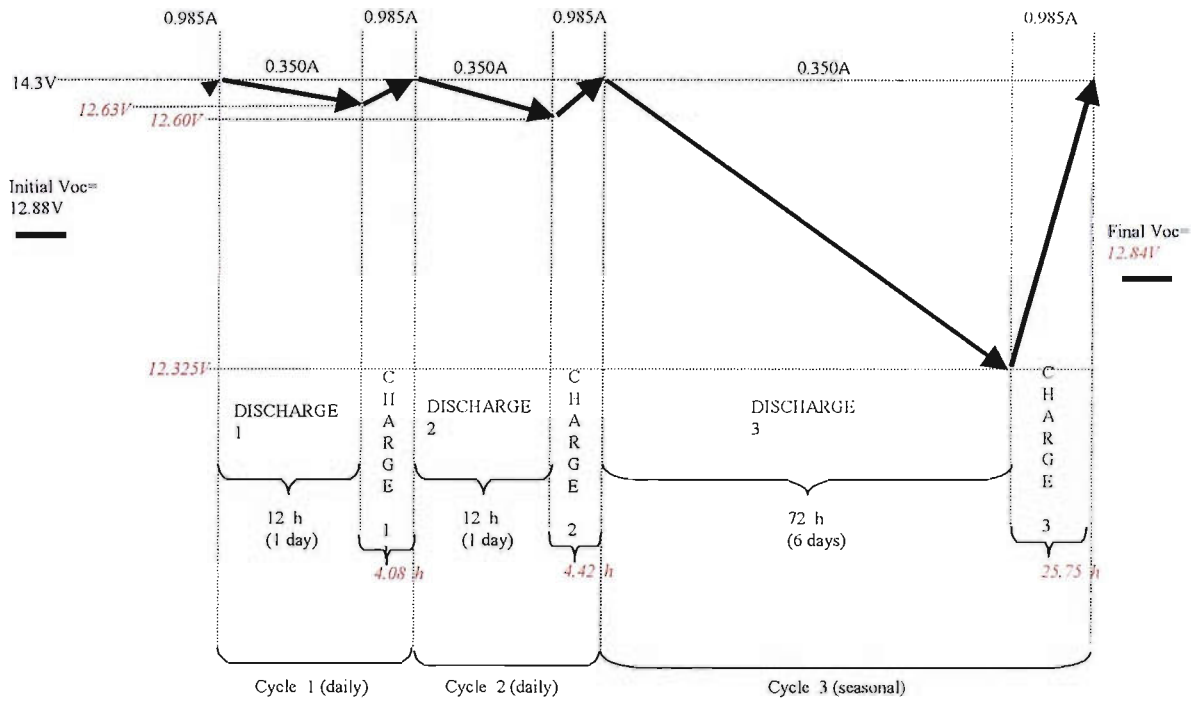

Figure 83 The experimental sequence

B. Results

Figure 84 a, shows the time profile of the cumulative charge received/given out by the battery. It is calculated by current integration and the charging efficiency is assumed equal to 1. Figure 84 b shows the net charge received/given out by the

battery after each charging cycle. Figure 85 shows the accumulative charge given out by the battery vs. voltage for all three discharging processes. Figure 86 shows the curves of the three battery charging processes. Table 7 shows the charge received and given out by the battery during each cycle as well as the net charge received/given out by the battery for each cycle.

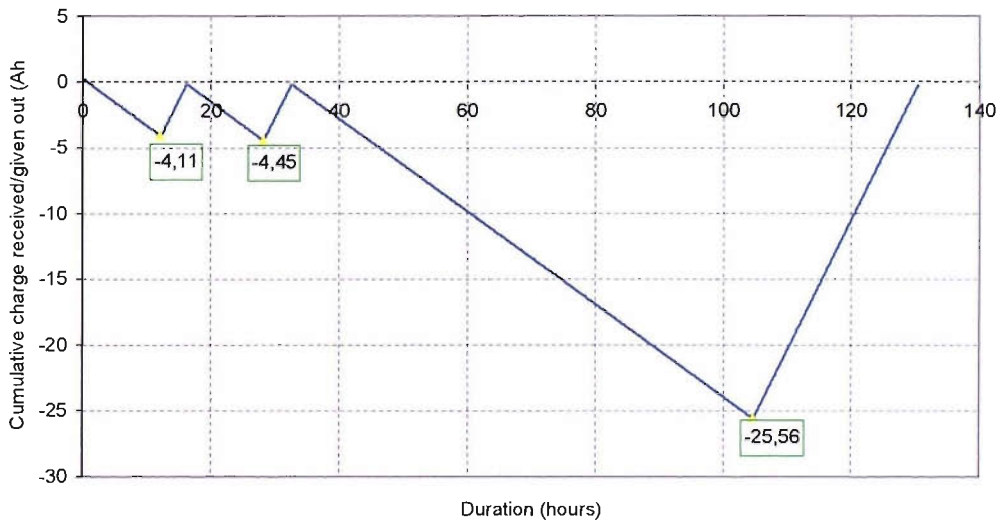

a

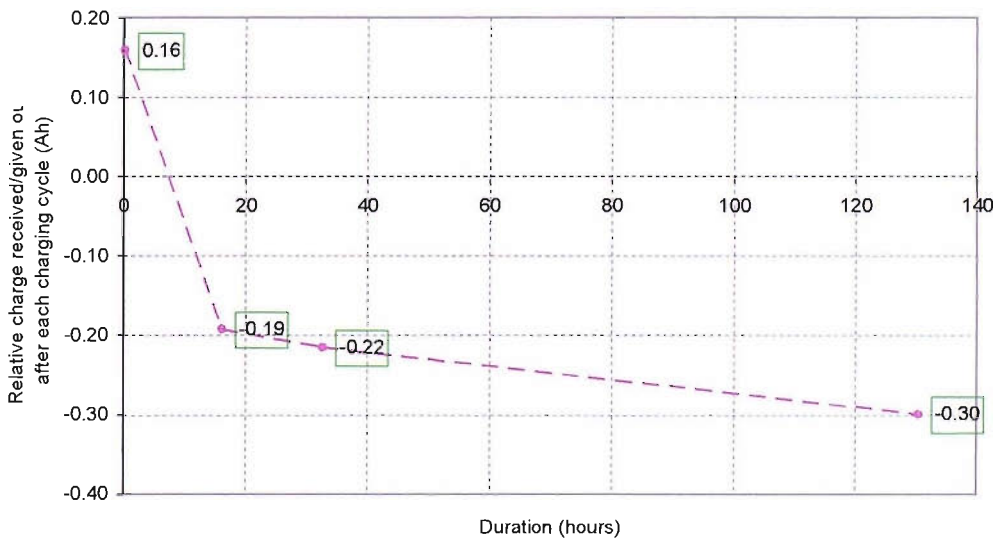

b

Figure 84 Time profile of the accumulative charge received/given out by the battery during each cycle (a) and the net charge received /given out by the battery (b)

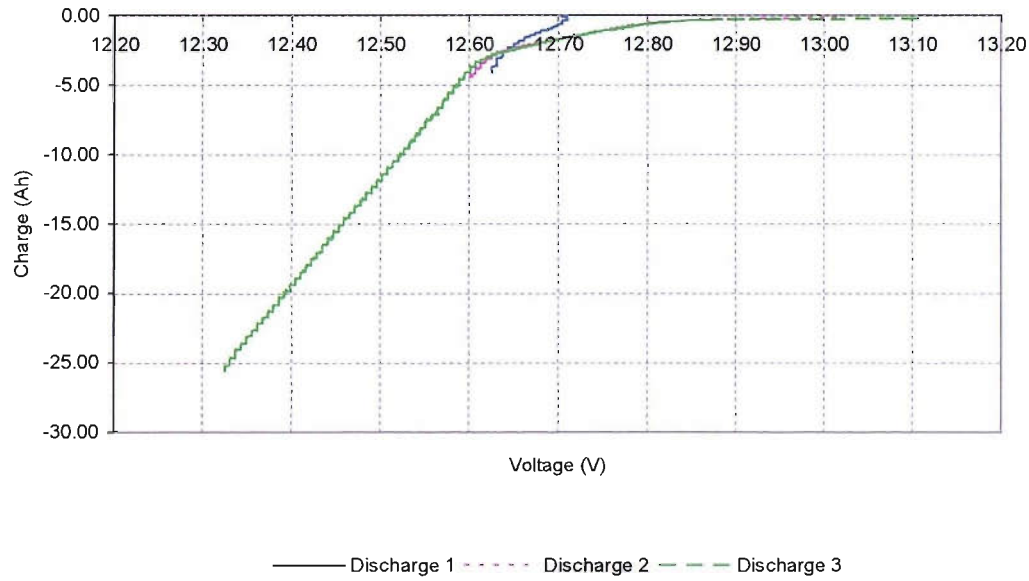

Figure 85 Charge given out by the battery vs. voltage for all discharging processes of the experiment shown in Figure 83

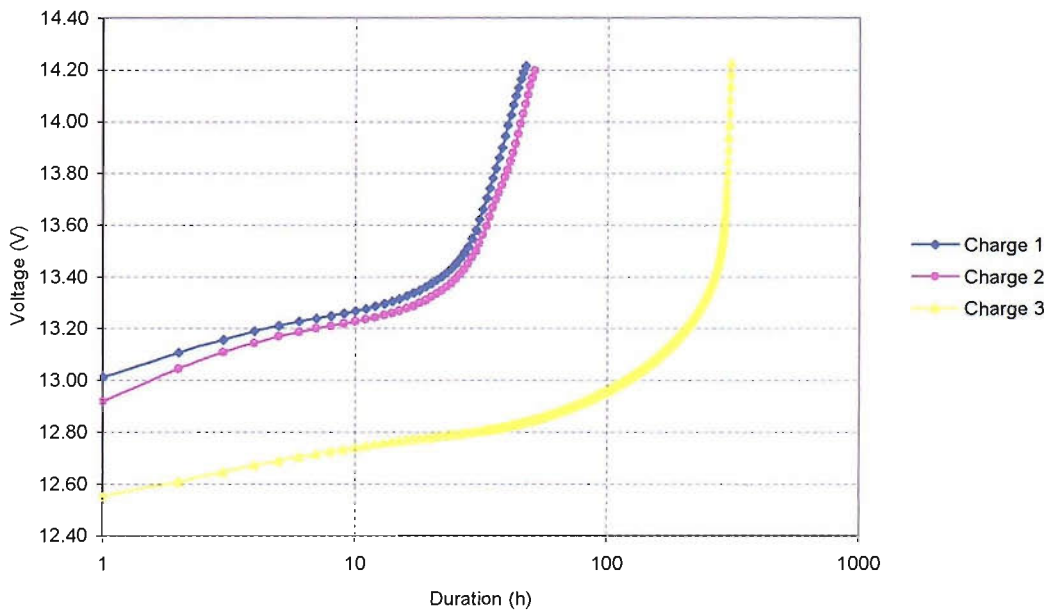

Figure 86 Battery charge curves

CHARGE				
	charge out (ah)		charge in (ah)	charge out-charge in (ah)
Charge up			0.164	-0.164
Cycle 1	4.32		3.98	0.34
Cycle 2	4.31		4.26	0.05
Cycle 3	First 12 h	4.22	25.31	0.07
	Total	25.38		
Total	33.99		33.71	0.28

Table 7 The total charge received/given out by the battery during each cycle

C.Discussion

The charge given out by the battery in each cycle is always more than the charge received by the battery. As a result it is seen in Figure 84 b that the values of the net relative charge exchange of the battery after each cycle show that the battery is losing charge (see also Figure 87). We cannot suggest that these values indicate the SOC of the battery with respect to the SOC at the beginning of the experiment, since there are mechanisms in the battery, which do not allow all the charge entering the battery to be converted in battery charge (see sections 5.2.3, 7.2.1). However, the SOC of the battery can only be lower than what these values indicate. One question is apparent here: Why is the cumulative charge lower in the second cycle and even lower at the end of the deep cycle since the charging rate remains the same and the voltage limit remains also the same? It seems that, as the cycling proceeds, the voltage rises more quickly with the charging current.

The difference between the charge given out by the battery and the charge received by the battery is independent of the depth of discharge (see third cycle in

Table 7), which means that should be close to the upper voltage limit that there is a difficulty for charge to enter the battery.

The charge loss during the whole process can be calculated in two ways. One way is from the initial and the final Voc, taking into account the manufacturer's data that relate the SOC and the Voc. The final Voc is 0.04V less than the initial. This corresponds (Figure 82) to about 0.04 reduction in the SOC, which multiplied by 100 Ah battery capacity gives 0.4 Ah less charge in the battery. The second way is by current integration (ignoring battery charging efficiency). It can be found that at the end of the experiment the battery has 0.3 Ah less. The difference between the values found from the first and the second way can be attributed to the fact that in the second way the charging efficiency is not taken into account.

The difference in the net cumulative charge at the beginning and the end of the first cycle, 0.16 and (–0.19) in correspondence should be reflected to the voltage drop from 12.63 at the end of the first cycle's discharge to 12.60 at the end of the second cycle's discharge. Similarly the difference in the net charge exchange at the beginning and the end of the second cycle are reflected to the voltage drop from 12.60 at the end of the second cycle's discharge to 12.59V, which is the voltage after 12h discharge in the third cycle.

The charge given out by the battery is the same during the first and the second discharge. However, the amount of charge received by the battery is larger during the second cycle (4.26Ah) (see Table 7) than during the first (3.98Ah). Therefore, in the first discharge cycle the difference between the charge given out by the battery and the charge received by the battery is larger than in the second.

7.4.2 Simulation of battery charging during a sunny day

A.Experiment

This experiment investigates the daily behaviour of the battery in the stand-alone PV system of section 3.3. To this end it reproduces the operation of a battery a sunny winter day: After the night discharge the battery is charged by the PV until the

regulator disconnects the PV at the upper voltage limit. In a sunny day, the PV array is then connected and disconnected at a frequency which depends on solar radiation and is imposed by the voltage limits set by the regulator. The initial open circuit voltage of the battery in the experiment is 12.81V; in other words, the battery is close to the full state of charge. The duration of the discharge is 15 h which corresponds to the night length on a winter day. The value of the discharge current (0.167A) is similar to the discharge current of each battery in the stand-alone PV system of section 3.3. The charging current (0.985A) is an approximate value of the current that charges each battery of the stand-alone system since the sunrise of a day until the charging is interrupted by the regulator for the first time. An interruptive discharge charge sequence then follows for 2.5 hours. The discharge current is set at the same value as before (0.167 A). The charge current is set to 2.648A, similar to the charging current of each battery at the midday of a sunny day, with in plane radiation 750 W/m^2. During this interruptive process the data are logged in a file every minute. The schematic diagram of the experiment is shown in Figure 87. The letters in italic indicate measured results.

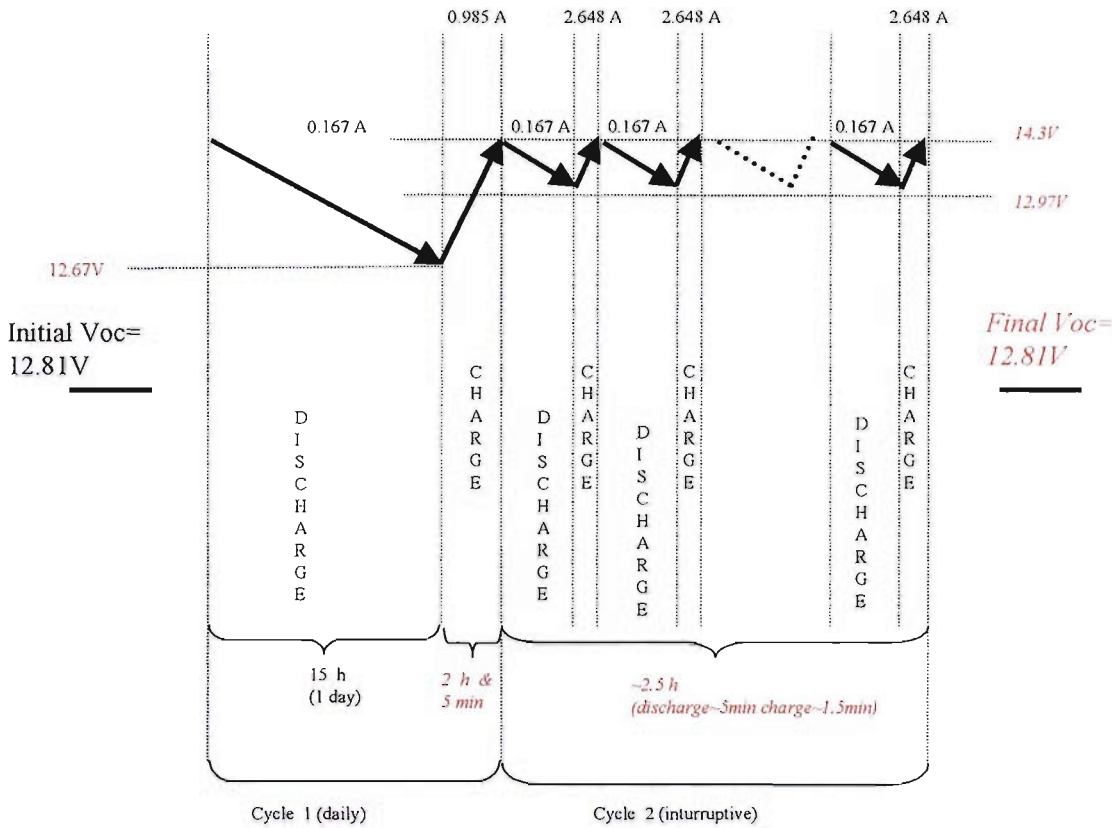

Figure 87 Schematic diagram of the experimental sequence

B. Results

Table 8 shows the charge received given out by the battery during the first cycle and during the interruptive process. Also shown is the efficiency of the total process Figure 88 a shows the time profile of the charge received/given out by the battery. Figure 88 b shows the charge received/given out at the end of each circle. Figure 89 shows the cumulative charge exchanged during the first discharge as a function of voltage. Figure 90 shows the charge curve of the first cycle.

	Charge (Ah)			Efficiency $(Q_{discharge}/Q_{charge})*100\%$
	First cycle	Interruptive	Total	93.8%
discharge	2.53	0.35	2.88	
charge	2.02	1.06	3.07	

Table 8 Charge received/given out by the battery during the experimental process of Figure 87.

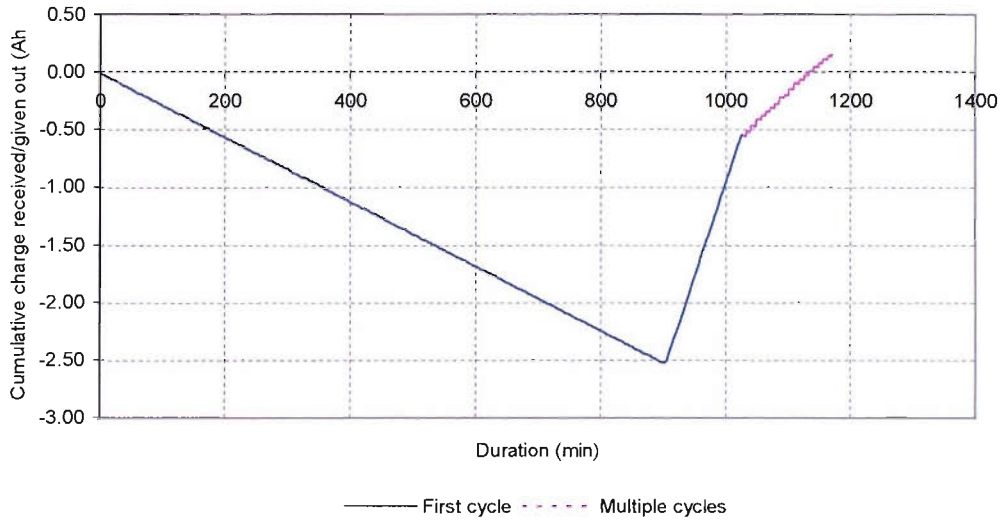

a

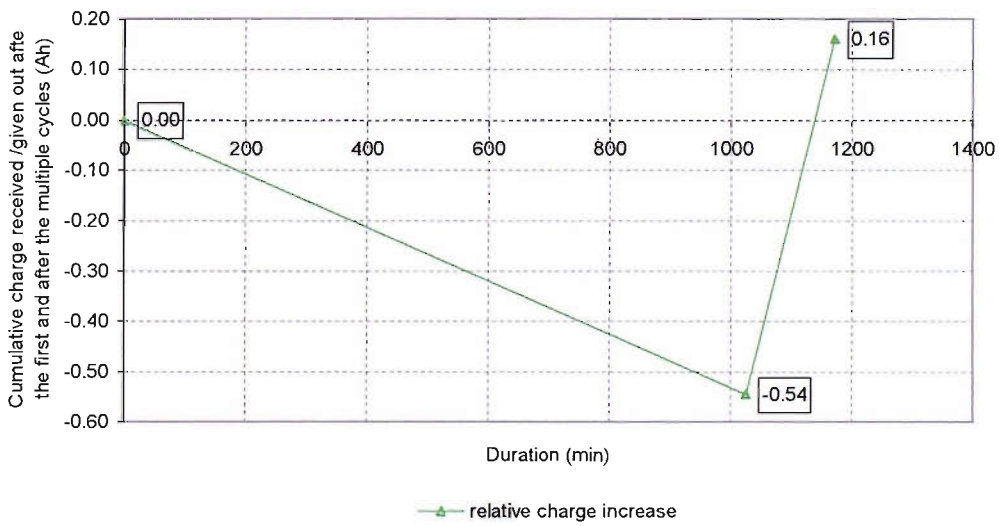

b.

Figure 88 Time profile of the cumulative charge received/given out by the battery (a) and time profile of the net charge received/given out by the battery at the end of the first circle and after the interruptive process (b)

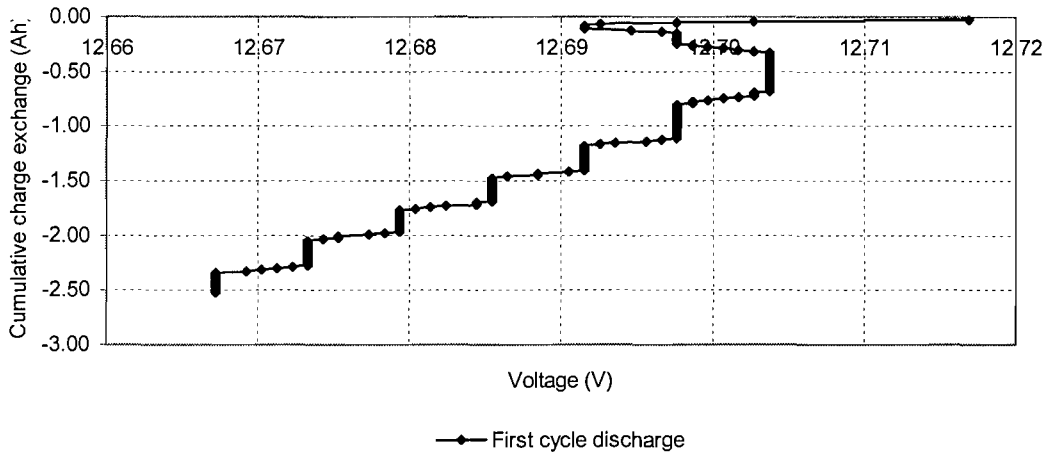

Figure 89 Cumulative charge exchange of the battery during the first discharge as a function of voltage.

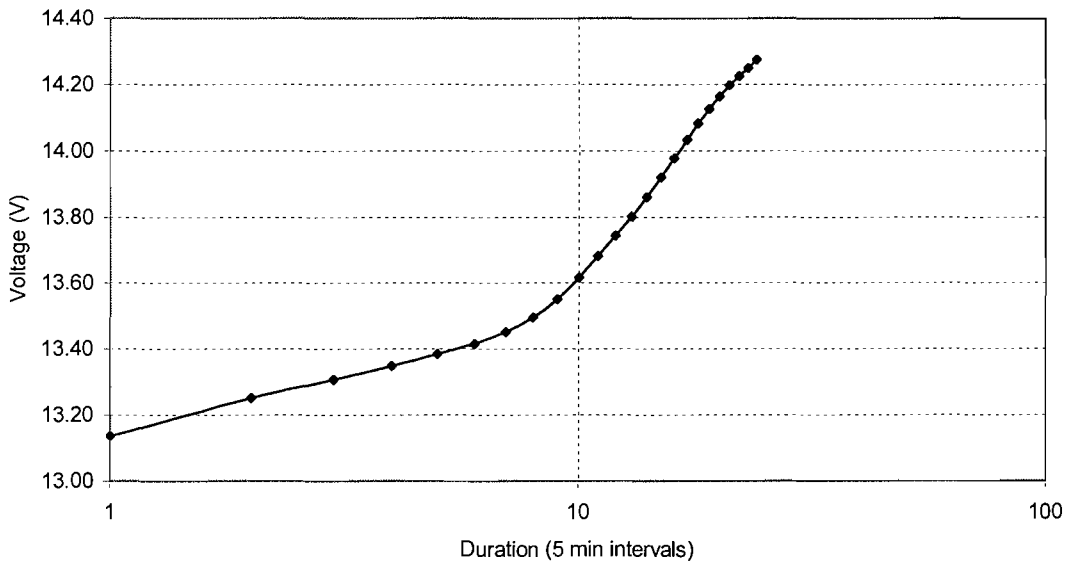

Figure 90 Charge curve of the first cycle

C.Discussion

Similarly with the previous experiment, after the first charge/discharge cycle, the amount of charge given out by the battery is larger than the amount of charge received by the battery (Table 8). The negative net amount of charge exchange at the end of the first cycle indicates that the charge in the battery has been reduced at least that much, as discussed in the previous experiment. Therefore, it is expected that had we disconnected the battery at that moment, the value of the open circuit voltage after rest would have been lower than the value of the initial open circuit voltage.

The interruptive process that follows will bring the battery to the initial SOC – the final open circuit voltage is the same with the initial (Figure 87). The net amount of charge exchange at the end of the whole process is positive (Figure 88).

In general, it can be observed smaller currents put more charge in the battery before the voltage reaches the cut off value, while larger currents will cause the voltage to rise and reach the cut off value quickly, before the initial value of the net charge exchange is reached.

The charging efficiency of the process calculated as described in section 5.2.3 is 94%. The charging efficiency is found higher than the efficiency referred to in the manufacturer's data (0.71 for SOC>0.9) and in the IEC 61427 (0.85 for SOC >0.9)[81]. However, it agrees with the values mentioned in literature[4,61] (see section 5.2.3).The high value of charging efficiency can be explained by the fact that the operation is below the full state of charge and there is no gassing (see Figure 90, charging curve).

7.4.3 Battery efficiency experiments

The purpose of these experiments is to relate the daily charging efficiency of the battery to the state of charge. Discharging/ charging cycles similar to the daily cycles of the battery are reproduced starting each time from a different state of charge. Each cycle starts from the battery at rest. Using the manufacturer's data, the SOC can be calculated from the Voc at the beginning and the end of each cycle.

These experiments take place in a situation when the battery is less than half discharged, as is usually the case in the operation of stand-alone systems. The minimum SOC reached by the battery of the stand-alone system during the monitoring period (calculated by charge integration is 0.68). This corresponds to the open circuit voltage of 12.55V as it can be found from the manufacturer's data (Figure 82). Two sets of experiments are performed here. In the first set, the battery starts at a low state of charge and is then charged to various states of charge to simulate the daily discharge/charge. The ultimate aim is to use this data to calculate the efficiency. The second set of experiments differs from the first only that the battery starts from a full state of charge.

In the first set of experiments, the battery is first discharged to a low level, with the final open circuit voltage 12.45V. The battery is charged for some time and the

open circuit voltage is recorded. The first 'daily' cycle starts at this point: the battery is discharged for 15hours and then charged until the amount of charge in the battery is equal to the amount of discharge. The final open circuit voltage is then recorded. Similarly with the previous experiment, the discharge and charge current were chosen close to the values observed in the stand alone system –discharge current (0.155A) similar to the night discharge current of the stand alone system and charge current equal to the average value of the small morning or evening charge currents of the stand alone system (0.985A). After the first cycle the battery is charged up a little to reach a higher SOC and the second cycle starts. The process is repeated to complete a third cycle. The currents that are used to charge the battery to a higher state of charge are set at values between 2A and 3.5A. The diagram of the experimental process is shown in Figure 91.

The second set of experiments consists again of three 'daily' cycles. To discharge the battery to different states of charge, starting from the initial full state, we either leave the battery to self-discharge, or a very low current-approximately equal to the night discharge current of the stand-alone system-is used. The diagram of the experiment is shown in Figure 92.

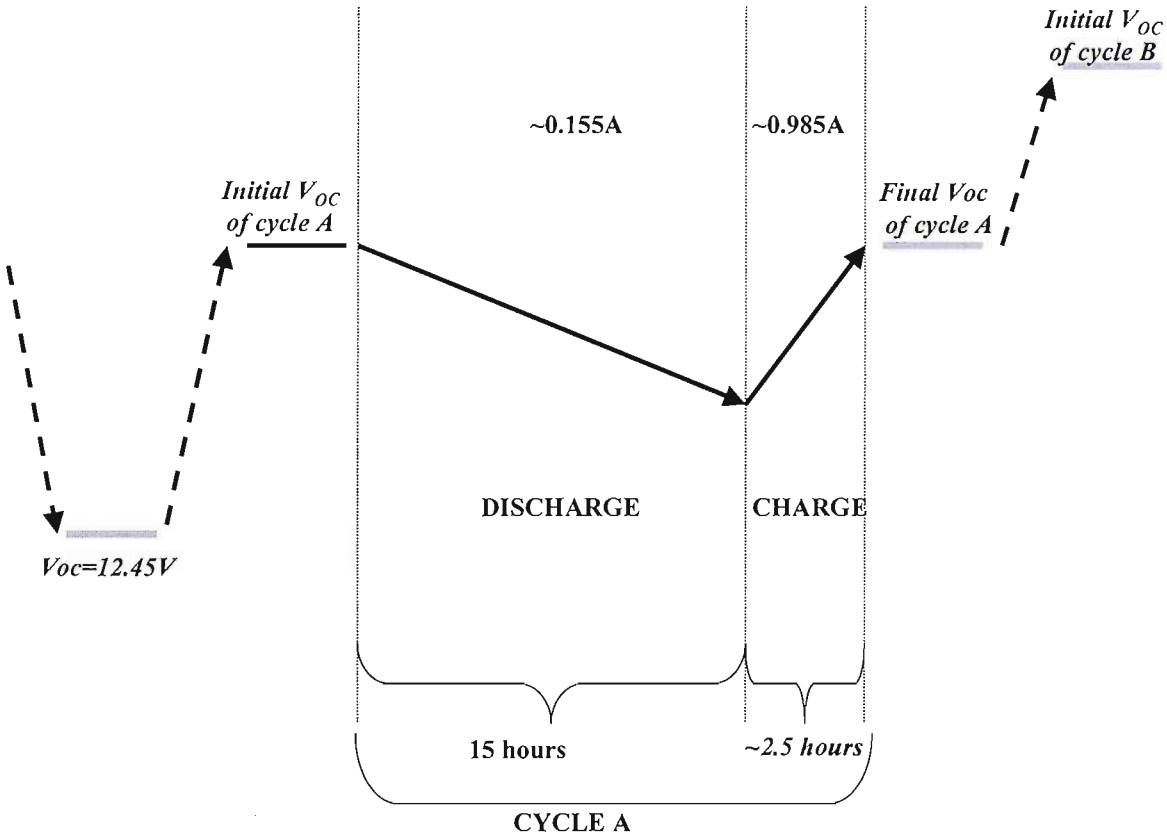

Figure 91 Experimental sequence of the first set of experiments. Only the first cycle is shown. The letters in italics correspond to the results while the Roman lettering corresponds to the settings. The dotted arrow lines show the initial charge/discharge sequence used to prepare the battery with the appropriate initial state of charge.

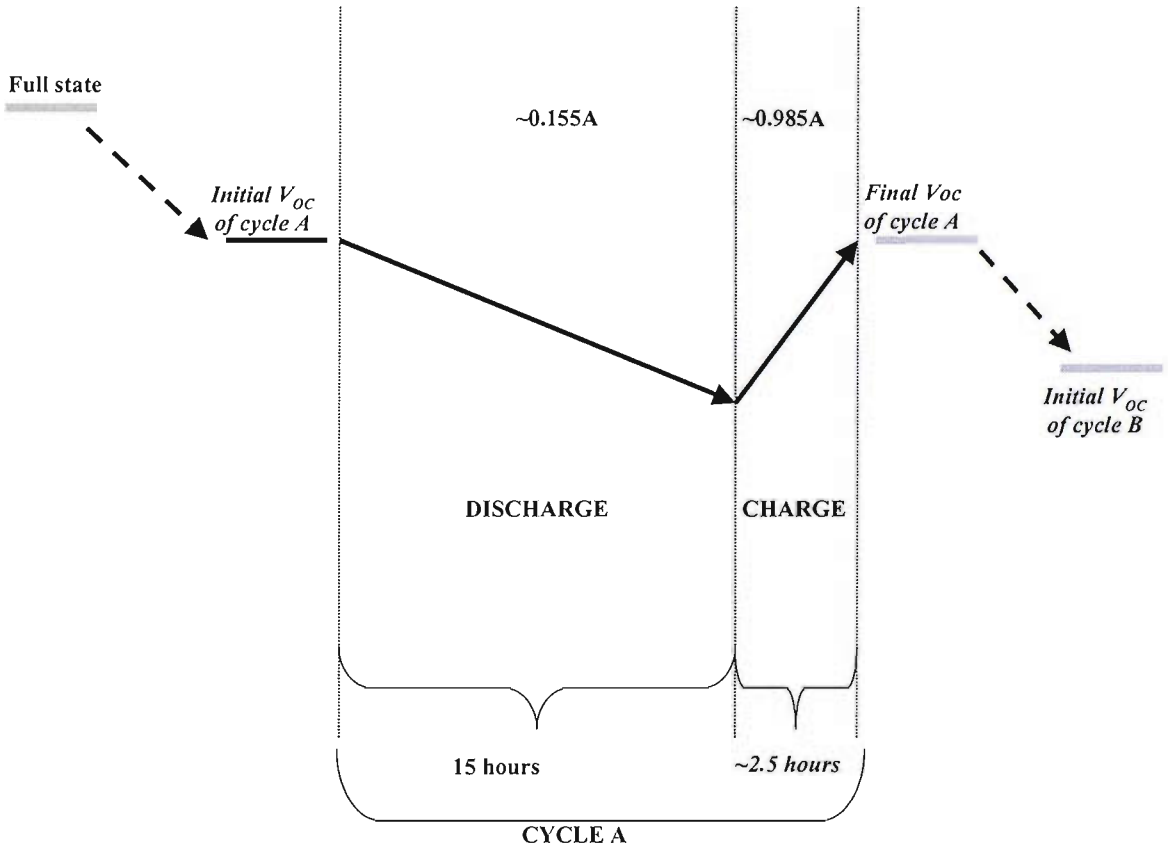

Figure 92 Experimental sequence of the second set of experiments. Only the first cycle is shown. The letters in italics correspond to the results while the Roman lettering corresponds to the settings. The dotted arrow lines show the initial charge/discharge sequence used to prepare the battery with the appropriate initial state of charge.

B. Results

The results of the two sets of the experiments, that is, the measured values of initial and final open circuit voltage of each cycle as well as the calculated- using curve fitting, corresponding values of state of charge, the calculated total charge-out and charge-in are shown in Table 9 (set one) and Table 10 (set two). According to the definition of the charging efficiency (see section 5.2.3):

n=charge out/charge in

n=(charge in-charge lost)/charge in

n=1-charge lost/charge in

The charging efficiency of the battery at different states of charge, as calculated from the results of the first set of experiments is shown in Table 9.

CYCLE No	A	B	C
Voc initial	12.563	12.671	12.779
SOC initial	0.694	0.812	0.934
Charge out	2.307	2.317	2.352
Charge in	2.430	2.359	2.428
Charge difference (in-out)	0.122	0.043	0.077
Voc final	12.557	12.658	12.765
SOC change that corresponds to charge difference	0.00122	0.00042	0.00077
SOC final	0.698	0.798	0.917
ΔSOC (SOC reduction)	0.003	0.014	0.017
Charge that corresponds to the SOC reduction (ΔSOC*100)	0.3	1.4	1.7
Efficiency	88%	41%	30%

Table 9 Results from the first set of experiments

CYCLE No	A	B	C
Voc initial	12.779	12.710	12.5962
SOC initial	0.993	0.856	0.730
Charge out	2.334	2.320	2.291
Charge in	2.336	2.417	2.299
Charge difference (in-out)	-0.002	-0.097	-0.008
Voc final	12.798	12.759	12.640
SOC change that corresponds to charge difference	0.00002	0.00097	0.0008
SOC final	0.955	0.911	0.778
ΔSOC SOC reduction	-0.022	-0.055	-0.048
Charge that corresponds to the SOC reduction (ΔSOC*100)	-2.2	-5.5	-4.8

Table 10 Results from the second set of experiments

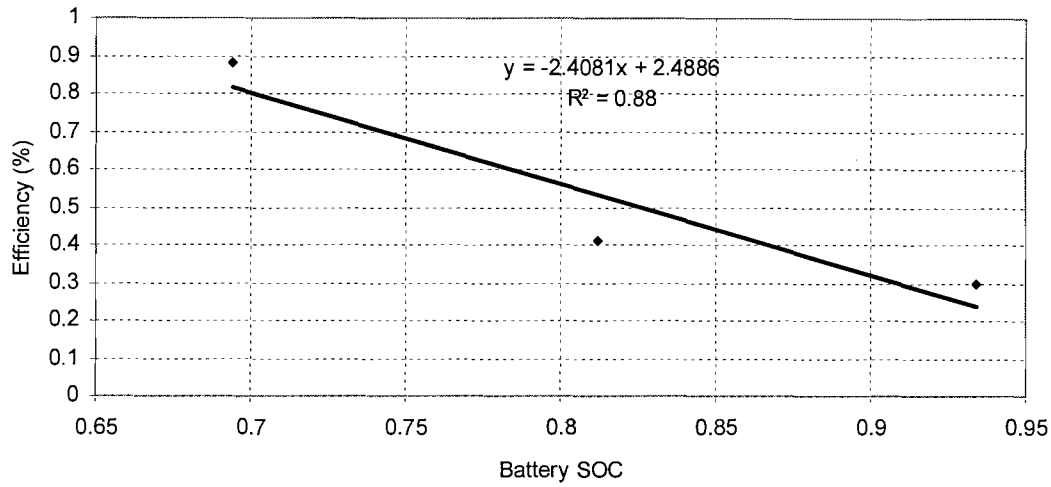

Figure 93 Efficiency of the battery at various states of charge calculated from the results of the first set of the experiments shown in Figure 91

C. Discussion

The results of the first test although they give surprising low values of efficiency, they are, similar with some results found in the literature: J.W. Steven and G.P.Convey, study in their paper[77] the incremental efficiency (the efficiency between two non-zero states of charge) at 22 °C of Torjan30XHS battery- a 12 volt flooded, lead antimony battery rated at 130Ah at the 20 hour rate by the manufacturer. Although, the battery type is different from the type used in the present work and there is not detailed description of the experimental process regarding the experiments conducted for the incremental efficiency, to allow for a direct comparison with the present study, the results show that the incremental efficiency is much lower than the overall efficiency (the overall efficiency is defined in the paper of J.W. Steven and G.P.Convey as the efficiency between zero SOC to the SOC under test). More specifically, they found that for states of charge higher than 80% most values are below 60% efficiency and states of charge close to the full state are represented of less than 50% efficiency.

However, the second set of the experiments conducted here put the results of the first test in doubt. The results of the second test show an increase in the battery SOC after each 'daily' discharge/charge cycle. Therefore, the results of the first and the second set are not consistent and although they cannot lead to an estimation of the

battery efficiency, they can lead to some interesting conclusions regarding the battery behaviour.

There seems to be a strong memory effect in the performance of the battery that is not reflected in the value of the open circuit voltage after rest. The memory effect is related with the battery charge or discharge before rest. As a result, the charging efficiency of the battery measured in this way is affected by the charge/ discharge history of the battery.

7.5 Conclusions

The battery performance has been studied, in the experimental stand-alone system presented in section 3.3 as well as through laboratory experiments.

The analysis of the stand alone system data has shown that, although relatively low values of solar radiation are adequate to meet the load demand, some energy from the battery is needed for more than 12 hours every day from November until April. The characteristic pattern of an almost full battery on a sunny day is an interruptive charge/discharge as imposed by the regulator and lasts many hours with consequent loss of energy. This energy loss, however, does not appear to be highly significant as there is surplus in energy in any case. More significantly, more charge enters the battery during periods of low solar radiation when it is charged at low currents and no interruptive charge/discharge takes place.

It is not possible to attribute one particular value of daily charging efficiency to an almost full battery under operation in a PV system. This is because the particular way of charging/discharging, which varies daily, seems to affect the efficiency when the battery operates close to the full state of charge. These intervals appear to have a little effect on the accuracy of the daily energy balance model since energy is likely to be dissipated by the charge regulator. There may, however, be an effect on the degradation of the battery which is not easy to quantify.

Laboratory experiments which studied a series of consecutive discharge/charge cycles showed that the battery state of charge is lower at the end of a subsequent cycle than at the end of the proceeding one. It is significant that the difference between the charge received and the charge given out does not depend on the depth of the cycle. To charge the battery to the initial state of charge, a very low current or an interruptive charge/discharge process should be used.

In addition, the results of laboratory experiments have revealed a memory effect of the battery charge/ discharge history on battery performance. The charge-discharge history is not reflected on the value of the open circuit voltage and this poses a difficulty in the quantitative estimation of the battery efficiency. It seems, however, that the loss of charge occurs only when the battery operates close to the full state of charge, in accordance with the literature[61].

8. VALIDATION OF THE MODEL BASED ON DAILY ENERGY BALANCE

8.1 Introduction

The model based on daily energy balance (or long-term model) is widely used as a tool in the system sizing (see chapter 9), mainly with the purpose to obtain analytical expressions regarding the relation between the generator size and the storage capacity of the battery. However, the model based on daily energy balance represents the complex operation of a stand-alone system in a very simplified way (chapter 6). There is little adequate research so far regarding the confidence with which we can apply these results to practical operation. Some issues regarding the simplifications of the model based on daily energy balance are of particular importance and are examined in this work. One is that the capacity of the battery is considered constant while, in reality, it depends on the current. The variation of the battery capacity with the current poses a difficulty in the specification of the battery capacity while the battery is in operation in the PV system, and this hinders the determination of the battery SOC. There is another reason, however, why the determination of the battery SOC is difficult: the charge received by the battery depends on the SOC (i.e., on the charge already in it), which, in turn, depends on various chemical reactions that degrade the battery, for example, sulfation (section 7.2.1). As a result, the charge actually available in the battery may be lower still. These issues affect the validity of the model based on daily energy balance and are the subject of this chapter. In this work we analyse the six months measured data, of the stand-alone system described in section 3.3 using excel software and we compare with the results from the model based on daily energy balance described in section 6.3.

The aim is to examine to what extent the model based on daily energy balance can provide information about the storage requirement of a stand-alone system. More specifically the objectives are:

- To calculate the battery state of charge from the experimental data during the operation of a PV system
- To determine the effective charging efficiency of the battery

- To analyse battery operation in terms of climatic cycles. In particular, to comment on the frequency at which the battery reaches the full state of charge, and the length of the time intervals for which it remains at full state (discharged during the night and fully charged during the day).
- To present the research up to day and identify the points that need further investigation regarding the validity of the model based on daily energy balance

It has been found in this work that the model based on daily energy balance approximates quite well the value of the minimum SOC reached by the battery over the winter season of the system, and it can be used in order to find the storage requirement of a system, but it does not approximate well the SOC of the battery close to the full state of charge.

This chapter includes five sections. Section 8.2 describes the calculation of the charge received given out by the battery and two methods are introduced for the calculation of the SOC. The first method and the results is presented in section 8.3 is based on current integration taking into account the effective charging efficiency. The second method and the results is presented in section 8.4 is based on voltage measurements and correlation of the voltage values with the integrating SOC without taking into account the charging efficiency. Section 8.5 is a discussion on the results of the two methods and section 8.6 the conclusions of the chapter

8.2 Estimates of the battery state of charge

The charge received/given out by the battery can be calculated on a daily basis by current integration. The charge can be expressed in days of storage- the resulting daily charge is divided by the measured daily load and the cumulative charge from the beginning of the monitoring period is calculated on a daily basis (Figure 94).

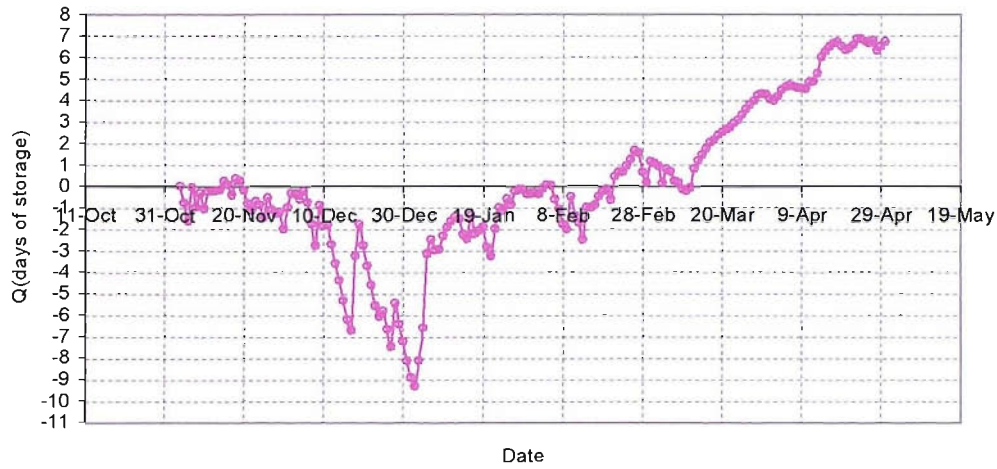

Figure 94 Cumulative charge Q received/given out by the battery

In some cases, for example, between the 14th and the 20th of November or after the 20th of February, the experimental results show that the net amount of cumulative charge received by the battery is becoming positive. This, however, cannot possibly mean that the initial battery capacity is increasing. Especially from the mid February and onwards the experimental results show an increase in the received charge that varies almost linear by time. The above observations mean that not all of the received charge is stored by the battery and some of this received charge is lost. This is expected because the charging efficiency of the battery is less than 1 (5.2.3). At the first sight it would seem that the charge stored in the battery can be determined from the data shown in Figure 94 by making use of the battery efficiency given by the manufacture or in reference data. This however is not the case. It appears (see section 5.2.3) that there is no standard way of defining charging efficiency. Figure 95 shows two charging efficiencies: supplied by the manufacturer for the battery type Sunlyte 12-5000X (used in this study) and according to IEC standard. The discrepancy between these two sources is evident. Therefore, the next step should be an estimate, using experimental results, of the profile of the battery state of charge in order to compare with the results from the model based on daily energy balance.

We use two models for the calculation of the state of charge of the battery from the measured data of the stand-alone system. One is by current integration taking into account the charging efficiency of the battery and the second is using the measured battery voltage. We shall show in 8.4 that the most consistent comparison is between the SOC at the sunset of one day and the battery voltage shortly before sunrise of the next day. The SOC is found by 5 min current integration of raw data (i.e. assuming charging efficiency equal to one) and dividing by the nominal battery capacity. The nominal capacity of the two batteries used in the system is 100 Ah each at the C/100 rate (see section 3.3.2). We should note, therefore, that since the total discharge current (0.3 Amps) is much lower than the current at which the nominal (rated) battery capacity is specified by the manufacturers, the actual capacity of each battery for this application will be higher than 100Ah. The battery capacity will be constant because the discharge current is constant (see section 5.2.3).

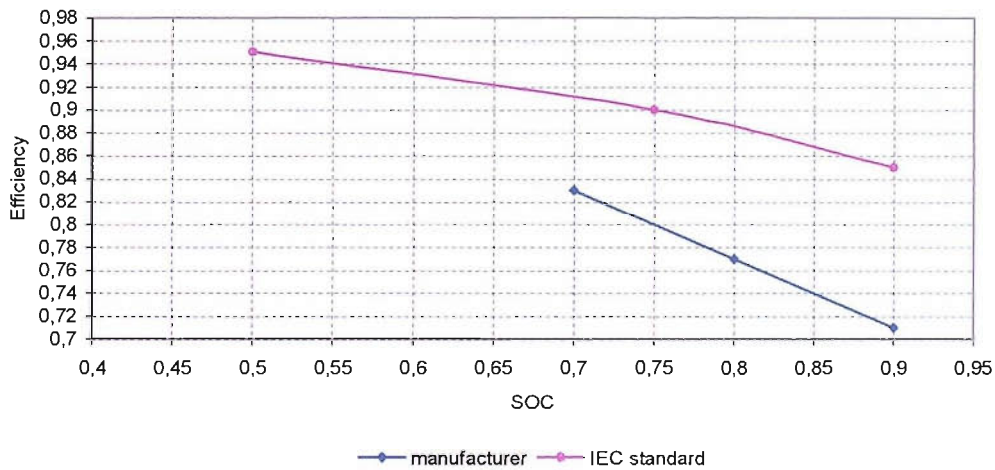

Figure 95 Battery charging efficiencies according to the manufacturer and according to the IEC standards

A correction should be applied to the results to allow for the different time of the day which is considered by the different methods. As discussed in section 6.3 the model based on daily energy balance calculates the SOC at the sunset. The experimental data, on the other hand, gives the cumulative charge at midnight. The cumulative charge calculated by integration of the experimental data should therefore be lower than the corresponding value found from the model based on daily energy

balance. The difference between the two values should be equal to the amount of charge given out by the battery between the sunset and midnight. This difference varies throughout the year, depending on the time of the sunset, with the maximum difference occurring in December when the midnight is about 7h after sunset. Even for this month, this difference is small, about 2.1 Ah, corresponding to about 0.3 days of storage.

The two models for the calculation of the SOC are presented in the following sections.

8.3 Determination of the SOC by current integration

The battery experiments in chapter 7 have shown that the loss of charge should occur close to the full state.

Therefore the profile of the battery 'true' SOC has been calculated considering the battery efficiency equal to 1 for all states of charge and zero when SOC is 1 (Figure 96):

If $SOC \geq 1$ and $Q_b > 0 \Rightarrow Q_b' = 0$

Where Q_b is the charge that will be received by the battery the next five minutes and Q_b' the increase in the battery charge the next five minutes.

This is a good approximation of charge being lost only close to the full state. Figure 97 shows the resulting SOC calculated by this model.

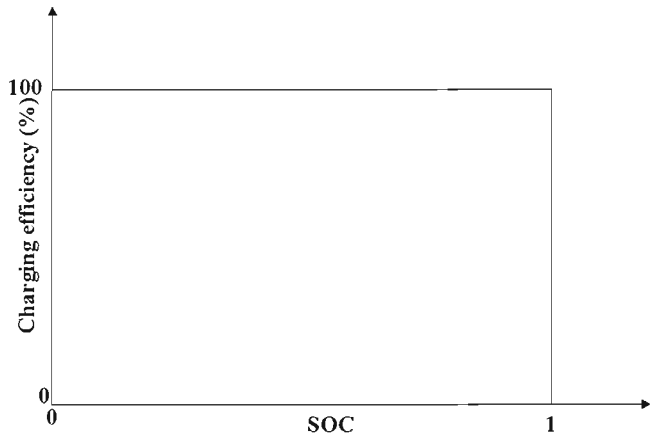

Figure 96 Efficiency variation in current integration model

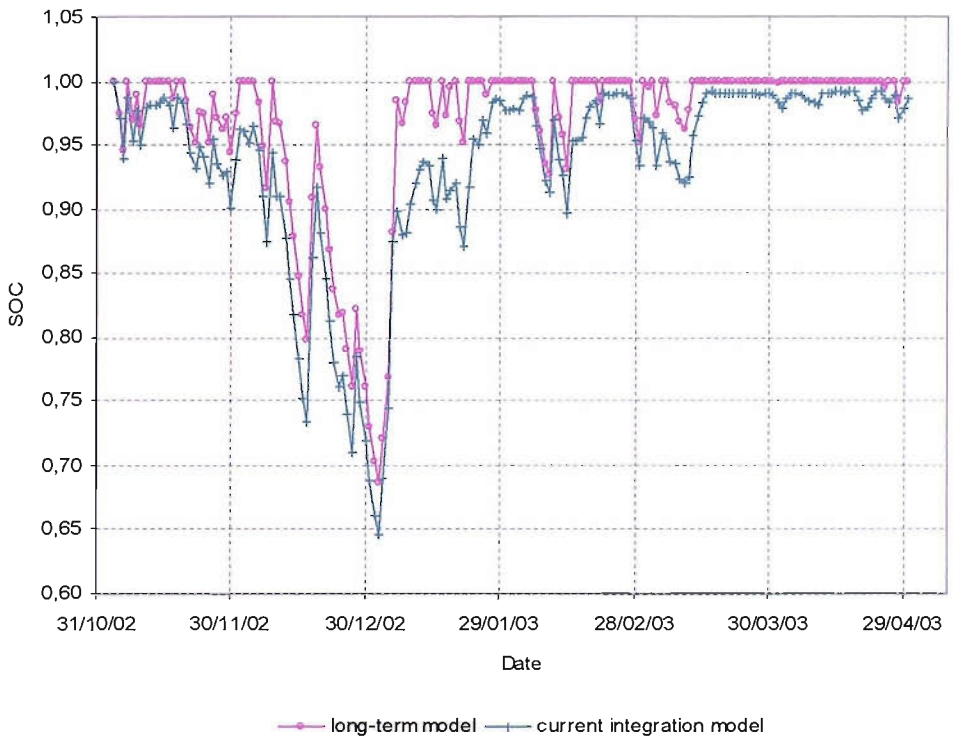

Figure 97 The current integration model gives the battery SOC assuming charging efficiency equal to zero when SOC≥1 and one in all other cases

8.4 Determination of the SOC from voltage measurements

One way of estimating the SOC of the battery at the end of a day is by disconnecting the battery just before the sunset (when the charging process stops), and

measuring the open circuit voltage. At least 48 hours should be allowed for the voltage to settle to a constant value. This voltage can then be converted to SOC using the manufacturer's data. In this method, we choose the voltage just before the sunrise of the next day to estimate the SOC of the battery that corresponds to the end (12:00pm) of the previous day. The reason for choosing the morning voltage is that during the night the battery is discharged slowly and at constant current. Thus,-almost independently of the charging/discharging process during the previous day,-the voltage is expected to settle at a value that will differ by a constant value from the open circuit voltage that would obtain if that time the battery had been disconnected and the voltage was measured after adequate rest. In order to allow for the same discharge duration for all days we choose the values of voltage at equal time intervals from the sunset time for all days. The same hour was selected as the sunset time for all days of the same month, as determined by ESRA software. ESRA software calculates the hourly monthly average values for a given location and a given tilt angle. It is therefore easy to select, for each month, the hour of the day for which the radiation becomes zero (sunset). The longest 'common' discharge time that we can allow for is 8 hours, since the shortest nights of the monitored period are those of April and last 8 hours.

Figure 97 shows the SOC of the battery as a function of the voltage in the next morning. To represent a meaningful procedure, only the points which correspond to the SOC below or equal to 0.95 are included in the graph. By choosing points with $SOC \leq 0.95$, we are considering only days at the first months of system monitoring, which are (December, January and February) for which the SOC calculated by integration rarely exceeds 1. This is because the battery almost never reaches the full SOC during these months, and because the cumulative errors are small, since we are still at the beginning of the integration process. In addition, when the SOC is lower than 0.95, the charging efficiency is approximately equal to 1 (see section 5.2.3). We have therefore reasons to believe that this method gives a good approximation to the true state of charge. However, there are no points at high voltage values, (higher than 12.5V), since those that correspond to SOC values greater than 0.95 are not included.

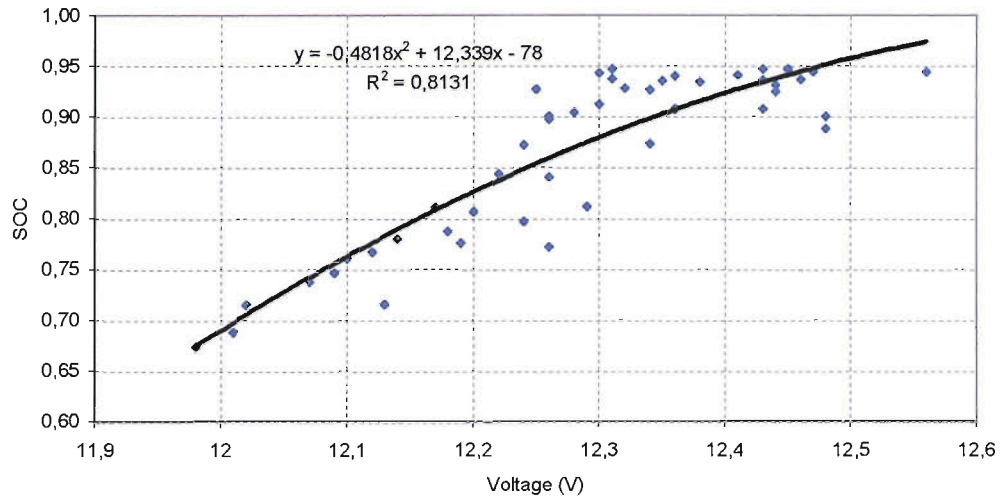

Figure 98 The SOC obtained by current integration and the voltage in the morning of the next day (points). Shown also is a polynomial fit to the measured data

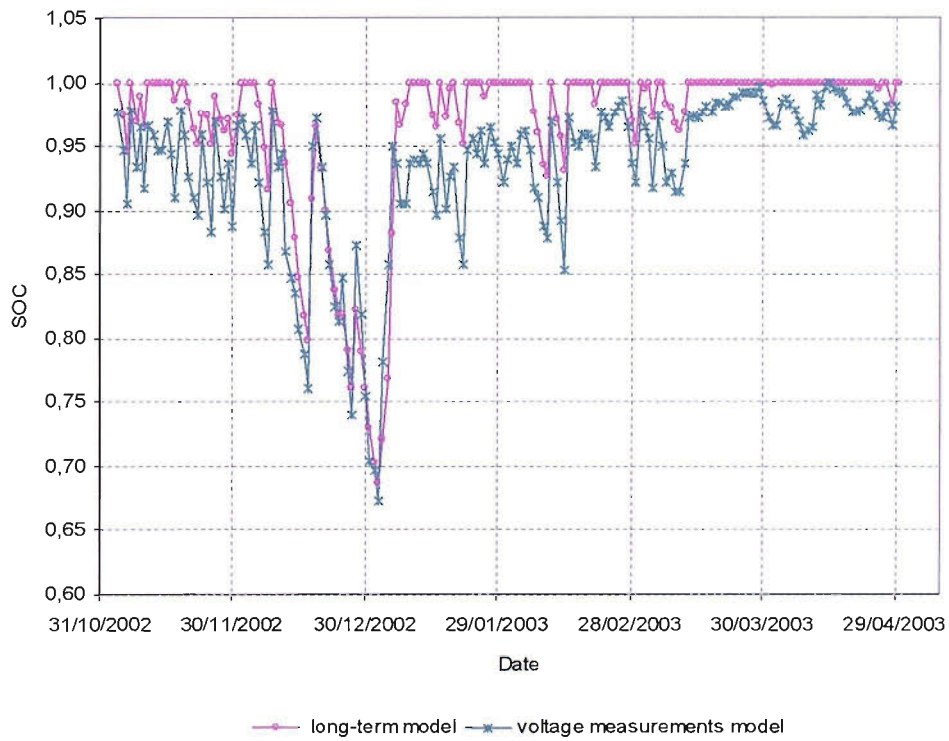

Figure 99 The voltage measurements model gives the battery SOC estimated from voltage measurements

A second order polynomial curve fitting is applied to the points. The limiting condition for the equation of the polynomial is to give the value one (fully charged battery) for the highest observed voltage value. All voltage values can now be converted to SOC values using the equation of the polynomial. The daily SOC is plotted as a function of time in Figure 99.

8.5 Discussion

From Figure 97 we can see that the minimum value of the battery SOC is represented well from the model based on daily energy balance. The SOC profile close to the full state of charge, however, is not represented very well by the model based on daily energy balance, especially when the battery recovers from deep discharge.

The conclusions regarding the SOC calculated by voltage measurements (Figure 99) are similar. Figure 97 and Figure 99 show that according to the model based on daily energy balance the battery is charged more often to the full state and remains at the full state for longer periods of time than the results of the experimental data show. For example, according to the model based on daily energy balance the deep discharge of the battery in winter starts in the 9^{th} of December and the battery becomes fully charged again in 6^{th} of January, that is, less than a month later. This difference between the results of the experimental data and the model based on daily energy balance should be attributed to the simplifications of the model including the fact that the charging efficiency is assumed unity when the battery is approaching the full state (see section 6.3). On the contrary for states of charge lower than 0.85 the results from the model based on daily energy balance agree very well with those from the analysis of the experimental data, since the effect of charging efficiency is not so strong.

Figure 100 compares the results of the two methods of calculation of the SOC and the results of the model based on daily energy balance. The results of the two methods of calculation are very similar.

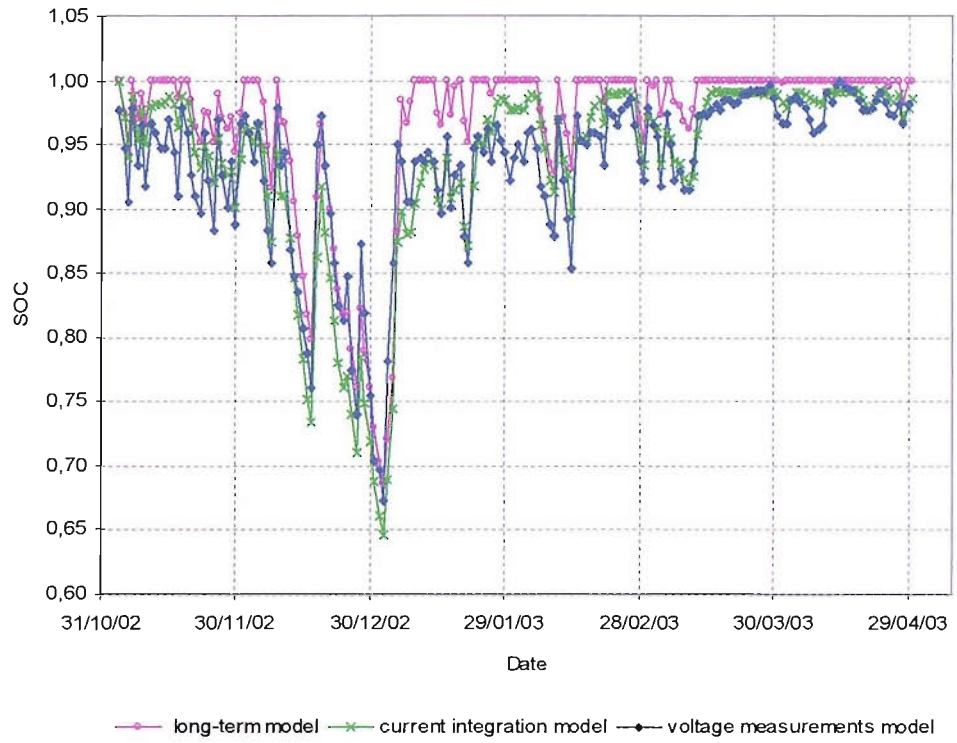

Figure 100 Approximation of the SOC using the two models for the analysis of the experimental data and the results from the model based on daily energy balance

8.6 Conclusions

The battery state of charge has been calculated from the experimental data for the months November to April by using two models: firstly, by current integration, assuming that the charging efficiency loss occurs only at full state of charge and secondly, by voltage measurements which were used to infer the battery state of charge at the end of the night's discharge. It has been found that both methods give similar profile of the state of charge. Furthermore, the results obtained using the two models for the lowest state of charge during a seasonal cycle are in close agreement with the results from the model based on daily energy balance. Therefore, the model based on daily energy balance can predict accurately the maximum storage required and can be used for system sizing purposes.

However, the model based on daily energy balance is not a good representation of the battery climatic cycling close to the full state of charge. It shows that the battery

reaches full charge more frequent than the analysis of the experimental results indicates and that it remains at the full state for longer periods. A more refined model of the battery behaviour, need to be used to account for the charge loss when the battery is nearly full.

9. SIZING OF STAND-ALONE PV SYSTEMS

9.1 Introduction

Virtually all PV system-sizing algorithms today are based on the statistics of solar radiation in the past. The sizing methods[82,83,84,85,86,87,88,89] use long-term monthly average radiation values and daily series of solar radiation data. In system sizing the day-to-day variations of solar radiation are very important. Different daily radiation patterns may well lead to the same monthly averages but to significantly different battery state of charge patterns as a function of time and therefore different LLPs. This is because a particular sequence of high and low daily radiation values might be more or less favourable to the system needs. However, when using sequences of measured past daily solar radiation data a limitation regarding the accuracy of the results is naturally arising since the 'historical' daily solar radiation profile is very unlikely to be repeated in the future[90]. All that has been proved so far is that the statistical properties of the solar radiation sequences make possible the generation of daily solar radiation series with the same features as the historical data. Generated data series are often used for system sizing when long series (more than 20 years) of daily radiation data are not available. The most widely used method for artificially generated radiation data is that of Augiar[91].

However, as mentioned by Lorenzo[7], long sequences of daily solar radiation values generated from shorter series of measured data do not necessarily produce more accurate results; Lorenzo[90] shows that predictions for loss of load probability (LLP) less than 10^{-2} are statistically meaningless which agrees with results previously presented by Klein[92].

In this chapter we will discuss a method for deriving the sizing curves from daily series of solar radiation data, developed previously in Southampton University[93] and we will present and discuss sizing curves from three locations-London weather station (UK), Salzburg airport (Austria), Heraklion (Greece)-derived using this method. Instead of using the concept of LLP we define here the reliability of supply as the duration of system operation without 'loss-of-load'.

In addition, in this chapter, we examine the effect of the long term solar radiation profile on the time profile of the minimum storage requirement for the case of Efford (UK) and for the case of Potsdam (Germany). Thus we demonstrate the sensitivity of the system output to the solar radiation statistics as a function of time.

The model based on daily energy balance (section 6.3) has been used in this work. It will be shown that the effect of varying the length of the period of data may be critical to the sizing results often leading to considerable under-sizing of the system.

In the case of Efford we find that the statistics of solar radiation has changed to a surprising degree over the past 36 years. Although the yearly average daily solar radiation has remained almost constant, the probability of a long sequence of days with low solar radiation has increased substantially. This has significant impact on the design of stand-alone PV systems, in particular, on the size of the battery: whilst 8 days of storage would have been sufficient to provide an uninterrupted supply in 1958, 13 days would have been needed in 1994. In the case of Potsdam, appears to be no significant trend in the storage requirement. The variation in the storage requirement among different years, however, is high and this increases the uncertainty with which we can specify the storage size.

Section 9.2 is an overview of the sizing and the sizing methods. Section 9.3 describes the methodology with which we obtain the sizing curves and presents the sizing curves of three locations based on 10 years of data. This section also describes the methodology used in order to obtain the minimum yearly storage requirement profile of a system. Section 9.4 is a discussion of the results of the new sizing approach. Also discusses the minimum storage requirement profile based on historical solar radiation data for two locations- Efford (UK) and Potsdam (Germany). Section 0 is the conclusions.

9.2 Literature review

9.2.1 Introduction

Sizing a stand-alone PV system means to determine, for a given location and load demand, the battery capacity, array size and array tilt angle in order to minimize the cost and meet the minimum acceptable level of system availability.

Availability is usually defined as the percentage of time that the power system is capable of meeting the load requirements. For system sizing studies system failures or interruptions due to maintenance are not taken into account and the availability is determined by the energy balance (see section 6.1) in the PV system. Availability[83] can vary widely depending on the application and the wishes of the user. For example, for stand-alone household systems in rural areas an availability level of 95% may be considered sufficient but for telecommunication systems a level of 99.99% may be required. The minimum acceptable level has a very important influence on cost. The system cost increases rapidly in trying to obtain the last few percent of availability[84].

Another way to express availability is the loss of load probability (LLP). This is the fraction of hours of load demand which cannot be met by the system. Therefore:

LLP=1-Availability

In addition, we can define the energy deficit as the fraction of load demand, which cannot be met by the system. In order to design PV systems and test their performance we use models based on daily energy balance (section 6.3) and modelling fo the system components (Chapters 4 and 5).

In this chapter a brief overview of the philosophy of the existing system sizing methodology will be presented (section 9.2.2) and the basic sizing method (section 9.2.3), which is also the most widely used in practice, will be analysed. Finally a brief reference to the analytical sizing methods is presented in section 9.2.4.

9.2.2 Sizing methods

There is no universally accepted method of sizing. Most suppliers have developed their own models and computer programmes. The several methods developed that do not require detailed simulation of the operation of the system components, for example, those of Barra[82], Chapman[83,84] , Bucciarelli[85,86], Sidrach-de-

Cardona[87,88] and Lorenzo[89] and those mentioned in several textbooks on PV systems[7,6,4,57] are based on the concept of the daily energy balance (section 6.1). In the simpler methods, usually those referred to in the textbooks[7,6,89,4] this design value is taken to be the mean daily solar radiation, either the yearly mean or the monthly mean radiation during the "worst month". The battery size - expressed typically as the number of storage days - is then estimated by experience and depends on the location.

The more sophisticated methods of sizing[82-90] use the concept of the loss of load probability (LLP) to determine analytical expressions for the generator and battery size. Using model based on daily energy balance (as discussed for example in section 6.3), it is possible to find the combinations of generator and battery size (the system sizing curve) that lead to the desired value of LLP. Thus, the methods described above-also referred to as analytical-allow the sizing of PV systems for a given location in a simple way, using just a few sizing parameters instead of long sequences of solar radiation data. Apart from approaching the problem of sizing in various ways, the several methods of sizing, use different assumptions to calculate the radiation on inclined surface.

After finding the combinations of storage size-generator size that lead to a fixed energy deficit, economic optimisation has to be carried out. Typically, this is done by finding the most optimum combination[94] of generator and battery size. It is important to note, that however, at the economic optimisation the need for battery replacements during the system lifetime is not usually taken into account.

9.2.3 Intuitive Method[6]

We will apply the method to the simplest stand-alone system, which consists of a generator a battery a load and a charge regulator. The charge regulator keeps the system voltage almost constant (within a maximum and a minimum limit as described in chapter 7.2.2). For simplicity we assume constant load and constant operating voltage. In some cases in the literature[6,7] this method of sizing is referred to as intuitive because it includes oversizing of the battery and the generator (in order to ensure good system reliability), based on experience.

It is convenient to express the radiation incident on a PV panel in peak solar hours (PSH), equal to the number of hours of the irradiance at standard test conditions (1kW/m2), which would produce the same radiation:

$$PSH = \int_0^{24} G\ (kW/m^2)dt \qquad (9.2.1)$$

In (9.2.1) we can approximate by G the hourly mean value of the in plane irradiance.

Therefore, PSH is numerically equal to the radiation in kWh/m^2 per day. The reason of expressing the radiation in peak solar hours is that we can find the energy (Wh) produced at constant voltage by a PV array during a day E_{PV} just by multiplying the peak power (W_p) produced under STC by the number of a certain typical average value of PSH. Therefore:

$$E_{PV}=W_p \cdot <PSH> \qquad (9.2.2)$$

Sizing method based on energy balance equates the energy supply (9.2.2) to the demand (daily load energy, L), from where the generator size can be calculated in W_p:

$$W_p \cdot <PSH> = L \qquad (9.2.3)$$

For example in locations where the solar radiation variations are not too pronounced throughout the year, the system sizing is based on the yearly energy balance (the average day of the average year). In this case, <PSH> is the yearly average daily PSH for the typical year at the location in question. The typical year consists of monthly average daily data of solar radiation averaged over several years of data.

In other locations, where the solar radiation varies considerably throughout the year, instead of the yearly average daily PSH we use the monthly average daily PSH of the worst month. The worst month is the month for which the ratio between

radiation and consumed energy is the least favourable. In case of constant load is the month with the less energy production.

The generator can be oversized by a factor F_{S1}. In other words, the size of the generator can be chosen to ensure that the energy produced during the design period exceeds the demand of the load by a margin, which depends on the designer's experience. Lorenzo, for example, suggests[90] F_{S1}=1.1 for southern Spain.

If the system sizing is based on the yearly energy balance then there might be an energy deficit for one or more months. In order to find the energy deficit all over the year, we should calculate the monthly average daily energy produced, then the monthly average daily energy deficit and sum the monthly average deficit over the year.

For the useful battery capacity (C_U in kWh), as defined in section 7.2.1, an empirical assumption can be made[7]

$$F_1 \cdot \overline{L} \le C_U \le F_2 \cdot \overline{L} \quad (9.2.4)$$

where the $\overline{L}$ is the monthly average daily energy consumption of the load and F_1, F_2 are constant factors and are the upper and lower limit in correspondence of the storage sizing factor F_{S2}. The storage sizing factor F_{S2} is the number of days without sunshine (or storage days) for which we design the system. The values F_1=3, F_2=5 are common values for rural electrification purposes recommended by Lorenzo, for Spain[90]. The actual choice depends on expected continuous days without sun for the location and the reliability that we aim to achieve. From (7.2.1) the total (nominal) battery capacity (C_B) needed can be obtained.

If the system sizing is based on the yearly energy balance then to find the total battery capacity needed we should add the energy deficit for a year in (kWh) divided by the depth of discharge.

If we want to take into account the energy lost in the controller we should divide the battery capacity found by the controller efficiency n_{con} to find the final battery capacity.

As an illustration of the sizing method based on energy balance, let us consider a stand-alone system located in Southampton. Let's assume a constant 12V and 0.3A load, which operates 24 hours. The daily consumption of the load will be 24*0.3*12=86.4Wh. The tilt angle of the modules will be chosen 66°, which is the latitude plus 15° (see section 2.10). The lowest depth of discharge of the battery will be chosen as 0.75. The available data for the long-term monthly average daily radiation on the horizontal and inclined surface are from the closest weather station, Efford (50.44° latitude) as given using ESRA[41] software.

The system sizing should be done for the worst month since the solar radiation varies considerably throughout a year (Figure 101). From ESRA software we find that the monthly mean daily radiation on the inclined surface for the worst month is 1.273 kWh/m^2. In this application we will ignore the losses in battery and controller, so using equation (9.2.3) we find that the required generator is 67.92 Watt peak power at least (F_{S1}=1). The useful battery capacity needed to allow for, say, 15 days of storage (F_{S2}=15)-a typical value for the UK- is 1.296 kWh from (9.2.4). The battery capacity C_B needed is 1.728kWh (or 144 Ah), from equation (7.2.1), section 7.2.1. In this case sizing the system for the yearly mean solar radiation would result in a very large battery.

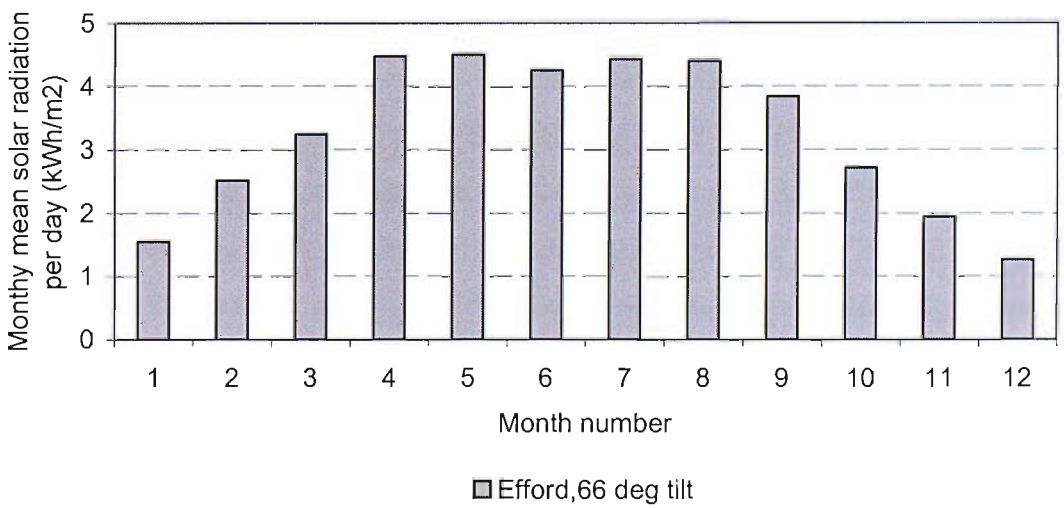

Figure 101 Energy supply to the photovoltaic generator.

9.2.4 Analytical methods of sizing

M. Sidrach-de-Cardona[87,88]

M.Sidrach-de-Cardona proposed an analytical expression of the array size as a function the following:

- The yearly mean daily radiation on the tilted surface
- The minimum value of the monthly mean radiation on the tilt surface
- The variation of the monthly mean daily radiation on the tilted surface
- A term that accounts for non-linearities in the way that the variation of monthly mean daily radiation on the tilted surface affects the array size for different storage sizes

The parameters of the model were estimated for three different LLP values and for storage sizes 3-6 days of storage. The daily solar radiation data used for the development of the model were from 1961-1990. The radiation on the array plane was calculated using the isotropic model for ground reflected radiation and Hay's anisotropic model for the diffuse.

M. Egido and E. Lorenzo[89,90]

This method is based on the observation that for each location the array size is related with the storage size by means of two parameters that depend on the LLP value. Thus using data from several locations in Spain M. Egido and E. Lorenzo constructed isoreliability maps for several values of LLP from which the values of the above parameters can be obtained. They used solar radiation data from 1972 to 1984. They further related each of the above parameters with the LLP value using two coefficients characteristic of the location. Therefore, there is the possibility to find the isoreliability curve for any value of LLP and for any location presented on the maps as follows: By choosing two values of LLP for which there are maps available, it is possible to find, using the maps, the values of the parameters that relate the array size and the storage size for each LLP value. Then, the four coefficients that relate the two LLP values with the location can be calculated. From those, the parameters that relate the array size and the battery size can be calculated for the desired value of LLP.

R.N. Chapman[83,84]

Instead of using the average radiation of the worst month to calculate the generator size R.N.Chapman uses the 'design insolation'. He defines the 'design insolation' as the variability of the radiation on the inclined surface- a polynomial function of the monthly average radiation on the inclined surface of the worst month. The method is based on the observation that the LLP is very similar for sites with the same design insolation on the inclined surface (for a given storage and tilt angle). R.N.Chapman developed a model based on daily energy balance which calculates the LLP for a fixed value of design insolation. The parameters of the polynomial, which defines the value of the design insolation, can be found iteratively, from the model based on daily energy balance for fixed storage and tilt angle, as those that minimize the deviation among the LLP values of different sites. 23.5 years of solar radiation data from 20 sites of the U.S. were used. The radiation conversion to the inclined surface was made using Liu and Jordan model.

The estimated values of parameters valid for the set tilt angle are used to generate array-sizing nomograms (design insolation as a function of monthly average daily horizontal radiation)

Storage-sizing nomograms (LLP as a function of days of storage) are generated by calculating LLP values for a range of storage values.

L. Barra[82]

L.Barra started from a geometric approach to the system-sizing problem. There are two extremes of system sizes: One, the PV system is small compared to the load, so all energy produced is transferred to the load. Two, the PV system is large enough to meet the load demand and charge the battery completely. In a system of co-ordinates where in the X axis we plot the amount of energy that is delivered to the load and the Y axis corresponds to the fraction of the load that is not covered the extremes mentioned above, correspond to the asymptotes of a hyperbola curve, the exact shape of which is linked with the storage capacity by means of two parameters. The values of the parameters were found from the best fit to the results of a simulation which gives the storage curve. Thus the equation that gives the array area as a function

of the storage capacity can be obtained. The solar radiation data used in the simulation were of the meteorological stations of the 'Aeronautica Militare Italiana'.

L.Luis and J.R. Bucciarelli[85,86]

The method of L.Luis and J.R. Bucciarelli treats the energy capture, storage and dispersion process as a random walk in the storage domain. To apply the technique one must know the variance as well as the mean of the probability density of the daily solar radiation on the plain of the array. There are two events: An increase in the energy in the storage by Δ with probability p, or a decrease in the energy in the storage by Δ with probability q. The probabilities p and q and the amount Δ are related with the variance and the mean probability density of the solar radiation. Then an equation that gives the number N of possible energy states of storage can be found as a function of the LLP for a day and a given array output. The storage capacity C, is $C=N^* \Delta$.

The above process was modified to account for the day to day correlation, depending on whether the previous day there has been an increase or decrease in the storage capacity.

9.3 Methodology

9.3.1 Sizing curves

The system considered here is the one described in section 9.2.2 and the sizing study will be done for three location-London weather station (UK), Salzburg airport (Austria), Heraklion (Greece). The minimum generator size is determined from the daily energy balance as described in section 9.2.2. Table 11 shows the weather and the system parameters of each of the three locations considered here, the monthly average daily radiation of the worst month and the minimum generator size that should be used. Firstly we consider array without oversizing (oversizing factor equal to 1). Then we consider larger arrays-the largest corresponds to oversizing factor 2.5. For each array size we determine the minimum necessary battery size so that there is no loss of load for the period under consideration.

	LONDON WEATHER CENTRE	SALZBURG AIRPORT AUSTRIA	HERAKLION
Latitude	51.52	47.8	35.32
Optimum angle	66	63	50
Monthly average radiation at the optimum angle (KWh/m2)	0.870	1.481	2.726
Minimum generator size (W)	99.4	58.34	31.69

Table 11 Weather and system parameters from three locations

The model based on daily energy balance of section 6.3 was used to find the battery state of charge (SOC). The input is 10 years (1981-1990) of daily solar radiation data on the horizontal plane for each of the three locations. The data have been processed to determine daily solar radiation on the inclined plane using ESRA software.

The battery size is determined by the following argument. Let us suppose that for a given generator size and a battery size (n days say) large enough to guarantee no loss of load, the battery reaches the lowest state of charge SoC_{min}. This happens during a climatic cycle when the battery is gradually discharged starting from a full state of charge on some day N_1, reaches SoC_{min} on a day N_2, and is finally fully charged on a subsequent day N_3. Figure 102 shows an example of three consecutive climatic cycles. Let us consider the third cycle, in which the battery reaches the lowest SoC and that determines the maximum amount of storage needed for the system. The energy deficit during the climatic cycle is the energy deficit until the day N_2 (inclusive). Given that the state of charge is calculated at the sunset of the day, the energy deficit until the previous day, day N_2-1, is:

$$E=n\cdot(1-SOC_{min})\cdot L \quad (9.3.1)$$

where n is the battery capacity in storage days that we used as input to the programme and L is the energy consumed by the load daily.

This energy deficit determines the battery size n_{min} which is needed for the system to supply the load without interruption. For this battery size, the SOC_{min} at the day N_2 is becoming zero and we therefore have

$$n_{min} \cdot L = n \cdot (1-SOC_{min}) \cdot L$$

Adding one day of storage to n_{min} to supply the load during the following night, the minimum required number of storage days n_{min} for this climatic cycle is therefore given by:

$$n_{min} = n \cdot (1-SOC_{min})+1 \quad (9.3.2)$$

It should be noted here that for the same generator size the length of the cycles remains the same provided that the system does not send load and the minimum SOC occurs the same day (Figure 103). The situation is different if we consider SOC profile for different generator sizes (Figure 104). The climatic cycles do not necessarily start and finish the same day and the minimum SOC during a time period may occur different days. Here, at day D1 in the first case and day D2 in the second.

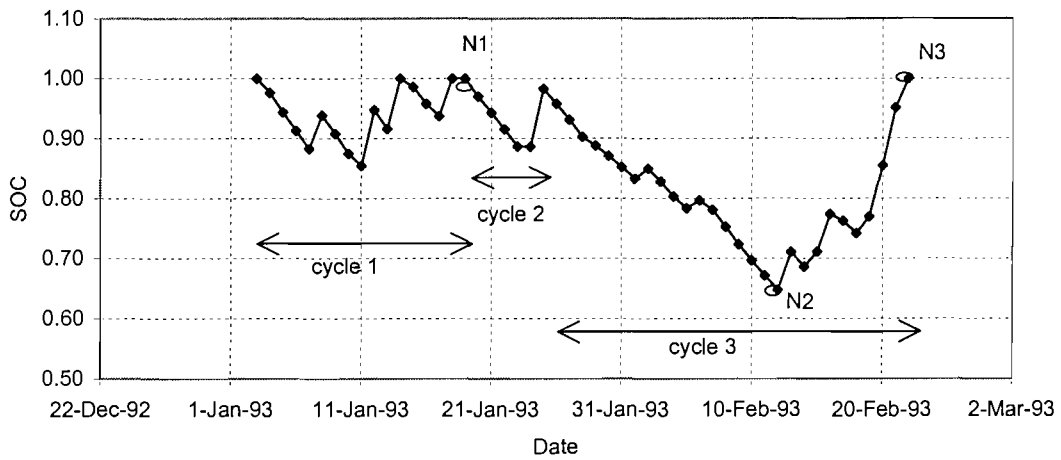

Figure 102 Example of climatic cycles from the system in Efford. Generator 108 Wh, battery 2400 Wh

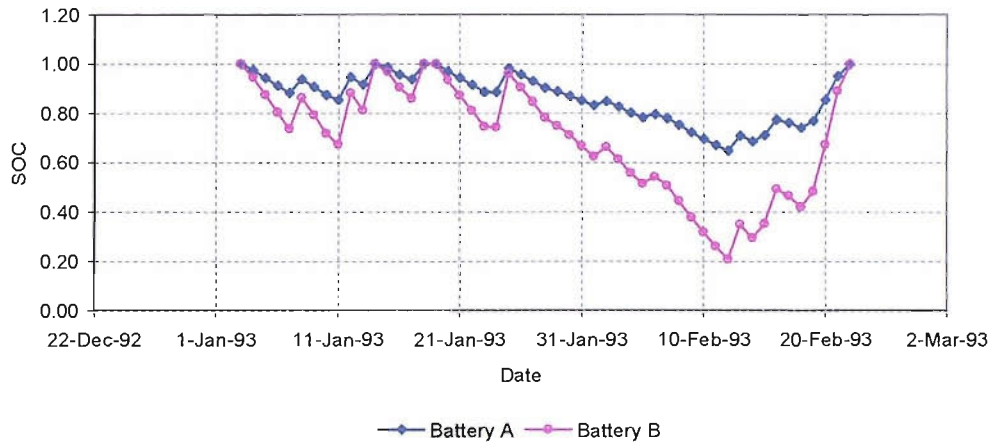

Figure 103 Battery SOC for the same generator size and different battery sizes, battery A, 2400 Wh and battery B, 1069 Wh

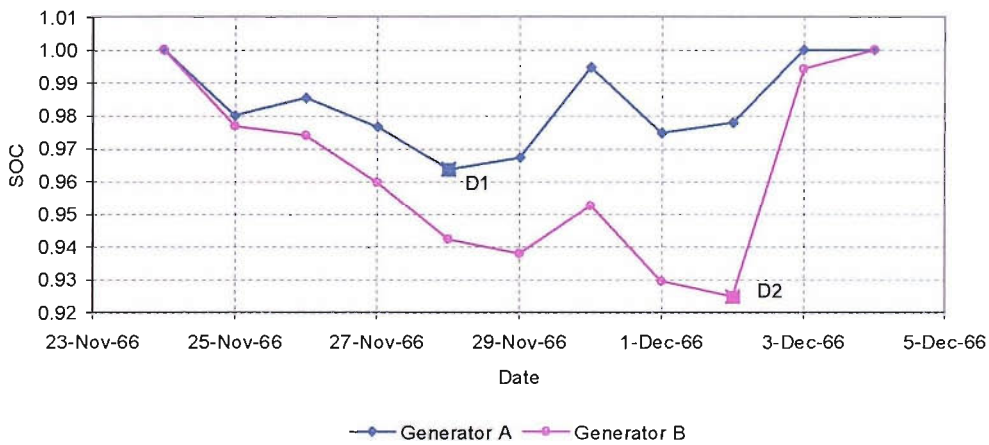

Figure 104 Battery SOC for the same battery size and different generator sizes, generator A, 108 Wh and generator B, 86.4 Wh

The sizing curve is constructed as follows:

We find n_{min} from (9.3.2) over the period in question as a function of the generator size, and thus determine the minimum storage required for the system to operate without shedding load for the minimum generator size. The above process is

repeated for larger generators- in essence, we oversize the minimum generator by a factor F_{S1} (see section 9.2.3). In this work, we illustrate this method by using the data for the 10-year period 1981-90, for three locations.

To obtain the most general description, the sizing curve is plotted in terms of the dimensionless variables C_A and C_S (see Lorenzo[7]). The generator capacity C_A is defined as the ratio of the daily energy produced by the generator divided by the daily energy consumed by the load (L). Therefore C_A is equal to the oversizing factor of the generator, $C_A=F_{S1}$ (see section 9.2.3). The storage capacity Cs is defined as the total maximum energy that can be extracted from the battery (C_U), divided by the daily energy consumed by the load (L). Therefore Cs is equal to the oversizing factor of the battery $C_S=F_{S2}$ and expresses the normalised useful battery capacity in days of storage (see section 9.2.3):

$C_S=C_U/L$

Figure 105 shows the results.

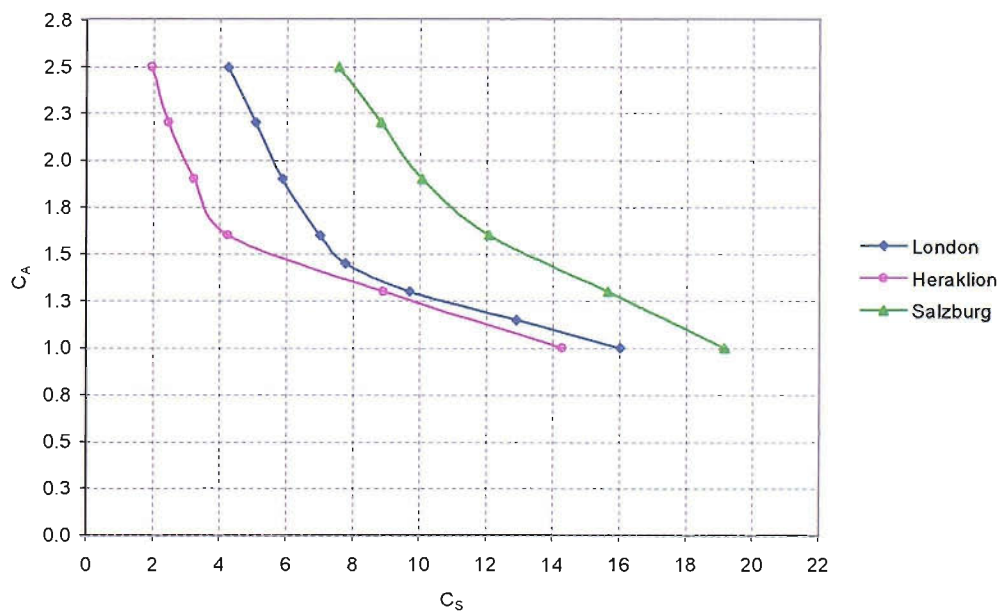

Figure 105 Sizing curves of three locations obtained using 10 years of daily radiation data (1981-1990) from ESRA software

9.3.2 Minimum storage requirement profile based on historical solar radiation data

We consider the PV system of section 9.3.1 in Efford. The optimum tilt angle is 66° to the horizontal and the long-term monthly average daily radiation of the worst month at this inclination is 1.216 kWh/m^2 according calculations made using ESRA[41] software. To supply a constant daily load L of 86.4 kWh we therefore need an array of at least equal daily energy output. Two system designs are considered here. In the first, the array is not oversized (oversizing factor F_{S1}=1, or C_A=1). The input is 36 years (1958-1994) of daily solar radiation data on the horizontal plane for Efford. The data have been processed to determine daily solar radiation on the inclined plane using ESRA software[41].

We consider only system configurations that they never shed the load, therefore, for each year, the battery size was determined, using the method described in 9.3.1, from the long-term energy-balance type model, developed in Matlab (section 6.3).

We find n_{min} from (9.3.2) for each year as a function of the generator size, and thus determine the minimum storage required as a function of time. The results are shown in Figure 106.

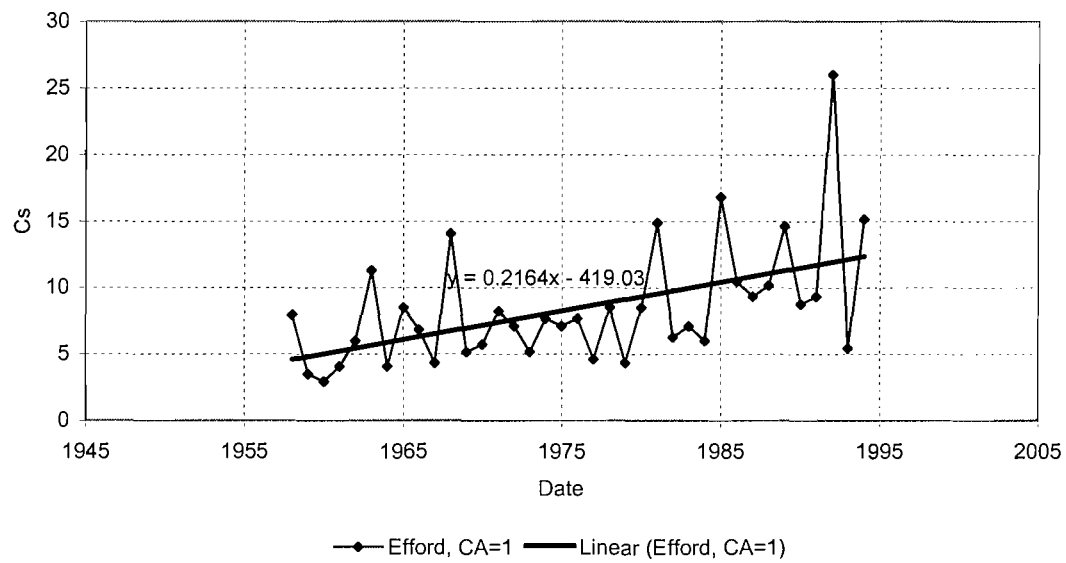

Figure 106 The minimum storage requirement in storage days in Efford as a function of time (1958-1994)

The sizing process described above has been repeated for the case of Potsdam (Germany). In this case the panel inclination should be 67° to the horizontal. The long-term monthly average radiation of the worst month (December) at this inclination is 0.785kWh/m2. Again the minimum generator size (no oversizing) has been used. Thus it is possible to compare the results with those from the system in Efford. Figure 107 shows the results of the storage requirement from Potsdam.

The input to the model based on daily energy balance is the daily solar radiation data on the horizontal surface from the Deutscher Wetterdienst, Meteorologisches Observatorium in Hamburg (Germany) and covers the years from July 1947 to June 2002, (54 years).

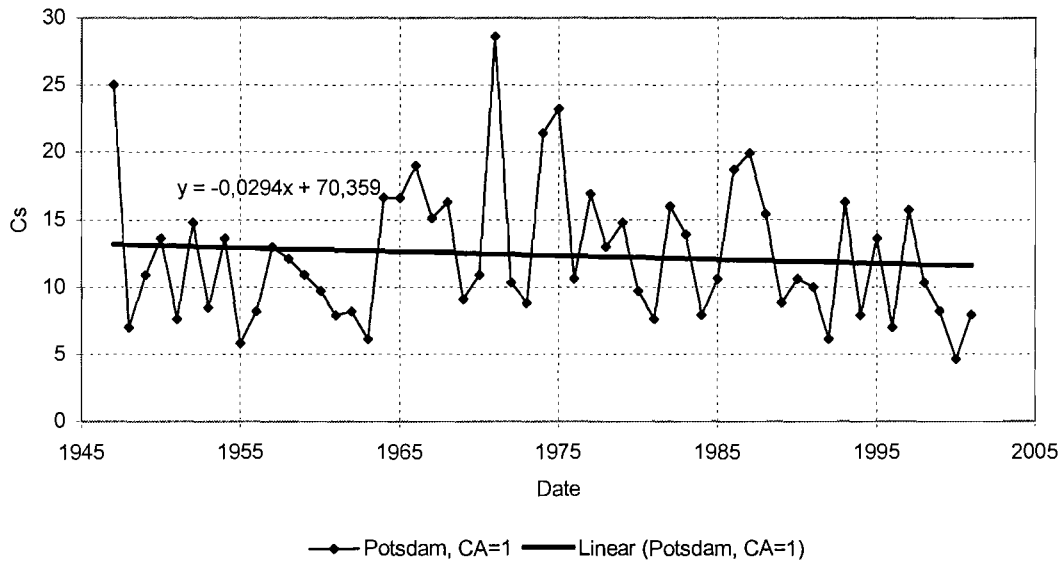

Figure 107 The minimum storage requirement in storage days for Potsdam (1947-2001). The oversizing factor of the generator is F_{S1}=1 (or C_A=1)

9.4 Discussion

9.4.1 Sizing curves

The LLP as a way of evaluating the reliability of a system does not give an idea about a number of important issues that should be considered in system design. For example, the time intervals between system failures or the length of the time that the

load remains disconnected each time that there is a failure is not taken into account. In addition we get no information about the DOD of the battery and the length of the time that the battery remains at low state of charge. Therefore it is questionable to what extent the LLP reflects the reliability of the system operation.

The sizing curves considered in this section define system configurations that supply the load without interruption. They reflect the way that the day-to-day correlations of the solar radiation affect the array-storage combination requirement. The results are still strongly dependent on the method used for the radiation conversion on the inclined surface (see section 6.4).

It is important to note that the shape of the sizing curves depends on the length of the daily radiation time series that we are using as input, or on the specific sequence of the years that are included in the time series that we are using for the derivation of the sizing curves.

Therefore, choosing the array storage combination of the curves derived using as an input a certain radiation time series, may lead to loss of load if we use as an input a longer time series or a time series of a different time period.

The monthly mean daily radiation of the worst month at the optimum tilt angle is higher in Salzburg airport than in London. However, it is seen that larger system (larger storage) it is needed in Salzburg airport. This should be attributed to the sequence of high and low daily irradiation values that seem to be more favourable to system needs in London than Salzburg although the monthly mean radiation is lower in London. Therefore, the sequence of high and low daily irradiation values is more critical for the system size than the monthly mean daily value of the solar radiation.

For Heraklion and C_A=1 the battery SOC becomes minimum during the winter of 1987. If we reconstruct the curve omitting the year 1987, we obtain a sizing curve which is in a better agreement with those presented by Lorenzo for telecommunications systems sizing in Southern Spain (Figure 106). The values of the sizing factors used are F_{S1}=1.2 and F_{S2}=6 (or array-storage combination C_A=1.2, C_S=6). Here we find that for F_{S1}= 1.3, F_{S2}=5.94 (or array-storage combination C_A=1.3, C_S=5.94), giving a reasonable agreement. The above, considerable change in sizing results, that occurs just by omitting one year of data highlights the effect that larger

time series may have on sizing. Using larger time series the possibility of them containing bad years in terms of favourable solar radiation patterns is increased and the sizing results may be affected dramatically. The effect of the long-term solar radiation profile in system sizing is examined in more detail in the next section.

An important observation on the sizing curves, is that although the presence of a 'bad' year, does change the shape of the curve (see Figure 108) when a combination of small generator and large battery has been used (left part of the sizing curve), may not affect it for combinations of large generator and small battery (left part of the curve). Therefore, combinations of large generator and small battery seem to be more likely to withstand unpredicted events of low solar radiation sequence (see also section 9.4.2). A larger generator, however, will cause the battery to be charged with higher current which may affect the battery life. The investigation of the effect of system operation on battery ageing, however, is beyond the scope of this thesis.

We should also note that by changing the oversizing factor of the generator the lowest state of charge of the whole period may occur at a different year. This is because (see section 6.4) the change in the generator size changes the profile of the battery state of charge. In the case of Heraklion, for example, the worst year is 1987 for generator oversizing up to 1.3, the year 1984 for generator oversizing 1.6 and 1.9 and the year 1983 for generator oversizing 2.2 and 2.5.

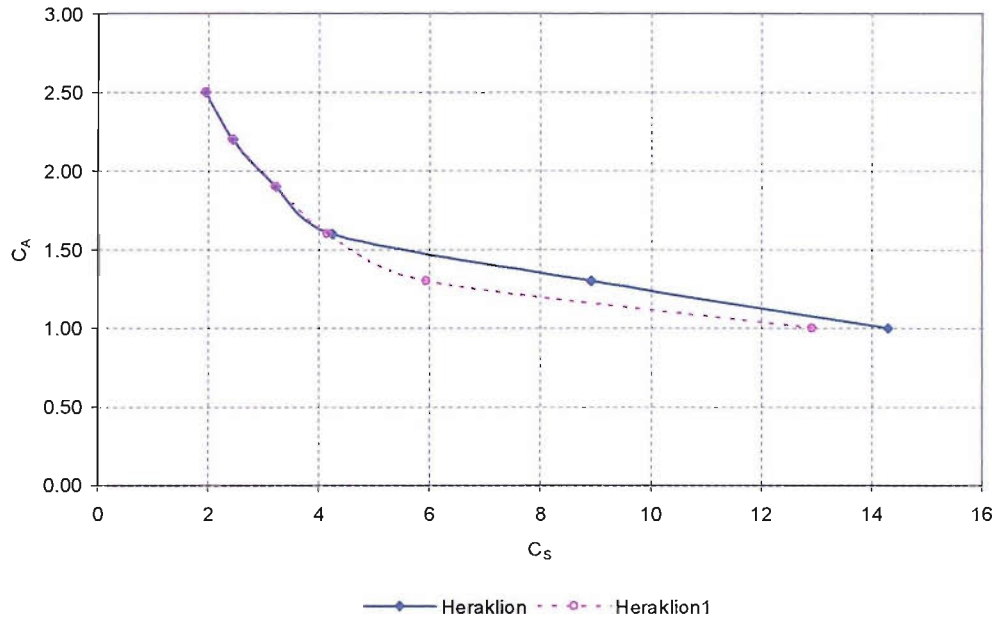

Figure 108 The sizing curve from Heraklion obtained using 10 years of daily radiation data from ESRA software. Heraklion1 is the curve that we obtain if we omit the year 1987- the worst year when we use the minimum generator size

9.4.2 Minimum storage requirement profile based on historical solar radiation data

It is seen that during the time period 1958-1994, there is a substantial increase in the storage requirement: by the end of the 36 years we need more than 3 times the number of storage days than during the first years of this period. However, there is a very small decrease found in yearly mean solar radiation during this period justifying the use of a fixed solar array in the analysis (Figure 109).

The importance of the above results in the system design is critical: Let's assume that on 1984 we are designing a system to operate for the next 20 years (until 2004). The system design is based, typically, on-say-25 years of solar radiation data from the past, for example from 1958 to1983, and the sizing curve of the system is derived using the above data series as described in section 9.3.1. If we chose to use the minimum generator size C_A=1, then from Figure 106 it is seen that the storage factor should be Cs=14.89 (or 14.89 days of storage). It is obvious from the graph that we will fail to account for the peaks in storage requirement of 1985, 1992 and1994,

and there will be loss of load the above three years. In particular in 1992, it is likely to have long duration of loss of load and low state of charge. The trend towards an increased storage requirement is unlikely to continue indefinitely and is likely to reverse at some stage in the future.

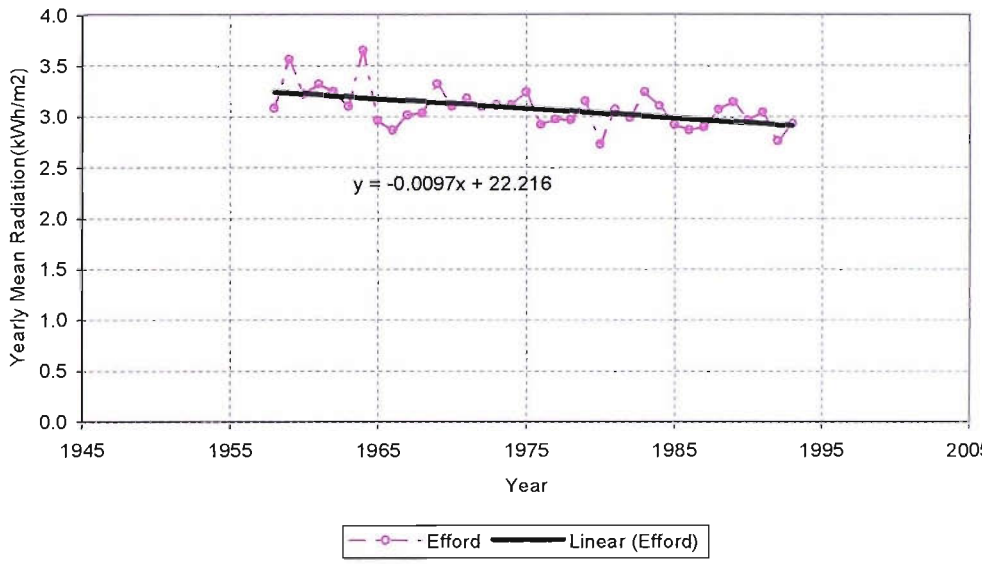

Figure 109 Yearly mean solar radiation in Efford at the optimum tilt angle

Given the small decrease in the yearly mean solar radiation (Figure 109), it appears that it is the change in the correlation of the day-to-day radiation values which leads to deeper discharges of the battery. Although the average irradiation changes little, there may be a systematic change in the 'persistence' of low solar radiation values over a longer period of time than hitherto. Thus, the design of PV system that will be used over a long period of time may have to be revised, and possibly based on solar radiation statistics more representative of future patterns than the currently available solar radiation data.

We should also note that the trend in the storage requirement is less pronounced when there is some oversizing of the generator. Figure 110 compares the minimum storage requirement in Efford, when the generator is oversized by a factor of 1.25 with that when we use the minimum generator size. Not only the trend is stronger when the generator is not oversized, but also the variation of the storage requirement

among the years is higher. Therefore there are two drawbacks when we are using combinations of small generator and large battery in system sizing. Firstly, the minimum battery size required the years with the highest storage requirement, will be far too large for most of the years of the system's operation. Secondly, the uncertainty with which the storage size is determined is increased. The latter explains the observation mentioned in section 9.3.1: that by choosing array storage combinations of large array and small storage it is much more likely to avoid loss of load in case the system encounters during its operation an unfavourable radiation pattern. For example, in the design case that is mentioned in this section, if instead of choosing the array storage combination of minimum generator size (C_A=1, C_S=14.89), the system is designed with generator oversizing, that corresponds, say, to the combination C_A=1.25, C_S=10.81, loss of load will occur only in 1994.

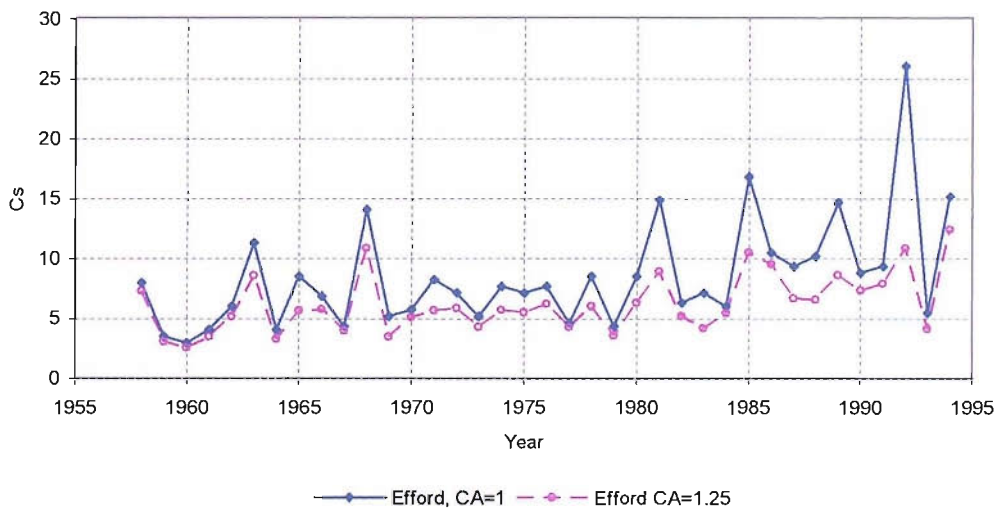

Figure 110 Minimum storage requirement for Efford, for the minimum generator size (C_A=1) and with oversizing the generator by a factor of F_{S1}=1.25 (or C_A=1.25)

In the case of Potsdam, the available radiation time series is longer than the one we used from Efford. Similarly with Efford, the change in the yearly mean solar radiation is small (Figure 111). Furthermore, the variability in the storage requirement is similar for both locations. Therefore, in the case of Potsdam, similarly with the case of Efford, 25 years of data are not necessarily adequate to size a system that

guarantees uninterrupted operation during its lifetime. If, for example, the system sizing is based on the 25 years of data from 1976 until 2001, we will fail to account for a possible increase in the future demand similar with those of the years 1947, 1971, 1974 or 1975. However, in contrast with the case of Efford the trend over the years 1970-1994 seems to indicate a trend towards a reduced requirement for storage and it continues to be so until the end of the available time series of data (2001). During the whole period that we examined, it is difficult to discern a strong characteristic trend in the Potsdam data. No correlation between the two data sets (from Efford and Potsdam) is apparent.

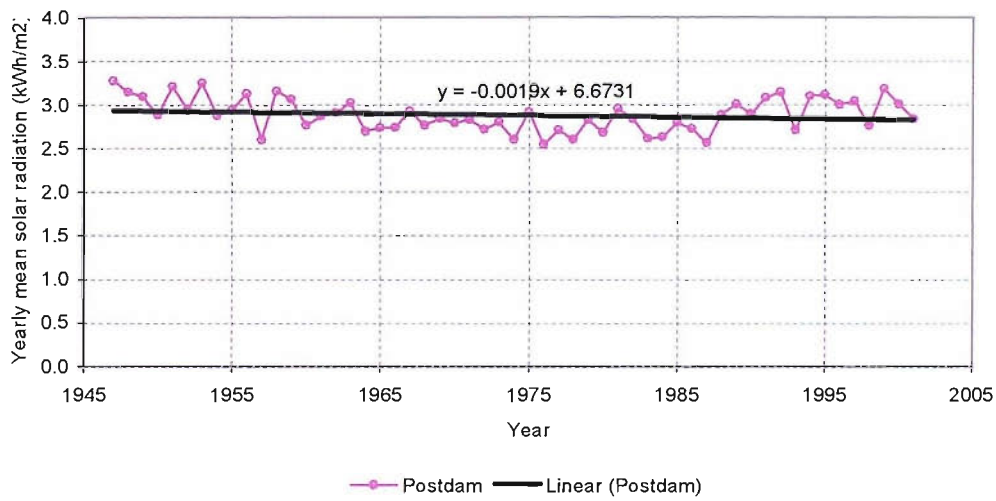

Figure 111 Yearly mean solar radiation in Potsdam at the optimum tilt angle

It will be shown now that the required storage found from the sizing results is an increasing function of the length of the time series used as input to system sizing.

Let us consider, for example, a five year frame in Figure 106, moving from 1958 to 1994 by one year step. One first determines the storage requirement for each 5 year period. The average storage required for the available time series of data (in this case, 1958 to 1994) can then be calculated. The final result can be interpreted as the storage requirement obtained from system sizing based on a typical 5 year series of solar radiation data. The whole process can be repeated using a 10 year frame, 15

year frame etc. The results are shown in Figure 112 and Figure 113 shows the results for the case of Potsdam.

Clearly, the use of a longer data series in system sizing, the sizing results in a larger storage requirement if the system is to operate without shedding load. Therefore, the longer the data series we use as input in system sizing the more likely is to design a system that will never shed load during its operation.

Figure 112 Resulting average required storage, in storage days, as a function of the length of the data series used in system sizing for the case of Efford

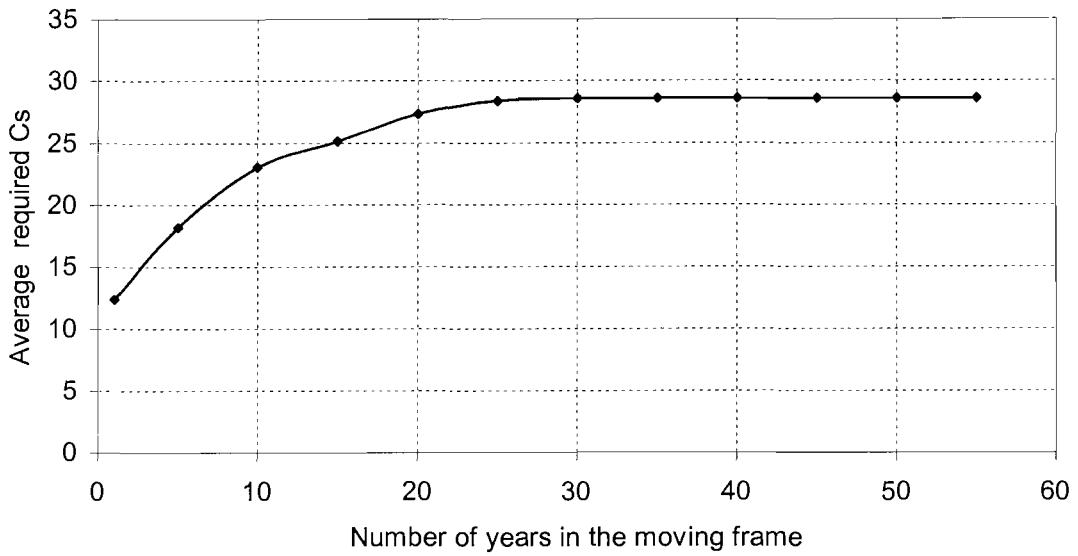

Figure 113 Resulting average required storage, in storage days, as a function of the length of the data series used in system sizing for the case of Potsdam

9.5 Conclusions

A new sizing approach has been developed based on the duration of system operation without loss of load. Using this approach, sizing curves have been obtained for three locations, (London, Heraklion, and Salzburg Airport). The curves were constructed using 10 years of solar radiation data (1981-1990) and discussed in some detail.

The new approach allows a detailed study of the long-term required storage. Thus, it has been found that there are significant variations in the storage requirement along the years and some trends in the behaviour from year to year even though the yearly average daily solar radiation changes little. The study in this work includes results from Efford (UK) and Potsdam (Germany). In the case of Efford there is a significant trend towards increased storage requirement between the years 1958-1994. The data for Potsdam (1947-2002) do not appear to follow a single significant trend but there are significant variations. Thus, the length of the time series or the particular years under consideration used in system sizing affects strongly the sizing results. Therefore, the results from the analytical methods (see section 9.2.2), which are based on the concept of LLP, do not only depend strongly on the model that has been used

for radiation conversion on inclined surface, (section 6.4), they also depend on the length of the daily time series that has been used in the derivation of the LLP sizing curves. In addition, day to day variations of solar radiation are critical for system sizing studies, while monthly average values may conceal a great deal of information regarding the available for years characterised by low solar radiation sequences.

These issues lead to the conclusion that future changes in the solar radiation patterns may need to be allowed for in an accurate design of PV systems.

The uncertainty in the minimum required storage capacity can be reduced by choosing a combination of large array and a smaller storage size. Clearly, such combination reduces the possibility of the loss of load in the event of an unpredicted unfavourable solar radiation sequence and makes for a more robust and dependable energy source.

There does not seem to be a correlation between the profiles of storage requirement of the two locations under study (Efford and Potsdam), although deeper similarities could be revealed by a more extensive research, bringing together a wider variety of locations.

10. PREDICTION OF FUTURE CLIMATE AND THE DESIGN OF PV SYSTEMS

10.1 Introduction

The future climate may be different than the climate today -especially if we take into account the predictions of the global warming. As the research on the climate change develops, artificially generated series of future solar radiation data are becoming available. One of the centres where data of this type are generated is the Hadley centre. No research has been done so far to assess whether these data could be used to advantage in PV system sizing.

Climate change may have an effect in the day to day correlations of the solar radiation. The principal aim of the present work is to examine the possibility of using artificially generated solar radiation data from climate change experiments in system sizing. The objective is to compare the resulting profile of storage requirement for Efford when the input is historical solar radiation data from the Met Office, with the corresponding profile when the input is artificially generated data from the Hadley Centre.

Using the model based on daily energy balance (section 6.3), it was found that the results are not in good agreement with those using solar radiation data from the past and therefore further research is needed.

Section 10.2 is an overview of the climate change, Section 10.3 presents the minimum storage requirement profile from Efford, using the Hadley data and compares it with that using the historical solar radiation data.

10.2 Overview of the climate change

10.2.1 Introduction

The weather is the fluctuating state of the atmosphere around us. The climate[95] is the average weather experienced over a long period, typically 30 years (more rigorously, it is a statistical description of weather, including variability and extremes as well as averages). The climate involves the components of the climate system and

these are the atmosphere, the ocean, the land surface, the cryosphere and the biosphere.

There are two primary factors, which determine how human activities change climate –the rate of greenhouse gas emissions and other pollutants and the response of climate to these emissions. The first of these factors can only be described using a range of scenarios, these scenarios depending on many different assumptions about how the world's population, economy, energy-technology and lifestyles will evolve. The second factor-the climate system response and the resulting regional patterns of climate change-can only be explored through the use of climate models.

10.2.2 Stage in climate predictions

Predicting climate in the future is a multistage process:

- Energy economy models that take into account such factors as growth in population, energy demand and technological change. Four scenarios were used by IPCC (Intergovernmental Panel on Climate Change), each of which describes a possible future world. Those scenarios where used for calculating future greenhouse gas and other pollutant emissions. A brief description of these scenarios is given in Table 12.
- Scenarios are constructed of future human related emissions of the main greenhouse gases. Green house gas is a gas, which 'traps' energy radiated by the earth within the atmosphere. Carbon dioxide (CO2) is the most important greenhouse gas being emitted by humans.
- Human related emissions are translated into atmospheric concentrations using carbon cycle models. We should note that carbon dioxide's atmospheric concentration responds very slowly to changes in the emissions. For this reason, even past emissions have not yet been fully reflected in the atmosphere. For other greenhouse gases, such as methane future concentrations are calculated using models that represent chemical reactions in the atmosphere. Unlike carbon dioxide, methane's concentrations respond to changes of the emissions much more quickly.
- Climate change experiments can be conducted using a climate model. The greatest uncertainty in model simulations comes from consequential effects on climate, which follow an initial warming. These effects are known as

'feedbacks' and they can act either to amplify the initial change or to reduce it. The melting of sea-ice, for example will reduce the amount of sunlight reflected and thus enhance the warming in high latitudes-a positive feedback. A warmer atmosphere will 'hold' more water vapour (a powerful greenhouse gas) and this too will act as a positive feedback. Possible changes in the characteristics of clouds in a warmer world are the most important source of uncertainty, since we do not even know if this particular feedback will be overall positive or negative.

- Climate change experiments can lead to climate change scenarios-coherent and internally consistent description of the change in climate by a certain time in the future, using a specific modelling technique and under specific assumptions about the growth of greenhouse gas and other emissions and about other factors that may influence the climate in the future. In contrast with the climate change scenarios, climate scenarios describe the future climates rather than possible changes in climate.

A1	Very rapid economic growth; Population peaks mid-century; social, cultural and economic convergence among regions; market mechanisms dominate. Subdivisions A1F1-reliance on fossil fuels; A1T-reliance on no-fossil fuels; A1B-A balance across all fuel sources
A2	Self–reliance; preservation of local identities; continuously increasing population; economic growth on regional scales
B1	Clean and efficient technologies; reduction in material use; global solutions to economic, social and environmental sustainability; improved equity; population peaks mid century
B2	Local solutions to sustainability; continuously increasing population at a lower rate than A2; Less rapid technological change than in B1 and A1

Table 12 The four scenarios used by IPCC (Intergovernmental Panel on Climate Change), each of which describes a possible future world

10.2.3 HadCM3 and other climate models

In order to make predictions of climate change, we have to calculate the effects of all the key processes operating in the climate system. Our knowledge about these processes can be represented in mathematical terms. Due to the complexity of the system the mathematical formulation is implemented in a computer program, which we refer to as a climate model. Various types of climate models are used for climate simulation and prediction.

The HadCM3 climate model is a sophisticated tool for simulating global climate used in Hadley centre. The model is based on the known laws of physics describing the transport of mass (including moisture) and energy; these equations are solved at intervals (typically 30 minutes) at a number of points forming a grid over the globe. In the HadCM3 model this grid is 2.5° in latitude by 3.75° in longitude (~300km grid interval). There are 19 vertical levels through the atmosphere. Figure 114 shows the model domains schematically. Apart from the HadCM3 model there is the regional climate model for Europe, HadRM3, ~50km grid interval. Local climate change is influenced greatly by local features such as mountains, which are not well represented in global models because of their coarse resolution. Models of higher resolution cannot practically be used for global simulation of long periods of time. Therefore, the regional climate models with higher resolution are constructed for limited areas and run for shorter periods (20 years or so). The regional climate model, developed in Hadley centre, HadRM3, takes boundary conditions from the coarser resolution global model simulations and provides a higher spatial resolution of the local topography and more realistic simulations of fine scale weather features. However, HadRM3 still exhibits systematic errors due to imperfect representation of even smaller scale features. For local climate change scenarios the experiments use the global coupled ocean-atmosphere model HadCM3 which drives a global model of the atmosphere alone, HadAM3H, ~ 120 km grid interval, which in turn is used to drive the regional model for Europe HadRM3. The above models have a 20-year history of development; have been carefully analysed and evaluated over many model generations.

A climate model has to represent the ocean as well as the atmosphere-not just the continuous transfer of heat, water and momentum across the air sea interface, but the ocean currents that transport vast amounts of heat between the equator and the

poles. Atmospheric models are now successfully coupled to deep ocean models to allow the transient changes in climate to be properly modelled. The ocean part of HadCM3 has twenty vertical levels and a horizontal resolution of 1.25° latitude by 1.25° longitude.

The model is run for many hundreds of (simulated) years. The starting point of the run represents the middle of the nineteenth century when any human influences would have been negligible (specifically the year 1860 was chosen as the start year to allow comparisons with global temperature observations). Over the period from 1860 to 1990, observed changes in greenhouse gasses and aerosols are used to simulate changes in the climate to date. Aerosols are microscopic droplets or solid particles in the atmosphere. They affect the thermal properties of the atmosphere by absorbing and scattering radiation and by aiding cloud formations. Although there are no measurements to show how the influence of aerosols on climate has changed over the past 150 years there are estimates of how sulphur dioxide emissions have risen. There are also future estimates of such emissions and these are used in a sulphur cycle model to calculate the accompanying rise in sulphate aerosol concentrations. The sulphur cycle -the generation of sulphate particles from sulphur dioxide- as well as the transport and removal by deposition and rain of the sulphate particles are included in HadCM3 and in the regional model HadRM3. This allows the effects of aerosols to be represented in the model. From 1999 onwards, a number of scenarios of future changes in greenhouse gases and aerosols are used. An important part of the process is model validation against observed data; work on this for HadCM3 and HadRM3 is currently in progress at the Hadley Centre and in the Climatic Research Unit at the UEA (University of East Anglia).

Apart from the HadCM3 and the models developed in the Hadley centre, there are other global climate models (Table 13). Whilst inter-comparison between model results is important and may reveal areas where there are significant differences or indeed similarities, there is no easy way of attaching higher or lower confidence to the results of one model over another. It is important to point out that agreement between models is not a 'proof' that they are correct, merely that given our current state of knowledge and modelling capability, all models are telling a similar story. Where differences between two models are large-and by this we mean larger that might be expected due to purely natural variability of climate-it is unlikely that both models can

be correct. As hinted above, determining which model is more likely to be correct is not a straightforward task.

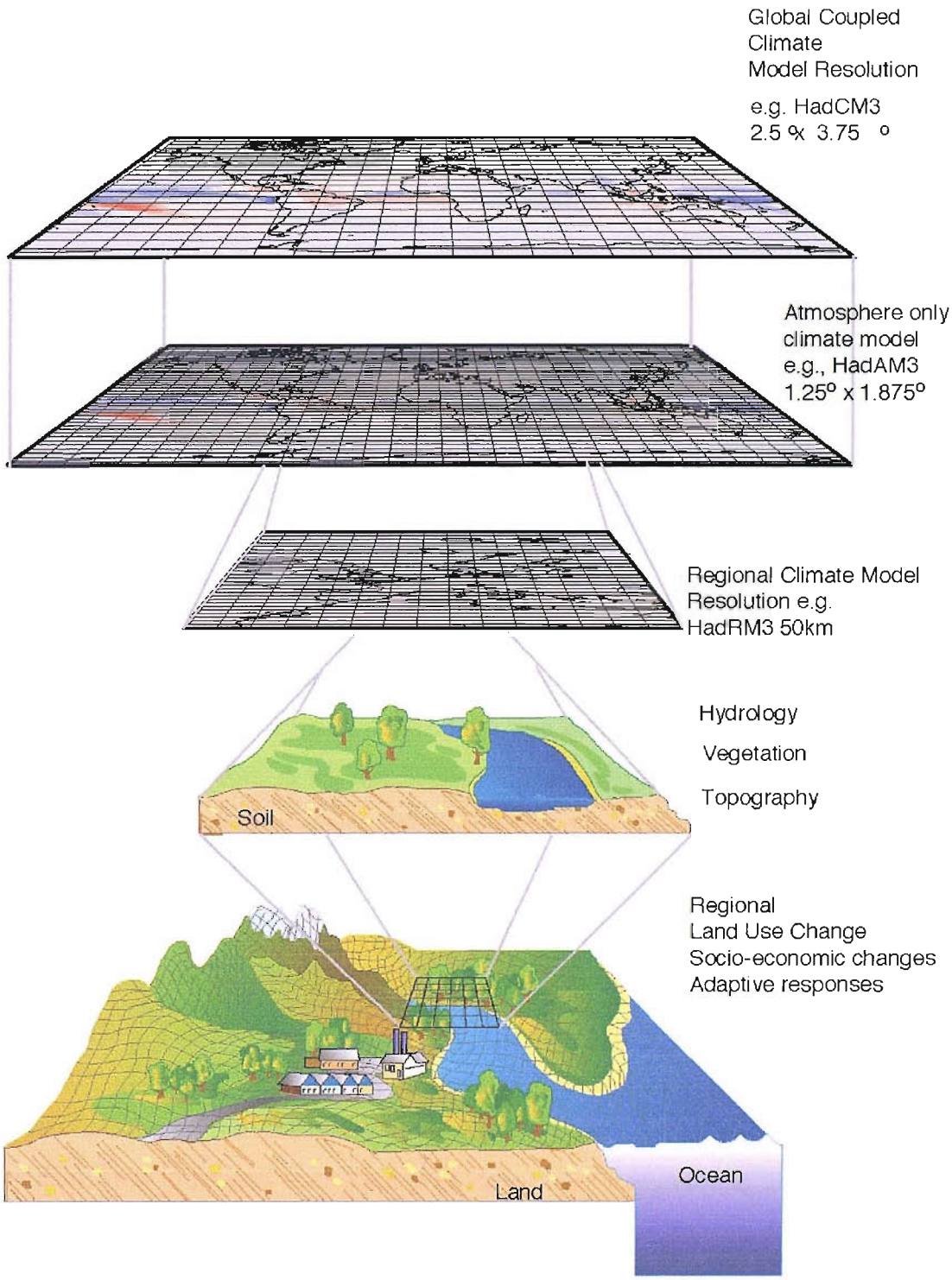

Figure 114 Schematic representation of the HadCM3 model domain

Model Name/Version	Country
CCCma	Canada
CSIRO Mk2	Australia
CSM 1.0	USA
DOE PCM	USA
MPI/DMI	Germany
GFDL R30c	USA
HadCM3	UK
MRI2	Japan
NIES-CCSR v2	Japan

Table 13 Global climate models

10.3 Application: Hadley Data

The data used in this section are the results from HadCM3 climate change experiments based on B2 scenario of medium-low emissions (see section 10.2.2). Since the aim of this work is the development of a new research methodology the choice of the scenario was arbitrary. The radiation values correspond to the 300KM grid interval that includes the area of Efford.

The methodology used here is the same with that of section 9.3.2. The graph in Figure 115 shows the minimum number of storage days required for a system to operate in Efford without shedding load. The generator oversizing factor is F_{SI}=1.25 (or C_A=1.25). In the first case we used the measured daily solar radiation data and in the second case the modelled daily solar radiation data from Hadley centre. The use of Hadley data leads in general to much higher storage requirement than the use of the actual data from the Met Office. There are two main reasons for the disagreement. The first is the great sensitivity of the battery SOC on the solar radiation pattern used as input when the solar radiation is low (section 6.4). As a result a yearly minimum battery SOC found using historical data and the corresponding one found using artificially generated data, may differ significantly even if the corresponding input daily solar radiation patterns differ little during the critical period where the minimum SOC occurs. Therefore, further research should include a statistical analysis and

comparison between the historical data and the solar radiation patterns especially during the winter period. The second reason is that the generated values of solar radiation may vary for different locations within the area specified by the 300 km grid used in the Hadley Centre experiments (section 10.2.3). This is because the daily solar radiation more than about 100 km away from a selected site is not representative of the daily solar radiation of the site unless the landscape is fairly flat[41]. In a mountainous area, the difference between the exact location of a site and the location of the representative whether station should be less than few hundreds meters. Therefore, the 300 km grid may be too large resolution for the case of Efford and further research is needed on this topic.

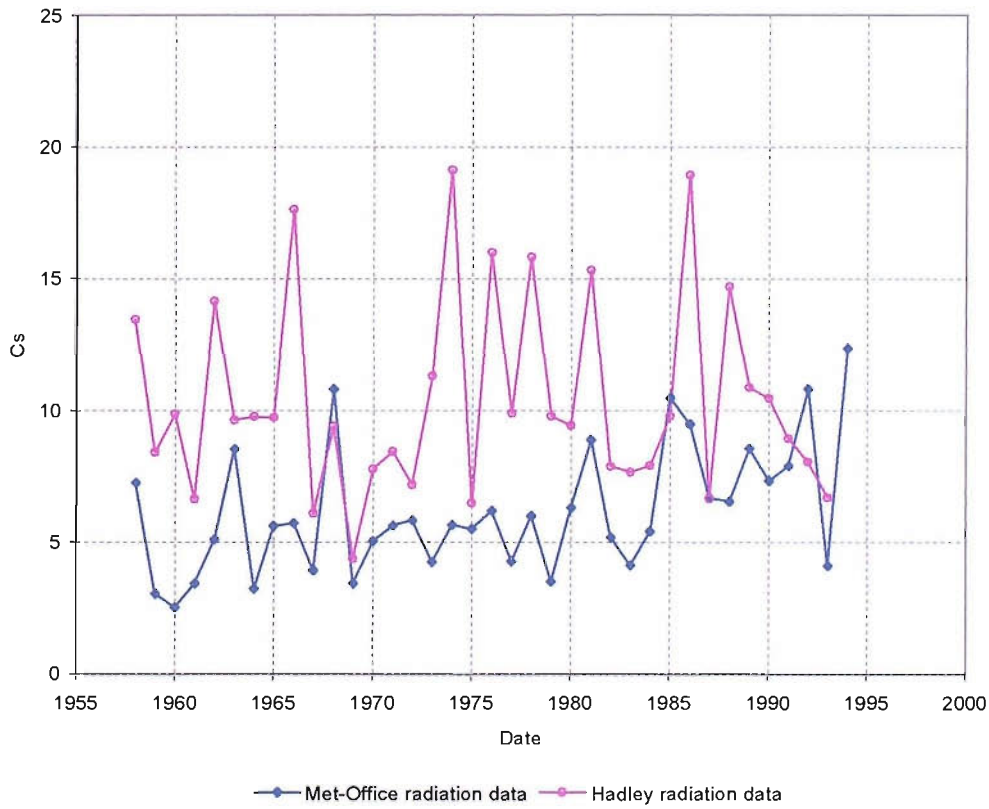

Figure 115 The storage requirement in Efford, using data from the Met Office and using data generated in Hadley Centre. The generator oversizing factor is F_{S1}=1.25 (or C_A=1.25)

10.4 Conclusions

It has been shown here how the sizing methodology presented in Chapter 9 can be applied to examine the possibility of using artificially generated future radiation series in system sizing. With the possible change in climate under way, such methodology may be critical for system configuration and component sizing. This study represents a first step in the research towards the incorporation of predicted solar radiation patterns in PV system design studies.

A comparison was made between the storage requirement of a typical system using historical solar radiation data and that using artificially generated daily solar radiation data from Hadley centre. The results were compared with the values obtained for Efford (UK) for the period 1958-1994. These preliminary results do not show agreement between the two storage patterns. This indicates the necessity of a detailed statistical comparison of the radiation patterns which are used as input to system sizing, although the sensitivity of the resulting battery state of charge on the solar radiation series during the low radiation winter months sets a limit in the accuracy of the daily energy balance model.

11. CONCLUSIONS

The principal aim of this thesis has been to develop and validate a new sizing approach to stand alone photovoltaic systems which uses observed time series of solar radiation to determine the required system size and the optimum configuration. The key element of this procedure is the analysis of climatic cycles by modelling based on daily energy balance, and the observation how a critical period in the solar radiation data affects the design and reliability of the PV system. To achieve this aim, the available procedures for conversion of measured solar radiation data to an inclined plane have been critically examined. An experimental stand-alone PV system has been constructed, monitored and the resulting data analysed in detail. A series of laboratory experiments has been conducted to determine the effect of realistic battery operation in a practical system on the simplified description using daily energy balance. An important result of the work has been to highlight the role of persistence of low solar radiation values on the reliability of the PV system. The following conclusions can therefore be made with regard to a robust system sizing process: Firstly, daily series of solar radiation data should be used for accurate sizing. Secondly, the longest data series available should be used if high reliability is to be achieved. The relationship between system reliability and storage size can be clearly seen from Figure 112 and Figure 113, which show the storage required as a function of the length of the time series of data required as an input in the sizing procedure.

The PV generator design requires the conversion of solar radiation data from the horizontal to the inclined plane of the array. To this end an overview of the methods for the calculation of the radiation on the inclined plane was presented and analysed using Matlab modelling. The conversion process always requires the decomposition of global solar radiation into beam, reflected (albedo) and diffuse fractions. Assumptions related with the anisotropy of the sky, the calculation of the ratio of beam radiation on the inclined surface to that on the horizontal surface, R_b, and the correlation of the fraction of the diffuse radiation with the clearness index are critical for the accuracy of the results.

To compare the theoretical predictions with measured data, daily radiation values from measured data at Southampton University were converted to the inclined

plane using Liu and Jordan model. Several existing correlations for the diffuse fraction were tried but the results were not in a good agreement with the measured values on the inclined surface. An improvement in the results has been achieved by deriving a correlation based on the measured data on the inclined surface especially during the winter months. The improvement refers to the values where the difference from the average value for the whole month is large. Sophisticated methods, thus need to be used for the radiation conversion to the inclined surface. In this work, the recent European Solar Radiation Atlas (ESRA) were used, where the methodology accounts for the anisotropy of the sky and the calculation of the ratio of beam radiation on the inclined surface to that on the horizontal surface, R_b, is carried out in a more accurate way.

Furthermore, it has been found that small differences in the radiation pattern may lead to substantial differences in the pattern of the state of charge of the battery during critical periods of system operation, for example, in the winter months. These discrepancies may be reduced or enhanced depending on the ratio of the generator size to the battery size.

PV generator operation was described using models for the solar cell and the PV generator that are available from literature. A model of the PV generator has been developed in Matlab and validated using experimental data from StaR photovoltaic facility. The results of the model were shown to be in a good agreement with the experimental data obtained from monitoring the operation of a PV generator connected to a variable resistor. The model therefore can be used as a designing tool in future study.

The construction and operation of lead-acid batteries (the most common type used in PV systems) have been reviewed. Emphasis has been given on the study of the charging efficiency of the batteries in stand-alone PV systems. A series of experiments has been conducted in the laboratory to study the models of battery operation and to deduce the charging efficiency. A loss of efficiency seems to occur when the battery is close to the full state of charge-an important feature of battery operation for the user of PV systems which allows a reasonably accurate description of the PV system for sizing purposes. A more detailed analysis of the battery, however, has proved a difficult task. The strong memory effect, in particular, did not

allow for a quantitative estimation of the charging efficiency when the battery is in operation in practice. The simplified "universal" models in the literature were found to depend on details of battery construction, and require a wide range of parameters to be determined in each specific case.

In addition, a stand-alone photovoltaic system has been constructed on the roof of Lanchaster building in Southampton University. A comprehensive monitoring system for the electrical and environmental parameters has been developed. The system was monitored for six months (November to April) and the results were used to validate a system model based on daily energy balance which has been refined from previous work at the Solar Energy Group at Southampton University. Two methods have been used for the analysis of the results in order to extract the profile of the battery SOC from the experimental data. The first is based on current integration, assuming charging efficiency equal to one when the battery is completely charged. The second is based on voltage measurements which were used to infer the battery SOC at the end of the night's discharge. Both methods were found to give similar results. One of the principal results of this work is the finding that, despite its simplifications, the energy model for the long-term performance of the PV system gives a good approximation of the lowest SOC reached by the system. As the efficiency drop occurs only when the battery operates at full state of charge, there is enough solar radiation, to provide with the extra charge needed. Therefore, the lowest state of charge reached by the system will not be affected. Apart from the charging efficiency the details of system operation do not seem to affect the energy balance of the system.

When the battery operates close to the full state of charge the experimental results are in less good agreement with those from the model. They show that it takes a longer time for the battery to reach the full state of charge after a period of deep discharge. In fact, in winter the battery hardly ever operates in full state of charge. Therefore, the model based on daily energy balance although suitable for system sizing purposes, is less appropriate for studies that address the battery life. The reason for this discrepancy appears to lie in the chemistry of battery operation when close to the full state of charge. In this region, the state of the battery –although important for

the battery life-is not described accurately by the model based on the daily energy balance.

A new methodology is suggested in this work which defines the reliability of supply in terms of the expected duration of system operation without shedding the load. In contrast with the traditional sizing techniques, based on loss-of-load probability, this method allows a detailed study of the time profile of the battery state of charge under real working conditions. Using this method the sizing curves of three locations-London (UK), Salzburg Airport (Austria) and Heraklion (Greece) were constructed from 10 years of solar radiation data from ESRA software.

The analysis of these sizing curves has shown that it is the sequence of high and low daily radiation values that is critical for the system size. On the contrary, the monthly mean daily values of the solar radiation may conceal the need for increased storage (or larger generator) for the years characterized by "persistence" of low solar radiation values. The exact shape of the sizing curves and therefore the sizing results depend strongly on the particular years under consideration of the daily solar radiation time series that has been used as an input.

The accuracy of the sizing methods relies on good availability or reliable past solar radiation data. It appears from our studies that the length of the data series that we use in system sizing may be critical for the sizing results. The study of long data series from Efford and Potsdam shows that, although it appears to be little correlation of the variations in storage requirement between the two locations, the variations are significant in both cases. Therefore, the length of the daily radiation time series (and hence also the length of continuous operation) should be used as the indicator of supply reliability. A combination of a larger array and a smaller battery smoothes the variations in storage requirement along the years and therefore reduces the dependence of the probability of loss of load on unfavourable radiation patterns that may appear in the future.

The above results are of importance, for system design, especially if we take into account the possibility of climate change. Generated data from Hadley centre have been used in this work to compare the sizing results from historical data and generated data. At present the agreement is not very good and further work is required to substantiate this result. A new methodology may also be needed to predict the

future trends in the pattern of the battery state of charge due to possible trends in the future solar radiation values.

12. FURTHER WORK

The following areas of further work have been identified as being worthwhile of investigation:

- Data from system monitoring of two or more consecutive years (November to April) should be used and analysed by means of the two methods described in this work (see chapter 8) in order to obtain the daily time profile of the battery state of charge. The results can then be compared with those from the model based on daily energy balance of the system as well as the SOC patterns of each year with the preceding one. The research will reveal possible effects on the battery SOC due to battery ageing. The model based on daily energy balance can then be modified accordingly. In addition, the model should be modified to account for the drop of the charging efficiency of the battery close to the full SOC.

- The battery state of charge data obtained from the model based on daily energy balance as well as the experimental data should be compared with results from a more detailed system model, for example, the model developed by Daniel Guasch Murillo and colleagues [72-74].

- The storage requirement over the years using historical daily solar radiation data, as described in Section 9.3.2, should be obtained having converted the radiation on the inclined surface using a different method (for example, the Liu and Jordan method), and for various system designs, in order to study the effect on the year to year variations of the storage requirement.

- Work described in Section 9.3.2 for Efford and Potsdam (the storage requirement over the years obtained using historical daily solar radiation data), should be repeated for other locations. The variability in storage requirement of different locations should be compared and examined for the existence of possible trends or correlations between the storage requirements at different locations.

- The historical solar radiation time series from Efford should be compared with the corresponding data from the Hadley Centre.

- Hadley radiation data from the regional model for the UK should be used to repeat the comparison carried out for Efford in section 10.3 of this work

13. REFERENCES

[1] J. Thornycroft and T. Markvart, Grid connection of PV generators: technical and regulatory issues, in: T. Markvart and L. Castañer, *Practical Handbook of Photovoltaics. Fundamentals and Applications,*Elesvier Science Ltd., Oxford, UK, 2003.

[2] Grid Connection of Photovoltaic Systems ETSU S 1394-P1, Dti, (1993).

[3] Low Voltage Grid-Connection of Photovoltaic Power Systems ETSU S/P2/00215/REP. Dti.

[4] F. C. Treble, *Generating Electricity from the Sun*, Pergamon Press, UK, 1991.

[5] S. R. Wenham, M. A.Green and M. E. Watt, *Applied Photovoltaics*, Centre for Photovoltaic Devices and Systems, Sydney, 1994.

[6] T. Markvart (ed), *Solar Electricity*, John Willey & sons, Chichester, 1994.

[7] E. Lorenzo et al., *Solar Electricity*, Progensa, Spain, 1994.

[8] J. A. Duffie and W. A.Beckman, *Solar Engineering of Thermal Processes*, 2nd ed. John Willey and Sons, USA, 1991.

[9] J.D. Meakin, *Current Topics in Photovoltaics*, Academic Press, London, 1990, Vol.4.

[10]N. Martin and J. M.Ruiz, 'Simple model fitting for PV modules spectral factors', *2nd World Conference and Exhibition on Photovoltaic Solar Energy Conversion*, Vienna, Austria, 2384 (1998).

[11] L. Castañer, S. Bermejo, T. Markvart and K. Fragaki, Introduction: energy production by a PV array, in: T. Markvart and L. Castañer, *Practical Handbook of Photovoltaics. Fundamentals and Applications,*Elesvier Science Ltd., Oxford, UK, 2003.

[12] D.L King, W.E. Boyson and J.A. Kratochvil, '*Analysis of Factors Influencing the Annual Energy Production of Photovoltaic Systems*', Proc. 29th IEEE Photovoltaic Specialist Conference, New Orleans, 1356, (2002).

[13] E.A. Sjerps-Koomen and E.A. Alsema, 'A model for a PV module reflection losses under field conditions', *13th European Photovoltaic Solar Energy Conference*, Nice, France, 751 (1995).

[14] R. Siegel and J. R. Howell, *Thermal Radiation Heat Transfer*, 4th ed., Taylor and Francis-Hemisphere, Washington, 2001.

[15] B. Y. H. Liu and R. C. Jordan, 'Daily Insolation on Surfaces Tilted Toward the Equator', *ASHRAE Journal*, **3(10)**, 53 (1962).

[16] B. Y. H. Liu and R. C. Jordan, 'The Long-Term Average Performance of Flat –Plate Solar Energy Collectors', *Solar Energy*, **7**, 53 (1963).

[17] J. P. Holman, *Heat Transfer,* 6th ed., Mc Graw-Hill, inc., New York, 1986.

[18] T. M. Klucher, *Evaluating Models to Predict Insolation on Tilted Surfaces*, Solar Energy, **23**, 111 (1979).

[19] J. E. Hay and J. A. Davies. 'Calculation of the Solar Radiation Radiation Incident on the Inclined Surface', *Proc.First Canadian Solar Radiation Data Workshop*, J.E. Hay and T.K. Won, eds. Ministry of Supply and Services Canada, 59 (1980).

[20] R. Perez, R. Seals, P. Ineichen, R. Stewart and D. Menicucci. 'A New Simplified Version of the Perez Diffuse Irradiance Model for Tilted Surfaces'. *Solar Energy*, **39**, 221 (1987).

[21] R. Perez, R. Stewart, R. Seals and T. Guertin. 'The development and verification of Perez Diffuse Radiation Model', *Sandia National Laboratoryoratories Contractor Report*, SAND88-7030, (Oct.1988).

[22] M. E. Herzog, *Estimation of Hourly and Monthly Average Daily Insolation on Tilted Surfaces*, M.S. Thesis, Trinity University, 1985.

[23] B. Y. H. Liu and R. C. Jordan. The Interrelationship and Characteristic Distribution of Direct Diffuse and Total Solar Radiation. *Solar Energy*, **4(3)**, 1 (1960).

[24] Choudhury, 'Solar Radiation at New Delhi', *Solar Energy*, **7**, 44 (1963).

[25] G. Stanhill, 'Diffuse Sky and Cloud Radiation in Israel', *Solar Energy,* **10 (2)**, 69 (1966).

[26] D. W. Ruth and R. E. Chant, 'The Relationship of Diffuse Radiation to Total Radiation in Canada', *Solar Energy*, **18**,153 (1976).

[27] M. Collares-Pereira and A.Rabl, 'The Average Distribution of Solar Radiation-Correlations between Diffuse and Hemispherical and between Daily and Hourly Insolation Values', *Solar Energy*, **22**, 155 (1979a).

[28]D. G. Erbs, S. A. Klein and J. A. Duffie, 'Estimation of the Diffuse Radiation Fraction for Hourly, Daily, and Monthly Average Global Radiation', *Solar Energy*, **28**, 293 (1982).

[29] S. E. Tuller, 'The Relationship Between Diffuse, Total and Extraterrestrial Solar Radiation', *Solar Energy*, **18**, 259 (1976).

[30] P. Bendt, M. Collares-Pereira and A. Rabl, 'The Frequency Distribution of Daily Radiation Values', *Solar Energy*, **27**, 1 (1981).

[31] J. K. Page, 'The Estimation of Monthly Mean Values of Daily Total Short-Wave Radiation of Vertical and Inclined Surfaces from Sunshine Records for Latitudes 40°N-40°S', *Proc. of the UN Conference on New Sources of Energy*, **4**, 378 (1964).

[32] J.K. Page, *Prediction of Solar Radiation on Inclined Surfaces*, Reidel (for the Commission of the European Communities), Dordrecht, Holland, 1986.

[33] J. W. Bannister, *Solar Radiation Records*, Division of Mechanical Engineering. Commonwealth Scientific and Industrial Research Organization, Australia, 1966-1969.

[34] D. T. Reindl, W. A. Beckman and J. A. Duffie, 'Diffuse Fraction Correlations', *Solar Energy*, **45**, 1 (1990a).

[35] J. F. Origill and K. G. T. Hollands, 'Correlation Equation for Hourly Diffuse Radiation on a Horizontal Surface', *Solar Energy*, **19**, 357 (1977).

[36] D. T.Reidl, *Estimating Diffuse Fraction Radiation on Horizontal Surfaces and Total Radiation on Tilted Surfaces*, M.S. Thesis, Mechanical Engineering, U. of Wisconsin-Madison, 1988.

[37] M. Macagnan, *Caracterización de la Radiación Solar para Aplicaciones Fotovoltaicas en el Caso de Madrid*, Ph.D. Thesis, Universidad Politéchnica de Madrid, 1993.

[38] M. Macagnan, E. Lorenzo and C. Jimenez, 'Solar radiation in Madrid', *Int. J. Solar Energy*, **16**, 1-14 (1994).

[39] S. A. Klein, 'Calculation of Monthly Average Insolation on Tilted Surfaces', *Solar Energy*, **19**, 325 (1977).

[40] S. A. Klein and J.C. Theilacker, 'An Algorithm for Calculating Monthly-Average Radiation on Inclined Surfaces', Trans. ASME, *J. Solar Energy Engrg.*, **103**, 29 (1981).

[41] *C.E.C. The European Solar Radiation Atlas*: Vols. I and II, Les Presses de l' Ecole des Mines, Paris, 2000.

[42] T. Muneer, 'Solar radiation model for Europe', *Building Serv. Eng. Res. Technol.*, 11, 153-163 (1990).

[43] R. Aguiar, 'Final tests of Diffuse Irradiation Models for ESRA Standard Set of Routines', European Solar Radiation Atlas Project, Contract JOU2-CT93-305, INETI, Report No. ESRA/INETI/Task II/19, Dep. Renewable Energies, Lisbon, 50 (1997).

[44] J.W. Bugler, ' The determination of hourly insolation on an inclined plane using a diffuse irradiance model based on hourly measured global horizontal insolation', *Solar Energy*, **19**, 477-491 (1977).

[45] C. Gueymard, 'An anisotropic solar irradiance model for tilted surfaces and its comparison with selected engineering algorithms', *Solar Energy*, **38**, 367-386 (1987), Erratum, *Solar Energy* **40**, 175 (1988).

[46] A. Skartveit and J.A. Olseth, 'Modelling slope irradiance at high latitudes', *Solar Energy*, **36**, 333-344 (1986).

[47] R. Perez, P. Ineichen, S. Seals, 'Modelling daylight availability and irradiance components from direct and global irradiance', *Solar Energy,* **44**, 271-289 (1990).

[48]*Photovoltaic Systems*, Fraunhofer Institute for Solar Energy Systems, Germany, 1995.

[49] *Universal Technical Standard for Solar Home Systems*, Thermie B SUP 995-96, EC-DGXVII, 1998.

[50]Lighting and overvoltage protection in Photovoltaic and solar thermal systems, Energie, European Commission, 2000.

[51] B. D. Hahn, *Essential Matlab for Scientists and Engineers*, John Willey & Sons, New York, 1997.

[52] A. Biran, M.Breiner, *Matlab For Engineers*, Addison Wesley, England, 1995.

[53] R. Kaiser, D. U. Sauer. 'Investigations on the long term prediction of the energy yield of stand-alone PV-systems', *12th European photovoltaic solar energy conference* (1994).

[54] S. M. Sze, *Physics of Semiconductor Devices*, John Willey & sons, New York, 1981.

[55] A. M. Green, *Solar Cells*, Operating Principles, Technology, and System Applications, Prentice-Hall, USA, 1982.

[56] R. Bronson, *Modern Introductory Differential Equations*, Schaum's outline series, Mc Graw-Hill, New York, 1973.

[57] R.J. Van Overstraeten and R.P. Mertens, *Physics, Technology and Use of Photovoltaics*, Adam Hilger, Bristol, 1987.

[58] F. Lasnier and T.G. Ang, *Photovoltaic Engineering Handbook*, IOP Publishing Ltd., 1990.

[59] H. Schmidt, D.W. Sauer and H.-G. Plus, *36 Cells for a standard module*, In 2nd World Conference and Exhibition on Photovoltaic Solar Energy Conversion, Vienna, Austria, 2203 1998.

[60] A. Vincent, *Modern Batteries, An Introduction to Electrochemical Power Sources*, Edward Arnold Ltd., ISBN 0-7131-3469-0 1984.

[61] D. Spiers and J.Royer, *Guidelines for the Use of Batteries in Photovoltaic Systems*, Canadian Energy Diversification Research Laboratory of CANMET (CEDRL), Canada, 1998.

[62] D. Linden and T.B. Reddy, *Handbook of batteries*, Third edition, McGraw-Hill, ISBN 0-07-135978-8 2002.

[63] D.Spiers, personal communication.

[64] C.M. Shepherd, *Design of primary and secondary cells*, J.Electrochem. Soc.112, 657 (1965).

[65] J.B. Copetti and F. Chenlo, 'Lead/acid batteries for photovoltaic applications, Test results and modelling', *J. Power Sources*, **47**, 109 (1994).

[66] S. Silvestre, D. Guash, U. Goethe and L. Castaner, 'Improved PV battery modelling using Matlab', *Proceedings of the 11th European Photovoltaic Solar Energy Conference and Exhibition*, Munich, 507-509 (October 2001).

[67] D. Guasch and S. Silvestre, 'Dynamic Battery Model for Photovoltaic Applications', *Progress in Photovoltaics: Research and Applications*, **11**, 193-206 (2003).

[68] D.G. Murillo, *Modelado y analysis de sistemas fotovoltaicos*, PhD. Thesis, Universitat Polytecnica de Catalunya, 2003.

[69] H. Gu, T.V. Nguyen and R.E. White, 'A Mathematical model of a lead-acid cell'. *J.Electrochem. Soc.*, **134**, 2953 (1987).

[70] Z. M. Salameh, M. A. Casacca and W. A. Lynch, 'A mathematical model for lead-acid batteries'. IEEE Trans. *Energy Conversion,* **7**, 93 (1992).

[71] J. N. Ross, T. Markvart and W. He, 'Modelling battery charge regulation for a stand-alone photovoltaic system', *Solar Energy*, **69(3)**, 181-190 (2000).

[72] S.Silvestre, D. Guasch, U.Goethe and L.Castaner, 'Improved PV Battery Modelling Using Matlab', *Proceedings of the 17th European Photovoltaic Solar Energy Conference and Exhibition*, Munich, 507-509 (October 2001).

[73] D. Guasch and S. Silvestre, 'Dynamic Battery Model for Photovoltaic Applications', *Progress in Photovoltaics:Research and Applications,* **11**, 193-206 2003.

[74] D. G. Murillo, Tesis Doctoral, Modelado y Analisis de Systemas Fotovoltaicos, Universitat Polytecnica de Catalunya, Barcelona, April, 2003.

[75] K. Levenberg, 'A method for the solution of certain problems in least squares. Quarterly of Applied Mathematics', **5,** Quarterly Journal 164-168 1994.

[76] D. Marquardt, 'An algorithm for least squares estimation of nonlinear parameters'. *SIAM Journal on Applied Mathematics*, **11**, 431-441 (1963).

[77] J.W. Stevens and G.P. Corey, 'A Study of lead-Acid Battery Efficiency Near Top-of –Charge and the Impact on PV System Design', *25TH PVSC*, May 13-17, Wasington , D.C (1996).

[78] A. Brunia, D. Schmal, H.P.W. Fransen, R.J.C. van Solingen, C.P.M Dunselman and T.C.J. van der Weiden, 'Analysis of Mechanisms and Causes of Deterioration of Lead-Acid Batteries in Photovoltaic Applications Based on Field Experience', 12th European Photovoltaic Solar Energy Conference, Amsterdam, The Netherlands, 418 (1994).

[79] G.W. Vinal, *Storage Batteries*, John Wiley, New York, 1955.

[80] W.B. Gu, C.Y. Wang and B.Y. Liaw, 'Numerical modelling of electrochemical and transport processes in lead-acid batteries', *J.Electorchem. Soc.*, **144**, 2053 (1997).

[81] Secondary cells and batteries for solar photovoltaic energy systems-General requirements and methods of test, 2002.

[82] L. Barra, S. Catalanotti, F. Fontana and F. Lavorante, 'An analytical method to determine the optimal size of a PV plant', *Solar Energy*, **33**, 509-514 (1984).

[83] R. N. Chapman, 'A Simplified Technique for Designing Least Cost Stand-Alone PV/Storage Systems',*19th IEEE Photovoltaic Specialist Conference*, New Orleans, 1117-1121 (1987).

[84] R. N. Chapman, *Sizing Handbook for Stand-Alone Photovoltaic/Storage Systems*, SAND87-1087, Sandia National Laboratoryoratories, Albuquerque, New Mexico, April 1987.

[85] L. L. Bucciarelli, 'Estimating loss-of power probabilities of stand-alone photovoltaic solar energy system', *Solar Energy*, **32(2)**, 205-209 (1984).

[86] L. L. Bucciarelli, 'The effect of day-to-day correlation in solar radiation on the probability of loss of power in a stand-alone photovoltaic energy system', *Solar Energy*, **36(1)**, 11-14 (1986).

[87] M. Sidrach-de-Cardona and L.L. Mora, 'A general multivariate qualitative model for sizing stand-alone photovoltaic systems', *Solar Energy Materials and Solar Cells*, **59**, 185-197 (1999).

[88] M. Sidrach-de-Cardona and L.L. Mora, 'A simple mode for sizing stand-alone photovoltaic systems', **55**, 199-214 (1998).

[89] M. Egido and E. Lorenzo, 'The sizing of stand-alone PV systems: a review and a proposed new method', *Solar Energy Materials and Solar Cells*, **26**, 51-69 (1992).

[90] E. Lorenzo and L. Narvarte, 'On the usefulness of Stand-Alone PV Sizing Methods', *Progress in Photovoltaics: Research and Applications*, **8**, 391-409 (2000).

[91] R.J. Aguiar, M.Collares-Pereira and J.P. Conde, 'Simple procedure for generating sequences of daily radiation values using a library of Markov Transition Matrices', *Solar Energy*, **40**, No.3, 269-279 (1988).

[92] S.A. Klein, W.A. Beckman. 'Loss of load probabilities for stand-alone photovoltaic systems', *Solar energy*, **39 (6)**, 499-512 (1987).

[93] T. Markvart, J.N. Ross and W.He, 'Battery charge management for minimum cost PV systems', *17th European Photovoltaic Solar Energy Conference*, Munich, Germany, **3**, 2549-2552, (October 2001).

[94] J.M Gordon, 'Optimal sizing of stand alone photovoltaic solar power systems', *Solar Energy Materials and Solar Cells,* **20,** 295, (1987).

[95] www.metoffice.gov.uk/research/hadleycentre/models/climate_system.html

APPENDIX A – PV GENERATOR MODEL

The formulas used in Matlab modelling for the calculation of the I-V of a PV generator are:

- To calculate the short circuit current of the generator under operating conditions

  $C_1=I_{SCMSTC}/1000$

  $I_{SC}=C_1*G_p$

  $I_{SCG}=I_{SC}*N_P$

- To calculate the open circuit voltage of the generator under operating conditions

  $V_{OCSTC}=V_{OCMSTC}/N_{SM}$

  C_2=NCOT(^{0}C)-20/80mW/cm^2 (we assume that C_2 is equal to 0.03 ^{0}C/W/m$_2$ and the error is less than 1%)

  $T_C=0.03*G_p+T_A$

  $V_{OC}=V_{OCSTC}-0.0023*(T_C-25)$

  $V_{OCG}=V_{OC}*N_S$

- To calculate the series resistance of the generator, we assume that it remains constant:

  $V_{tstc}=(1.381*10^{-23}*(273+25))/1.602*10^{-19}$

  $vocstc=V_{OCSTC}/ V_{tstc}$

  $FFO_{STC}=(vocstc-ln(vocstc+0.72))/(vocstc+1)$

  $P_{MAXSTC}=P_{MAXMSTC}/N_{SM}$

  $FF_{STC}=P_{MAXSTC}/(V_{OCSTC}*I_{SCMSTC})$

  $r_{sstc}=1-FF_{STC}/FF_{OSTC}$

  $R_S=r_{sstc}*VOCSTC/I_{SCMSTC}$

  $R_{SG}=R_S*N_S/N_P$

- To calculate the thermal voltage of the cell under operating conditions

  $V_t=(1.381*10^{-23}*(273+T_C))/1.602*10^{-19}$

- To calculate the I-V curve of the generator

  $I_G=I_{SCG}[1-exp(V_G-V_{OCG}+I_GR_{SG}/mN_sV_t)]-(V_G+I_GR_{SG})/R_{PG}$

- The power at any instant is in general the product of the voltage and the current

The parameters used in the above equations are:

C_1=constant of proportionality

I_{SC}=short circuit current of the solar cell under operating conditions

T_C=cell temperature under operating conditions

V_{tstc}= The thermal voltage of the cell under standard test conditions

v_{ocstc}=normalized open circuit voltage under standard test conditions

v_{oc}=normalized open circuit voltage under operating conditions

P_{MAXSTC}=the maximum power of the cell under standard test conditions

FFO_{STC}=fill factor of an ideal solar cell under standard test conditions

FF_{STC}=fill factor of a solar cell under standard test conditions

r_{sstc}=normalized series resistance under standard test conditions

R_S=series resistance of the cell

R_{SG}=series resistance of the generator

R_{PG}=parallel resistance of the generator

V_t=thermal voltage of the cell under the operating conditions

m=ideality factor

I_G=current of the generator under operating conditions

V_G=voltage of the generator under operating conditions

APPENDIX B-STaR DATA ACQUISITION SYSTEM

The data acquisition system at StaR (Southampton Test and Reference) facility consists of a DAQ card (CIO-DAS08/Jr-AO) and five multiplexers (CIO-EXP32/16) in which all the DC voltages and currents are connected to monitor system and environment parameters. The DAQ card, CIO-DAS08/Jr-AO, is in one of the AT slot in a computer and the multiplexers are on the racks (interface). DATALAB is an icon-based software with which an interface programme to DAQ hardware was developed. For the experiment this programme was modified and datalab was used for both monitoring and logging the data.

APPENDIX C-CURRENT AND VOLTAGE SENSING

Current sensing			
	PV	Battery	Load
Voltage range used	0.25V	0.25V	0.25V
Voltage error(%)= Voltage range used/ Nominal system voltage=0.25V/12V	2 %	2 %	2 %
Maximum expected values of current	~7 A	~6.7 A	~0.3 A
Calculated values for the current sensing resistors R=V/I	35.71 mOhm	37.31 mOhm	833 mOhm
Specifications of resistors used	33 mOhm 4Watt rating at 70°C	33 mOhm 4Watt rating at 70°C	740 mOhm (two of 370 mOhm in series) 1Watt rating at 70°C
Calibrated values of the resistors	34.2 mOhm	34.2 mOhm	719 mOhm
Maximum expected values of voltage readings $I \cdot R_{calibrated}$	0.239 V	0.221 V	0.216 V
Maximum power consumption on the current sensing resistors $P=I^2 \cdot R_{calibrated}$	1.68 Watt	1.48 Watt	0.0647 Watt

Voltage sensing			
	PV	Battery	Load
Voltage range used	2.5 V	2.5 V	2.5 V
Maximum voltage expected	~22 V	~22 V	~22 V
Chosen value for R_1	27.4 kOhm	27.4 kOhm	27.4 kOhm
Calculated values for the resistor R_1 $\frac{R_2}{R_1+R_2}=\frac{V_2}{V}=\frac{1}{10}$	246.6 kOhm	246.6 kOhm	246.6 kOhm

APPENDIX D-PUBLICATIONS

1. **A. Fragaki** and T. Markvart, 'Does climate change affect the design of stand-alone PV systems?', *Progress in Photovoltaics.* Paper accepted on 9/10/2004.

2. L. Castañer, S. Bermejo, T. Markvart and **K.Fragaki**, Energy production by a PV array, in: T. Markvart and L. Castañer (Ed), *Practical handbook of Photovoltaics. Fundamentals and Applications,* Elsevier Science Ltd., Oxford, UK, 2003, 517-529.

3. L. Castaner, S. Bermejo, T. Markvart and **K.Fragaki**, Energy balance in stand-alone systems, in: T. Markvart and L. Castañer (Ed), *Practical handbook of Photovoltaics. Fundamentals and Applications,* Elsevier Science Ltd., Oxford, UK, 2003, 531-541.

4. **A. Fragaki** T. Markvart, 'Does global warming affect the design of stand–alone PV systems?', Poster, *1st SWH International Conference*, Segovia, Spain, 155, (2003).

5. **A. Fragaki** and T. Markvart, 'Solar radiation data and photovoltaic system modelling', *Proceedings of the Eighth Postgraduate Conference in Engineering Materials,* University of Southampton, 33-34, (2002).

6. **A. Fragaki** and T. Markvart, 'Photovoltaic systems', *Proceedings of the Seventh Postgraduate Conference in Engineering Materials,* University of Southampton, 5-6, (2001).